Cocrystallization and Particle Size Reduction of Active Pharmaceutical Ingredients (APIs) Using Supercritical Carbon Dioxide Crystallization or Spray Drying

by

Lauren MacEachern

Submitted in partial fulfilment of the requirements for the degree of Doctor of Philosophy

at

Dalhousie University

Halifax, Nova Scotia

May 2024

Dalhousie University is located in Mi'kma'ki, the ancestral and unceded territory of the Mi'kmaq. We are all Treaty people.

TABLE OF CONTENTS

LIST OF TABLES

LIST OF FIGURES

ABSTRACT

Modern active pharmaceutical ingredients (APIs) often exhibit poor aqueous solubility, leading to poor bioavailability. Methods to improve dissolution include altering solid form (salts, polymorphs, cocrystals), creating amorphous dispersions, and particle size reduction. In this study, cocrystallization and particle size reduction of two nonionizable anthelmintic drugs, niclosamide (NCS) and praziquantel (PZQ), are investigated. The research aims to understanding parameters that influence cocrystal formation and particle size of materials prepared by spray drying and rapid expansion from supercritical solution (RESS).

An NCS-urea cocrystal with mean particle size of 2 μm was prepared by spray drying with yield up to 73%. However, the process required large volumes of organic solvent. Feasibility of using CO_2, a greener solvent, for preparation of the cocrystal was evaluated at different process conditions. Addition of between 2.7—3.5 % cosolvent significantly impacted cocrystal formation at 40 °C and 20 MPa. Adding 2-propanol increased cocrystal formation by 50—60% compared to neat $scCO_2$, while cyclohexane reduced cocrystal formation by between 20—35%, and water hindered cocrystal formation. However, even with cosolvent, NCS was not sufficiently soluble to form a cocrystal using RESS. Furthermore, although a cocrystal was formed it did not exhibit improved solubility in biorelevant conditions.

PZQ exhibited better solubility than NCS in $scCO_2$ and was pursued to demonstrate the impact of solvent choice and processing parameters on cocrystal formation in $scCO_2$. During the research a novel crystalline form of PZQ was discovered which was stable for up to 7.5 weeks and exhibited up to 20% improved solubility in biorelevant media. Adding cosolvent to $scCO_2$ allowed for PZQ and coformer, malonic acid, to crystallized by RESS. While addition of acetone and tetrahydrofuran did not produce pure cocrystal, methanol and ethanol were successful. Investigation of RESS with MeOH cosolvent led to production of particles as small as 600 nm with yields above 65% and acceptable crystallinity and residual solvent.

This work showed that with careful selection of process solvent(s) both spray drying and RESS are feasible processes for preparing phase pure co-crystals and simultaneously generating micron or sub-micron size particles which may be advantageous over mechanical particle size reduction methods.

LIST OF ABBREVIATIONS AND ACRONYMS USED

Å	Angstrom
AAS	Atomization and antisolvent
API	Active pharmaceutical ingredient
BCS	Biopharmaceutical classification system
BET	Brunauer-Emmett-Teller Surface Area Measurement
C	Celcius
CF	Coformer
CHF3	Trifluoromethane
CSS	crystallization from supercritical solution
DCM	Dichloromethane
DEE	Diethylether
DMF	Dimethylformamide
DMSO	Dimethylsulfoxide
DOE	Design of experiments
DSC	Differential scanning calorimetry
EOS	Equation of state
EtOAc	Ethyl acetate
EtOH	Ethanol
FaSSGF	Fasted state simulated gastric fluid
FaSSIF	Fasted state simulated intestinal fluid
FDA	Food and Drug Administration
FeSSIF	Fed state simulated intestinal fluid
FT	Fourier Transform
GAS	gas antisolvent
GC	Gas chromatography
GRAS	generally regarded as safe
HPLC	High-performance liquid chromatography
ICH	International council for harmonization
IPA	Isopropanol

IPAc	Isopropyl acetate
IR	Infrared
K	Kelvin
KF	Karl Fischer
LAG	Liquid assisted grinding
MeOH	Methanol
MPa	Megapascal
MtBE	Methyl tert-butyl ether
NBM	Nabumetone
NCS	Nicolsamide
NCS-UR	Nicolsamide-urea cocrystal
NMR	Nuclear magnetic resonance
NSAID	Nonsteroidal anti-inflammatory drug
OFAT	One factor at a time
PSD	Particle size distribution
PZQ	Praziquantel
RESS	rapid expansion from supercritical solution
RH	Relative humidity
SAS	supercritical antisolvent
scCO2	Supercritical carbon dioxide
SCF	Supercritical fluid
SEA	supercritical enhanced atomization
SEM	Scanning electron microscopy
SOP	Standard operating procedure
TFE	Trifluoroethanol
TGA	Thermogravimetric analysis
THF	Tetraydrofuran
TPD	Ternary phase diagram
WHO	World Health Organization
XRPD	X-ray powder diffraction
°	Degree

θ	Theta
<	Less than
>	Greater than
>>	Much less than
μm	Micrometer
mm	Millimeter
g (mg)	Gram (milligram)
L (mL)	Litre (millilitre)

ACKNOWLEDGEMENTS

I would like to express sincere thanks to my supervisor, Dr. Azadeh Kermanshahi pour, and my co-supervisor, Dr. Sophia He, for their mentorship and guidance throughout this process, particularly when we had to navigate the unforeseen challenge of the COVID-19 pandemic. A great thank you also goes to my mentor, Dr. Mahmoud Mirmehrabi, who encouraged me to pursue this new challenge and supported me throughout the program. I would also like to thank supervisory committee members Dr. Su-Ling Brooks and Dr. Sohrab Rohani for providing thoughtful feedback during our meetings.

I would like to extend my gratitude to my BRL lab-mates for collaboration in advancing this research— particularly Rishi Walwyn-Venugopal for his help with the spray dryer, and Grace O'Connor and Dr. Jamileh Shojaei for their help with troubleshooting and operation of the supercritical reactor.

I also owe thanks to Dean Grijm and Michael Ruffolo of the PEAS Department for their help with troubleshooting equipment, Dr. Vivek Trivedi for introducing a collaboration after being meeting at ISSF, and to Xiang Yang of the Electron Microscopy Center at Saint Mary's University for collecting beautiful images throughout various stages of the research.

Finally, thank you to my husband and family for their continued patience and support (and patience again) throughout this process. Without them, completing this thesis would not have been possible.

1 CHAPTER 1: INTRODUCTION

1.1 BACKGROUND

Active pharmaceutical ingredients (APIs) can be differentiated according to solubility and permeability. The most common system used to categorize APIs by their solubility and permeability is the Biopharmaceutics Classification System (BCS) which divides APIs into four classes, illustrated in Figure 1.1. Solubility is considered high when the dosage of the drug is soluble in ≤ 250 mL aqueous media between pH 1 and 6.8 at 37 °C, while high permeability is considered when the drug exhibits more than 85% recovery of the drug in the urine.[1] When APIs do not meet the criteria for high solubility and permeability, they are categorized as 'low'. For compounds falling into Classes II, III, or IV either solubility or permeability of the drug should be improved which is done through modification of the solid-form, dosage form, or formulation. Based on a review of the top 200 orally administered drugs in 2006, it was estimated that between 25 and 44% of drugs were Class I (high solubility and permeability), while 31-35% of drugs were Class II (low solubility, high permeability), 16-35% were Class III (high solubility, low permeability), and just 4-7% were Class IV (low solubility and permeability).[2]

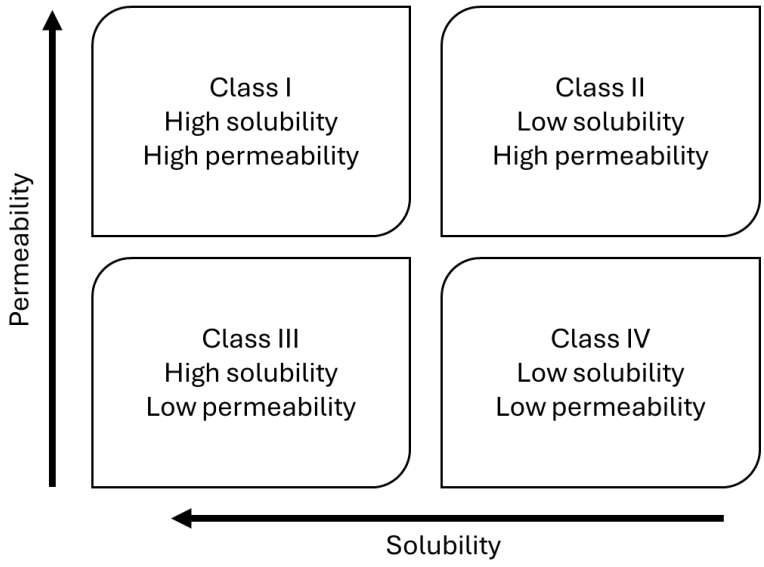

Figure 1.1- Summary of BCS classification of APIs.

The main driver for modification of BCS Class II APIs is to increase the solubility of the drug in-

vivo which can be achieved through modification of the solid-form (forming salt, cocrystal, or amorphous) and particle size reduction.[3–5]

Particle size reduction of APIs increases the material's specific surface area, leading to increased dissolution rates when compared to larger particles of the same material.[6] Using conventional crystallization techniques the ability to reduce particle size is limited. A lower limit around 1 μm has been suggested, but in practice this is rarely attained using industrially relevant crystallization methods.[7] Therefore, secondary processes are typically employed such as jet milling, nano milling, ball milling, or high-pressure homogenization.[6–8] When secondary micronization processes are used, a conventional batch crystallization typically precedes the mechanical particle size reduction step. However, some processes are able to crystallize materials with small particle size in a single step, such as spray drying and supercritical fluid crystallization, which may mitigate concerns related to generation of amorphous material or chemical instability due to mechanical stress.[9–15]

Ionizable APIs that exhibit poor solubility often developed as a salt form to improve solubility or other physical properties. At a high-level, solubility improvement of salts compared to freeform is related to equilibrium of the ionized and nonionized forms of the API, pKa of the compound, the counterion, and the pH of the dissolution media.[16,17] Solubility of pharmaceutical salts is generally strongly dependent on the pH of dissolution media, exhibiting a maximum solubility at pH_{max}, the point where the freeform and counterion can coexist as solids in a slurry. The pH_{max} for a given salt is influenced by the pKa of the API and the solubility of the salt form and freeform of the API.[16] To identify suitable salts for the purpose of improved bioavailability, pH_{max} should be high (for basic APIs) and low (for acidic APIs) to ensure some solubility improvement is expected in biorelevant conditions. Salts are generally well-accepted and easier to isolate in comparison with crystals or amorphous solids, which is why they are a first option for solubility improvement of ionizable APIs.

For non-ionizable APIs where salt formation is not possible, the use of cocrystals or amorphous solid can improve solubility. Amorphous solid and cocrystals are often hypothesized to follow a "spring-parachute" effect to improve kinetic or apparent solubility, which relates to the high-energy (thermodynamically unstable) amorphous state of an API.[4] For an amorphous API, it follows that due to the high free energy of the amorphous material, the solubility in a given

media should be greater than a compound's thermodynamically stable solid-phase. The initial kinetic dissolution of the metastable amorphous is often referred to as the "spring" while the "parachute" stage encompasses the transition from a high-energy (more soluble) phase towards equilibrium solubility of a thermodynamically stable (less soluble) crystalline phase. It is generally accepted that the gradual transition from amorphous to thermodynamically stable crystalline API follows Ostwald's Rule of Stages through formation of metastable forms. Cocrystals are suspected to follow a similar path—first the cocrystal formed through hydrogen bonding dissociates into its components, generating amorphous API *in-situ*, which then behaves similarly to amorphous API as described above.[4] The improvement in kinetic solubility allows for better absorption of the solubilized drug while in the gastrointestinal tract before conversion to the lower-solubility, more thermodynamically stable form.

In general, using a crystalline solid for the drug substance can be more desirable than using amorphous because it allows for more consistent processing/isolation and can often have a chemical stability advantage in the solid-state (i.e. during storage).[18–20] For ionizable compounds, salts are often used to improve the solubility of BCS Class II APIs, and for non-ionizable compounds cocrystals may be used. According to the United States Food and Drug Administration (FDA), a cocrystal is a crystalline material comprising two or more different molecules (often described as API and coformer) in the same crystal lattice.[21] A cocrystal should have a well-defined stoichiometry and interact non-ionically by hydrogen bonding. A cocrystal is often considered as a special case of a solvate or hydrate, but the second component, the coformer, is a solid at ambient conditions. Coformers are often selected from known compounds that are generally regarded as safe (GRAS) or from a list of pharmaceutically acceptable compounds that are not pharmaceutically active. However, in some instances coformers with therapeutic effects are used.[22–24]

Cocrystals approved by the FDA include both drug-drug cocrystals and more conventional cocrystals with only one pharmaceutically active component. Examples of cocrystals with two pharmaceutically active components include Seglentis (Esteve Pharmaceuticals) which comprises celecoxib and tramadol hydrochloride, used for acute pain treatment, and Entresto (Novartis) which comprises sacubitril and valsartan, for cardiovascular issues.[22,23] Cocrystals with only one active component include examples such as Stelagtro (Merck) which comprises

ertugliflozin (active) and l-pyroglutamic acid (inactive) and Abilify (Bristol Myers Squibb) which comprises apriprazole (active) and fumaric acid (inactive) which are used in the treatment of type 2 diabetes and schizophrenia, respectively.[23,24]

Cocrystals can be prepared using a range of methods which fall into two main groups— methods suitable for screening, and methods suitable for scale-up. Screening methods are suitable for small-scale (tens of milligrams) and are designed to enable high-throughput screening to identify cocrystal forms. Screening methods include liquid assisted griding (LAG), evaporative crystallization, co-melting, and reactive crystallization.[25,26] On the other hand, methods suitable for scale-up are not amenable to high-throughput screening and are suitable once a target cocrystal form has been identified and needs to be produced on gram-scale quantities and above. Such methods can include conventional batch crystallization, spray drying, and supercritical fluid (SCF) crystallization.[25]

1.2 Knowledge Gap and Objective

Significant work has been done exploring crystallization of APIs using $scCO_2$, specifically rapid expansion from supercritical solution (RESS). However, most of the work is done for single component APIs that exhibit relatively high solubility in $scCO_2$. There is a limited body of work exploring $scCO_2$ crystallization of multicomponent systems such as cocrystals or for APIs that are not highly soluble in $scCO_2$. Finally, direct comparison of process parameters and product attributes between $scCO_2$ processes and conventional crystallization is often overlooked. The knowledge gaps that provided motivation for the research presented in this thesis were:

- Expanding on characterization of select cocrystals of BCS Class II APIs to identify if cocrystal formation and particle size reduction offers an advantage compared to commercially available freeforms.
- Systematic approach for solvent or cosolvent selection in $scCO_2$ processes.
    - Although the proposed research focuses on $scCO_2$, selection of conventional organic solvents is a key decision when designing a crystallization process and can have a profound impact on the process. Selection of an optimal solvent system may be addressed simply by assessing the solubility profiles of API and co-former. Although the impact of solvent is not equal for all compounds, it can

imfluence morphology, yield, co-crystal phase purity, or polymorph. The solvent class must also be considered because it will have implications on product specifications.

- Comparison of process details and product attributes for APIs crystallized in $scCO_2$ vs. conventional crystallization in organic solvents.
    - Supercritical CO_2 processing is sometimes considered to be an environmentally acceptable alternative to conventional crystallization organic solvents. However, there is an energy usage and cost associated with heating and pressurization of CO_2. Also, due to the low solubility of many pharmaceuticals in $scCO_2$, cosolvent additives may be required for a successful co-crystallization by methods like RESS. The quantity of organic solvent required for an SCF crystallization versus conventional crystallizations should be compared while taking into consideration process yield and product attributes such as crystallinity, particle size, and residual solvent content.
- Reporting of key process parameters and details to facilitate process comparison, scale-up assessment, and technology transfer.
    - For crystallization by RESS the reporting of relevant process parameters is often limited. To ensure that the research community can maximize progress on co-crystallization in SCF the reported work can be presented with more detail whenever possible which can help to better identify critical areas for improvement.
- Better understanding of optimizing a SCF co-crystallization to improve yield.
    - Yield loss is often speculated to be from loss during collection due to small sample size, but if processes such as RESS are to become more industrially relevant in the pharmaceutical industry yield loss should be understood and addressed. Mass balances of processes are not often reported, but can be used to identify process shortcomings through comparing mass of solids in mother liquor, collection vessel, or other components of equipment.

1.3 Scope of Thesis

This PhD research is aimed toward understanding parameters that influence formation and particle size of cocrystals prepared using techniques such as spray drying and supercritical CO_2 crystallization which offer the possibility of cocrystallization and production of small (possibly sub-micron), uniform particles in a single process. Although this research focuses on the influence of process conditions on the solid-state properties of the produced solids, the ultimate goal of preparing material using these methods is to improve bioavailability of BCS Class II APIs that have low solubility. The research is divided into four main sections:

- Literature review (Chapter 2)
    - A thorough literature review of cocrystallization with a focus on cocrystals produced in $scCO_2$ was conducted. The literature review identified gaps in the research, which guided the research summarized within this thesis.
- Model compound screening and selection (Chapter 3)
    - BCS Class II compounds were compared based on safety (dosage), price and availability, potential to form cocrystals, and novelty. Three compounds were experimentally assessed and ultimately two compounds were carried forward to evaluate in more detail.
- Crystallization of a niclosamide-urea cocrystal by spray drying and $scCO_2$ processing (Chapter 4 & 5)
    - A niclosamide-urea cocrystal was found to readily form during initial assessment. To gain an understanding of experimental development of ternary phase diagrams (TPDs), a TPD of the cocrystal was prepared in IPA. Furthermore, the cocrystal was prepared by spray drying and attempted to be prepared by $scCO_2$ processing. Solubility of the cocrystal prepared by spray drying was compared to the neat API. Due to low solubility of NCS in $scCO_2$, even with the addition of a cosolvent, it was not a suitable cocrystal for crystallization in $scCO_2$, but the impact of cosolvent choice on success of cocrystal formation in $scCO_2$ was still evaluated and related to theoretical TPDs.
- Crystallization of a praziquantel-malonic acid cocrystal in $scCO_2$ (Chapter 6 & 7)
    - Due to the low solubility of niclosamide in $scCO_2$, praziquantel was selected as a

second model compound in support of this research. A baseline understanding of praziquantel's behavior in $scCO_2$ was developed, which led to discovery of a novel crystalline form that exhibited improved solubility in biorelevant media and was physically stable in humidity stressed conditions for up to 7.5 weeks. After developing a baseline understanding, the impact of processing conditions on product attributes such as phase-purity, yield, solvent content, and particle size was evaluated.

For each model compound in this research, it was attempted to develop a systematic approach for selecting a suitable process and solvent for preparation of a chosen cocrystal which involved exploration of ternary phase diagrams (measured or hypothesized) and solubility measurement in solvents with different properties including $scCO_2$. Processes were judged based on the ability to prepare the target form with acceptable properties such as crystallinity, phase purity, particle size, and yield. To the best of our knowledge, the influence of solvent choice on (co)crystallization by the RESS method $scCO_2$ has not been previously studied. Addition of an appropriate cosolvent to $scCO_2$ crystallization may allow for APIs to be crystallized with small particle size by RESS, even if they exhibit low solubility in pure $scCO_2$, making this crystallization technique feasible for a wider range of compounds.

2 CHAPTER 2: LITERATURE REVIEW; SUPERCRITICAL CARBON DIOXIDE FOR PHARMACEUTICAL CO-CRYSTAL PRODUCTION

2.1 ABSTRACT

Pharmaceuticals in Biopharmaceutics Classification System (BCS) Class II (low solubility, high permeability) are often modified to improve kinetic solubility. Co-crystallization and micronization are common methods for improving dissolution rate. The basis of understanding co-crystallization processes is solubility and phase stability. In the majority of co-crystallization processes, conventional solvents are utilized. Co-crystallization using supercritical carbon dioxide as co-solvent and anti-solvent can offer advantages over conventional co-crystallization including greener solvent choice and production of small, uniform particles without additional micronization. Gas antisolvent is the most widely reported supercritical fluid (SCF) co-crystallization process possibly due to its versatility in solvent selection, and similarities to conventional antisolvent processes. This review focused on exploring critical co-crystallization parameters and feasibility of SCF techniques. In this review it was identified that solvent choice proves to be one of the most critical parameters, impacting morphology, yield, phase purity, or polymorphic outcome to different extents. It was also identified that a systematic study of solubility to design co-crystallization processes is needed to optimize SCF co-crystallization yield and throughput. Furthermore, focus on solubility and modeling of multi-component systems and development of ternary phase diagrams can lead to robust, tailored co-crystallization processes in SCF systems, transitioning this technology to become more common in industry.

2.2 INTRODUCTION

2.2.1 Solubility and Supersaturation- The Basis of Crystallization

A supercritical fluid is defined as any fluid at conditions beyond its critical point. All fluids can form SCFs in theory; however, the practicality of the critical point must be taken into account. Some substances are inert, non-flammable, and safe with attainable critical points. Examples of such gases are carbon dioxide (CO_2) and trifluoromethane (CHF_3). The critical points of CO_2 and

CHF_3 are 31.3 °C/7.4 MPa and 25.93 °C/4.7 MPa, respectively.[27] Of these two SCFs, CO_2 is by far the most widely studied because it is non-toxic, environmentally friendly, and recyclable. Water could also be a desirable SCF due to abundance and non-toxicity. However, the melting point of most pharmaceutical compounds (free molecule, co-crystal, and salts) is below the critical temperature of water (374 °C), which makes supercritical water incompatible for pharmaceutical processing.[27] For example, multiple databases of pharmaceutical compounds' melting points showed that less than 10% had melting points above 250 °C.[28,29]

SCFs exhibit properties in between a vapor and a liquid. The SCF density is similar to a liquid, allowing for solvation power, while viscosity and diffusivity are similar to that of a vapor, allowing for mass transfer. Changes in operation conditions such as pressure and temperature alter the properties of an SCF, and therefore the solvation power. This allows $scCO_2$ to be used instead of a conventional organic solvent.[30]

Solubility and supersaturation are the basis of any crystallization process. In order to develop a robust crystallization process, solubility of the compound(s) of interest must be well understood in the solvent system. For the case of conventional crystallization processes, solubility is assessed as a function of temperature and composition in the case of a multicomponent solvent system. In the case of supercritical systems, solubility should be assessed as a function of temperature and pressure (or density of the fluid), and composition for SCF/organic solvent systems.

The solubility assessment method for supercritical systems differs from that of conventional solvents. Typically, solids will be loaded into the high-pressure cell or equilibrium vessel along with glass beads to allow for better mass transfer and mixing. Direct measurement of solubility of compounds in supercritical fluids can be time consuming and might not be straightforward. Generally, for a supercritical system only one solubility measurement can be done at a time (i.e. one temperature, pressure, composition). Both pressure and temperature should be well controlled during the measurement and care must be taken with the collection of materials for analysis. Since the SCF expands as the vessel is de-pressurized care needs to be taken to ensure the volume or mass of solvent and solute is accurately determined. For this reason, the solubility assessment stage of process development for a supercritical system comprises significantly more time than for a conventional crystallization solubility assessment. There are a number of

variations on a simple solubility assessment, which are not discussed in detail in this paper.[31–35] In all cases, a slurry is allowed to equilibrate at a given pressure and temperature. Solids (or supernatant) are then collected to be analyzed using gravimetry or spectrophotometry methods. In the literature, solubility measurements are often carried out in triplicate.

There have been a number of models proposed for predicting solubility of compounds in supercritical fluids in general, or specifically in supercritical carbon dioxide ($scCO_2$). The models include empirical or semi-empirical, equation of state (EoS) in combination with group contribution (GC) models, solution models, and artificial neural network (ANN).[36–48] Empirical or semi-empirical methods are quite popular and are based on a number of independent variables such as temperature, pressure, and/or density of the supercritical fluid. There are at least 24 proposed density-based models to date.[37]

When solubility of a compound in the process solvent system is understood, process parameters can be selected to control nucleation and growth during crystallization. Common process parameters include solute concentration, solvent system composition, temperature profile, pressure profile (for supercritical systems), mixing regime, and antisolvent dosing regime. Solute concentration, solvent composition, temperature, and antisolvent dosing all directly relate to supersaturation of a given system. Altering these parameters during a crystallization process can impact polymorph, morphology, particle size and chemical purity. The fundamentals of crystallization are essentially the same for single component active pharmaceutical ingredients (APIs) and co-crystals, but the relationship between API and co-former should be considered when designing a co-crystallization process.

Solvent system (both composition and solute concentration) can have a profound impact on the product. The solvent system chosen impacts inter- and intra- molecular interactions during crystallization.[49–51] Use of different solvents, or even additives and impurities, can impact which sites on the crystal faces are available for hydrogen bonding during crystal growth. The growth rate of different crystal faces can then be modified thus altering particle morphology.[50,52] Solvent choice can also impact polymorphic outcome.[53] Degree of supersaturation and consequently, solution concentration impacts nucleation and growth rates, affecting particle size due to difference in concentration of the bulk vs the particle surface.[54,55] Particle size is a function of supersaturation, where particle size generally

decreases with increasing supersaturation due to increased nucleation rate. [56,57] As a result varying solvent temperature, API concentration, and solvent composition (i.e. antisolvent dosing regime) can be used to tune particle size. Solution concentration also determines the throughput of the crystallization, which is an important factor if the aim is scale up of a process. For example, if a crystallization process with 200 g/L solute (API) concentration is carried out in a 5 L reactor, throughput is 1 kg API. However, for a process with 20 g/L API, the throughput in the same 5 L reactor is only 100 g. Therefore, it is desirable to carry out the former process with more throughput, given its higher potential for scale up.

Mixing during crystallization is a critical factor as well impacting mass and heat transfer, shear, antisolvent dispersion, compound suspension, nucleation and growth during a crystallization process. [52] Impeller speed, type, and material of construction can impact crystallization. In general, fast nucleation leads to smaller particle size and slow nucleation can give larger particle size. However, a broad PSD may also be obtained at higher supersaturation due to agglomeration of smaller particles. When designing a process and assessing factors such as particle size, bulk density, and yield, any differences in mixing regime should be considered. [52]

The above parameters also impact results obtained from crystallization in high pressure systems. Solvent choice and solution concentration extends to SCF systems where an organic solvent is also used (gas antisolvent (GAS), supercritical antisolvent (SAS), supercritical enhanced atomization (SEA)). [51,58–62] Mixing has also been found to be a critical factor in success of co-crystal formation in some SCF processes. [34] However, the extent of the impact of these parameters is dependent on the system. The influence of process parameters on SCF crystallization will be discussed in more detail in the following sections. In this review we aim to identify areas of improvement for future research by suggesting a more systematic approach, robust reporting methodology, and considerations when selecting scale-up systems.

2.2.2 Supercritical Fluid for Pharmaceutical Co-crystal Production

There are several potential benefits to crystallization of an API or co-crystal by SCF techniques. These can include a greener solvent choice, elimination of an additional filtration/drying step, removal of residual organic solvent, ability to adapt to a continuous process, and to produce small particle size with narrow particle size distribution. For some APIs reducing residual solvent to below International Council for Harmonization (ICH) guidelines can be difficult due

to the morphology or particle size of the product. [63] Processes, which use $scCO_2$ as a solvent and do not incorporate organic solvent (crystallization from supercritical solution (CSS), rapid expansion from supercritical solution (RESS)), eliminate the need to remove organic solvents from the final product by drying at elevated temperatures or incorporating various washing steps. SCF processes can be used to isolate co-crystal particles much smaller than 1 μm diameter in a one-step crystallization process without added thermal or mechanical stress; i.e. no secondary milling step is required. [64] The use of SCF at large scale for crystallization of pharmaceuticals is still a novel technique with few companies advertising the service.

The United States Food and Drug Administration defines a co-crystal as a crystalline material comprising two or more different molecules (API and co-former) in the same crystal lattice. [21] The components have a well-defined stoichiometry and interact non-ionically (i.e. via hydrogen bonding). According to the FDA a co-crystal is considered a special case of solvate or hydrate where the second component, i.e. co-former is a solid at regular conditions (room temperature, atmospheric pressure). [21] Co-formers are often selected from known compounds that are generally regarded as safe (GRAS) or from lists of pharmaceutically acceptable counterions and are not pharmaceutically active. [3,65,66] However, in some instances co-formers with therapeutic effects can be used (e.g. sulfamethazine-theophylline). [67]

APIs are more commonly falling into the BCS as class II, which is a low solubility, high permeability compound. [68] The main driver for modification of BCS Class II APIs is an increase in kinetic solubility of the compound in vivo. Kinetic solubility of BCS Class II compounds can be improved by various methods such as using an amorphous solid form, formulation optimization, salt or co-crystal formation, and particle size reduction. [3–5]

Improved solubility of co-crystals has been attributed to the “spring parachute” effect. [4] The “spring parachute” concept suggests that a co-crystal dissociates to form amorphous or nanocrystalline drug in solution, giving rise to high initial solubility (the spring). The amorphous drug then follows Ostwald’s rule of stages, transitioning through metastable polymorphic forms until reaching the thermodynamically stable form and thus, equilibrium solubility. The transition through metastable polymorphs gives high apparent solubility (the parachute). The phenomena of “spring parachute” or enhanced co-crystal solubility has been shown for a number of co-crystals in literature. [3,4,69,70]

Improved solubility of amorphous dispersions also follows the “spring parachute” effect. [4] However, physical stability of an amorphous phase over extended time is often a concern because amorphous is the highest energy (least thermodynamically stable) phase. [18,19] As such, advanced solid state characterization is required to ensure long term stability and homogeneity of the amorphous phase. [20] Generation of an amorphous dispersion also typically proceeds a conventional crystallization, thus adding a step in the drug manufacture process.

Particle size reduction can also give rise to improved dissolution rate. [4,5,71] However, reduction in particle size via conventional crystallization is limited. A lower limit for particle size obtained from conventional crystallization is on the order 1 μm. [7] In practice, the particle size is rarely obtained below about 20 μm using conventional crystallization techniques that are viable from an industry perspective. To further reduce particle size, a micronization process such as jet milling is needed. [7,8] Novel particle size reduction methods such as “nano milling” have been found to produce particle sizes less than 200 nm. [8] Milling processes are widely used, but can result in degradation due to thermal and mechanical stress, loss in crystallinity, or change in polymorph. [13,72] In some cases physical instability dominates, where complete conversion from a crystalline form to amorphous is observed after milling. [13] However, chemical stability is also impacted by milling with some studies showing above 5 wt.% increase in chemical impurities after milling. [14,15] A SCF process can allow for both cocrystal formation and micronization in a single process without added thermal or mechanical stress. For example, the RESS process can be used to isolate particles much smaller than 1 μm diameter in a one-step crystallization process; i.e. no secondary milling step is required. [64]

The success of hydrogen bonding of co-crystals can often be predicted using a synthon approach. A supramolecular synthon is a spatial arrangement of intermolecular interactions, such as hydrogen bonding. A number of supramolecular synthons have been reported in the literature and can be used to aid in co-former selection when screening for co-crystals. [73,74] The functional groups of the API are assessed (e.g. amide, carboxylic acid) and then potential co-formers are selected based on ability to form homo- or hetero-synthons with the functional groups of the API. [70,75,76] Generally a wide range of co-formers containing the desired synthons are selected for screening. Co-crystal screening often takes a high throughput approach where 10-20 co-formers are screened using various techniques such as liquid assisted grinding

(LAG), co-evaporation, and co-melting. [26,77,78] All co-former/API pairs are screened using the mentioned approaches and unique crystalline "hits" are identified. The physicochemical properties of "hits" are then assessed and ranked by properties such as phase and chemical purity, melting point, morphology, chemical and physical stability, and solubility in biorelevant media.

Some examples of the supramolecular synthons common in co-crystals (carboxylic acids and amides) are shown in Figure 2.1 through Figure 2.3. Carbamazepine, for example, can form hydrogen bonds in both the homodimer and heterodimer motifs shown below. [76]

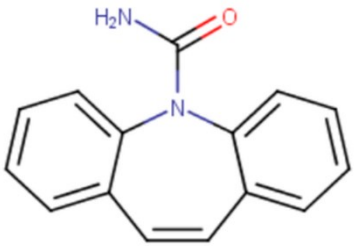

Figure 2.1- Carbamazepine.

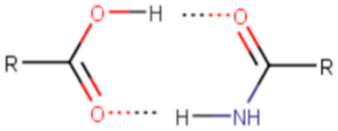

Figure 2.2- Carboxylic acid amide heterosynthon.

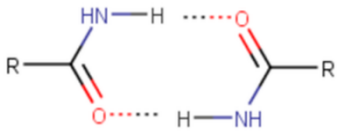

Figure 2.3- Amide homosynthon.

Although the synthon approach can be used to narrow down the initial list of co-formers, pairs are not guaranteed to successfully form a co-crystal. [77,79,80] As such, co-former selection is

largely experimental. Research is ongoing to find a predictive model for success of co-crystallization. [81–84] Factors such as geometry, steric hindrance, and solvent interaction all play a role in a successful co-crystallization. [85,86]

The choice of solvent can influence successful formation and physical stability of co-crystals. This can be depicted using a ternary phase diagram (TPD), where solubility of both API and co-former impact the co-crystal stability region, Figure 2.4 and Figure 2.5. The solubility is dependent on solvent, temperature, and pressure and a TPD depicts the phase stability in one set of conditions. A congruently saturating system is depicted in Figure 2.4 where an API and co-former have similar solubilities in the solvent system at a given temperature and pressure. In the congruently saturating system, it is possible to crystallize a 1:1 co-crystal from solution through evaporation (following the dotted arrow from region 1 to 4). In the same system, the co-crystal will be stable in a slurry containing a 1:1 stoichiometric mixture of API and co-former. When the components exhibit significantly different solubility in a set of conditions, then the stability region is shifted and a co-crystal may not be obtained by solution-based screening methods, Figure 2.5. [85–88] In Figure 2.5 the co-former exhibits higher solubility than the API and during evaporation the API or mixture of API and co-crystal will be isolated (following the dotted arrow from region 1 to region 2 and 3). In an incongruently saturating system, the co-crystal will not be stable in a slurry containing 1:1 stoichiometric mixture of API and co-former. Isolation of a phase pure co-crystal from slurry requires excess of one component: in Figure 2.5 excess co-former is required. The importance of TPDs in relation to co-crystallization in SCF will be discussed in more detail throughout the review.

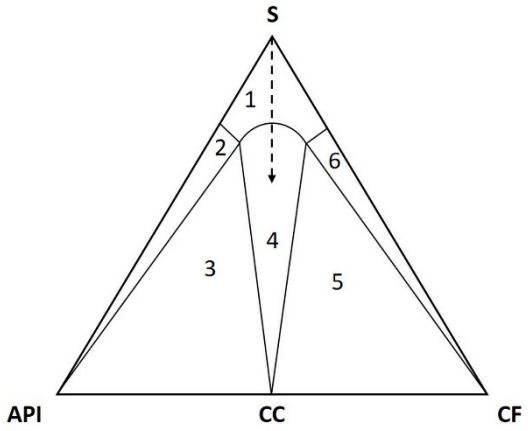

Figure 2.4-Congruently saturating ternary phase diagram for API, co-former (CF), and solvent (S). Co-crystal (CC) stoichiometry is 1:1. Regions defined in the phase diagram are solution (1), API as solid phase (2), API + CC as solid phase (3), CC as solid phase (4), CC + CF as solid phase (5), and CF as solid phase (6).

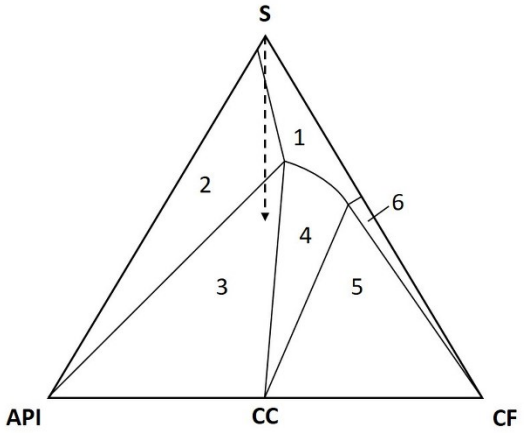

Figure 2.5- Incongruently saturating ternary phase diagram for API, co-former (CF), and solvent (S). Co-crystal (CC) stoichiometry is 1:1. Regions defined in the phase diagram are solution (1), API as solid phase (2), API + CC as solid phase (3), CC as solid phase (4), CC + CF as solid phase (5), and CF as solid phase (6).

Co-crystals can also arrange differently in the crystal lattice giving rise to polymorphism of the co-crystal. Solvent not only impacts the success rate of forming a co-crystal but also it can influence the polymorphism of the co-crystal. [49,89,90] Hydrogen bonding ability of solvent

and interaction with solute can dictate which crystalline form of a compound is obtained. [49] The role of solvent and crystallization regime effects on polymorph extends to use of $scCO_2$ as well. [53,91,92] The method of co-crystal production can also impact polymorph. Fucke *et al.* showed that up to 4 crystalline forms of a piroxicam co-crystal could be obtained by varying the method of generation e.g. co-melting, LAG, and solution methods. [80]

Scale-up methods for producing co-crystals include antisolvent crystallization, hot melt extrusion (HME), spray drying, high shear granulation, slurry crystallization, and SCF crystallization. [25,26]

Exploring various aspects of co-crystal preparation using supercritical fluid (SCF) crystallization ranging from system configuration and process parameters to technoeconomic perspectives is the focus of this review. The review identifies the need for a systematic approach to co-crystallization process design in high pressure systems and experimental determination of phase stability regions of co-crystals in high pressure systems.

2.3 Co-Crystallization in Supercritical Fluids

As with organic solvents, an SCF can be employed in a process in one of three ways: as a solvent, as a cosolvent (or additive), or as an antisolvent. The most common methods reported in the literature for co-crystal preparation in supercritical fluids are RESS, CSS, GAS, and SAS. For RESS and CSS, the SCF is considered as the solvent. For GAS and SAS, the SCF is considered as the antisolvent. Whether CO_2 is a solvent or antisolvent will depend on the solubility of the compound of interest. If solubility is low in $scCO_2$, then an organic solvent is employed and CO_2 is added as antisolvent. In these cases, residual organic solvent levels in the final solids must still be monitored. If solubility in $scCO_2$ is sufficient then CO_2 can act as a solvent and residual solvent in the final product need not be considered.

Crystal engineering and particle size control in supercritical systems is based on the same principles as in conventional crystallization: solubility and supersaturation. Some process parameters which influence solubility and supersaturation in a supercritical system differ from conventional crystallization because pressure is now a factor. Influential parameters applicable to both conventional and SCF crystallization include solvent selection, concentration (throughput), and mixing. Parameters such as cooling/heating rates and antisolvent (gas or conventional

solvent) dosing rates also influence both conventional and SCF processes. However, the temperature/pressure dependence of solubility in a high pressure system alters the design of a cooling profile or dosing regime. Another factor applicable to SCF systems which is not encountered in conventional crystallization is depressurization rate. The methods of particle size control and fundamentals of crystallization are essentially the same for single component APIs and co-crystals in SCF systems, although the stability region of the co-crystal must be considered.

Two important responses for a co-crystallization process are the product yield and co-crystal phase purity. If the work is focused on identifying formation of co-crystals or new polymorphic forms of a co-crystal, then yield may not be an important response and co-crystal phase purity takes priority. In this review the phase purity and yield for SCF co-crystallization processes were summarized whenever available. Of course, other properties such as residual solvent, particle size, solubility profile, physical stability, and chemical purity are also important responses in crystallization. Residual solvent, particle size, and purity can all be dependent on the solvent system and designed crystallization regime. While solubility profile is related to surface area, particle size and polymorph. Physical stability can be intrinsic to the compound, but also can depend on chemical purity, residual solvent and polymorph. However, these were not consistently reported in the selected literature and thus are not summarized here.

To our knowledge there are two published reviews with a focus on pharmaceutical co-crystallization in SCF, Table 2.1. The review by Pando *et al.* focuses on process details for co-crystallization of pharmaceuticals by a variety of SCF techniques. Padrela *et al.* gave a broader overview of crystallization of pharmaceuticals in SCF including examples of co-crystals. Padrela *et al.* gave special consideration to scale-up and industrial implementation of crystallization in SCF along with detailed lists of existing literature and reports of crystallization of pharmaceuticals. In this review we aim to cover the middle ground between both reviews with a focus on co-crystallization only.

Table 2.1- Reviews focusing on co-crystallization of pharmaceuticals in SCF.

Authors	Focus	Ref
Pando *et al.*	Preparation of pharmaceutical co-crystals using SCF. Focus was on	[93]

Authors	Focus	Ref
	process details for RESS, SAS, CSS, AAS, SEA, and GAS.	
	Conclusions and future perspectives included: suggestions to further explore trends due to temperature and pressure, ensuring co-crystal purity and yield were reported, continued modeling, and encouraging pharmaceutical companies to develop processes with low environmental impact.	
	$scCO_2$ for production of pharmaceutical nanoparticles using multiple techniques with an emphasis on co-crystals. Focus was given to considerations for scale-up and industrial implementation, listing scale-up related challenges and opportunities for the various SCF processes.	
Padrela *et al.*	Conclusions and future perspectives included: encouraging more fundamental experimental data and reliable models to control final product properties to aid in scale up, discovering methods to mitigate difficulty in handling and characterization of micro- and nano-powders, and suggesting more collaboration with industry to facilitate process optimization and scale-up studies. Major considerations for scale-up included throughput, ability to operate in batch or continuous mode, difficulties when collecting fine particles, and clogging of nozzles in atomization processes.	[12]

2.3.1 CSS Crystallization

CSS uses SCF as solvent and typically no additional co-solvent or antisolvent is used. However, sometimes in the CSS technique small amounts of a co-solvent are added to improve solubility of the solute in CO_2. The CSS technique does not use atomization. To recrystallize a compound via the CSS method solids are loaded into a high-pressure chamber. The SCF (CO_2) is pressurized into the vessel to dissolve the solutes at a specified temperature and pressure and after some time the vessel is depressurized by venting the chamber and solids are collected directly from the same vessel, Figure 2.6. In the CSS method, parameters which can be varied in the process include pre and post expansion pressure and temperature, solute concentration(s), mixing, and depressurization rate. Solids produced via the CSS technique do not require further drying.

In the CSS method, similar solubilities of the API and co-former are crucial since the de-pressurization is uniform and there is no other solvent present to retain excess of one component

or the other. The CSS method requires that both the API and co-former exhibit solubility in $scCO_2$ or $scCO_2$ with small amount of a co-solvent. If the desired outcome is a co-crystal, better mixing has also been shown to lead to co-crystal formation. [34]

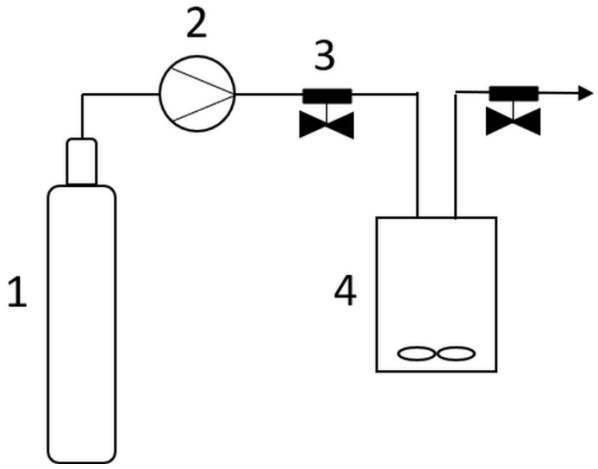

Figure 2.6- Schematic for CSS process. (1) CO2 supply, (2) high-pressure pump, (3) vents, (4) high-pressure vessel with mixer.

Co-crystallization by CSS has been reported to some success by two groups. Padrela *et al.* attempted to generate an indomethacin–saccharin co-crystal via a CSS method (flowing $scCO_2$ over a physical mixture of solids for 90 hours at two different pressures), but they found it was not successful. [94] They attributed the failure to form a co-crystal to low solubility of the pure substances and inability to dissolve the crystals of starting material, but in their later work they found mixing to be the most important factor for co-crystal formation. [34] Padrela *et al.* were later successful at producing co-crystals of theophylline, indomethacin, and carbamazepine with saccharin in a 2 hour CSS process employing mechanical mixing.[34] In the same work, Padrela *et al.* studied the kinetics of co-crystallization in a theophylline–saccharin system and found that approximately 80% of the co-crystal formation was complete within 30 minutes, after which the formation slowed and reached near 100% completion in 2 hours. At constant pressure, an increase in temperature gave a decrease in completion of co-crystallization. Higher temperature at constant pressure equates to decrease in CO_2 density, and thus solvation power.

Co-crystallization in SCF is not only applicable to typical pharmaceuticals, but also to natural

products. Recently, Ribas *et al.* produced co-crystals of a natural product, curcumin, with two co-formers. [95,96] Co-crystallized curcumin by CSS gave improved solubility over neat curcumin. In their work particles ranged from about 25-35 μm diameter and dissolution rate was not correlated to the size. This echoes that particle size must not be neglected when comparing dissolution rates between unique co-crystals or neat API.

In all reported successful CSS co-crystallizations the scale of experiment was less than 500 mg of API and product yields were not reported, Table 2. In theory if the pores in the filter are small enough to collect all solids, the yields should be near 100% because solids are collected directly from the chamber. The rate of depressurization in the experiments was also not reported. Homogenization and mechanical mixing of components in the co-crystal appears to be a more critical factor than equilibration time. Of the reports summarized in Table 2.2 the longest equilibration time (without mixing) did not lead to formation of a co-crystal. However, when mixing was employed, it successfully resulted in co-crystal formation within 1-2 h of equilibration time. Padrela *et al.* directly compared CSS processes with and without mixing. They found that without mixing co-crystallization was hindered, illustrating the importance of mixing and transport phenomena. [34] In another paper, Cuadra scaled down a carbamazepine-saccharin co-crystal formation previously reported by Padrela from 400 mg to 9 mg. [97] They found that even with mixing, the co-crystallization was not complete until 20 h, as opposed to 2 h in Padrela's work. In addition, mixing does not guarantee successful formation of a co-crystal. In the same paper, Cuadra observed only partial co-crystal formation of 5-fluorouaracil with urea, thiourea, and pyrazinamide after stirring for 20 h with addition of MeOH co-solvent. [97] Co-crystal formation was not observed without co-solvent. It may be possible to produce co-crystals with CSS even if the solubility of both components is low and affinity to form a co-crystal is high, with sufficient mixing and addition of co-solvent. Co-crystal formation in conventional solvents is also possible by LAG even when both components solubility is less than 2 mg/mL. [85]

Table 2.2- Co-crystallization reports employing CSS.

Ref	API	Co-former	Scale, g of API	Pressure, MPa	Temperature, °C	Time, h	Product yield, %[a]	Co-crystal phase purity
[94]	Indomethacin	Saccharin	0.085	14, 22	50	≤ 90	~ 100	~ 0%

[34]	Theophylline	Saccharin	0.4	20	50	2	N.D.	~ 100%
[34]	Carbamazepine	Saccharin	0.4	20	50	2	N.D.	~ 100%
[34]	Indomethacin	Saccharin	0.4	20	50	2	N.D.	~ 100%
[95]	Curcumin[b]	n-acetylcysteine	0.3	9	45	1	N.D.	~ 100%
[96]	Curcumin	Nicotinamide	N.D.	9	45	1	N.D.	~ 100%
[97]	5-fluorouaracil[c]	Urea, thiourea, pyrazinamide	0.009	20	40	20	N.D	< 100%

Note. N.D. not disclosed. [a] yield calculated as collected mass/processed mass. [b] 0.5 mL cosolvent was added. [c] 0.02 mL cosolvent was added to some experiments.

2.3.2 RESS Crystallization

The principle of the RESS technique is similar to the CSS method, but instead the solution is depressurized by spraying through a nozzle. Small amounts of co-solvent are sometimes added to improve solubility of the solute in CO_2 in the RESS technique. The solutes are dissolved in the SCF (CO_2) in a high-pressure chamber at a specific temperature and pressure. Rapid expansion of the solution through the atomizer nozzle reduces solvation pressure and particles precipitate into a secondary collection vessel (this could be a filter/collection bag), Figure 2.7. Nucleation and growth are rapid from the homogeneous solution. Solids produced via the RESS technique do not require further drying. In the RESS method, parameters, which can be varied in the process include pre and post expansion pressure and temperature, solute concentration(s), and geometry of the spraying system including spraying distance and the nozzle set-up. The impact of these parameters on crystallization of an API should be well understood when designing a robust process. Specifically, the geometry of the nozzle/atomizer/capillary has been found to have the most profound impact on the final particle size distribution. [59,98,99] Although mixing is critical for process like CSS outlined in the previous section, mixing is not applicable for the atomization-type SCF processes such as RESS, SAS, SEA, and atomization and antisolvent (AAS).

Typically, an increase in nozzle diameter and length leads to an increase in particle size. Hezave *et al.* explained this phenomena using the pressure gradient across the nozzle: a shorter length gives steeper pressure gradient and smaller particles, while a longer nozzle has a gradual gradient, lower supersaturation and lower nucleation rate, thus larger particles. [59] An increase in nozzle diameter has also been shown to increase mean particle size. [59] Spraying distance

has also been shown to impact particle size, it was speculated that increase in spraying distance increased the size by allowing longer time for growth. [99,100] In addition, the type of nozzle (orifice vs. capillary) has also been shown to yield significantly different particle size for a study with aspirin. [99] The system set-up can change the particle size distribution (PSD), even if all other parameters are kept constant. This is a key point to keep in mind when designing scale-up systems.

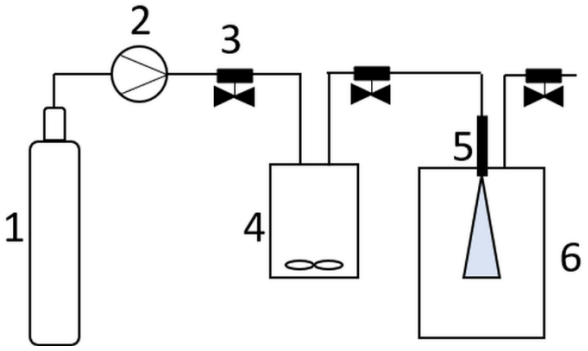

Figure 2.7- Schematic for RESS process. (1) CO2 supply, (2) high-pressure pump, (3) vents, (4) high-pressure vessel with mixer, (5) nozzle, (6) collection chamber.

If a co-crystal is desired, then both the API and co-former should exhibit reasonable solubility in the SCF in the specified temperature and pressure range. In an ideal scenario, the solubility of the API and co-former are similar, i.e. the system is congruently saturating and evaporation from stoichiometric solution is expected to yield phase pure co-crystal (Figure 2.4). However, phase pure co-crystals have been generated from incongruently saturating systems by spray drying, a technique employing rapid evaporation of solvent. [101] Co-crystals can be formed by the RESS method even if solubility differences are an order of magnitude, but the affinity of the API to co-former should be high compared to the solvent. In general, RESS has not been widely studied in the literature for co-crystallization of pharmaceuticals. Limited information is available for both screening and process development of co-crystals, Table 2.3.

Most work reported on RESS co-crystallization takes a screening approach. The reported results focus on the solid form characterization such as XRPD (X-ray powder diffraction) and thermal analysis, while process details, yield and phase purity are neglected. To the best of our

knowledge the reports of co-crystal screening by RESS are limited to the work of Vemavarapu *et al.* and Herrmann *et al.*. [102,103]

Vemavarapu *et al.* approached co-crystal screening in $scCO_2$ by dissolving physical mixtures of API/additive (co-former) at an 8:2 ratio. [103] In some of the mixtures reported by Vemavarapu *et al.* presence of the second component (additive) lead to an increase in solubility of the main component in the SCF. They hypothesized that this was due to formation of eutectics on the basis of increased solubility and also lower melting of the resulting compositions. In some cases, the additive lead to formation of a different polymorph or conversion to low crystallinity or amorphous solids. Herrmann *et al.* attempted to form co-crystals of ibuprofen and cholesterol with caffeine, but a co-crystal phase was not obtained. [102]

Process development for RESS co-crystallization has been reported by only one group, Müllers, Paisana, and Wahl. [104] Müllers *et al.* reported a method to crystallize an ibuprofen-nicotinamide co-crystal at 2 g scale using a 5 L reactor vessel. Co-crystallization essentially went to completion (96% phase purity based on heat of fusion), but the product yield with respect to dissolved solid was low (20%). It was suggested that low product yield could be due to inefficient particle collection and nozzle blockage, though the loss was not quantified. The successful co-crystallization of ibuprofen-nicotinamide by RESS may be attributed to solubilities of both components being the same order of magnitude in $scCO_2$ under the operating conditions used. [100,105] Although the process reported by Müllers *et al.* was not optimized for throughput or yield, it provides a good example of work in which sufficient process details are reported. The co-crystals produced by RESS also showed improved dissolution compared to neat ibuprofen due to small size and high surface area.

In most reports of RESS co-crystallization the scale of experiment and process parameters (e.g. nozzle geometry) were not reported likely because the goal was screening for a co-crystal phase and not process development.

Table 2.3- Co-crystallization reports employing RESS.

Ref	API	Co-former	Scale, g API	Pressure, MPa	Temp, °C	Nozzle diameter, µm	Expansion chamber temperature, °C	Product yield, %[a]	Co-crystal phase purity

[104]	Ibuprofen	Nicotinamide	2	30	50	150	50	20	96%
[102]	Ibuprofen, cholesterol	Caffeine	N.D.	10-30	N.D.	N.D.	N.D.	N.D.	0 (did not form co-crystal)
[103]	Salicylic acid, aspirin, tolbutamide, piroxicam, theophylline, phenytoin, indomethacin, naproxen	Various	N.D.	7.6-62	35-100	N.D.	N.D.	N.D.	N.D.

Note. N.D. not disclosed. [a] yield calculated as collected mass/processed mass.

2.3.3 GAS Crystallization

The GAS process uses the SCF as an antisolvent and requires a conventional organic solvent to dissolve the compound of interest. To recrystallize a compound using the GAS method the solid is dissolved in an organic solvent inside a high-pressure vessel equipped with a filter. The solution is pressurized with SCF (CO_2) via a dosing pump to lower solvating power and precipitate out the compound. Two methods can be used to dose the CO_2 into the solution for GAS: bubble the gas directly into the solution or add the gas to the headspace above the solution and allow it to diffuse into the liquid solution. The former reduces the equilibration time and there is no diffusion delay. CO_2 is typically bubbled through the solution to enhance mass transfer. This can be done by dosing CO_2 directly into the solution (depicted in Figure 2.8) or by introducing CO_2 through a frit in the bottom of the high-pressure vessel. [106,107] The resulting solids are collected by a filter in the high-pressure vessel and the SCF/solvent mixture is collected in a secondary depressurization vessel, Figure 2.8. The solids on the filter in the high-pressure vessel are washed with the SCF to remove excess organic solvent. Solids are collected from the higher-pressure chamber and CO_2 can be recovered from the secondary depressurization vessel.

In this method CO_2 replaces a typical organic antisolvent. It makes the formation more environmentally friendly since the gas can be recovered. The solids recovered are dried by passing SCF (CO_2) over the precipitated solids for some time prior to depressurizing. In the GAS technique, the crystallization is a function of the antisolvent addition rate (or pressure change over time). [31] As with a typical organic solvent atmospheric crystallization (e.g. cooling,

antisolvent) the process must be designed such that it falls within the co-crystal stability region. This means that the input constituents may not be stoichiometric, but the rate of precipitation will occur in a stoichiometric manner.

Contrary to the CSS technique, low solubility of some APIs in $scCO_2$ makes GAS a good technique for co-crystallization of pharmaceuticals. GAS has been the most widely reported technique for supercritical co-crystallization to date with about 40% of publications using this method, Table 2.4. Some common solvents used for GAS are tetrahydrofuran (THF), ethanol (EtOH), methanol (MeOH), and acetone. Solubility of API and co-former can be assessed in various organic solvents easily by a gravimetric method, clear point method, or spectrophotometry method to select the appropriate solvent. The solubility as a function of solvent composition, pressure, and temperature should be understood in order to best design a GAS process. Parameters which can impact the solids obtained by GAS include solvent choice and solvent volume, temperature, pressure, solute concentration(s), and antisolvent addition regime.

The impact of pressure and temperature on the final product depends on the solubility profile of the solute(s). For the GAS process specifically, the pressure profile (CO_2 antisolvent dosing rate) impacts nucleation and growth rates. [61,62] Faster dosing rate (higher supersaturation) leads to higher nucleation rate, which agrees with what is observed for conventional crystallization. Differences in dosing profile impact not only particle size, but also polymorph, chirality, and yield. [61,108,109] However, it is important to note that each system (solvent, API, co-former) will be unique and a universally robust process does not exist.

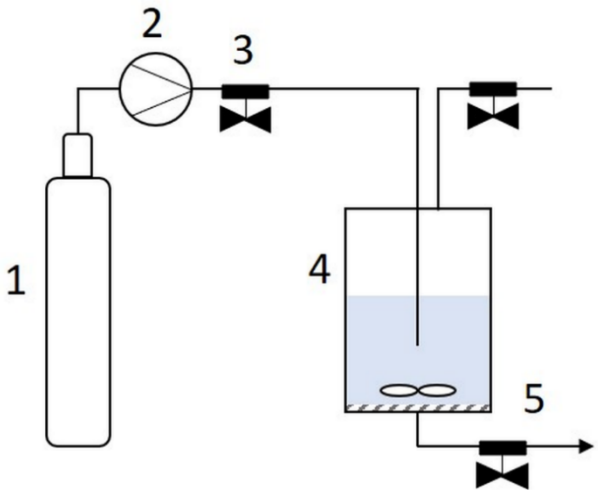

Figure 2.8- Schematic for GAS process. (1) CO2 supply, (2) high-pressure pump, (3) vents, (4) high-pressure vessel with mixer, (5) filter.

Most reports of co-crystallization by GAS are carried out at 0.25 – 2 g scale. In one case, the reported scale of experiment was 1 "mole" of carbamazepine (which is 236 g), but it is unclear from the report if the authors were referring to actual mass used or simply referring to molar ratios because this scale is much larger than usual. [110] In general for GAS co-crystallization processes, relevant process parameters are well reported. The size of the high-pressure vessel in GAS co-crystal reports varies from 37 mL to 2 L with most vessels falling near the half liter volume. To the best of our knowledge, prior research has not particularly focused on scalability of co-crystals by GAS.

The relative volume of organic solvent used to dissolve the API and co-former varied significantly between reports as well, from as low as 4 L/kg up to 100 L/kg (4 – 100 volumes). The difference in volume of solvent used is due to differences in solubility of APIs. Some studies are done at the highest possible concentration to ensure rapid precipitation on introduction of CO_2. [106] The temperature range for all reported processes fell between 25 – 45 °C and final pressure between 9 – 11 MPa. The pressure and temperature conditions are determined by the miscibility region of the organic solvent with CO_2. The CO_2 dosing rate is typically reported as mass per unit time, but sometimes is reported as a function of volume or pressure. Ober *et al.* also provide a general pressure profile for a GAS co-crystallization process, illustrating the impact of dosing on pressure.[31] A non-linear pressure increase is observed when CO_2 dosing is controlled by constant mass or volume. In Table 2.4 where CO_2 dosing was reported by

volume, the mass dosing rate was estimated based on the expected CO_2 density under the operating conditions stated in the report. The reported system temperature and pressure were used to calculate CO_2 density by solving roots of the Peng Robinson EoS.

Yield is reported in less than half of the processes reported in Table 2.4 and ranges from 20 – 75.4%. Cases of low yield such as the work of Neurohr *et al.* (naproxen-nicotinamide) or Kotbantao and Charoenchaitrakool (ketoconazole-4-aminobenzoic acid) did not provide any information on the possible ways that the product was lost. [109,111] For example, when experiments are carried out only at 250 – 300 mg scale, it is possible that product loss during collection and transfer of micronized solids could significantly impact yield. Even in work where the product yield is high (> 70%), there is still value in reporting and quantifying where product loss occurs. Ober *et al.*, who achieved a product yield of 75% for an itraconozole-succinic acid co-crystal, noted that an excess of co-former was used to minimize unco-crystallized itraconozole and that product loss due to collection is expected to be minimized on scale-up. In one report of a naproxen-nicotinamide co-crystal yield increased with slower CO_2 dosing, better mixing, and also increased concentration of API and co-former in the solvent. [109]

Equilibration time can also impact yield. Increasing hold time at final conditions allows the system to reach equilibrium and supersaturation to approach unity, thus maximizing yield. More insight into the GAS co-crystallization could be gained by quantifying the product losses by mass balance. It is also possible that yields of co-crystallization processes could be improved using slower dosing rates, sufficient mixing, and longer hold times at final temperature and pressure. In some cases, it is also possible that a different solvent choice would alter product yield. Kotbantao and Charoenchaitrakool reported yields of 17.6% using EtOH as solvent, which increased to 56.2% when acetone was employed instead. [111] The difference in yield should be due to differences in solubility in the final composition if all other parameters are equivalent. This illustrates the importance of understanding the solubility profile of a co-crystal when designing a crystallization process.

In almost all cases co-crystal phase purity is able to be extracted from the literature for GAS co-crystallization. Phase purity is often determined qualitatively by analytical techniques such as XRPD, differential scanning calorimetry (DSC), or Fourier transform infrared (FT-IR). High performance liquid chromatography (HPLC) coupled with the aforementioned analytical

techniques has also been used to quantify API and co-former content in a co-crystal. [109] Techniques such as XRPD and DSC can also be employed quantitatively, but they are not as straightforward as HPLC for quantification of phases and thus are most often used qualitatively when reporting phase purity. In most reported cases, co-crystal phase purity is high (either by quantitative or qualitative assessment), suggesting that GAS processes can be designed to produce phase pure co-crystals, Table 2.4. In cases where co-crystal phase purity is low it is possible that a different solvent could lead to a higher phase purity co-crystal. Quantitative assessment of co-crystal phase purity is critical when the aim is design of a robust co-crystallization process. However, when the research goal is screening for new co-crystal forms, qualitative assessments of form purity are sufficient.

Although mixing is also critical during a crystallization process, there do not appear to be any studies on impact of mixing for GAS co-crystallization to date. As with conventional crystallization the mixing rate, reactor geometry, CO_2 dosing pump set-up and impeller type could impact homogeneity, yield, and particle size in a GAS process. [52]

GAS can produce co-crystals of varying size, depending on the system and process parameters. Particle sizes of co-crystals produced by GAS have ranged from sub-micron to almost 500 μm. [109,112] CO_2 dosing rate is accepted to have the most profound impact on PSD by GAS, where faster dosing leads to smaller particles. [61,109] However, other parameters such as mixing and concentration also have some impact but to a lesser extent. [61,109] The interaction between all parameters has not been thoroughly studied for a co-crystal system. Size of co-crystals produced by conventional antisolvent crystallization to GAS was compared by Pessoa *et al.*. [112] When using isoniazid as a co-former, the GAS co-crystals were larger than those prepared by conventional methods and the opposite trend was observed when using nicotinamide as a co-former, despite employing the same crystallization regimes. This illustrates the importance of understanding the phase stability regions and solubility for a given system when trying to engineer particles of a target size.

Erriguible *et al.* modeled a GAS process using data from a naproxen-nicotinamide co-crystal, studying the effects of solute concentration and antisolvent ($scCO_2$) addition rate on particle size. [113] The model employed the quaternary solubility dataset of naproxen-nicotinamide in acetone/$scCO_2$, previously measured. [114] They found the initial concentration of API and co-

former did not have a large impact on the particle size and antisolvent addition rate impact was found to be the same as with conventional antisolvent crystallization techniques (faster addition gave higher nucleation rate, less growth, smaller particles). Calculated particle size distributions were in good agreement with the experimentally measured values. The yields for modeled processes were reported, but predicted yields based on solubility were not given. Continued efforts similar to those of Erriguible *et al.* and Revelli *et al.* can help researchers better understand co-crystallization processes in SCF. The solubility data used for the population balance model is valuable in understanding co-crystallization processes in relation to a TPD because TPDs are experimentally determined by solubility measurement. Typically the API and co-former molar ratios are varied and the equilibrium solubility of the mixture is assessed in the desired solvent system. This solubility assessment method could be extended to development of a TPD by varying the ratio of naproxen to nicotinamide in a given solvent composition, temperature, and pressure. In addition, the solid phase composition would have to be characterized by means of XRPD or an appropriate alternative technique. Once the TPD is developed, the population balance model could be used to model a given process, select appropriate process parameters to tune particle size, or determine safe operating range for a given system. Together the solubility assessment and co-crystallization population balance model could aid in designing robust and tailored co-crystallization processes.

Table 2.4- Co-crystallization reports employing GAS.

Ref	API	Co-former	Scale, g of API	Solvent, volume, mL	Pressure, MPa	Temp, °C	CO_2 dosing rate, g/min	Vessel volume, L	Product yield, %[a]	Co-crystal phase purity
[110]	Carbamazepine	Nicotinamide	~ 200 [b]	EtOH, 6-8	11	40	~ 50 [c]	2	N.D.	~ 100%
[106]	Itraconozole	Succinic acid	0.25	THF, 10	10.3	40	Variable (4 bar/min)	0.037	75.4	< 100%
[31]	Itraconozole	L-malic acid	0.25	THF, 10	10.3	40	1	0.037	N.D.	~ 100% + amorphous
[109]	Naproxen	Nicotinamide	1.6	Acetone, 40	10	35	25	0.49	20-63	98%
[61]	Naproxen	Nicotinamide	1.6-3.76	Acetone, 40	10	37	3, 20	0.49	64-72	99%
[108]	Naproxen	Nicotinamide	1.96	Acetone, 40	10	37	2, 11, 20	0.49	N.D.	~ 100%
[115]	4-aminosalicylic acid (ASA)	Nicotinamide	0.4-1	Acetone, N.D	11	36	20	0.49	60	~ 100%
[115]	5-ASA, 3-ASA	Nicotinamide	0.4-1	Acetone:DMSO, 40	-	-	-	-	N.D.	0 (did not form co-crystal)
[116]	Sulfamethoxazole	L-malic acid	1.25	Acetone, 5	9	45	~ 0.8 [b]	N.D.	N.D.	< 100%
[111]	Ketoconazole	4-aminobenzoic acid	~ 0.25-0.3	Various, 5	9	25-45	~ 1.4 [b]	N.D.	13.2-56.2	~ 100%
[117]	Mefenamic acid	Paracetamol	N.D.	Acetone, 5	9	25-45	~ 1.8 [b]	N.D.	N.D.	< 100%
[107]	Mefenamic acid	Nicotinamide	N.D.	Acetone, 5	9	25-45	~ 1.8 [b]	N.D.	N.D.	<< 100%
[112]	Resveratrol	Isoniazid	0.3	EtOH, 25	9	45	10	0.6	N.D.	~ 100%
[112]	Resveratrol	Nicotinamide	0.3	EtOH, 15	9	45	10	0.6	N.D.	< 100%

Note N.D. not disclosed. [a] yield calculated as collected mass/processed mass. [b] reported scale was 1 mole API. [c] Flow rate reported in mL/min converted to g/min using CO_2 density estimated at given temperature and pressure using Peng Robinson EoS.[105]

2.3.4 SAS Crystallization

SAS is a technique which combines spray drying (atomization) with antisolvent precipitation. The compound of interest is dissolved in a conventional organic solvent and sprayed through an atomizer nozzle into a high-pressure collection chamber, which has been pressurized with the SCF, Figure 2.9. The collection chamber temperature and pressure are controlled. The particles are formed rapidly by decrease in solubility due to SCF as antisolvent. The resulting solids are collected by a filter in the high-pressure collection vessel and the SCF/solvent mixture can be collected in a secondary depressurization vessel. Drying is required for the SAS technique and can be accomplished by pumping SCF (CO_2) through the collection chamber to remove excess organic solvent after precipitation. Parameters that impact solids obtained by SAS include solvent system, temperature and pressure, solute concentration(s) and flow rate, CO_2 flow rate, and nozzle geometry.

Impact of process parameters will depend on the system and the range of conditions studied and any interaction between the parameters. For processes where solute(s) are atomized or sprayed, the pressure in the expansion chamber has been shown to affect particle size, morphology, and polymorph. [99,118,119] A DOE approach to SAS crystallization of sulfasalazine in THF found that concentration of the solution was found to have little to no impact on PSD, but higher CO_2 flow rates gave rise to smaller particles due to faster supersaturation of the system.[120] Other groups have also found that low operating temperature, pressure, and solution flow rate, coupled with high CO_2 flow rate, larger nozzle diameter gave rise to small crystals. [121] As was discussed for RESS, the system design, specifically the spray nozzle diameter also impacts the particle size in SAS. [120,121] The influence of process parameters on other solid phase properties such as polymorph, morphology, and phase purity for some co-crystals are outlined below.

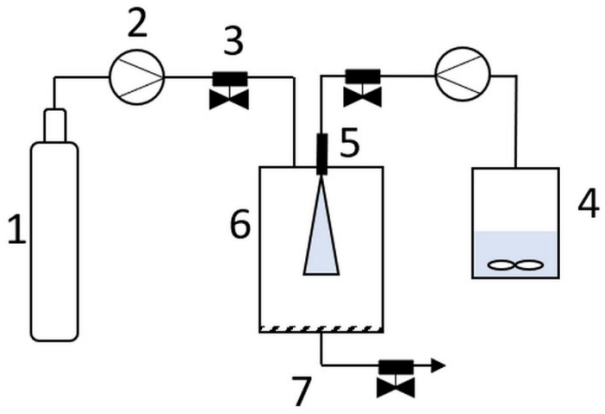

Figure 2.9- Schematic for SAS process. (1) CO2 supply, (2) high-pressure pump, (3) vents, (4) vessel containing organic solvent/solute solution, (5) atomizer, (6) high-pressure collection chamber, (7) filter.

SAS has been the second most common reported method for co-crystal production in SCF, after GAS. Similar to reports of GAS in literature, co-crystallization by SAS has also been carried out at small (< 1 g) scale and in many cases the scale is not reported. First, the API and co-former are dissolved in organic solvent, which has included alcohols, acetone, dichloromethane (DCM), and even high boiling solvent dimethylsulfoxide (DMSO). The solutions tend to be dilute, upwards of 30 volumes, where reported, Table 2.5.

In general, process parameters are well reported in the SAS co-crystallization literature. Flow rates, nozzle size, and precipitation chamber conditions (size, pressure, and temperature) are reported in most studies. However, the scale of the process is not always reported. The nozzle diameters vary between 100 – 254 μm and precipitation chamber volume varies from 100 mL to above 1 L. Despite the differences in nozzle and precipitation chamber geometry, the precipitation chamber pressure and temperature are often similar. Chamber pressures have been reported between 9-15 MPa, with a mode of 10 MPa. Chamber temperatures are reported between room temperature and 60 °C, with near 40 °C being common to most reports.

Product yields for co-crystallization via SAS are similar to those from GAS, ranging from 10 – 70% where reported. In about half of the SAS co-crystallization papers the product yield is not reported, Table 2.5. Cuadra *et al.* illustrated impact of solvent choice on product yield where use of DCM gave a 40% yield and MeOH gave 65% yield. [53] However, significant variability in yield can be obtained even when using a single solvent system. In a more recent paper, Cuadra

et al. found that product yield of a 5-fluorouracil-urea co-crystal varied from 10 to 50% when the SAS process was repeated in triplicate. [97] It is likely that yield loss in SAS can also be attributed to difficulties in product collection. In the study of a naproxen-nicotinamide co-crystal, Neurohr *et al.* reported product yields from 63-70%. However, the difference of 7% was deemed not significant due to variations in process parameters and difficulties in particle collection. [122] Thus for SAS processes operating at small scale (< 1 g), it may be difficult to draw conclusions on yield trends if variation between duplicate experiments is high without conducting mass balance.

The co-crystal phase purity is typically also easily deduced form the SAS reports based on XRPD data, thermal analysis, or IR spectroscopy even if not explicitly reported. However, a co-crystal can appear to be phase pure based on these characterizations while still containing small amounts of excess API or co-former either as amorphous material or below detection by the analytical techniques. Neurohr *et al.* illuminated this by showing that solid state characterization agreed with a phase pure co-crystal, but HPLC analysis showed that the phase purity varied between 94 – 100%.[123] Neurohr *et al.* found that when the flow rate ratio of solution to SCF was low (< 0.04 mL solution/g CO_2) for the naproxen–nicotinamide system, co-crystal phase purity was low. In the case of a low phase purity, evidence of a physical mixture was easily observed by XRPD, FT-IR, and HPLC analyses. As such, where phase purity is reported based on XRPD, thermal analysis or FT-IR the percentage given is approximate in Table 2.5.

In SAS co-crystallization reports, solvent is a commonly varied parameter. As mentioned earlier, the solvent choice can also have a significant impact on co-crystal polymorph and particle morphology. Cuadra *et al.* showed that depending on the solvent system, variation in polymorphic form was observed for a carbamazepine-saccharin co-crystal. [53] Use of MeOH gave a pure crystalline phase during the initial screening, while EtOH and DCM led to mixtures of crystalline forms. However, during further studies using MeOH the crystalline form differed with pressure and temperature. [53] In this example, the acceptability of solvent should also be considered before selection of a solvent system for further development. Solvents such as EtOH are considered Class III with allowable limits of 50 mg/day (or 0.5 wt.%) while MeOH is Class II with an allowable limit of 30 mg/day (or 0.3 wt.%). [63]

Multiple studies have also looked at impact of solvent choice on the particle morphology.

[53,94,124] In two cases, changing solvent varied morphology between plates and needles. [53,94] Padrela *et al.* found that co-crystals of indomethacin-saccharin prepared with EtOH were a mixture of needle-like and block/plates, while morphology was more uniform using THF as a solvent. [94] [83] In another report, Neurohr *et al.* were able to use differences in morphology and particle size distribution as evidence of phase inhomogeneity. [123] Conversely, in another example the use of either EtOH or acetone produced similar moprhology. [124] This illustrates that solvent selection is a critical factor when designing an SAS process. Not only can solvent choice impact morphology and polymorph, but it also must be considered in terms of maximum allowable solvent in a final drug substance.

A goal of particle production by atomization techniques is often obtaining small particle size. SAS has been able to successfully yield small particles for co-crystals, ranging from 0.2-10 μm. [53,94] However, small particle size is not a guarantee of SAS. A naproxen-nicotinamide co-crystal produced by SAS consistently produced uniform particles with distributions centered near 300-400 μm, regardless of the flow rate of solution concentration. [123] Another study showed particle size control was challenging for diflunisal co-crystals, illustrating the importance of understanding phase behavior as a function of temperature and pressure when aiming to tune PSD of a co-crystal. [123] In general, there has not been a one size fits all trend for control of particle size by SAS techniques.

Solvent choice should be considered a critical factor in SAS co-crystallization, but other parameters such as flow rate ratio, pressure and temperature can also impact the polymorph and phase purity. One study of a diflunisal-nicotinamide co-crystal showed that temperature, pressure, and components concentration had little impact on the final product. [124] On the other hand, Cuadra *et al.* observed two unique crystalline forms of a carbamazepine-saccharin cocrystal prepared by supercritical antisolvent (SAS). [53] The resultant crystalline form was dependent on both solvent and temperature. They also found that at constant concentration and pressure, an increase in temperature by 20 °C lead to generation of a mixture of crystalline forms. [53] Even more stark than a mixture of co-crystal polymorphs, variation of flow rate in SAS can be the difference between formation of a phase pure co-crystal or a heterogenous mixture of co-crystal with pure components. [122] This can be taken as an illustration of uniqueness of different systems. Depending on the API, co-former, and solvent choice, variation

of process parameters can have a profound impact on product or little to no impact. Systematic crystallization development based on solubility for co-crystals in high pressure systems should continue to be explored.

Table 2.5- Co-crystallization reports employing SAS process.

Ref	API	Co-former	Scale, g of API	Solvent, volume	Flow rate ratio (solution/SCF), mL/g	Nozzle diameter, µm	Precipitation chamber volume, L	Precipitation chamber temperature, °C	Precipitation chamber pressure, MPa	Product yield, %[a]	Co-crystal phase purity
[94]	Indomethacin	Saccharin	0.03	EtOH, acetone, THF, MeOH, ~ 8-9	< 0.2	200	N.D.	RT	~ 9	N.D.	~ 100%
[124]	Diflunisal	Nicotinamide	0.45 - 0.9	EtOH, acetone, 30	0.05	100	1.35	35-40	10-12	70	> 99%
[125]	Paracetamol	Dipoclinic acid	N.D.	MeOH, 20	0.033	254	0.1	40	10	N.D.	~ 100%
[122]	Naproxen	Nicotinamide	N.D.	Acetone, N.D.	0.12-0.5	180	0.32	37	10	63-70	94-100%
[122]	Naproxen	Nicotinamide	N.D.	Acetone, N.D.	0.04	180	0.32	37	10	55-62	<< 100%
[53]	Carbamazepine	Saccharin	0.08-0.9	MEOH, EtOH, DCM, DMSO, 30	0.05	100	0.5	40-60	10-15	40-65	~ 100%
[126]	Paracetamol	Trimethylglycine	N.D.	MeOH, DCM, 50	N.D.	N.D.	N.D.	N.D.	N.D.	N.D.	N.D.
[127]	Paracetamol	5-nitroisophthalic acid	N.D.	MeOH, 20	0.033	254	0.1	40	10	N.D.	~ 100%
[97]	5-fluorouracil	Urea, thiourea, pyrazinamide	0.08-0.15	MeOH, 30	0.05	100	0.5	40	7-15	10-70	≤ 100%

Note. N.D. not disclosed. [a] yield calculated as collected mass/processed mass.

2.3.5 SEA and AAS Crystallization

The AAS technique is similar to SAS. For SAS set-up, the collection chamber is pressurized with CO_2 while a solution (in organic solvent) is atomized into the SCF and collected at high pressure. While for AAS, the solution in organic solvent is mixed with the SCF in the coaxial nozzle to precipitate solids, and then the solids are collected in a chamber at near atmospheric pressure.

The methodology for SEA is similar to that of SAS and AAS, but the $scCO_2$ and solution are mixed prior to atomization and depressurization. A schematic for the AAS and SEA process is shown in Figure 2.10. The compound solution and SCF are prepared separately, but mixed prior to flowing through the atomization nozzle. Droplets formed during atomization are dried in the collection chamber near atmospheric pressure. The collection chamber is temperature controlled. Solids are collected from a filter in the chamber and chamber walls, while the solvent and CO_2 are passed through. As with SAS, parameters which impact the solids obtained by SEA and AAS include solvent system, temperature and pressure, solute concentration(s) and flow rate, CO_2 flow rate, and nozzle geometry.

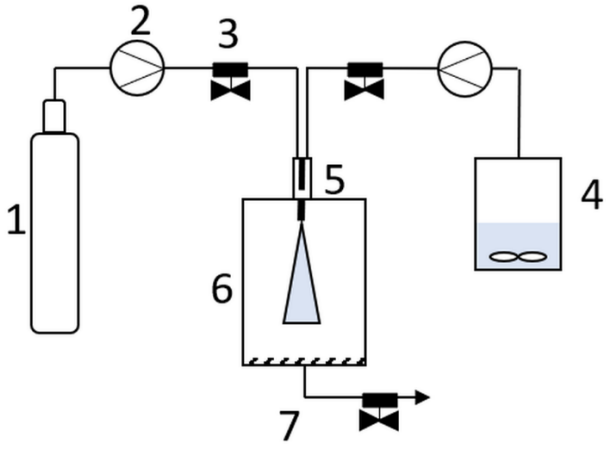

Figure 2.10- Schematic for AAS and SEA process. (1) CO2 supply, (2) high-pressure pump, (3) vents, (4) vessel containing organic solvent/solute solution, (5) atomizer, (6) high-pressure collection chamber, (7) filter.

Reports of co-crystallization by SEA and AAS in the literature are limited, with three reports of co-crystallization by SEA and one using AAS, Table 2.6. In three separate pieces of work a

screening approach was employed either with a variety of APIs and a single co-former, a single API and variety of co-formers, or a single co-crystal with a variety of solvents. All reports of co-crystallization by SEA were conducted at less than half gram scale.

Yields were not reported for any of the SEA or AAS co-crystallizations summarized in Table 2.6. For most cases, presumably it was not reported because the goal was screening. Co-crystal phase purity was inferred from XRPD or DSC data, thus the reported co-crystals are considered as approximately phase pure.

For SEA and AAS processes the solutions of API were dilute, all being upwards of 100 volumes. These are low throughput processes even compared with reported SAS co-crystallization. In some cases the low concentration may be due to low solubility of the API or co-former in the selected solvent. For screening style experiments the throughput is not a critical aspect. But, for a scalable crystallization process the solvent volume should ideally rival that of conventional crystallization (generally under 20 volumes). Overall, the process parameters for all reported SEA and AAS are similar in the four different papers. Process parameters for SEA were consistent between all reports, likely since these were conducted in the group of de Azevedo.

As with SAS, parameters such as pressure, temperature, and solute concentration can also impact the product. Padrela *et al.* found that for a theophylline-saccharin co-crystal the solution concentration and CO_2 pressure had little impact on PSD, while higher temperature gave rise to higher mean particle size. [128] Co-crystallization of an indomethacin-saccharin by AAS was also used to demonstrate process parameter effects. [94] Similar morphologies were able to be obtained for different solvent systems. However, the particle size differed depending on solvent and pressure. The AAS results were compared to solids obtained by SAS, demonstrating a significant morphology differences when employing a different atomization technique. [94] Although there is limited literature on co-crystallization by SEA and AAS, it should follow that the degree of dependence on process parameters varies from system to system.

A main advantage of using supercritical atomization techniques for screening is that the generated solids can exhibit small, uniform particle size. In a study, screening using LAG was compared to screening using SEA for 6 APIs with a saccharin. Although both LAG and SEA could produce the same crystalline form, SEA gave smaller, more uniform particle size. [128] In another example, various co-crystals of theophylline prepared by SEA were all less than 2 μm

diameter. [129] As previously discussed, solubility of an API is influenced by both particle size and solid form. Comparison of solubility of different co-crystals is more reliable if they are all produced with similar particle size and surface area. For the purpose of screening, SEA also tends to favor kinetic crystalline forms of a material, therefore can also be a valuable tool in both co-crystal and polymorph screening. [128]

Table 2.6- Co-crystallization reports employing SEA and AAS.

Ref	Process	API	Co-former	Scale, g of API	Solvent, mL	Pressure, MPa	Temperature, °C	Flow rate ratio (solution/SCF), mL/g	Nozzle diameter, µm	Precipitation chamber temperature, °C	Co-crystal phase purity
[128]	SEA	Indomethacin, theophylline, caffeine, sulfamethazine, aspirin, carbamazepine	Saccharin	0.02-0.03	EtOH, 7.9	8	50	0.06-0.13	100	50	~ 100%
[130]	SEA	Theophylline	Saccharin	0.25	THF, 89	8	50	0.28	100	50	~ 100%
[131]	SEA	Theophylline	Urea, saccharin, gentisic acid,salicylic acid, glutaric acid, sorbic acid, 1-hydroxy-2-naphthoicacid, oxalic acid, maleic acid and nicotinamide	0.5	THF, 89	8	50	0.08-0.28	100	50	~ 100%
[94]	AAS	Indomethacin	Saccharin	0.03	EtOH, acetone, THF, MeOH, EtOAc, ~ 8-9	6-12	50-70	< 0.2	200	RT	~ 100%

Note. RT is room temperature. Product yield for all processes were not disclosed.

2.4 Current Status and the Path Forward

2.4.1 Process Details

In general, reporting of process parameters for co-crystallization processes by SCF varies between authors and depends on techniques employed. For GAS, SAS, SEA, and AAS co-crystallization, relevant process parameters are often well reported. However, for CSS and RESS the reporting of relevant process parameters is often limited. To ensure that the research community can maximize progress on co-crystallization in SCF the reported work can be presented with more detail whenever possible, regardless if the goal is screening or process development. With more information surrounding the process, researchers can better identify critical areas for improvement. First, the scale of the process should be reported for all experiments. This includes reporting the input mass of solids (and mass or molar ratio for co-crystallization). For some processes such as RESS and CSS it is crucial to differentiate between the input mass and dissolved mass, as there can be an initial extraction stage followed by a pre-expansion stage. [98,132,133] The pressure and temperature of the chamber can differ between these two steps, and thus the concentration of dissolved solids also varies. However, examples of the two-stage process in co-crystal reports to date were not found. In addition to input solid mass, any additive mass such as glass beads should also be reported because it can impact the result.

Second, the reactor set-up should also be reported in sufficient detail. This includes parameters such as chamber volume, nozzle geometry, spray distance, and precipitation chamber volume. Stirring methodology (overhead stirrer, magnetic stir bar, no stirring) should also be reported. In particular for the CSS process mixing was found to be a critical factor in successful co-crystal formation. [34] For RESS crystallization the nozzle geometry has been found to have the most profound impact on particle size and should be reported with detail if particle size analysis is conducted on the resulting solids. Nozzle type (orifice vs. capillary), length, and diameter have been shown to yield different particle size. [59,98,99] The nozzle set-up can change the PSD, even if all other parameters are kept constant. This is a key factor when designing scale-up systems or doing technology transfer.

For co-crystallization by GAS, the CO_2 flow rate is a critical parameter for co-crystallization, impacting nucleation and growth. Reporting CO_2 flow rate using mass of CO_2 whenever possible is preferred over a volume flow rate. Reporting flow as a volume is not as direct because the

density of $scCO_2$ varied significantly as a function of pressure. Many authors report dosing rate as a function of volume, but this may be due to the dosing pump used for the experiment. In cases where dosing pumps operate by volume flow rates, conversion to mass flow rate is trivial. But to ensure an accurate conversion, the pressure and temperature during dosing must be clearly reported. Even a crude method such as weighing the CO_2 tank before and after a constant dosing rate process can provide an approximate mass dosing rate. Wherever possible reporting pressure ramp along with the mass dosing rate is encouraged. This allows the solubility profile to be better understood as a function of antisolvent dosing which can have a profound impact on crystallization processes. Such details may not be necessary for screening purposes, but should be considered when fine tuning a co-crystallization process.

One major aspect of a robust process is ability to appropriately scale-up and obtain reproducible results. When authors report process parameters in sufficient detail it can allow for comparison between processes and more facile technology transfer. This provides an opportunity to study the scalability and reproducibility of processes even if the work is being conducted in different laboratories.

2.4.2 Co-Crystallization Yield

Yield is a key response in any crystallization process, especially for high value products such as pharmaceuticals. In conventional solvent systems yields above 90% are achievable with reasonable throughput processes. [134] The highest reported yield for a supercritical co-crystallization process is 75% (GAS, itraconozole–succinic acid). [106] However, for many reports the yields are less than 50%. SAS processes tended to give more consistent yields, where reported, varying from 40 – 70%, while GAS gave a wider range of product yields, varying from 13 – 75%. Yield loss is often speculated to be from loss during collection due to small sample size and the nature of micronized solids. [104,106] Due to scale of the reported SCF co-crystallizations to date (often < 1 g) the loss during collection of product can be significant. However, when yields are less than 50% there should be other factors leading to low yield such as solubility in the final solvent composition.

One area overlooked in the current research is better understanding of optimizing a SCF co-crystallization to improve yield. A simple mass balance to account for yield loss during the process could illustrate shortcomings of a given process. Alternatively, solubility of the co-

crystal in the final solvent composition (assuming it falls within a co-crystal stability region) can be considered and theoretical yields determined. If solubility is not determined prior to the crystallization work, mass balance can also be used to calculate approximate solubility in the final composition by collecting all solids from the mother liquor in cases where conventional organic solvent is employed.

Mass balance of mother liquor is most applicable to GAS, CSS, and SAS where solids are filtered. However, mass balance applies to all processes including RESS, SAS, SEA and AAS where atomization is employed. Mass balance can be used to determine yield by comparing mass of solids in mother liquor, collection vessel, or other components of equipment such as a high-pressure vessel, given the values are in good agreement. When yield is reported, it is also encouraged to outline how product yield was calculated. This is of particular importance for processes such as CSS or RESS where there could be a two-step extraction process. Initial extraction often occurs in a separate vessel from the pre-expansion vessel, thus the quantity of solid added to the extraction vessel does not necessarily agree with the quantity in the pre-expansion vessel. [98,132,133] In such cases it is important to specify what values are used for yield calculation. This will not only aid in a better clarification of yield in published work, but also give researchers guidelines on what product losses to expect when handling these micronized compounds at similar scale.

Although the product yields are often overlooked in reports of co-crystallization by SCF, phase purity is well reported or easily interpreted based on reported characterization. For the purpose of screening, a qualitative assessment of co-crystal phase purity is sufficient using analytical methods such as XRPD, DSC, and FT-IR. However, for process studies, a more quantitative characterization is warranted, which is often done by chromatography.

2.4.3 Controlling Particle Size

One of the advantages of SCF processes is the ability to form a cocrystal and micronize the material in a single process. As discussed in the earlier sections, particle size influences dissolution rate, where a smaller PSD (higher surface area) gives rise to improved dissolution. Thus, control of particle size of API from a crystallization process is critical to ensure a consistent dissolution profile in the final drug product.

A number of studies have shown that reduction of co-crystal particle size improves overall dissolution. [95,104,135] Curiously, in one example initial dissolution (first 15 minutes) of larger particles was actually the same or greater than the smaller particles. [135] This could arise from powder inhomogeneity or presence of fines in a sample. This Illustrates that a single value (e.g. d50 or d90) is not always sufficient to describe the nature of a powder sample. A full PSD should be reported whenever possible. Analysis of surface area is also a valuable measurement for correlation to dissolution and is encouraged when possible.

There are a limited number of systematic studies on particle size of co-crystals produced by high pressure methods. The impact of pressure and temperature on the final product depends on the solubility profile of the solute(s). Both solute concentration and degree of supersaturation impacts nucleation and growth rates, which in turn impacts particle size. [51,58–62] In some co-crystallization studies, clear trends are observed between process parameters and particle size. Examples include impact of dosing rate in GAS or CO_2 flow rates in SAS. [61,109,120,121] However, there are also examples where process parameters are varied but clear correlations between parameters and particle size are not readily observed. [109,123] For example in a GAS co-crystallization when mixing rate was high, the CO_2 dosing rate clearly impacted particle size, but with lower mixing the impact of dosing rate of particle size was not as pronounced. [109] In another example, efforts to reduce particle size in an SAS process were not effective, despite varying process parameters (solute concentration and flow rate, CO_2 flow rate), PSD for all experiments were essentially the same. [122] This illustrates that absence of trends does not mean a parameter has no impact, but more likely indicates interactions between parameters.

Identification of interaction between process parameters is challenging when using a one factor at a time (OFAT) design approach. Design of experiments (DOE) approaches can be used to identify interaction of parameters and are recommended when the goal is process understanding and optimization. Along with approaching process design systematically, such as with DOE, it has also been suggested that knowledge of phase behavior would be useful in better understanding the impact of process parameters on PSD and morphology. [124] This leads to the following discussion on importance of understanding phase behaviour in the next section.

2.4.4 Ternary Phase Diagrams (TPDs)

Another gap in co-crystallization research in SCF is a systematic study of phase stability in the

ternary system comprising API, co-former, and supercritical solvent. TPD development has aided researchers in understanding co-crystallization processes in conventional solvent systems for over 10 years. [87,88,136,137] TPDs are used to illustrate the stability region of a co-crystal in a given solvent system. Depending on the selected conditions (i.e. solvent system, temperature) the co-crystal stability region can vary significantly. [88] Two unique cases are shown in Figure 2.4 and Figure 2.5. Boundaries of the co-crystal stability region can aid in defining safe operating parameters for a robust crystallization process. For example, if a system is incongruently saturating (Figure 2.5) then a solution crystallization starting with the desired stoichiometry may not be favorable. [87] An excess of one component can be added to the system to ensure the isolated solid phase falls within the co-crystal stability region. The component in excess remains in solution and would be removed during filtration and washing steps. TPDs are most relevant to processes operating closer to equilibrium conditions such as GAS or CSS where antisolvent dosing or depressurization are controlled. However, development of TPDs can aid in better understanding of co-crystallization by SCF in any regime.

Theoretical TPDs have been used to describe results obtained from GAS, SCF co-crystallization of a naproxen-nicotinamide co-crystal. [108,109] To the best of our knowledge, there is not a published work for an experimentally generated TPD of a co-crystal in a supercritical system. This is likely because the methodology for TPD development in a supercritical system needs to be modified from that of a conventional solvent system. In conventional systems a large number of experiments can be set up simultaneously. It is straightforward to prepare slurries in ambient conditions and add seed crystals of desired phases. The slurries are generally stirred until equilibrium is reached (days to weeks) before sampling for solid phase data and concentration of components in supernatant. However, for supercritical equipment setups groups are often limited to running experiments in sequence. For each data point on a TPD the system of interest should reach an equilibrium state. The logistics of seed introduction into a high-pressure system also need to be considered. Thus, developing a complete TPD in a supercritical system will be a more complex task than in conventional solvent systems. Systematic solubility assessments of quaternary systems (API, co-former, solvent, $scCO_2$) such as that done by Revelli *et al.* can help set the groundwork for development of TPDs in SCF systems. [114] The methodology could be extended to development of a TPD by varying the ratios of API to co-former for a given solvent composition, temperature, and pressure.

Theoretical TPDs can help provide insight when explaining co-crystallization results in SCFs, following the examples set by Neurohr *et al.* when full experimental determination is not feasible. If processes such as GAS are employed as the final co-crystallization step of an API then continued work on TPD development in supercritical systems should continue. If complete TPDs are not feasible, probing the stability of a process with a small number of data points on a proposed TPD can still provide insight into acceptable process space and boundaries of a co-crystal stability region. For example, extended slurries using mixtures of API and co-former with varied molar ratio can aid in identifying if a system is congruent or incongruently saturating. The solid phase identity after slurry can be used for identification of phase stability boundaries.

2.4.5 Technoeconomic Assessment

Supercritical CO_2 is often quoted as being an alternative to conventional crystallization because $scCO_2$ is a more environmentally acceptable solvent. [138,139] However, for many pharmaceutical SCF processes $scCO_2$ is used as an antisolvent. Despite still employing organic solvents, SCF processes generally produce small and narrow particle size distributions, eliminating the need for an additional micronization step.

Technoeconomic assessment is often overlooked when considering SCF crystallization (co-crystallization) process implementation at large as an alternative to conventional crystallization in organic solvents. Although CO_2 is a more inert solvent than conventional solvents, there is an energy usage and cost associated with heating and pressurization of CO_2. Also, due to the low solubility of many pharmaceuticals in $scCO_2$ it is often employed as an antisolvent in SCF crystallization and co-crystallization. As such, the quantity of organic solvent required for an SCF versus conventional system should be compared. Over 70% of reports of supercritical co-crystallization employ an organic solvent such as acetone, ethanol or THF. While the use of organic solvent for pharmaceutical SCF co-crystallization may not be avoidable, the throughput of the process should be considered. For example, a carbamazepine–nicotinamide cocrystal was successfully prepared with 90% yield using only 14 volumes solvent. [134] SCF co-crystallization processes reported to date tend to be dilute, commonly employing 100 volumes organic solvent. Compared to conventional co-crystallization techniques this is not a scalable throughput where 6 to 20 volumes are usually used.

Kurniawansyah *et al.* performed an economic assessment for crystallization by GAS, SAS, and

ARISE (atomized rapid injection solvent extraction) of a model compound with EtOH as solvent. [140] GAS was the least costly (6 – 13 USD/kg), while SAS and ARISE were higher cost (64 – 385 USD/kg and 52 – 255 USD/kg). The greatest contributor to cost of raw materials was solvent used and the cost per kg could be reduced by increasing the solution concentration (increasing throughput). SEA/SAA were not discussed directly in the analysis, but the cost would likely be similar to SAS due to process similarities. For CSS and RESS processes organic solvent does not contribute to the cost, but RESS and CSS were not considered in Kurniawansyah *et al.*'s analysis. The pressure used in the SCF crystallization techniques should also be considered. In co-crystallization by RESS, pressures were generally higher than the other techniques. Pressures up to 62 MPa were reported for RESS, while pressures using other SCF techniques were 15 MPa or lower. Although organic solvent will not contribute to cost of RESS, the cost of greater CO_2 compression should be considered. Depending on the required CO_2 compression and volume of organic solvent, the most economically viable process will likely vary depending on the compound and solubility.

A technoeconomic assessment is not necessary when the goal of research is screening. However, it is important to consider production (crystallization) when determining the most promising solid form of an API. For high value products such as pharmaceuticals, the cost of SCF crystallization may be a minute factor in the selection of a crystallization method and the benefits of simultaneous recrystallization and micronization can outweigh the cost. Nevertheless, in order to facilitate a technoeconomic assessment experimental research must be reported in sufficient detail. Scale, solvent (including CO_2) quantities, pressure, temperature, and yield can be included in all research publications even if the focus is screening.

2.5 Concluding Remarks

Co-crystallization of pharmaceuticals is still a young field, and co-crystallization in SCF is even younger. As such, we have aimed to identify knowledge gaps and potential research areas. The majority of work to date on co-crystallization in supercritical fluids has taken a screening approach where the goals of the work are often determining differences between solvent used and/or the co-formers used. However, it is still important to report process-related parameters and responses for screening work whenever possible. Reporting of the key factors such as scale and product yield, reactor set-up, nozzle geometry, and dosing rates is encouraged because it can

aid in better technology transfer, scale-up assessment, and comparison between different studies. For dosing regimes, reporting of the mass rate and pressure profile are advised whenever possible as these are unambiguous.

A feasible scale-up process should robustly produce the desired polymorphic form, yield a crystalline product with desired PSD, exhibit reasonable yield (> 85% is typical), produce a high purity solid product, and have low residual solvent content. For a co-crystal, the co-crystal should also be phase pure (i.e. homo-crystals of API and/or co-former are not present).

RESS and CSS processes are generally not suitable for scale-up of pharmaceutical co-crystals because of solubility limitations of pharmaceutical compounds. Although CSS may not be a viable method for scale-up of co-crystals, it is suitable for screening purposes. Co-crystals can form within 1-2 hours during CSS, allowing for straightforward screening. It is possible that like LAG, co-crystal formation can proceed by CSS even with low component solubility if mechanical energy is sufficient. Although RESS also employs $scCO_2$ as a solvent, successful co-crystallization by the method is limited and not well studied. Unlike CSS, the solids collected from RESS are formed due to rapid expansion of the SCF solution from a nozzle. RESS is likely more limiting during screening than CSS because of low solubility of pharmaceutical compounds. Undissolved solids in the vessel are often contained by a filter. Intrinsically this gives less than 100% theoretical yield unless both components are completely dissolved. Also, if a co-crystal exhibits lower solubility than its two pure components in $scCO_2$, a co-crystal phase could precipitate in the vessel which would in turn not be collected during the evaporation step. A two-pronged approach to screening by RESS/quasi-CSS could involve collected of the sprayed solids as well as those confined in the vessel. Mechanical mixing in the high-pressure chamber may provide sufficient energy to form a co-crystal in the solid state, while rapid evaporation potentially also leads to co-crystallization.

Techniques employing $scCO_2$ as an antisolvent tend to be more feasible for SCF co-crystallization process design. However, most reports of SCF antisolvent co-crystallization use dilute solutions of API and co-former often up to 100 volumes organic solvent. In screening studies the low solute concentration is imposed by low solubility of the API and can be accepted. But for a recrystallization process design a more systematic solvent selection should be employed to design a process with good throughput. Of the SCF antisolvent techniques, GAS has

been the most commonly reported for co-crystallization to date. This may be due to its versatility in solvent selection, similarities to conventional antisolvent processes, and mode of solids collection directly from a filter in the vessel. Despite this, product yields reported for GAS co-crystallization are generally low (< 75%) and justification of low yield is often not discussed in detail. A more systematic approach to solvent selection based on solubility could help improve yields. It is not possible to predict a product yield in a particular system if solubility of the co-crystal product in the final composition is unknown.

Although the work summarized in this review focuses on $scCO_2$, selection of conventional organic solvents should not be neglected. Throughout all reports of co-crystallization summarized here, solvent choice has been shown to have the most profound impact on the process. In many instances, selection of an optimal solvent system may be solved simply by assessing the solubility profiles of API and co-former. Although the impact of solvent is not equal for all systems, it will always have some impact on morphology, yield, co-crystal phase purity, or polymorph. If process scale-up is a consideration the solvent class must also be considered because it will have implications on the product specifications. For example, use of EtOH could give slightly lower yield than THF in a process, but it is likely much more straightforward to design a process with residual EtOH < 0.5% than it is to design a process with THF < 0.07%.

Perhaps one of the largest gaps in SCF co-crystallization is the fundamental understanding of phase stability and solubility in supercritical systems. In-depth studies of every screened co-crystal are not necessary (or feasible) as they are far from the objective. However, researchers have already shown that SCF can be added to the co-crystal screening repertoire of techniques. The focus can now be shifted towards better understanding of why SCF systems can generate phase pure co-crystals and how to design robust SCF co-crystallization processes. The basis of designing thoughtful co-crystallization processes is understanding solubility of co-crystals and their components in a given system. Researchers have made many advances in understanding of pharmaceutical co-crystals in conventional solvent systems in recent years. The synthon approach has been widely accepted and is now employed in almost all co-crystal research. [73–76,79,141] In addition, thermodynamic stability of co-crystals in conventional solvent systems has also been well reported and can be utilized in co-crystallization process design. [85–

88,136,142] We can draw on those methodologies to aid in developing a more robust understanding in novel high-pressure systems. Work focusing on solubility and modeling of multi-component systems in SCF and relating results to proposed TPDs in supercritical systems are starting to lay the foundation for development of TPDs and tailored co-crystallization processes in SCF systems. [108,109,113,114]

Overall, supercritical co-crystallization can be a viable alternative to co-crystallization in conventional systems offering the added benefit of removing any secondary processing such as micronization. With further study, we are confident that higher throughput SCF co-crystallization processes are developable and also reasonable from an economic standpoint when compared with their conventional crystallization counterparts.

3 CHAPTER 3: MODEL COMPOUND SCREENING AND SELECTION

3.1 INTRODUCTION

A common way to categorize drugs is by BCS class, which divides drugs on the basis of solubility and permeability. There are many comprehensive reviews classifying commercially available drugs by BCS class.[2,68,143] The objective of the research presented in this thesis is related to improvement of poorly soluble APIs through cocrystallization and particle size reduction. As such, comprehensive lists were assessed and a small selection of suitable BCS class II drugs were selected to screen for use as model compounds. The selection criteria for this work included BCS classification (class II required), availability and cost, typical dosage (for safety consideration), and potential for cocrystal formation. For brevity, only the three candidates which underwent some characterization and screening are included in this chapter.

Niclosamide (NCS) is on the World Health Organization (WHO) list of essential medicines and is an anthelminthic used to treat tapeworm infestations.[144] A typical NCS dosage is 500 mg.[144] Due to NCS low aqueous solubility (between 1—13 μg/mL) it is a suitable candidate for exploring methods to improve bioavailability.[145] NCS is polymorphic with at least one anhydrous form, two hydrates, and solvates with solvents such as tetrahydrofuran (THF), dimethylformamide (DMF), dimethylsulfoxide (DMSO), methanol (MeOH), tetraethylene glycol (TEG), and diethyl ether (DEE).[145–149] Cocrystals of NCS with a variety of coformers including urea and caffeine have also been published, and some showed improved solubility over neat NCS in an isopropanol (IPA)/water mixture.[147,150,151] As shown in Figure 3.1, NCS has a hydrogen bond donors (e.g. OH, amide hydrogen) and acceptor (e.g. amide and nitro-group oxygen). There was not any existing literature regarding processing of NCS in supercritical fluids at the time of this research, nor was there a comparison of solubility in biorelevant media or a scaleable process for crystallization.

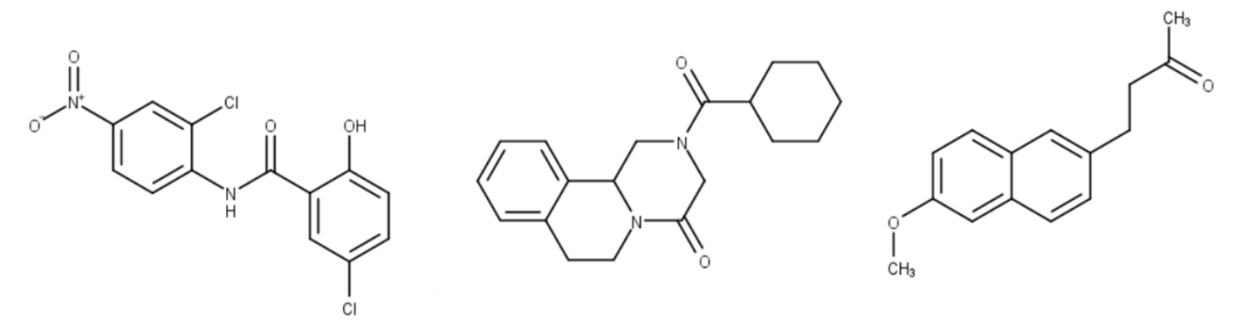

Figure 3.1- Molecular structure of niclosamide (left), praziquantel (center), and nabumetone (right).

Praziqnatel (PZQ) is also on the World Health Organization (WHO) list of essential medicines. It is an anthelmintic used to treat the parasitic worm disease, schistosomiasis.[152] PZQ is administered as a tablet of between 150 mg or 600 mg dosage and is provided as a racemate, (*RS*)-PZQ.[144,153] PZQ has a minimum measured aqueous solubility of 0.4 mg/mL between pH 1.2 and 6.8 and is therefore considered a BCS Class II drug.[143] Therefore some research efforts have focused on methods to improve the solubility of PZQ.[154–156] PZQ can crystallize in different forms including (*RS*)-PZQ racemate (Form A), hemi-hydrates of both (*R*)- and (*S*)-enantiomers, and two lower-melting anhydrous forms (Form B and C), which were identified in 2018-2019 through solvent-free milling.[156–158] Form B melts 30 °C lower than Form A and has lower heat of fusion, indicating a metastable polymorph. Furthermore, the solubility of form B in water was twice that of Form A and Form B was observed to be physically stable in ambient conditions for 12 months.[156] Form C was also a metastable, lower melting form which exhibited improved aqueous solubility compared to Forms A and B. However, Form C showed limited physical stability and will convert back to form A during storage.[158]

PZQ has two carbonyl oxygens (C=O), which are H-bond acceptors and can be used for co-crystal formation, as shown in Figure 3.1. PZQ has been shown to form co-crystals with a variety of carboxylic acids using LAG and evaporative crystallization techniques.[153,157] Solubility of PZQ co-crystals in biorelevant media in comparison to (*RS*)-PZQ Form A has not been reported.

PZQ solid lipid nanoparticles (SLNs) have been prepared using a mixture of $scCO_2$ and dichloromethane (DCM) at 100 mL-scale.[159] The PZQ-SLNs had an average particle size of 25 nm and showed approximately double the in-vitro drug release compared to free PZQ in a pH

7 phosphate buffer.[159] Aside from preparation of SLNs, the behavior of PZQ in $scCO_2$ has not been previously studied.

NBM is a nonsteroidal anti-inflammatory drug (NSAID) which is commonly used to treat arthritis.[160] NBM is given as a high-dose (750 mg) oral tablet exhibiting a minimum aqueous solubility between of 15 µg/mL pH 1.2 and 6.8 and falls into BCS class II.[143] NBM has at least two known crystalline anhydrous forms which exhibit different morphology and melting point.[160] NBM can form H-bonds through the carbonyl oxygen, as shown by the structure in Figure 3.1, and therefore is a candidate for co-crystallization. NBM co-crystals are reported in the literature with a variety carboxylic acids and saccharin and were prepared using an evaporative crystallization method.[161] However, the co-crystals were not characterized beyond differential scanning calorimetry (DSC) and infrared (IR) spectroscopy. Solubility improvement of cocrystals compared to NBM Form 1 in biorelevant media and production through a scalable method have not been explored.

The solubility of NBM has been measured in $scCO_2$ by Su and Chen.[162] The solubility of NBM was between 3.9×10^{-5} and 2.7×10^{-3} mol fraction over the range 308 K/10 MPa to 328 K/22 MPa. Because of relatively high solubility in CO_2, NBM was a good candidate for RESS crystallization to improve surface area (reduce particle size). RESS successfully gave a reduction in particle size of NBM (from 32.6 to 3.3 µm) and the particle size reduction resulted in a significant improvement in the dissolution rate of NBM in aqueous media.[163]

The goal of this screening was to narrow down suitable API candidates to use during the scope of this thesis. The three compounds were subjected to solubility screening in a variety of organic solvents at room temperature (RT) and in $scCO_2$. Solids subjected to high-pressure experiments were analysed by XRPD to evaluate potential change in polymorph. Compounds were also subjected to an abbreviated cocrystal screening through co-evaporation to identify propensity for cocrystal formation.

3.2 Materials and Methods

3.2.1 Materials

NCS (>98% purity), was used as received without further purification from Millipore Sigma, Lot #: 058M4059V. Praziquantel (>98% purity, Form A), was used as received without further

purification from TCI America, Lot #: KM430-AB. Nabumetone (analytical standard grade) was used as received without further purification from Millipore Sigma, Lot #: MKCN3727.

3.2.2 XRPD

X-ray powder diffraction (XRPD) was performed using a Bruker D8 Advance in reflection mode with a Cu Kα source. The scan range was 4-30° 2θ with 0.03° 2θ step size. Samples were prepared on Si zero-return wafers.

3.2.3 Solubility in Organic Solvents

Solubility measurements were conducted using a gravimetric or addition method. For the gravimetric method, an excess of solid was suspended in 1 mL of solvent at room temperature to form a slurry. The slurries were stirred for a minimum of two days to equilibrate. Supernatant from the slurries was weighed (m_{sup}) in a tared vial of known mass (m_v) on a Mettler Toledo balance (± 0.0001 g) and then evaporated to dryness at 50 °C in atmosphere and then 50 °C under vacuum. The solid residue was weighed (m_{sol}), and the masses were used to calculate solubility. In the case where mass difference between m_{sol} and m_{sup} was less than 0.0001 g (not detected) the solubility was reported as << 1 mg/mL. For the addition method, the solid (30-40 mg) was weighed into a 2 mL vial and a stir bar was added. Then 100 µL solvent was added. If the solids did not dissolve, solvent was added in 30 µL increments until dissolution.

3.2.4 Solubility in $scCO_2$

Solubility of APIs was measured in $scCO_2$ using a simple gravimetric method in the SFT-10 system as described in section 5.3.2.1 Solubility Assessment in CO2.

3.2.5 Cocrystal Screening

Between 30 and 40 mg of API was weighed into a 4 mL vial. Then approximately 1.1 eq. of the selected co-former was weighed. Acetone or EtOH (3 mL) was added, the solution was stirred at 50 °C and allowed to evaporate to dryness. Co-milling was done by weighing API and co-former in a ball mill, adding 1 volume heptane, and milling for 30 s using a ¼” stainless steel ball. The recovered solids were analyzed by XRPD.

3.3 Results and Discussion

3.3.1 Characterization of Three Compounds

3.3.1.1 XRPD Analysis

Bulk NCS showed XRPD diffraction peaks characteristic of both anhydrous (NCS-A) and monohydrate (NCS-H) forms, the diffractograms are shown in Figure 3.2. [147,148] The diffractogram of NCS-A prepared in IPA agreed with powder diffraction data of van Tonder *et al,* and are also shown in Figure 3.2. [145] NCS-H characteristic peaks include 7.69, 9.47, 11.63, 12.78, 16.94, and 27.26 °2θ while NCS-A characteristic peaks appear at 6.61, 13.07, 13.81, 17.28, 19.89, and 26.81 °2θ. PZQ used for experiments was Form A which exhibits characteristic peaks at 4.01, 6.33, 8.02, 8.21, 15.39, 1644, and 20.11 °2θ. Finally, NBM has characteristic peaks at 7.99, 21.54, and 24.06 °2θ.

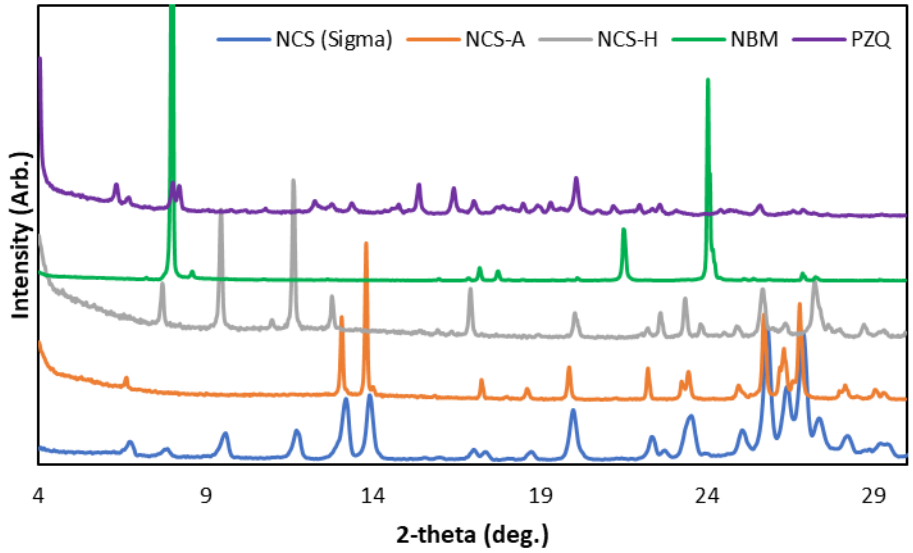

Figure 3.2- XRPD diffractograms of niclosamide (NCS; from Sigma, anhydrous, and hydrate forms), nabumetone (NBM) form A, and praziquantel (PZQ) form A.

3.3.1.2 Solubility Assessment in Conventional Solvents

Solubility of NCS, PZQ, and NBM was evaluated in a range of conventional Class 2 and Class 3 organic solvents. The results are summarized in Table 3.1. In general, NCS exhibited the lowest solubility in most organic solvents, giving less than 20 mg/mL solubility in the solvents tested except for THF. NBM solubility was high in solvents such as DCM, THF, 2-MeTHF, EtOAc,

and ACN with all solvents giving more than 190 mg/mL solubility. PZQ solubility was highest in MeOH, DCM, and THF with more than 120 mg/mL solubility, while other solvents showed between 40 and 80 mg/mL solubility.

In cases where slurries were obtained, solids were analysed by XRPD after the experiment to evaluate polymorphism. In the case of PZQ and NBM there was no evidence of new polymorphs, while with NCS multiple unique XRPD patterns were observed. The mixture of NCS-A and NCS-H converted to NCS-A in IPA and EtOAc.[147] After a slurry in THF, a mixture of NCS-A and a previously reported THF solvate was observed.[146] After a slurry in MeOH, another unique XRPD pattern was observed, however it did not agree with previously reported NCS polymorphs.

Table 3.1- Solubility result for three APIs in organic solvents at room temperature.

Solvent	**Solubility (mg/mL solvent)**		
	NCS	**PZQ**	**NBM**
MeOH	19	128	-
EtOH	12	66	-
acetone	20	73	> 300
DCM	9	> 500	> 400
THF	52	178	> 300
2-MeTHF	-	> 60	192 – 236
EtOAc	11	41	219 – 269
IPA	13	42	-
ACN	-	80	268 – 349

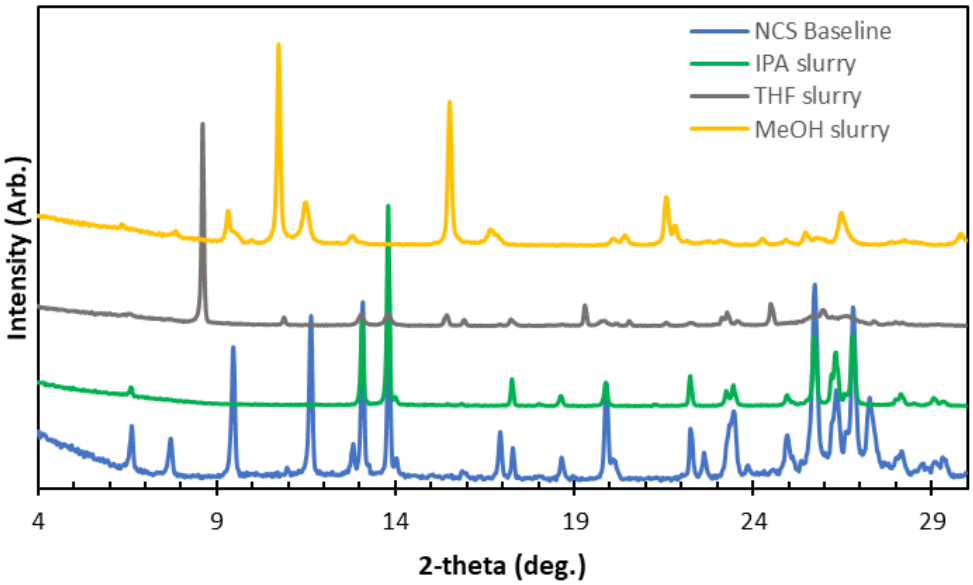

Figure 3.3- Unique XRPD patterns (different polymorphs/solvates) observed after slurrying NCS in various solvents compared to input material (mixture of anhydrous and hydrate).

3.3.2 Solubility Assessment of Three Compounds in CO_2

A limited number of solubility measurements of NCS, PZQ, and NBM were conducted in $scCO_2$ to help determine if neat CO_2 was a feasible solvent for crystallization of if addition of cosolvent would be necessary to improve solubility. Solubility of NCS was the lowest of the three compounds while NBM exhibited the highest solubility in the conditions tested and the results are summarized in Table 3.2. Solids remaining in the high-pressure vessel were collected for XRPD analysis after the experiments to evaluate polymorphism. In the case of NBM there was no evidence of a change in polymorph− the characteristic peaks in XRPD diffractograms of recovered solids were in agreement with the input material as given in Figure 3.4. In the case of NCS, the input material was a mixture of a hydrate and anhydrous form.[147,148] After exposure to $scCO_2$ the XRPD showed characteristic peaks only from the anhydrous form, while the characteristic peaks of the hydrated form were no longer present which is discussed in more detail in Chapter 5: Cocrystal Formation of Niclosamide and Urea in Supercritical CO2 and Impact of Cosolvent and is therefore not discussed here. The diffractograms for the NCS experiment are shown in Figure 3.5. However, in the case of PZQ, the XRPD diffractogram of recovered solids exhibited new, unique characteristic peaks which indicated a potential new

polymorph as shown in Figure 3.6. In addition to the change in XRPD pattern a distinct morphology change was also observed from a fine powder to elongated needle-like solids, shown in Figure 3.7. A thorough investigation of the novel polymorph of PZQ is presented in Chapter 6 and is therefore not discussed here.

Table 3.2- Solubility of three APIs in $scCO_2$.

Compound	Pressure, MPa	Temperature, °C	Hold time, h	CO_2 density, g/cc	Solubility, $Y \times 10^4$
NCS	20	40	24	0.8308	0.08
	18.1	40	25	0.8195	3.41
PZQ	12.9	40	24	0.7403	0.48
	33.6	61	24	0.8533	> 4.21[a]
NBM	9.4	40	24	0.5608	5.86
	26.2	60	24	0.7979	48.2

[a] no solid remaining in pan after measurement. After de-pressurization a sticky substance was deposited in the vessel.

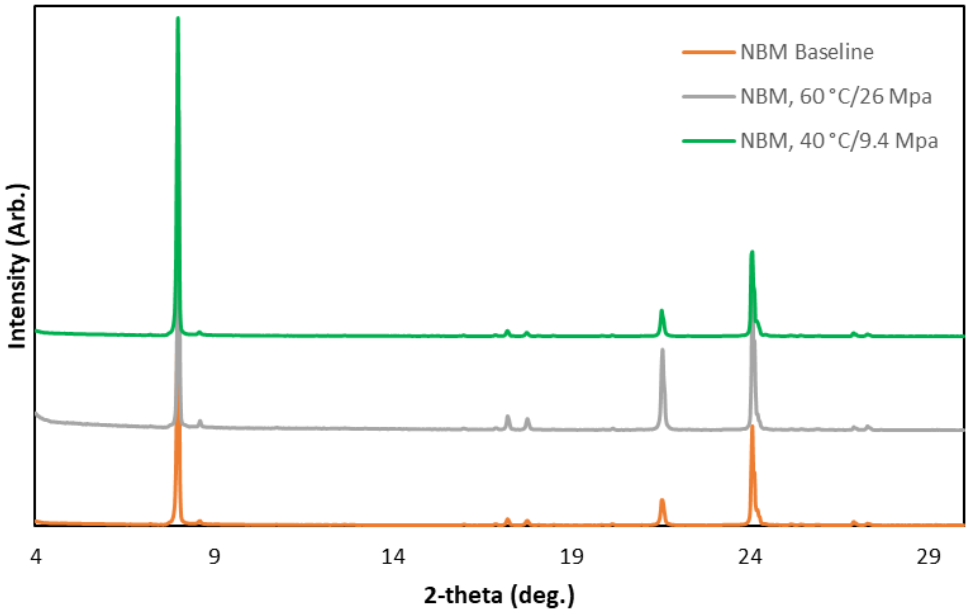

Figure 3.4- NBM XRPD diffractogram after exposure to $scCO_2$ for 24 h showing there was not a polymorphic transformation.

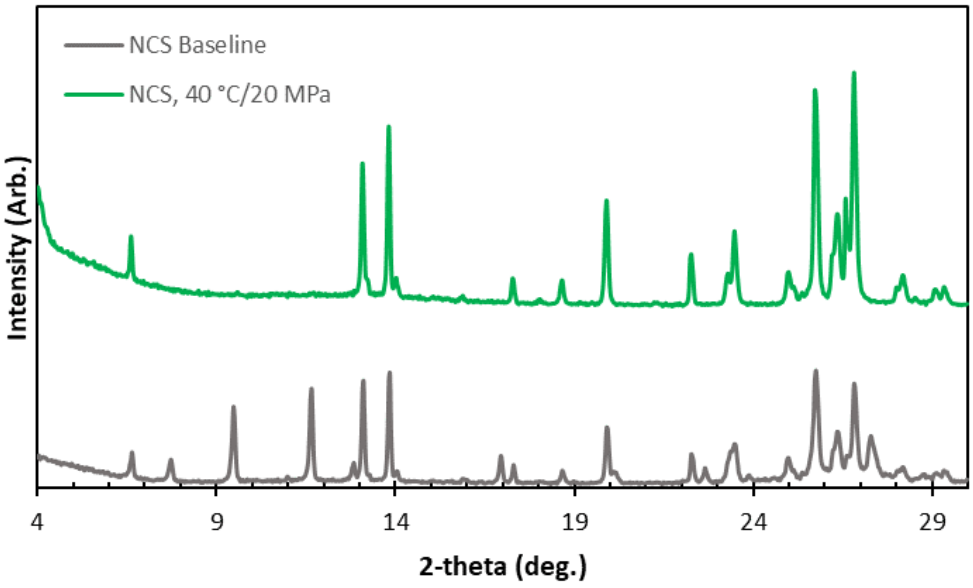

Figure 3.5- NCS XRPD diffractogram after exposure to $scCO_2$ for 24 h.

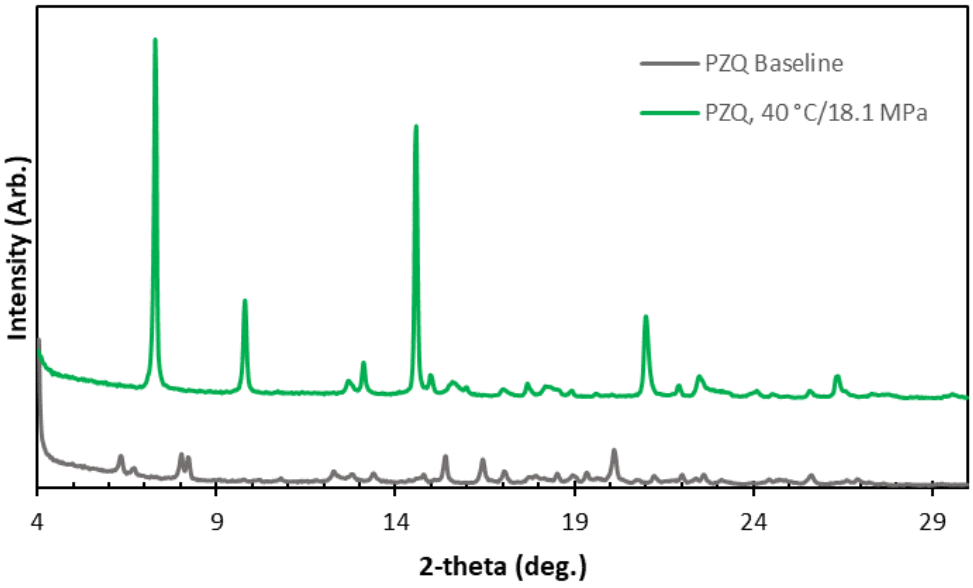

Figure 3.6- PZQ XRPD diffractogram after exposure to $scCO_2$ for 24 h indicating a polymorphic transformation.

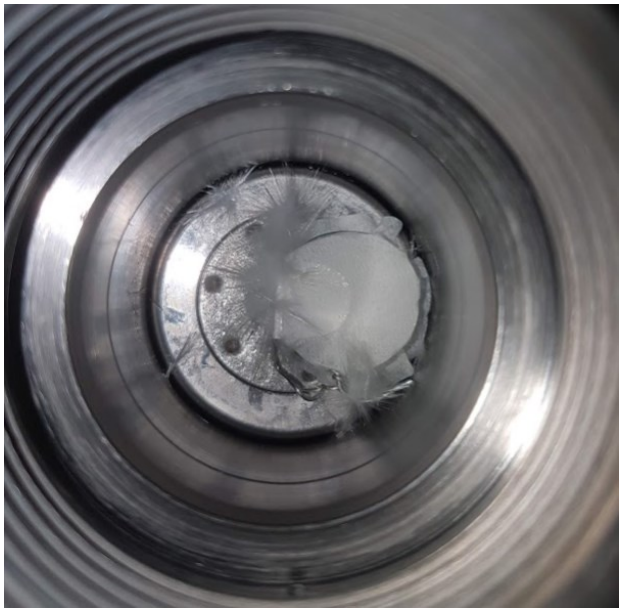

Figure 3.7- PZQ solid exhibiting needle-like morphology after exposure to $scCO_2$ for 24 h.

3.3.3 Cocrystal Screening in Conventional Solvents

The propensity of NCS, PZQ, and NBM to form cocrystals using a conventional co-evaporation method was explored. Coformers were selected based on functional groups of the API and coformer which have the ability to form hydrogen bonds. Figure 3.8 depicts the coformers used in the screening of three compounds, which include functionalities such as aliphatic and aromatic carboxylic acids, amides, and carbonyls.

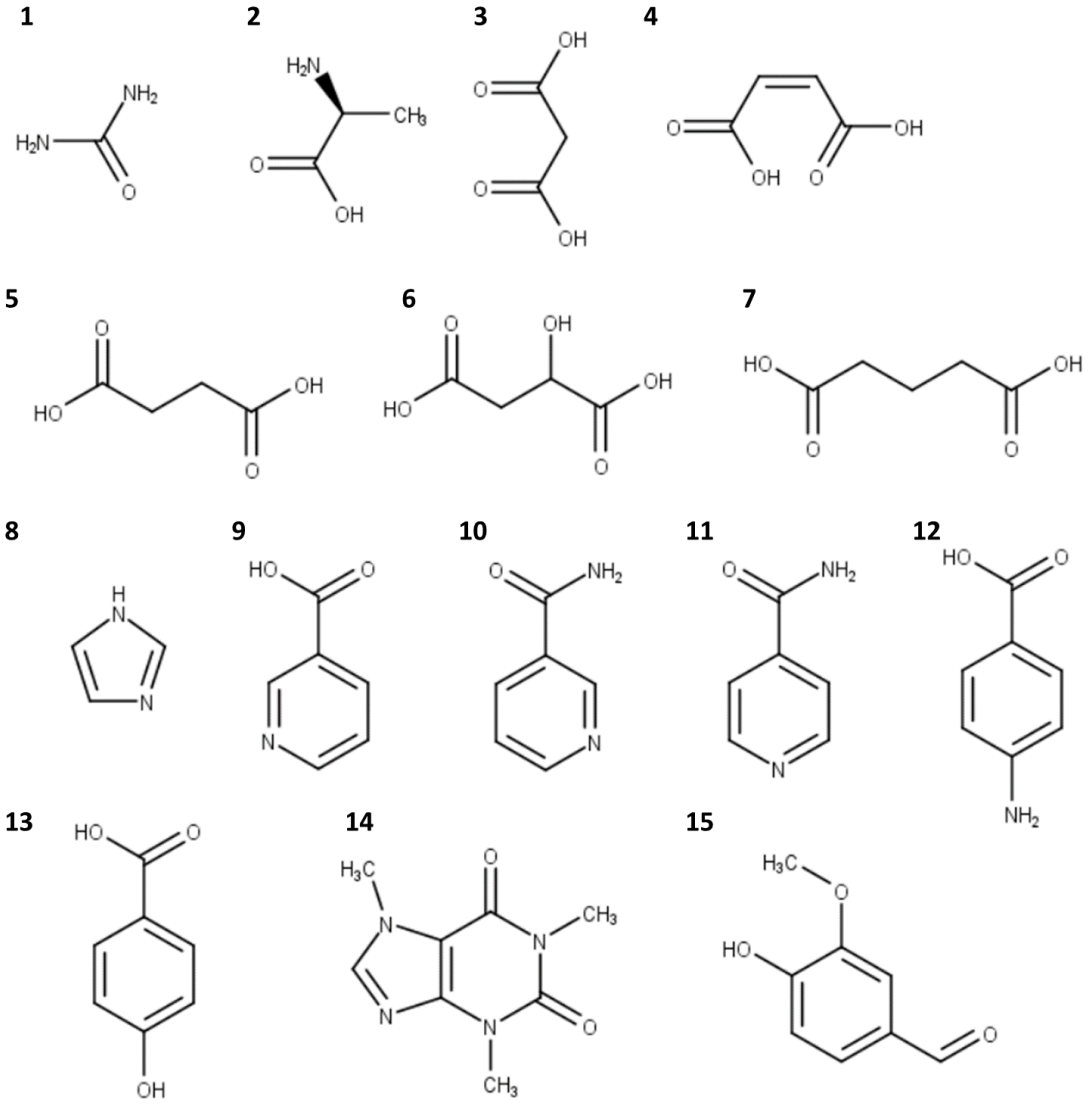

Figure 3.8- Structure of coformers used during screening.
1- urea, 2- L-alanine, 3- malonic acid, 4- maleic acid, 5- succinic acid, 6- malic acid, 7- glutaric acid, 8- imidazole, 9- nicotinic acid, 10- nicotinamide, 11- isonicotinamide, 12- 4-aminobenzoic acid, 13- 4-hydroxybenzoic acid, 14- caffeine, 15- vanillin.

Between seven and ten coformers were screened for each compound and the results are summarized in Table 3.3.

NBM did not form a cocrystal by the co-evaporation method with any of the selected coformers, as indicated by XRPD analysis where only characteristic peaks of NBM and the coformer were

observed. It must be noted that co-crystals of NBM with malonic acid and glutaric acid have been reported in literature.[161] The co-crystals were also prepared by co-evaporation in EtOH. However, the solvent was evaporated under vacuum, unlike this work where evaporation was at atmospheric pressure. The concentration of the solutions used was also different, 0.1 mM, while in this study the concentration was 40-60 mM. The variation in evaporation method and concentration is possibly why the malonic acid and glutaric acid co-crystals were not isolated in this screening. Supporting data for the results from NBM cocrystal screening are given in Appendix B.

Co-crystals of NCS with the co-formers shown in Table 3.3 have already been reported in literature with the exception of nicotinic acid.[147,150,151] Nicotinic acid was included because of carboxylic acid and pyridine functionality. NCS showed some evidence of cocrystal formation with all of the tested coformers except 4-aminobenzoic acid. In experiments with caffeine, imidazole, isonicotinamide, and nicotinamide characteristic peaks of NCS and coformer were not observed by XRPD which indicates complete formation of the cocrystal. Experiments with nicotinic acid and urea showed unique peaks in the XRPD indicating cocrystal formation, but also some characteristic peaks of either NCS or coformer in varying quantity. Supporting data for the results from NCS cocrystal screening are given in Appendix B.

PZQ did not form a cocrystal with L-alanine, nicotinamide, or urea in the co-evaporation experiments and formed a gel when screening with maleic acid, malic acid, and vanillin in acetone. Evidence of cocrystal formation was observed when screening with 4-hydroxybenzoic acid, glutaric acid, malonic acid, and succinic acid in both acetone and EtOH, while evidence of cocrystal formation with malic acid and vanillin was observed only in EtOH. Co-crystals with the above co-formers, with the exception of vanillin, have been reported in literature. Further discussion and supporting data for the results from PZQ cocrystal screening are given in Appendix B.

Table 3.3- Results of cocrystal screening of three APIs by co-evaporation in acetone and EtOH.

Coformer	NCS		PZQ		NBM	
	acetone	EtOH	acetone	EtOH	acetone	EtOH
4-aminobenzoic acid	×	×	-	-	-	-
4-hydroxybenzoic acid	-	-	✓	✓	×	×
caffeine	✓	✓	-	-	-	-

Coformer	NCS		PZQ		NBM	
	acetone	EtOH	acetone	EtOH	acetone	EtOH
glutaric acid	-	-	✓	✓	×	×
imidazole	✓	✓	-	-	-	-
isonicotinamide	✓	✓	-	-	-	-
L-alanine	-	-	×	×	×	×
maleic acid	-	-	gel	gel	×	×
malic acid	-	-	gel	✓	×	×
malonic acid	-	-	✓	✓	×	×
nicotinamide	✓	✓	×	×	×	×
nicotinic acid	✓×	✓×	-	-	-	-
succinic acid	-	-	✓	✓	×	×
urea	✓×	✓	×	×	×	×
vanillin	-	-	gel	✓	×	×

Note. Hyphen indicates the experiment was not performed. Symbol × indicates that solids were mixture of API and coformer by XRPD (cocrystal not formed), ✓ indicates a unique XRPD pattern was observed compared to API and coformer reference, while ✓× indicates a mixture of new peaks with API or coformer reference was observed.

3.4 Conclusions

NCS, PZQ, and NBM were evaluated for the purpose of selecting a model compound for the research presented within the scope of this thesis. The three compounds were evaluated based on solubility in conventional organic solvent, solubility in $scCO_2$, tendency to form a cocrystal, and novelty of the research.

In general, NBM exhibited the highest solubility in conventional organic solvents and in $scCO_2$ in comparison to PZQ and NCS. NCS exhibited the lowest solubility in $scCO_2$ of the three compounds and the data obtained in this study were in reasonable agreement with literature values (see Appendix D: Solubility Measurement Method Development and). After exposure to $scCO_2$ for 24 h without mechanical agitation, NBM did not show evidence of change in polymorph, while a mixture of NCS-A and NCS-H converted to only NCS-A after exposure, and PZQ exhibited new peaks in XRPD after exposure indicating formation of a novel polymorph.

Between eight and ten coformers were selected to screen with the three compounds using a co-evaporation method in two solvents—EtOH and acetone. Although cocrystals have been previously reported with NBM, they were not observed during the limited screening in this study. Both PZQ and NCS showed evidence of cocrystal formation with multiple coformers from both solvents tested. Namely NCS showed evidence of cocrystal formation with 4-aminobenzoic

acid, caffeine, imidazole, isonicotinamide, nicotinamide, nicotinic acid, and urea. While PZQ showed evidence of cocrystal formation with 4-hydroxybenzoic acid, glutaric acid, malic acid, malonic acid, succinic acid, and vanillin.

Based on the preliminary results for solubility, ease of co-crystal formation, and novelty, PZQ and NCS were selected as model compounds to move forward. NCS and PZQ exhibited lower solubility in $scCO_2$ compared to NBM, but one objective of the work presented in this thesis is to explore the impact of cosolvent selection on cocrystal formation. Therefore, NCS and PZQ are suitable candidates to investigate cosolvent/$scCO_2$ mixtures. Both PZQ and NCS also readily formed cocrystals with a variety of coformers, while NBM did not. Furthermore, PZQ and NCS exhibited interesting behavior from a polymorphism perspective when exposed to $scCO_2$ while NBM did not exhibit polymorphism in the range of conditions explored.

4 CHAPTER 4: TERNARY PHASE DIAGRAM DEVELOPMENT AND PRODUCTION OF NICLOSAMIDE-UREA CO-CRYSTAL BY SPRAY DRYING

Reprinted with permission from L.A. MacEachern, R. Walwyn-Venugopal, A. Kermanshahi-pour, M. Mirmehrabi, Ternary Phase Diagram Development and Production of Niclosamide-Urea Co-Crystal by Spray Drying, J. Pharm. Sci. (2020) 1–11.

4.1 Abstract

In this work, a ternary phase diagram was developed for a Niclosamide-urea co-crystal (NCS-UR) in isopropanol (IPA) using a combination of slurry and solvent addition methods. The ternary phase diagram showed that solubility of Niclosamide and urea differed by an order of magnitude in IPA, leading to an incongruently saturating system. Spray drying was explored as a method to generate NCS-UR. Co-crystals with small, uniform particle size were successfully prepared by spray drying from equimolar solutions with yield up to 73%. Co-crystals were phase pure by X-ray powder diffraction (XRPD) and differential scanning calorimetry (DSC) from all conditions explored. Somewhat similar particles were obtained at inlet temperature of 70 °C (mean size of 2.0 μm) compared to 85 °C (2.8-3.4 μm). Based on the TPD, isolating phase pure co-crystal through solution crystallization in IPA would require excess urea. However, spray drying did not require excess co-former. The in-vitro solubility of NCS-UR was compared to anhydrous NCS in biorelevant media. NCS-UR did not give improvement in solubility at 1 h or 24 h. Overall, this work showed that spray drying is a feasible process for preparing phase pure co-crystals for an incongruently saturating system and simultaneously generating micron size particles.

4.2 Introduction

One of the struggles of modern active pharmaceutical ingredients (API) is poor aqueous solubility. This problem has stimulated a significant amount of research in improving the kinetic solubility of APIs through amorphous solid form, formulation optimization, salt or co-crystal formation, and particle size reduction.[3–5] Improved solubility of co-crystals is attributed to the "spring parachute" effect.[4] The "spring parachute" concept suggests that a co-crystal dissociates to form amorphous or giving rise to high initial solubility (the spring) then transitions

through metastable forms (the parachute) until reaching the thermodynamically stable form and equilibrium solubility. Co-crystallization is an established technique of improving the aqueous solubility of an API and is becoming more popular in the pharmaceutical field.[3,4,21,26,28,69,70,76] The molecules that API are bonded with in a co-crystal are mostly generally regarded as safe (GRAS) compounds.[3,26,65,66] However, co-formers with therapeutic effects are also reported.[67]

Solubility of API and co-former in a given solvent system influences the phase stability and successful isolation of a co-crystal. The phase stability and solubility are most often visualized through ternary phase diagrams (TPDs). TPDs are an essential tool for solution based methods and can be used to define the compositions of API, co-former and solvent where the co-crystal is stable at equilibrium.[26,87,164] Co-crystal components can be considered as congruently or incongruently saturating. Incongruently saturating components can pose problems for solution-based methods because an excess of one component is required to obtain a phase pure co-crystal. This is particularly challenging using evaporative, melt, or grinding techniques where the excess component is not removed by filtration. In evaporative methods, this can lead to addition of undesired Class 2 solvents to push the co-crystal towards congruent saturation.[11,63,165] Use of Class 2 solvents in a scalable process is discouraged due to low limit of allowable residual solvent according to International Council for Harmonization (ICH) guidelines.[63]

A challenge of co-crystallization methods is scale-up. Co-crystallization methods such as liquid assisted grinding (LAG), evaporative crystallization, or co-melting are not easily adapted to a larger scale.[166] Slurry crystallization is viable at large scale batch mode, but continuous crystallization might be challenging.[166] One method that can be more readily scaled-up for co-crystallization is spray drying.[165,167–169] Spray drying can offer the advantages of continuous crystallization and isolation while producing a solid with small and narrow particle size distribution.[9–11] Spray drying can also be advantageous when preparing incongruently saturating co-crystals. Reports have shown that stoichiometric solutions can be used to generate phase pure co-crystals by spray drying in incongruently saturating systems.[101,168] This result means that addition of undesirable Class 2 solvents, as mentioned in the above paragraph, for solubility modification may be avoided with optimized spray drying parameters.

The final product of a spray drying process is influenced by the drying gas flow rate, inlet

temperature, solution feed rate, solvent, concentration of solute in the feed solution, as well as the geometry of the system. [170,171] The atomizing gas flow and solute concentration have significant impact on particle size, while solution feed rate and solvent can also contribute to differences in particle size. [170] Morphology of spray dried particles can also vary significantly which depends on the crystal lattice and diffusion of solute during rapid evaporation. [168,170] For example, a theophylline (TPY)-urea co-crystal had flake-like morphology, while TPY-saccharin exhibited irregular morphology when spray dried from the same solvent. [168] In another example, a Dapsone-caffeine co-crystal was prepared in three different solvents and all solids exhibited spherical morphology. [169]

Niclosamide (NCS) is an anthelmintic drug typically used for the treatment of tape worm in both humans and animals and is part of the World Health Organization's list of essential medicines. [144] NCS anhydrous form has an aqueous solubility of 13 µg/mL, while the hydrates exhibit even lower solubility of < 1 µg/mL. [145] As such, NCS falls in the Biopharmaceutical Classification System (BCS) as a class II drug (low solubility and high permeability). Co-crystals of NCS with a variety of co-formers have been reported in literature. [147,150,151] A NCS-urea co-crystal prepared by LAG with ethly acetatewas shown to give about two-fold solubility improvement compared to neat NCS in 40% isopropanol (IPA) in water at 37 °C using solids with similar particle size. [147] However, solubility assesment in biorelevant media was not investigated. The impact of particle size on dissolution of NCS co-crystals also has not been investigated. In addition, NCS co-crystals have not been prepared by scaleable techniques, such as spray drying, to the best of our knowledge.

The current work investigates spray drying as a co-crystallization process for NCS and the co-former, urea, in a Class 3 solvent, isopropanol (IPA). Here, a process is reported to reproducibly prepare phase pure NCS-UR co-crystals with small particle size. One objective of the co-crystallization is improvement of solubility of NCS in biorelevant media through combination of co-crystallization and particle size reduction. Another objective of the work is to obtain solubility data of anhydrous Niclosamide (NCS-A) and NCS-UR co-crystal in biorelevant media, which has not been reported in literature to the best of our knowledge.

4.3 Materials and Methods

4.3.1 Materials

NCS (>98% purity), was used as received without further purification from Millipore Sigma, Lot #: 058M4059V. Urea (>99% purity) was sourced from Fisher Chemical, Lot # 145423. Analytical grade 2-propanol (>99% purity) was sourced from Fisher Chemical, Lot # 185686.

4.3.2 X-ray Powder Diffraction

X-ray powder diffraction (XRPD) was performed using a Rigaku MiniFlex 600 in reflection mode with a Cu Kα source. The scan range was 4-30° 2θ with 0.05° 2θ step size. Samples were prepared on Si zero-return wafers.

4.3.3 Thermal Analysis

Differential scanning calorimetry (DSC) was performed using a Mettler Toledo DSC^{3+}. Samples (~3 mg) were weighed directly into hermetic aluminum pans with pin-hole. All measurements were performed under nitrogen gas flow from 30-250 °C at a rate of 10.0 °C/min. Simultaneous thermogravimetric analysis and differential scanning calorimetry (TGA/DSC) was performed using a Mettler Toledo TGA/DSC^{3+}. Samples (5-10 mg) were weighed directly in hermetic aluminum pans with pin-hole and analyzed from 30-250 °C at a rate of 10.0 °C/min.

4.3.4 Scanning Electron Microscopy

Scanning electron microscopy (SEM) for samples SD-1 through SD-7 was performed using a Hitachi Cold Field Emission SEM, model S4700 with 3 kV beam and 12.5 pA beam current. Samples were mounted on carbon tape and sputter coated with approximately 20 nm Au-Pd layer using a Leica EM ACE200 sputter coater. SEM for samples SD-8 and SD-9 was performed using a TESCAN MIRA3-LMU FESEM with 5 kV beam, approximately 7 nm beam spot size, and 250-260 pA beam current. Samples were mounted on carbon tape and sputter coated with approximately 15 nm Au layer using a BIO-RAD PS3 sputter coater.

4.3.5 Particle Size Analysis

Particle size distribution (PSD) of solids was assessed by analysis of SEM images. ImageJ was used to process 50 to 100 particles from each SEM image. [172]

4.3.6 Proton Nuclear Magnetic Resonance (^{1}H NMR)

^{1}H NMR was performed using a Nanalysis 60e NMReady 60 MHz spectrometer. Solids were dissolved in 0.75 mL deuterated tetrahydrofuran (THF-d_8) with two drops (approximately 30 μL) of D_2O to aid in solubility. Solutions were transferred to NMR tube (Wilmad 5 mm thin wall 8″ 200 MHz, 506-PP-8). The measurement conditions were 128 scans with 1.0 s relaxation delay and 3.7 s acquisition time at 33 °C.

4.3.7 Brunauer-Emmett-Teller (BET) Surface Area Measurement

BET analysis was performed on Micrometrics Gemini VII. The samples (200–250 mg) were degassed at 165 °C with a gentle flow of nitrogen gas for at least 16 h. Between 8 and 13 glass beads were added to the balance tube to compensate for low surface area of the samples. A 10-point analysis was used to determine BET surface area. Measurements were performed at P/P^0 values of 0.05, 0.08, 0.10, 0.15, 0.18, 0.20, 0.23, 0.25, 0.27, and 0.30.

4.3.8 NCS-UR Seed Formation

NCS-UR seed was prepared by co-evaporation. Approximately equimolar amounts of NCS (160 mg) and urea (35 mg) were dissolved in 20 mL of IPA and the solution was allowed to evaporate at 50°C while stirring. The resulting solids were dried under vacuum (< 0.5 mbar) at 50 °C for four hours.

4.3.9 NCS Anhydrous Form Preparation

Anhydrous NCS (NCS-A) was prepared by weighing about 300 mg NCS in a scintillation vial and adding 3 mL IPA. The mixture was stirred at 50 °C for 1 h and then filtered under reduced pressure. The solids were dried at 50 °C (-29.5 inHg) for 18 h. The dried solids were gently ground in a mortar and pestle to reduce particle size prior to characterization and solubility assessment.

4.3.10 TPD development

Slurries were prepared with varying compositions of NCS, urea and IPA at a 150 mg scale (total solid mass). All slurries were seeded with approximately 1 mg of NCS-UR co-crystal seed and were allowed to stir at room temperature (RT, 20-24 °C) for 5-7 days. Solids were filtered using 5 μm filter paper and XRPD analysis was conducted on the filtered solids (wet cake) to determine phase identity.

For NCS and urea, solubility points were determined by a solvent addition method similar to Reus procedure. [173] Slurries were created using 30 mg solid (total solid mass) with varying compositions of NCS, urea in IPA. The quantity of IPA, NCS and urea were recorded at each dissolution point, which was used to determine the solubility points on the TPD.

4.3.11 Spray Drying

Spray drying experiments were conducted using a Buchi Mini Spray Dryer B-290, which operates in a co-current flow direction in combination with a B-295 Inert Loop and is depicted in Figure 4.1. The spray dryer uses a two-fluid nozzle with a 0.7 mm diameter nozzle tip with compressed nitrogen at a pressure of 552 kPa as the atomizing gas. The atomizing gas flow was 246 L/h for all experiments. The spray dryer was equipped with a 0.33 m long × 0.15 m diameter spray cylinder, 330 mL high performance cyclone, and 45 mL collection vessel. Stock solutions of NCS, urea, or their mixtures were prepared in IPA at ambient conditions (3.3–7.5 mg/mL). A total of 200 mg solid was used for each experiment. For co-crystallization experiments equimolar solutions of NCS and urea in IPA were used. A total of 3 g solid was used for SD-8 and SD-9. The stock solution was fed to the spray dryer with a peristaltic pump (3 - 6 mL/min) and a high-performance cyclone was used to separate the solids from the gas stream. Evaporated alcohol was condensed in the sealed inert loop. Stock solution concentration and temperature of inlet and outlet were varied.

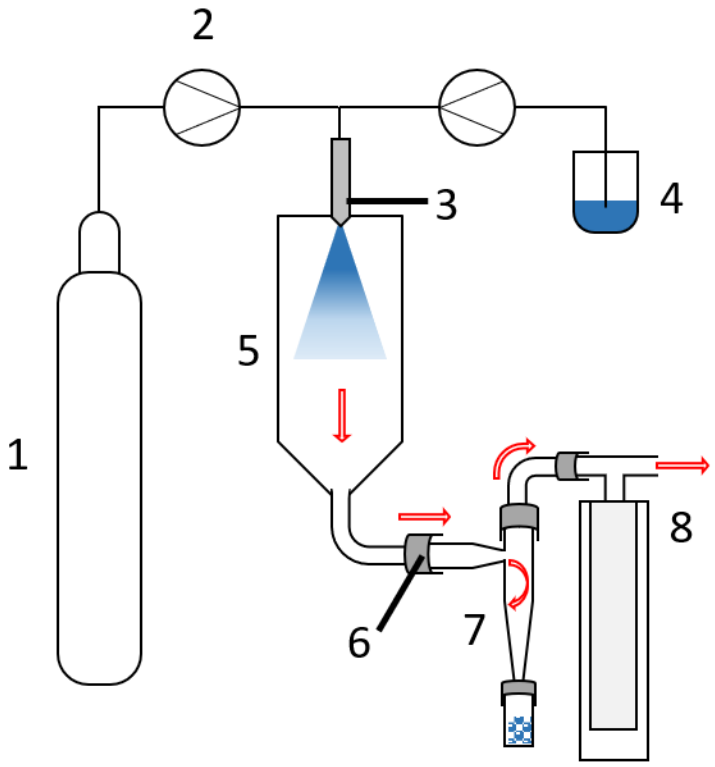

Figure 4.1- Schematic of spray dryer. 1- nitrogen supply, 2- pumps, 3- atomizer and inlet temperature, 4- feed solution, 5- drying chamber, 6- outlet temperature, 7- cyclone and collection vessel, 8-vent to inert loop through a bag filter. Arrows indicate direction of flow.

4.3.12 Solubility in Water and Biorelevant Media

Fasted state simulated gastric fluid (FaSSGF) was prepared using Biorelevant powder (Biorelevant.com). First, 0.200 g NaCl (Fisher Chemical) was dissolved in 90 mL of distilled water. The pH was adjusted to 1.6 using 1 N HCl (Millipore Sigma) and water was added to fill to volume in a 100 mL volumetric flask. Biorelevant powder (6 mg) was dissolved in 50 mL of salt solution and made up to 100 mL using the salt solution.

Fasted state simulated intestinal fluid (FaSSIF) was prepared using Biorelevant powder (Biorelevant.com). First, a phosphate buffer was prepared by dissolving 0.042 g of NaOH pellets (Fisher Chemical), 0.395 g $NaH_2PO_4.H_2O$ (Fisher Chemical), and 0.619 g NaCl in 90 mL distilled water. The pH was adjusted to 6.5 by adding 1 N NaOH solution or 1N HCl and distilled water was added to fill to volume in a 100 mL volumetric flask. Biorelevant powder

(0.224 g) was dissolved in 50 mL of the phosphate buffer solution and made up to 100 mL using phosphate buffer solution. The prepared solution was allowed to stand for 2 h as per Biorelevant instruction.

Solubility in water and simulated fluids was carried out at 37 °C on a stirred heating block (ThermoFisher). Solids (~4.5 mg) were weighed in 4 mL and 2.25 mL of distilled water or simulated fluid was added. All samples were prepared in triplicate. The thin slurries were stirred until the sampling time. Approximately 1 mL of the slurry was drawn using a syringe and filtered through a 0.45 µm PTFE filter directly into an high performance liquid chromatograph (HPLC) vial for analysis.

HPLC analysis for solubility assessment was done using an Agilent 1260 Infinity II HPLC equipped with a Waters XBridge C18 column (4.6 × 15 mm, 3.5 µm). A calibration line was built using NCS-A prepared at various concentrations (1.12, 5.6, 11.2, 56, 154, and 308 µg/mL). Triplicate samples were prepared for 154 µg/mL. The slope was calculated as 7.2289 mAu(mg/mL)$^{-1}$ with a correlation coefficient (R^2) greater than 0.99. Concentration of NCS-A and NCS-UR in water and simulated fluids were calculated by comparing the NCS peak area to the calibration line (Figure 4.2).

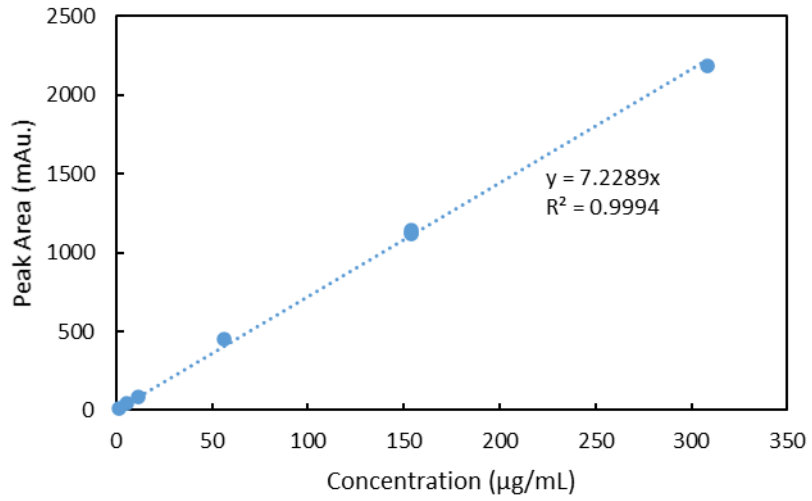

Figure 4.2- HPLC calibration curve for NCS-A.

4.4 Results and Discussion

4.4.1 Characterization of NCS, Urea, and NCS-UR

Bulk NCS showed XRPD diffraction peaks characteristic of both anhydrous (NCS-A) and monohydrate (NCS-H) forms, the diffractograms are shown in Figure 4.3. [147,148] The diffractogram of NCS-A prepared in IPA agreed with powder diffraction data of van Tonder *et al,* and are also shown in Figure 4.3. [145] The urea diffractogram showed characteristic peaks at 22.4-22.5° 2θ. TGA/DSC of the starting NCS material showed that it was a physical mixture of NCS-A and NCS-H. [145] Based on mass loss in TGA (1.15% w/w), approximately 22 % w/w of the starting material was NCS-H, which can be found in Figure 4.4. The melting onset of NCS-A was 231 °C and urea was 134.5 °C by DSC, and their thermograms are shown in Figure 4.5.

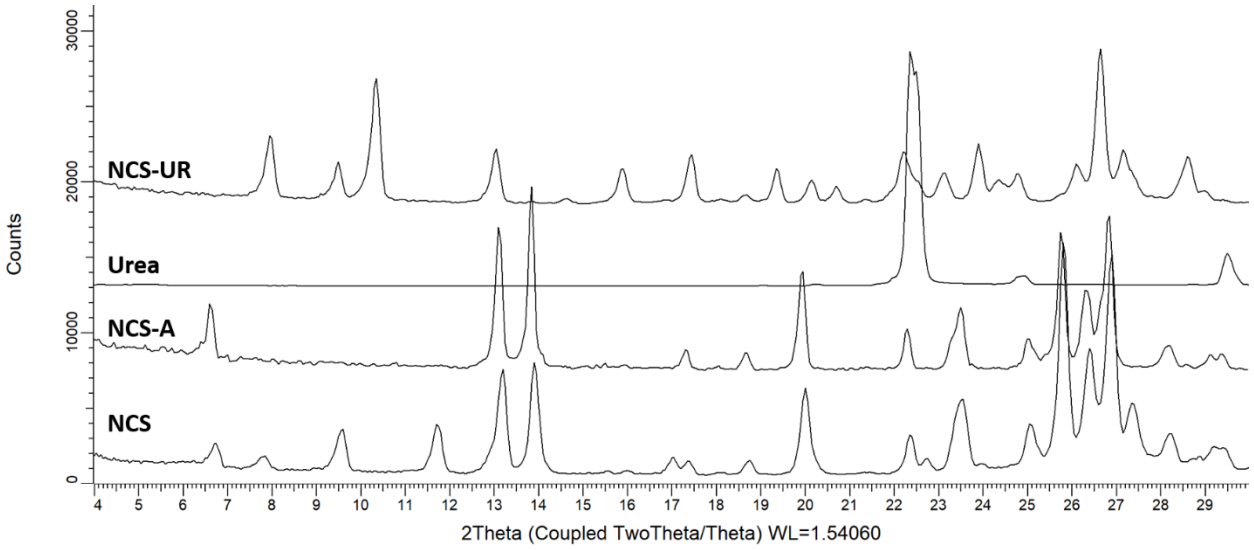

Figure 4.3- XRPD diffractograms of NCS, NCS-A, urea and NCS-UR formed through co-evaporation.

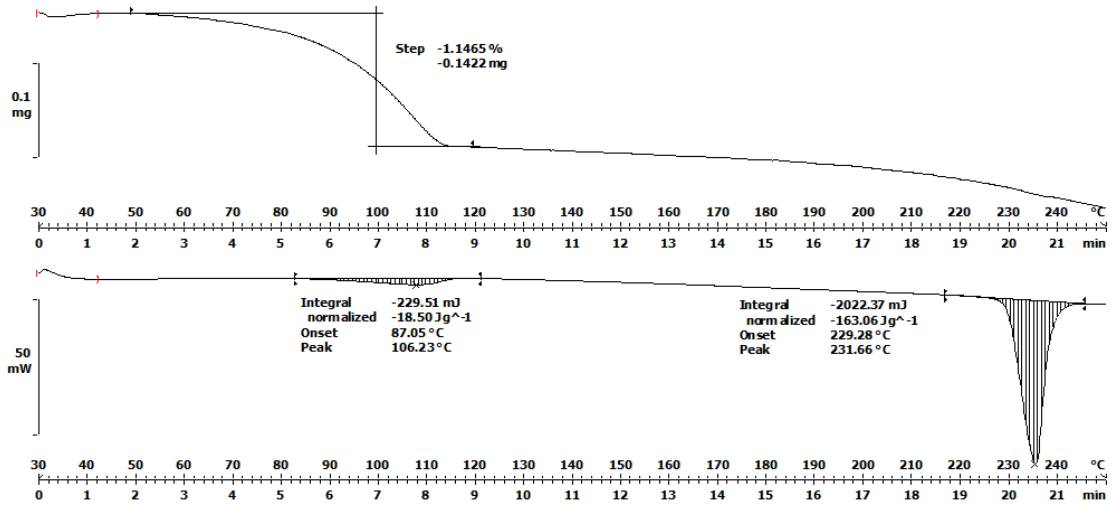

Figure 4.4- Simultaneous TGA/DSC thermograms of NCS.

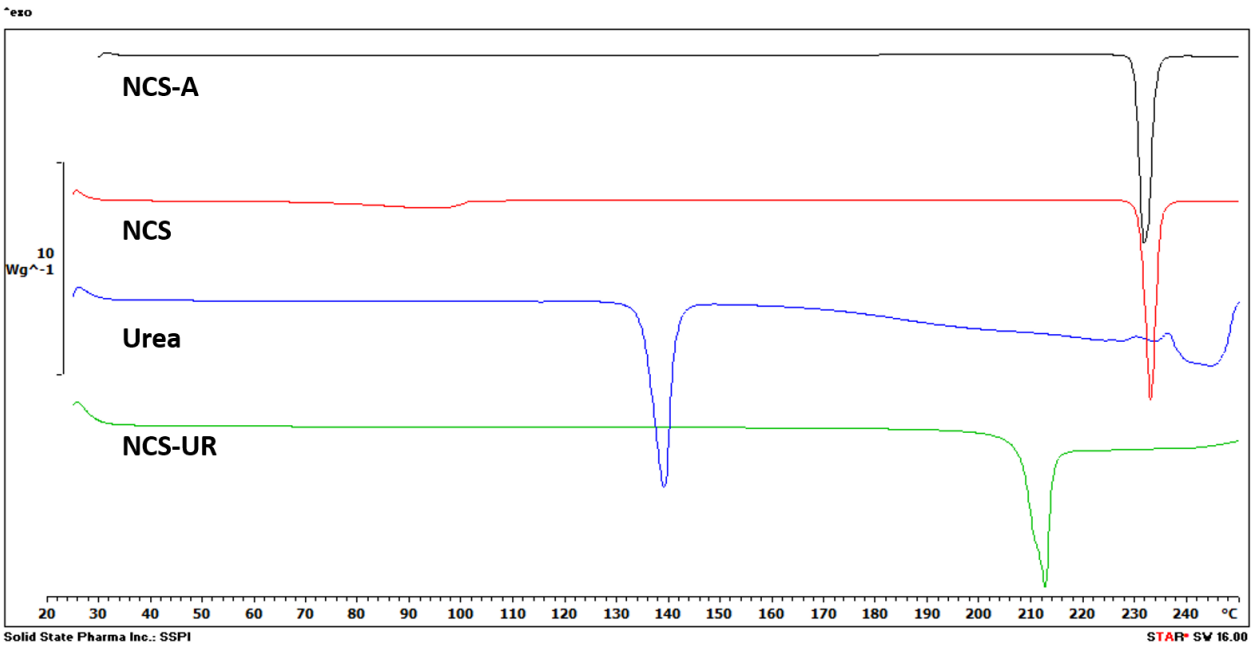

Figure 4.5- DSC thermograms of NCS-A, stock NCS, urea, and NCS-UR formed through co-evaporation.

Co-evaporation was successful in producing NCS-UR as confirmed by XRPD and DSC. Based on XRPD and DSC analysis, the co-crystal was phase pure because NCS and urea were not detected. However, determining the detection limits for NCS and urea by these analytical techniques were considered outside the scope of this work. The overlay of the XRPD

diffractograms of NCS, NCS-A, urea and NCS-UR formed through co-evaporation are shown in Figure 4.3. The diffractogram obtained for NCS-UR agrees with the co-crystal reported by Sanphui. [147] The structure and hydrogen bonding motif of the co-crystal was determined by Sanphui and is shown in Figure 4.6. [147] The NCS-UR co-crystal is formed through O–H···O (d-a 1.80 Å, ∠176.6 °) hydrogen bonding between OH of NCS and carbonyl of urea, and N–H···O (d-a 2.17 Å, ∠154.3 °) hydrogen bonding of NCS amide oxygen to urea amine. There is only one reported polymorph of the NCS-UR co-crystal. In addition, throughout this work there was no evidence of a different polymorphic form of NCS-UR by XRPD or DSC analysis. However, the crystallization of NCS-UR has only been reported from two solvent systems: ethyl acetate (EtOAc) by Sanphui, and IPA (this work). [147] Thus, the polymorphic landscape of NCS-UR is rather unexplored.

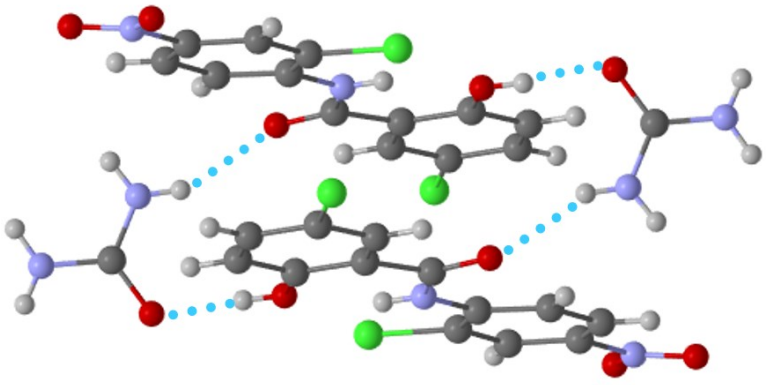

Figure 4.6- Hydrogen bonding of NCS-UR using single crystal diffraction data from Sanphui. [147]

NCS-UR was characterized by DSC and showed a melting onset of 209 °C, between the melting onsets of urea and NCS-A, also agreeing with previous reports. [147] [29] The melting onset of NCS-UR also agrees well with the predicted melting temperature based on the correlation proposed by Perlovich. [28] Pervlovich's correlation predicts 193 °C, a 3.4% (16 °C) difference, which is within the standard deviation reported for the correlation. The predicted melting onset was obtained using equation (2).

$$T_{fus}(\text{NCS-urea}) = A + B \cdot T_{fus}(\text{NCS}) \quad (2)$$

where A and B were determined by fitting known melting points of 11 urea-containing co-crystals to equation (2). The values of A and B obtained for urea co-crystals were 139.66 and

0.648, respectively. [28]

4.4.2 TPD Development

A TPD was successfully developed for NCS-UR in IPA at room temperature using the XRPD data from slurry solids as well as solubility points from the solvent addition method. A total of 37 data points were used to construct the TPD with 21 slurry compositions and 16 from solubility points. For solubility assessment, mixtures of NCS-A and urea were prepared varying from 100% NCS-A to 100% urea in 10% increments by mass ratio (i.e. 90%, 80%, …, 10% NCS). Between 1.2 and 2.5 mL of IPA were gradually added incrementally while stirring to dissolve the solids. As the mixtures neared the dissolution point, the volume of solvent added in each aliquot was decreased to determine the saturation concentration more accurately. To define the solubility line near the eutectic of NCS-A and NCS-UR, solubility points at compositions of 82-86% NCS were assessed at 100 mg scale. Between 6.17 and 6.25 mL of IPA were added for each of these experiments in a similar manner as described above. The solubility points were plotted on the TPD by calculating mole fractions of NCS-A, UR, and IPA at the dissolution point.

To assess the composition of solid phase, slurries were prepared varying from 100% NCS-A to 100% urea in 10% increments by mass ratio (i.e. 90%, 80%, …, 10% NCS-A). A constant volume of IPA (3 mL) was added to the slurries. To better define the phase boundary between ‘N+S’ and ‘N+CC+S’, as well as ‘U+CC+S’ and ‘U+S’ regions (which can be seen in Figure 4.7 and Figure 4.8), additional slurry points were added. The compositions of slurries were determined based on the expected location of the phase boundaries. The slurries comprised 92-98% NCS-A (with 2-8% UR by mass) and 0.5-8% NCS-A (with 92-99.5% UR by mass), respectively. IPA was added to the solid mixtures to maintain a molar ratio of 98 or 95%, respectively. A constant mole ratio of IPA was selected for the additional series of slurries to produce a horizontal line of data points that crossed the expected phase boundary, in contrast to the constant volume of IPA in the first series which produced a diagonal line. After filtration and XRPD analysis of the solid phase, the data was overlaid on the TPD. The solubility points in combination with solid phase data were used to determine the phase boundaries.

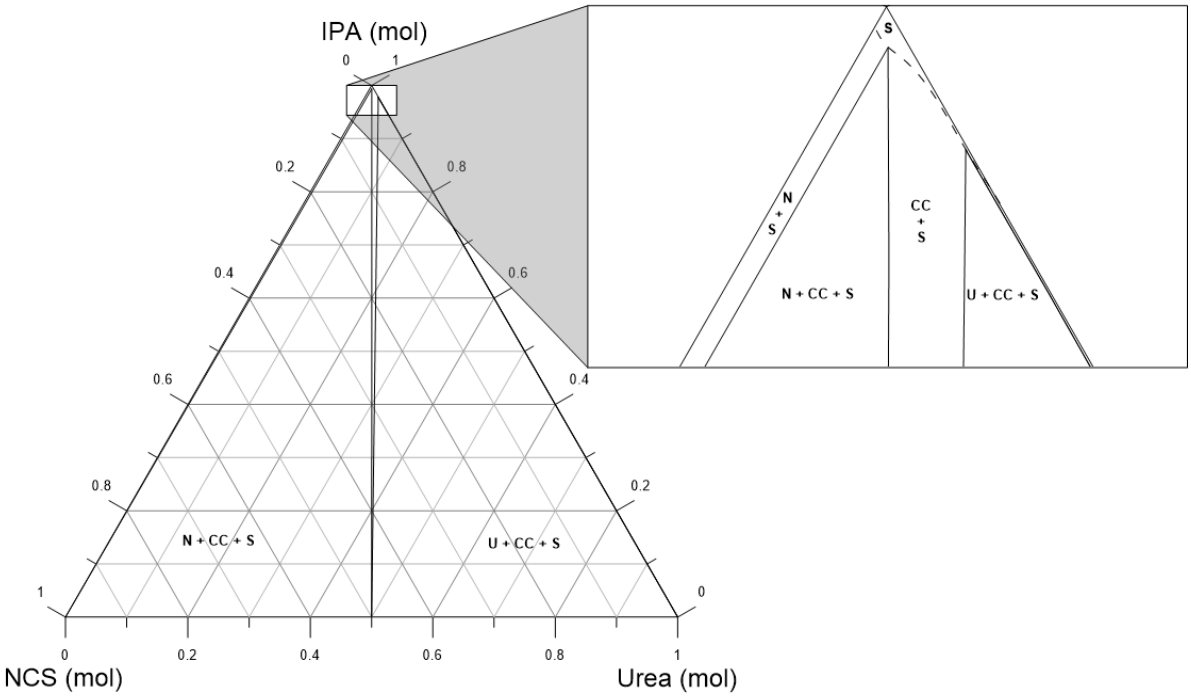

Figure 4.7- Full TPD for NCS, urea and IPA between 20 and 24°C in mol fractions. Specific regions where each phase is present are defined; S: solution, N: NCS-A, CC: NCS-UR co-crystal, U: urea.

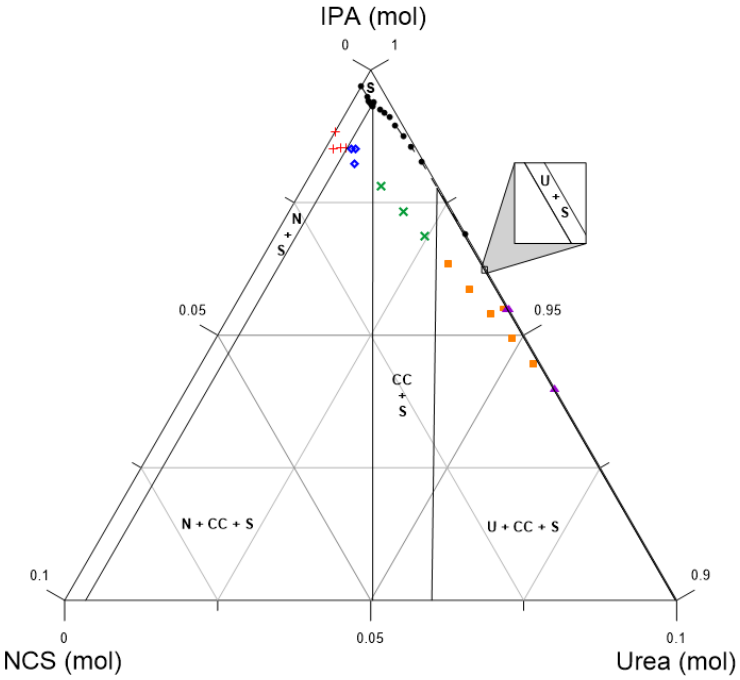

Figure 4.8- Zoom of TPD for NCS, urea and IPA between 20 and 24°C in mol fractions. Specific

regions where each phase is present are defined; S: solution, N: NCS-A, CC: NCS-UR co-crystal, U: urea. solvent addition solubility points (circles, black), and solid phases from the slurry: NCS (+, red), NCS + NCS-UR (open diamond, blue), NCS-UR (×, green), NCS-UR + urea (filled square, orange), urea (filled triangle, purple).

Figure 4.7 and Figure 4.8 show the TPD developed along with the data points used for solubility and solid phase determination. The co-crystal stability region is skewed slightly to the right meaning that the NCS-UR system is incongruently saturating in IPA. Evaporative techniques can produce the co-crystal with equimolar solutions, which was observed from co-evaporation from IPA solution.

When developing a solubility line in a TPD by means of solvent addition, the solid phase data must be obtained separately to better define the phase boundaries. In this work a combination of solvent addition method and solid form data from slurries was used to determine the stability regions. The results indicate that the co-crystal is stable as the single solid phase in the IPA solvent system at RT only when urea is present in at least stoichiometric (1:1) quantity. A mixture of NCS-A and NCS-UR is observed at sub stoichiometric urea amounts. In such a system, a slight excess of urea could be added, and the co-crystal will be isolated by filtration. In a process such as spray drying, it is possible that excess urea is not required to produce a pure form of the co-crystal. It has previously been shown that metastable forms are accessible by spray drying methods. [101,174] Thus, spray drying was explored as a process for producing NCS-UR.

4.4.3 Production of NCS-urea Co-crystal by Spray Drying

Spray drying of NCS-UR was explored using equimolar ratios of components in solution. Based on the TPD, evaporation from a 1:1 solution should produce a pure form of the co-crystal. Parameters explored during spray drying of NCS-UR included concentration of feed solution, varying from 3.3 to 7.5 mg/mL, and inlet temperature, varying from 70 to 128 °C, Table 1. One series of experiments varied the inlet temperature, while another maintained constant inlet temperature and the feed solution concentration varied. The feed solution concentration can impact particle size and cyclone efficiency. An increase in the feed solution concentration is expected to give rise to larger particles due to more solid being available for particle formation.

A consequence of larger particle size is improved cyclone efficiency, which leads to better yield. [170] The temperature can also impact efficiency (yield) because a drier solid will adhere less to the cyclone and be collected in higher quantity in the collection vessel. [170,175] The temperature range of 70 to 128 °C was selected based on the boiling point of IPA. Drying of droplets can be achieved at temperatures lower than the boiling point of the feed solvent, so a lower value of 70 °C was selected. [101,175] The upper limit of 128 °C was selected to produce an outlet temperature above the boiling point of the solvent. A wide span of temperature was selected to assess impact on particle size, co-crystal form purity, and yield. The feed solution concentration range was selected to be undersaturated based on the solubility of the co-crystal components in IPA. Specifically, solubility of the less soluble component, NCS-A, in IPA was determined at 13.2 mg/mL by the solvent addition technique. Thus, the feed solution concentrations were prepared at less than 50% saturation of NCS-A.

Solids were recovered directly from the collection chamber for calculation of yield and characterization by XRPD, DSC and SEM. Yields from spray drying experiments were calculated on a molar basis, assuming 1:1 stoichiometry of the collected product, equation (1).

$$Yield(\%) = 100 \times {mol_{NCS-UR}}/{mol_{NCS}} \quad (1)$$

Yields of the 200-mg spray drying runs varied from 45% (90 mg) to 73% (146 mg), Table 1. The product yields obtained from experiments may be low because the drying process could result in generation of fine solids, which consequently entrain from the cyclone. Due to static nature of the solid prepared by spray drying, there was also a tendency for some solids to retain in the cyclone instead of accumulating in the collection chamber. While the variation in yield at 200 mg scale is high, the nature of the solid and challenges with collection make interpretation of trends in yield inconsequential.

Spray drying was successful in generating spherical particles as observed by SEM shown in Figure 4.9. The spherical 3-D morphology can offer improvements on the 2-D needle like morphology of bulk NCS (mixture of NCS-A and NCS-H) in terms of flowability. For three of the runs (SD-4, SD-5, SD-7) particle size was assessed through image analysis and the cumulative distributions are shown in Figure 4.10. All three solids had average particle size of less than 5 μm diameter, Table 4.1. The solids from run SD-7 (lowest drying temperature)

exhibited slightly narrower PSD. This may be attributed to the slower drying and longer time to reach the particle "locking point" during evaporation. [175] Cyclone efficiency increases with particle size, therefore the smaller particles from SD-7 (2.0 μm) compared to SD-5 (3.4 μm) likely also contributes to the observed decease in yield for SD-7. [176] However, PSD determination through image analysis can be biased and further studies at larger scale would be required to understand the impact of spray drying parameters on particle size in this system.

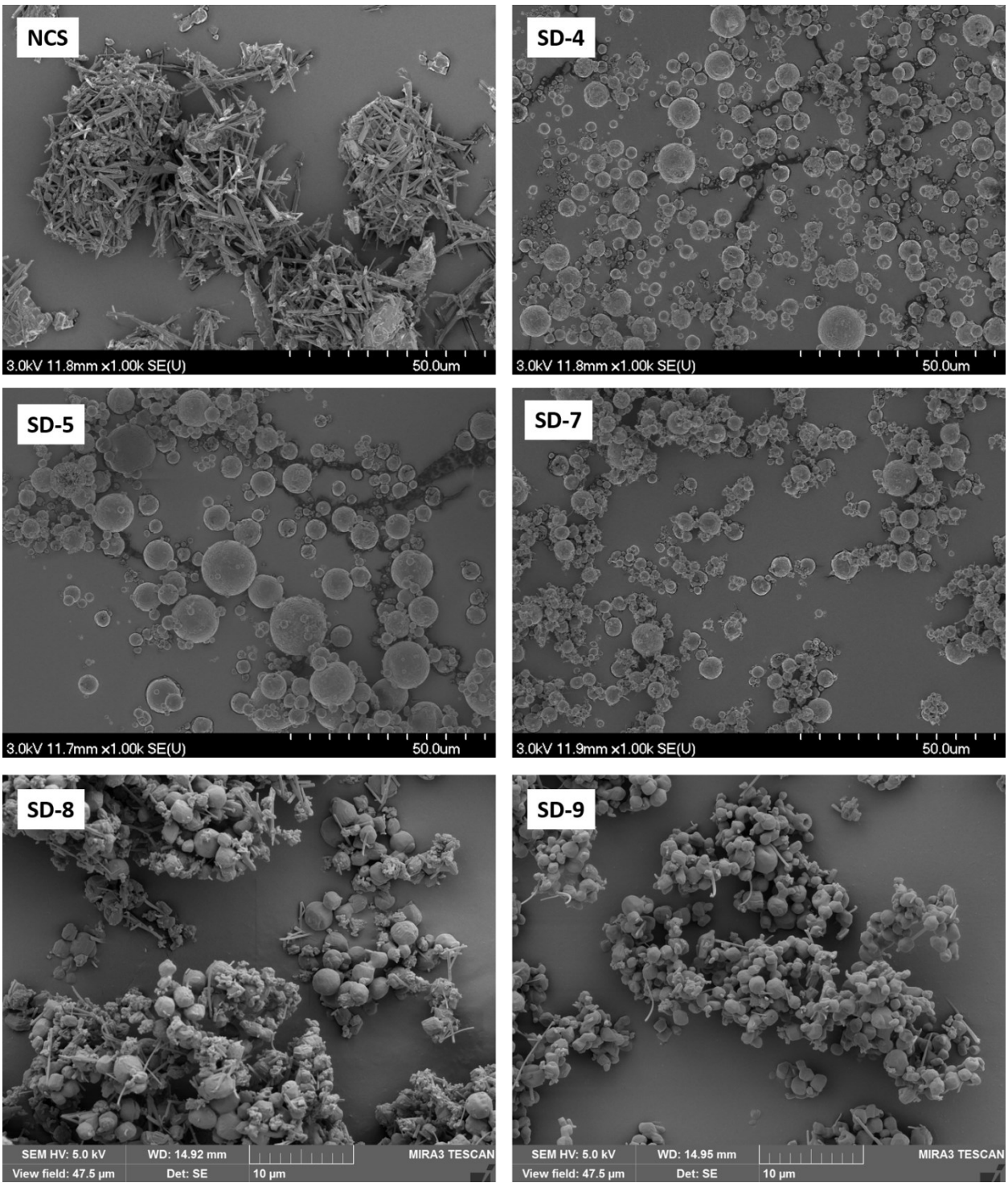

Figure 4.9- SEM images of bulk NCS (NCS-A and NCS-H) and solids obtained from SD-4, SD-5, SD-7 and 3 g scale SD-8, SD-9.

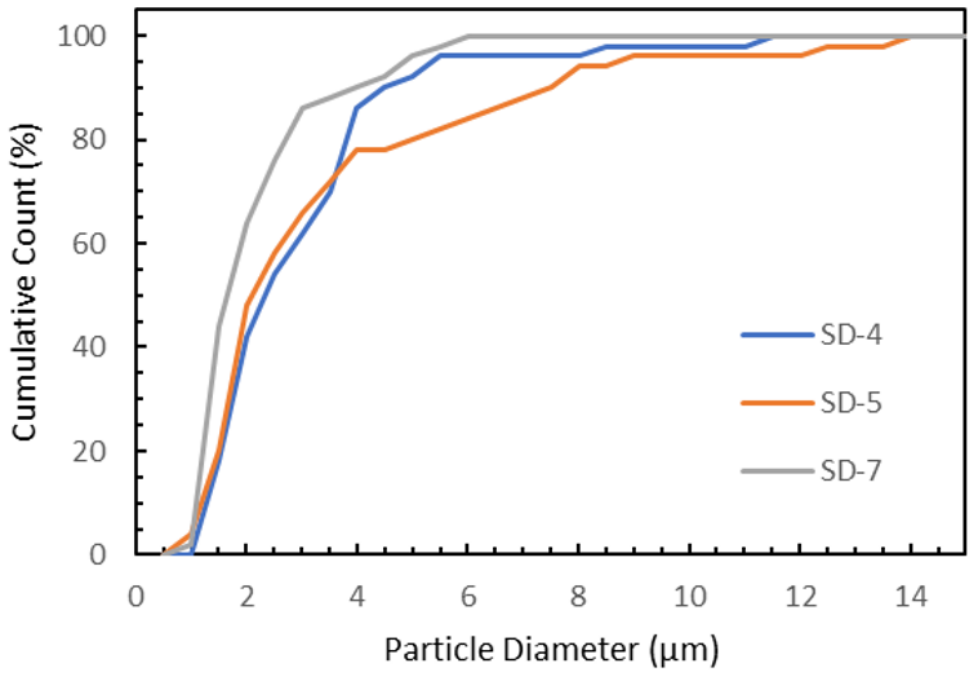

Figure 4.10- Cumulative particle size distribution of solids from SD-4, SD-5, and SD-7 based on analysis of 50 particles.

The solid phase purity of product was assessed by XRPD and DSC analysis. In all instances, the samples appeared phase pure by XRPD and are shown in Figure 4.11. DSC analysis of solids also agrees with phase pure co-crystals which is observed by the single endothermic events in Figure 4.12. However, the limit of detection of these two techniques for this data set has not been determined.

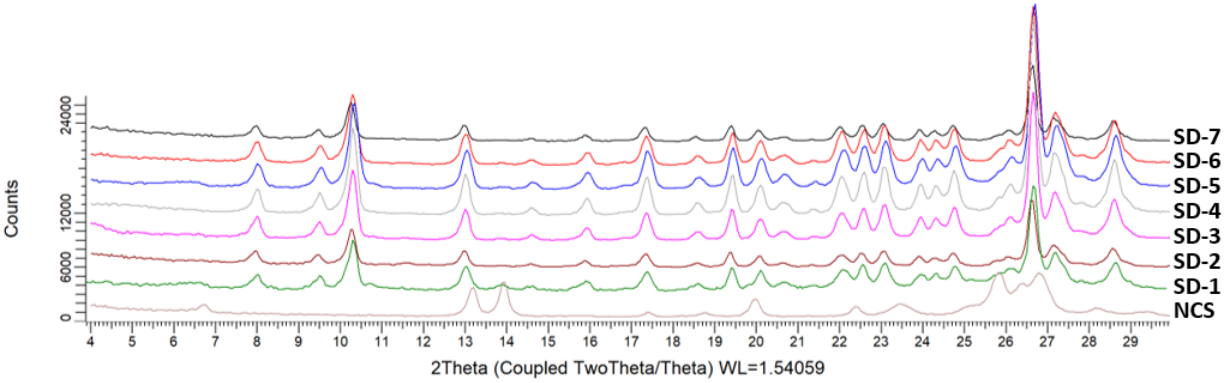

Figure 4.11- XRPD diffractograms of spray dried NCS-UR runs 1 through 7. Spray dried NCS reference shown on the bottom.

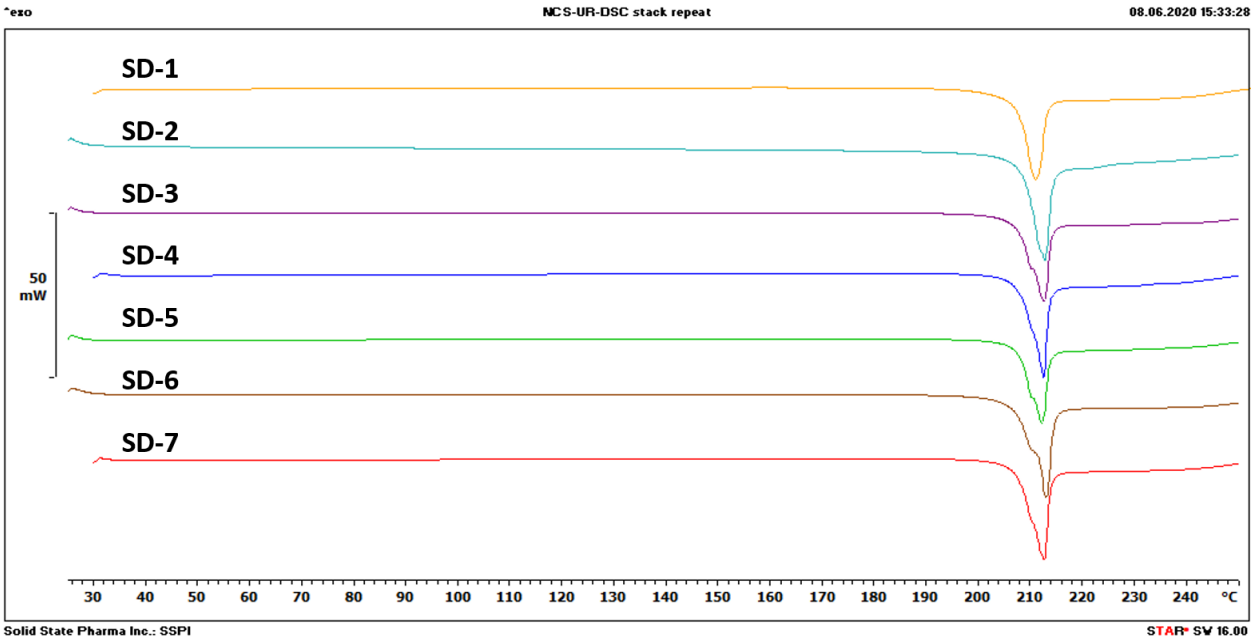

Figure 4.12- DSC thermograms of spray NCS-UR runs 1 through 7.

Table 4.1- Spray drying experiment operating parameters and summary of resulting solids.

Test	Concentration (mg/mL)	Inlet Temperature (°C)	Outlet Temperature (°C)	Aspirator (m^3/h)	Yield (%)	XRPD Result	DSC Result	Average Particle Diameter
Co-evap	9.8	n/a	n/a	n/a	~ 100	CC	CC	N.D
SD-1	5	128	88	30	59	CC	CC	N.D
SD-2	5	100	59	30	60	CC	CC	N.D
SD-3	5	90	52	30	62	CC	CC	N.D
SD-4	5	85	50	39	N.D.	CC	CC	2.8 ± 1.8[1]
SD-5	7.5	85	52	39	69	CC	CC	3.4 ± 2.8[1]
SD-6	3.3	85	50	39	73	CC	CC	N.D
SD-7	5	70	40	39	45	CC	CC	2.0 ± 1.1[1]

Note. n/a not applicable; N.D. not determined. [1] Results from image analysis of 50 particles.

Spray drying is a rapid process so co-crystal formation is heavily influenced by kinetics, while TPDs represent equilibrium systems at a specific temperature, therefore the direct application of TPDs to spray drying is limited, but they can still be used to explain experimental results. Even the fastest drying processes did not show evidence of crystalline NCS-A or urea in the spray dried particles. NCS-A has lower solubility than urea in IPA by about an order of magnitude, which could possibly lead to NCS precipitating if the process were stressed (e.g. higher evaporation temperature). However, neither NCS-A nor urea were observed supporting that this is a phase pure co-crystal. Due to the nature of the crystallization method (evaporation), techniques such chromatography and nuclear magnetic resonance may not illustrate the phase purity since components should still be present in an equimolar ratio. Further investigation into amorphous content may be required to determine true phase purity.

4.4.4 Scale-Up and Solubility Study

Two spray drying experiments were scaled up to 3 g for additional characterization such as residual solvent content, surface area, and solubility assessment. The method parameters were selected based on runs SD-2 and SD-4, Table 4.1. The concentration, flow rate, and aspirator were held constant for both experiments at 5 mg/mL, 6 mL/min, and 39 m^3/h. The product yield for the experiments were between 47 and 49% w/w. Mass balance showed that a significant portion of the product was lost to the cyclone (14 to 18% w/w). The solids collected were approximately phase pure NCS-UR co-crystal based on XRPD and DSC analysis, which can be found in Figure Figure 4.13 and Figure 4.14. ^{1}H NMR showed that the residual IPA in the collected solids was 0.50 and 0.48 wt.% for SD-8 and SD-9, respectively, falling within acceptable limits based on the ICH residual solvent guideline for IPA (5000 ppm, 0.5 wt.%). [63] The NMR spectra and peak areas are given in Figure 4.15 and Figure 4.16.

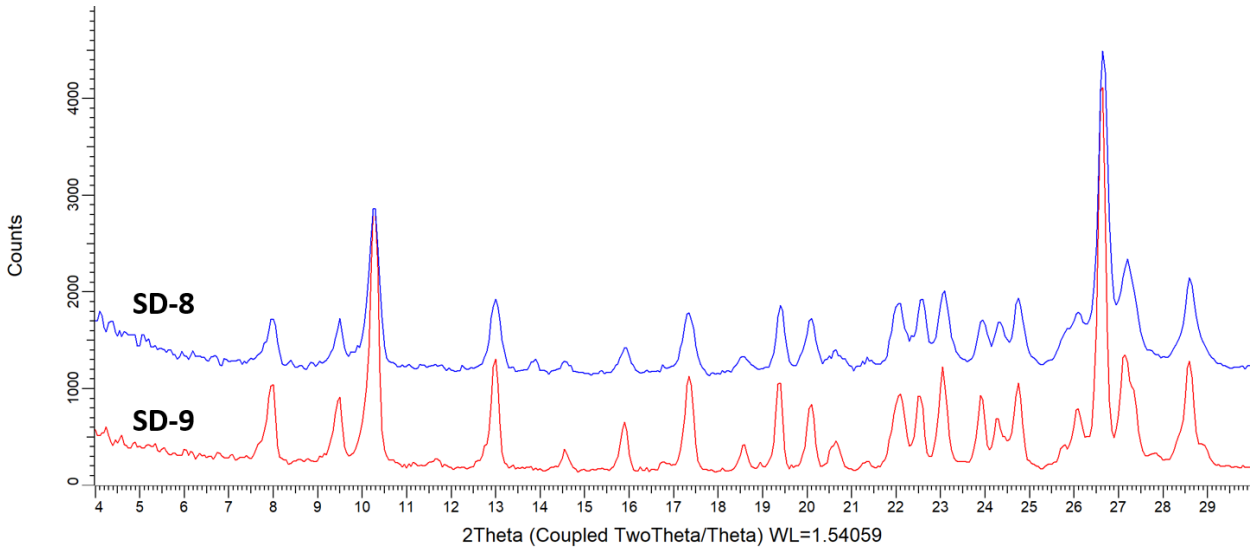

Figure 4.13- XRPD diffractograms of solids from 3-g scale runs SD-8 and SD-9.

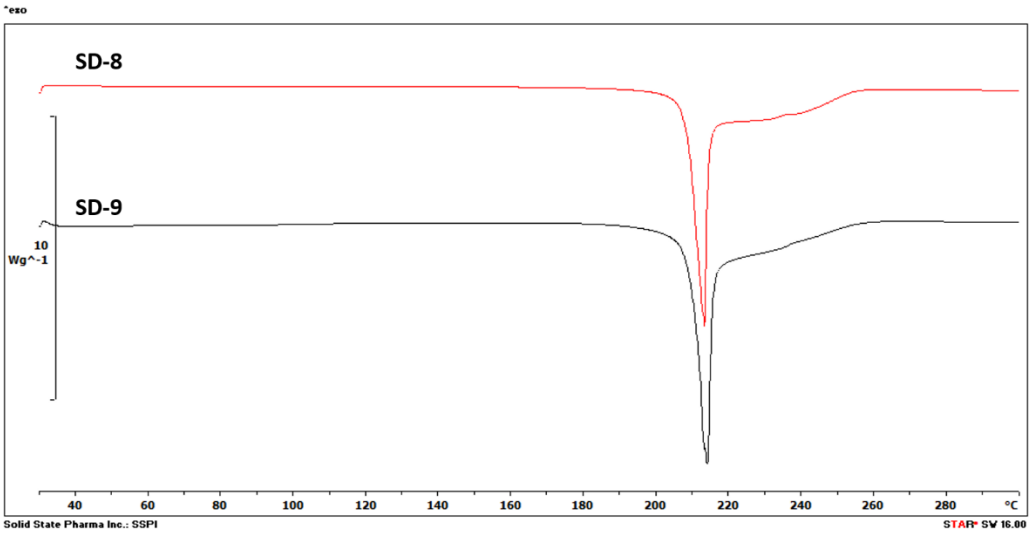

Figure 4.14- DSC thermograms of solids from 3-g scale runs SD-8 and SD-9.

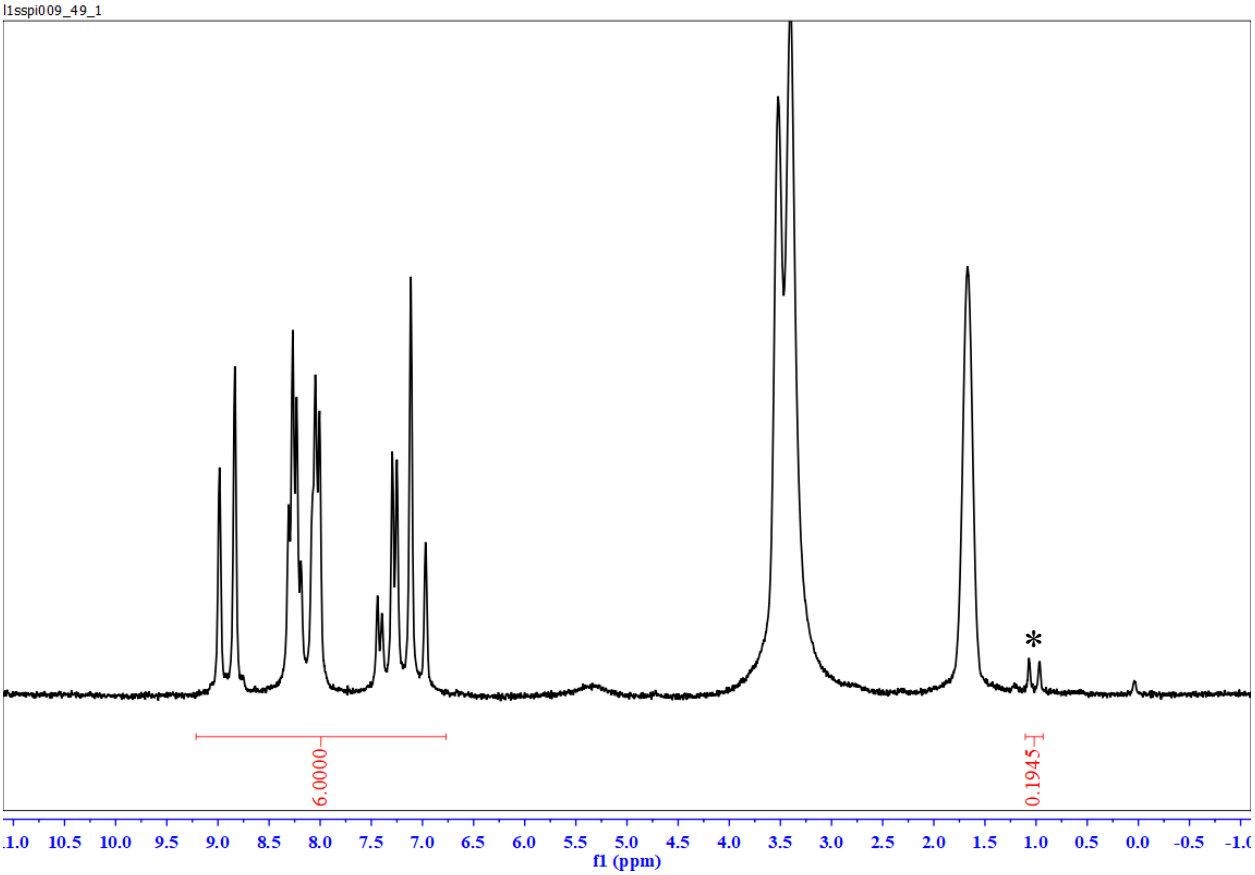

Figure 4.15- ^{1}H NMR of solids from 3-g run SD-8. IPA doublet indicated with asterisk.

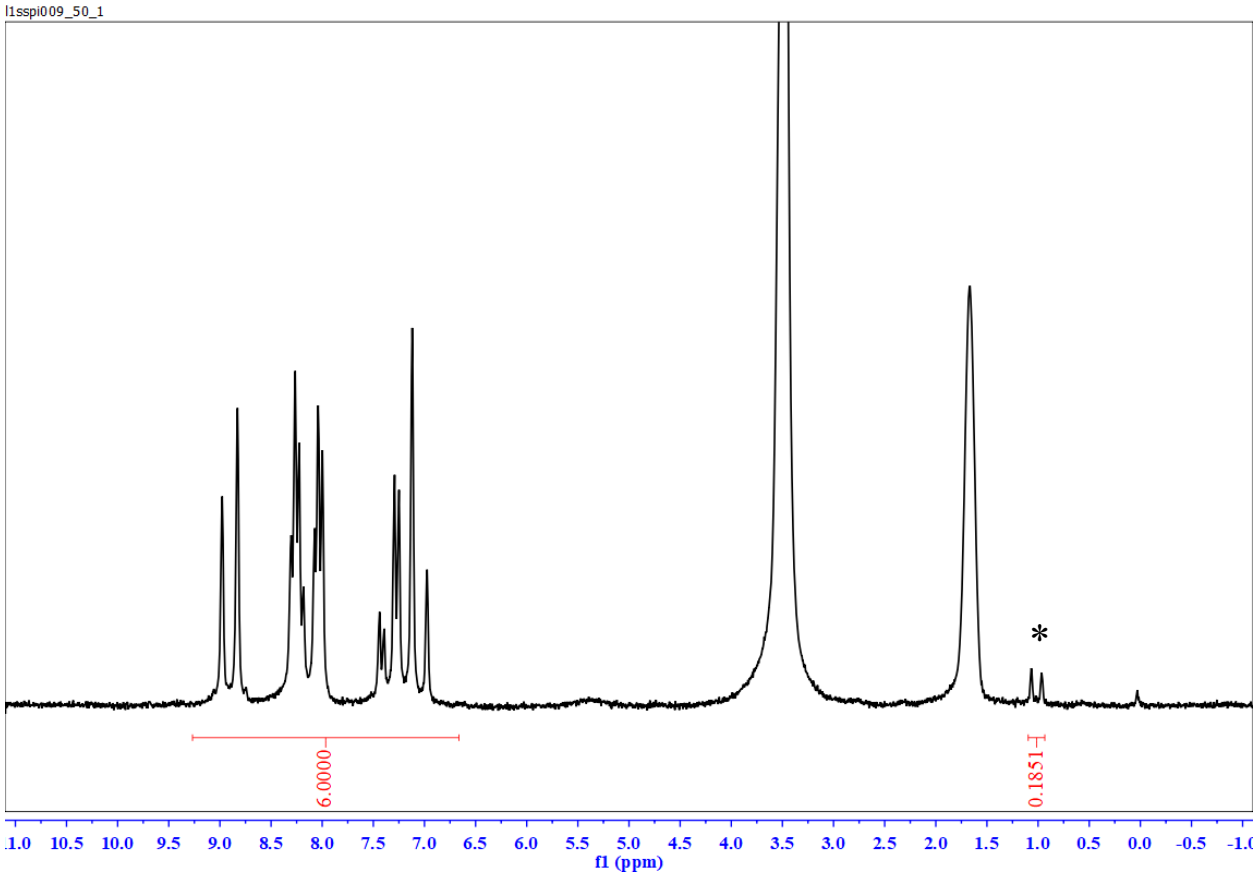

Figure 4.16- 1H NMR of solids from 3-g run SD-9. IPA doublet indicated with asterisk.

Particle size and surface area of pharmaceuticals directly impacts the dissolution rate, so the solids obtained from SD-8 and SD-9 were subject to particle size and BET surface area analyses. The particle size of the solids from 3 g scale experiments was estimated by image analysis of 100 particles and is summarized in Table 4.2 and Figure 4.17. The average particle size from image analysis of solids from SD-8 was 1.4 µm and of solids from SD-9 was 1.2 µm. The observed average particle size follows the same trend as observed in the small-scale experiments, Table 4.1 1, but the 0.2 µm difference is within the error of analysis. The mean particle size for SD-8 and SD-9 are notably lower than the small-scale experiments based on image analysis. However, the error for the image analysis of the 200-mg scale runs (SD-4, 5, and 7) is substantial due to small sample size and thus, the results for SD-8 and SD-9 are not statistically different. The lower drying temperature in run SD-9 (51 °C) gave rise to smaller particles with more narrow distribution than the particles obtained from SD-8 with a slightly higher drying temperature (58

°C). The surface area of SD-8 and SD-9 were 1.32 and 0.93 m^2/g, respectively, the details of which are found in Figure 4.18 and Figure 4.19. Although the particle size for run SD-8 is slightly larger than SD-9, the SEM images show that the particles from SD-8 qualitatively exhibit more irregular texture in comparison to SD-9. This may be why SD-8 has higher surface area than SD-9. In addition, some cord-like particles were observed in the SEM of SD-8 and SD-9 which were not observed at small scale. However, there was no evidence of a different polymorph of NCS-UR, nor excess NCS or UR by XRPD and DSC analysis.

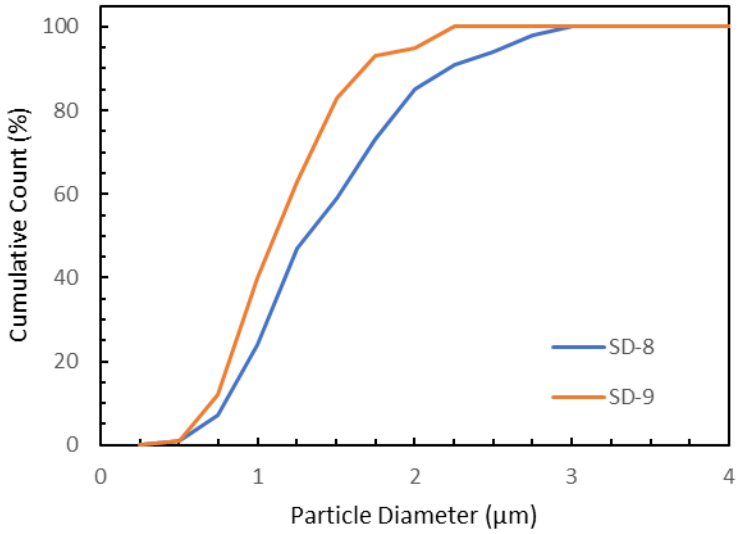

Figure 4.17- Cumulative particle size distribution of solids from 3-g runs SD-8 and SD-9 based on analysis of 100 particles.

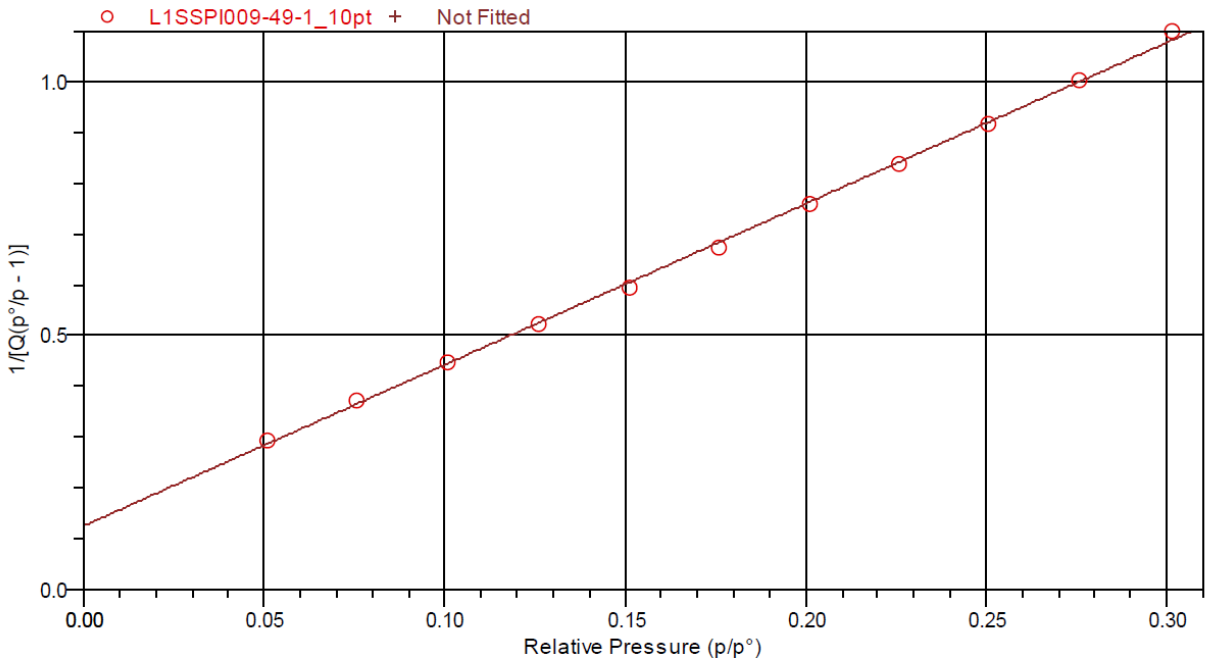

Figure 4.18- BET surface area plot for solids from 3-g run SD-8.

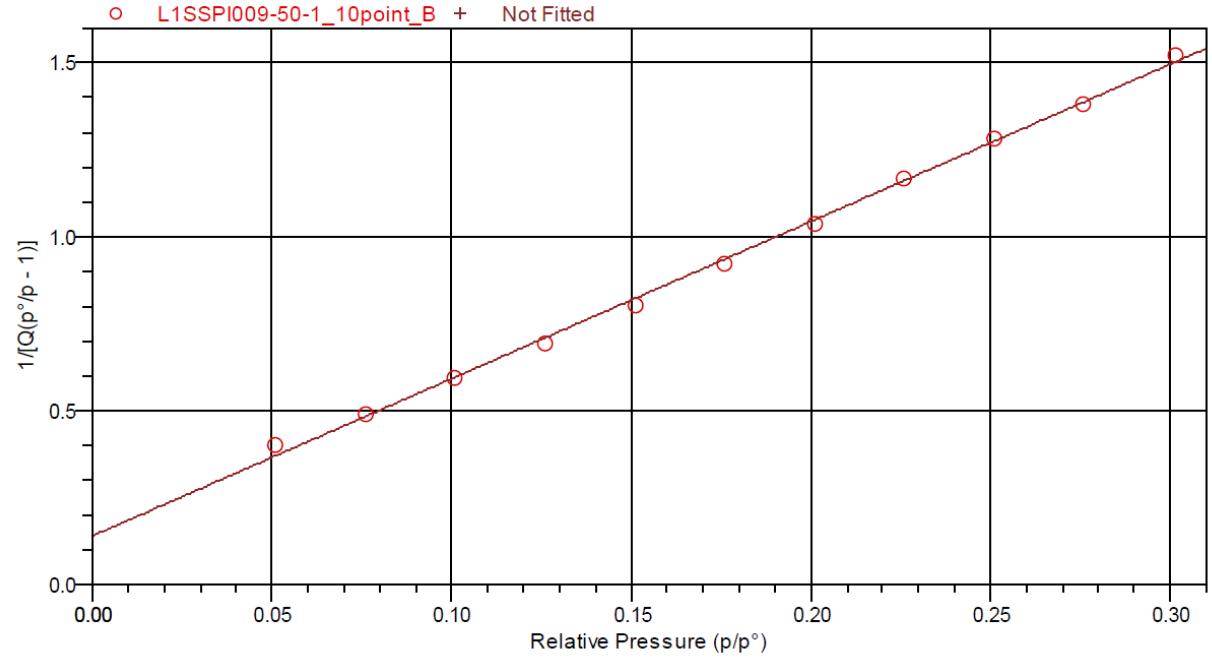

Figure 4.19- BET surface area plot for solids from 3-g run SD-9.

Table 4.2- Parameters and results from 3-g scale spray drying experiments.

Test	Inlet Temperature (°C)	Outlet Temperature (°C)	Yield (%)	Mass collected from cyclone (%)	XRPD Result	DSC Result	Average Particle Diameter (µm)	Residual IPA (wt.%)	BET Surface Area (m^2/g)
SD-8	100	58	49	18	CC	CC	1.4 ± 0.6[1]	0.50	1.32 ± 0.01
SD-9	85	51	47	14	CC	CC	1.2 ± 0.4[1]	0.48	0.93 ± 0.01

[1] Results from image analysis of 100 particles.

The solubility of NCS-UR was assessed in 40% IPA in water and NCS-UR by Sanphi *et al.* [147] In their paper, NCS-UR showed approximately a 2-fold improvement in solubility over NCS at 2 h and 24 h timepoints. However, to the best of our knowledge, there has not been a comparison of NCS-UR to NCS-A in biorelevant media. The solubility of spray dried NCS-UR was compared to NCS-A in water and biorelevant media at 37 °C to determine if the co-crystal with small particle size would provide an improvement in kinetic (1 h) or equilibrium (24 h) solubility compared to NCS-A. The solubility in water showed variability between triplicate samples compared to buffered media. At both 1 h and 24 h timepoint, the results for NCS-A and NCS-UR were not statistically different in water. This may be due to inhomogeneity in sampling with small quantities. The pH of the samples in water was similar for NCS-A (7.81) and NCS-UR (7.59 – 7.79) at the 24 h mark. In FaSSIF (pH 6.5) there was less variability between triplicate samples and NCS-A exhibited improved solubility compared to NCS-UR at both timepoints. At 1 h, SD-9 exhibited improved solubility compared to SD-8, which is likely related to the smaller particle size of the solids. Solubility at 24 h was statistically the same for SD-8 and SD-9. Likewise, the pH at 24 h was similar for NCS-A (6.60) and NCS-UR (6.53 – 6.54) in FaSSIF. Solubility was below detectable limits (BDL) in FaSSGF (pH 1.6) at all timepoints for NCS-A and NCS-UR. After stirring for 24 h, solids from water and FaSSIF slurries were recovered for XRPD analysis. The XRPD of solids recovered from the slurries agreed with NCS-H as shown in Figure 4.20.

Table 4.3- Solubility in water and biorelevant media for NCS-A and NCS-UR.

Input Solid	Fluid	Solubility (µg/mL)		XRPD Result after 24 h Slurry
		1 h	24 h	
NCS-A	Water	7.3 ± 4.2	11.3 ± 5.7 (pH 7.81 ± 0.09)	NCS-H
	FaSSGF	BDL	BDL	n/a
	FaSSIF	12.0 ± 0.2	10.1 ± 0.2 (pH 6.60 ± 0.08)	NCS-H
NCS-UR SD-8	Water	5.7 ± 3.0	7.4 ± 0.5 (pH 7.59 ± 0.11)	NCS-H
	FaSSGF	BDL	BDL	n/a
	FaSSIF	7.6 ± 0.4	5.9 ± 0.7 (pH 6.53 ± 0.01)	NCS-H
NCS-UR SD-9	Water	9.4 ± 2.8	6.4 ± 2.5 (pH 7.79 ± 0.26)	NCS-H
	FaSSGF	BDL	BDL	n/a
	FaSSIF	8.9 ± 0.6	6.7 ± 0.8 (pH 6.54 ± 0.01)	NCS-H

Note. Error given based on triplicate samples. pH of solution shown in brackets at 24 h timepoint.

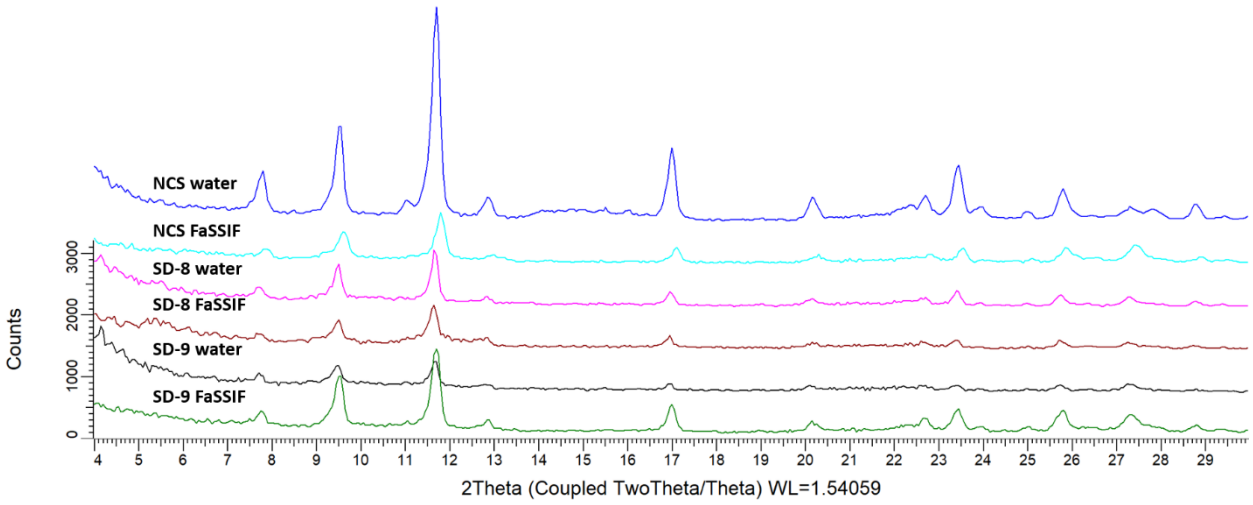

Figure 4.20- XRPD diffractograms of solids isolated from slurries in water and FaSSIF after 24 h solubility assessment.

Although NCS-UR was shown to improve solubility in 40% IPA, the measurements in this work did not show solubility improvement in water and biorelevant media at 1 h and 24 h time points. However, it is possible that an improvement in solubility will be observed *in-vivo* during the transition of NCS-UR to NCS-H due to the spring-parachute effect. [4]

4.5 Conclusion

A TPD was developed at room temperature for NCS-UR in IPA using a combination of equilibrium slurry experiments and solvent addition. The work illustrated that a TPD can be developed for compounds such as urea, where solubility assessment by chromatographic techniques is not straightforward or readily accessible. A combination of well-designed slurry experiments and solubility assessment can be used to determine phase boundaries on the TPD. At equilibrium, NCS-UR was stable when urea was present in at least stoichiometric quantity. This identified that crystallization by a non-equilibrium method such as spray drying could be appropriate for scale-up of a co-crystal.

NCS-UR was successfully prepared by spray drying from stoichiometric solutions, despite being part of an incongruently saturating system. The inlet temperature was varied from 70 to 128 °C and feed solution concentration was varied between 3.3 and 7.5 mg/mL. Phase purity of the co-crystal was determined by XRPD and DSC. All spray drying conditions in this work successfully generated phase pure co-crystal within the detection limits of the analytical methods employed.

The best product yields obtained in this work were 69% and 73% at 200 mg scale when an inlet temperature of 85 °C was used.

The spray drying method was successfully scaled-up to 3 g and two inlet temperatures (85 and 100 °C) were tested. The scaled-up solids were assessed by XRPD, DSC, BET, SEM, ^{1}H NMR and were used to assess solubility in biorelevant media. The solids from scale-up exhibited spherical particles with average diameter between 1.2 (85 °C) and 1.4 µm (100 °C) and surface area between 0.93 (85 °C) and 1.32 m^2/g (100 °C). Residual IPA fell at acceptable concentration of 0.48 to 0.50 wt.% for the 3-g scale experiments. Despite a previously reported improvement in solubility in 40% IPA, the solubility of NCS-UR in water and biorelevant media did not show improvement compared to NCS-A at either 1 h or 24 h. The solids recovered after the solubility measurements agreed with NCS-H by XRPD, indicating that the co-crystal dissociated during the measurement. Thus, it is possible that an in-vitro improvement in solubility would be observed due to the spring-parachute effect, even though it was not captured at the 1 h dissolution sampling point in this study. The spring effect (higher kinetic dissolution) for the NCS-UR co-crystal may be observed directly *in-vitro* if the dissolution is monitored by a technique such as UV or HPLC between time zero and one hour. A substantial spring effect, even in such a short timeframe, can have a significant impact on exposure.

The current study demonstrated the feasibility of industrial applicable processes for NCS-UR by spray drying a phase pure co-crystal at small scale. Phase pure NCS-UR can be successfully prepared by spray drying under various conditions. Although formation of the co-crystal and reduction in particle size did not offer a solubility advantage in biorelevant media at 1 h and 24 h timepoints *in-vitro*, it is possible that an improved kinetic dissolution between time zero and 1 h could lead to *in-vivo* improvement due to the spring-parachute effect. A different co-former may give suitable improvement in solubility. In addition, it is recommended to include solubility assessment at biorelevant pH as criteria for selection of a suitable co-crystal of NCS.

5 CHAPTER 5: COCRYSTAL FORMATION OF NICLOSAMIDE AND UREA IN SUPERCRITICAL CO2 AND IMPACT OF COSOLVENT

Reprinted with permission from L. MacEachern, A. Kermanshahi-pour, M. Mirmehrabi, L. Ajiboye, V. Trivedi, S. Rohani, Q. He, Cocrystal formation of niclosamide and urea in supercritical CO_2 and impact of cosolvent, J. Sup. Flu. (2023) .

5.1 ABSTRACT

A cocrystal of niclosamide and urea was attempted for the first time using a crystallization in supercritical solvent (CSS). Experiments were conducted at 40 °C or 60 °C between 3.3 and 29.4 MPa in CO_2. Cocrystal formation showed a dependence on the state of CO_2 with no cocrystal formation below the critical point and consistently showed partial conversion above the critical point. The addition of 0.5 mL (2.7-3.5 mole%) cosolvent was found to have significant impact on cocrystal formation at 40 °C and 20 MPa. Addition of 2-propanol increased cocrystal formation by between 50 and 60% compared to neat $scCO_2$, while cyclohexane reduced cocrystal formation by between 20 and 35%, and water completely hindered cocrystal formation. The impact of hold time, cosolvent, solubility in relation to ternary phase diagrams, and inter- and intra-molecular hydrogen bonding are discussed.

5.2 INTRODUCTION

Modern active pharmaceutical ingredients (APIs) commonly fall into the ‘low solubility’ category (Class II) of the Biopharmaceutical Classification System (BCS) which impacts their bioavailability [68]. As such, low-solubility APIs should be modified to improve kinetic solubility and in turn, bioavailability. For ionizable APIs, forming a salt is often used to improve solubility. However, for non-ionizable APIs, salt formation is not possible and alternative complexes such as cocrystals must be used as a method to improve solubility. During cocrystal screening, the most common methods used to generate cocrystals include liquid assisted grinding (LAG), co-evaporation, reactive crystallization, or slurry crystallization [26,77,78]. Most of these methods use conventional organic solvents in the process. However, cocrystals can also be formed using solventless methods such as neat grinding (without addition of solvent), co-melting or contact cocrystallization, or using non-conventional solvents such as supercritical fluids, namely supercritical carbon dioxide ($scCO_2$).

The use of $scCO_2$ is promising for cocrystal screening and scale-up, due to the opportunity to remove/minimize conventional organic solvent(s) from the process and generate sub-micron particles. Supercritical methods for cocrystal formation often include an organic solvent to aid in dissolution of the cocrystal formers. Such methods include supercritical antisolvent (SAS), gas antisolvent (GAS), and supercritical enhanced atomization (SEA) or atomization and antisolvent (AAS). In these methods, the API and coformer are typically dissolved in a conventional organic solvent and $scCO_2$ is used as an antisolvent. These methods are attractive because many pharmaceuticals have poor solubility in $scCO_2$, but these processes still take advantage of $scCO_2$'s ability to rapidly de-supersaturate a solution and produce small, uniform particles. Supercritical methods which do not use significant quantities of organic solvent include rapid expansion from supercritical solution (RESS) and crystallization from supercritical solution (CSS). In these processes, the API and coformer will typically dissolve in the supercritical phase and are crystallized either by rapid expansion through a nozzle (RESS) or gradual depressurization of the vessel (CSS). However, the use of RESS and CSS for cocrystal formation is not as widespread as the solvent-containing methods likely due to the high cost associated with the supercritical technology and poor solubility of most compounds and low reported rate of success [177].

A cocrystal screening with saccharin and multiple coformers using CSS, explored the impact of mechanical agitation and cosolvent [94,178]. It was proposed that the rate of cocrystal formation appeared to be dependent on the phase equilibria and dissolution rate of the cocrystal formers. For example, a saccharin cocrystal with theophylline (more soluble) formed at a faster rate than with indomethacin (less soluble) [94,178]. Aside from solubility, mechanical agitation was also identified as a key parameter in cocrystal formation rate [94,178]. There are also examples which indicate that variation in rate of conversion to cocrystal may be expected due to different mixing mechanism, reactor geometry, particle size, scale, etc. as well. For example, two research groups found that the reaction time to obtain complete conversion to a carbamazepine-saccharin cocrystal varied, Padrela et al. [6] obtained the phase-pure cocrystal within 2 h while Cuadra et al. [8] required 20 h reaction time [97,178]. In another CSS screening with 5-fluorouracil, experiments without added cosolvent did not lead to cocrystal formation despite mixing [97]. However, addition of MeOH consistently led to partial cocrystal formation. The results of the 5-fluorouracil study suggested that sufficient solubility of components (e.g. through addition of cosolvent) is

required to get successful cocrystal formation [97]. CSS cocrystallization is somewhat analogous to slurry crystallization in conventional organic solvents. Therefore, it is important to consider the solubility of components and theoretical ternary phase diagram of a given system to understand conditions which favor the cocrystal as it tends toward equilibrium.

When discussing cocrystal formation through a slurry crystallization method, it is important to consider ternary phase diagrams (TPD) when trying to identify conditions favorable to obtaining a phase-pure cocrystal in the solid phase. TPDs are graphical representation of the phase equilibrium at given compositions of the API, coformer, and solvent [87,164]. Development of a TPD for a given system can identify compositions at which the cocrystal is stable at equilibrium. The conditions where a cocrystal is stable are dependent not only on the API and coformer, but also on the solvent system. If solubility of one component is substantially greater than the other in a given solvent, a cocrystal with 1:1 stoichiometry may not be stable in a slurry with equimolar ratio of both components.

On the other hand, there are a number of reports of cocrystals which have formed simply through "contact" cocrystallization whereby the two components are mixed together and then left to sit without any further manipulation [179–181]. In contact cocrystallization, there is no organic solvent or mechanical agitation. The coformer urea has been shown to spontaneously form cocrystals with both salicylic acid and caffeine without mechanical agitation or organic solvent-mediated methods. Silva *et al.* [179] investigated urea-salicylic acid cocrystal formation and the role of humidity. Raman mapping showed that cocrystal formation above urea's deliquescence point occurred at the interface between urea and salicylic acid particles without any physical mixing or mechanical grinding [179]. In 2007 *Jayasankar et al.* [181] proposed a mechanism of cocrystal formation under deliquescent conditions whereby a saturated aqueous solution at the hygroscopic particles surface gives way to cocrystal nucleation and growth. In another example, formation of a urea-caffeine cocrystal has occurred during storage when relative humidity (RH) was low (< 30%) and without mechanical mixing [180]. The cocrystal formation that occurred during storage after milling was attributed to inter-particle contact which increased due to smaller particle size when compared to an experiment with un-milled materials, suggesting that 'contact' cocrystal formation is not necessarily mediated by deliquescence.

Niclosamide (NCS) is an anthelmintic drug used for the treatment of tape worm and is part of the

World Health Organization's list of essential medicines [144]. Niclosamide is known to be polymorphic, with a known anhydrous form, multiple hydrates, and solvates with a diverse range of solvents [145,146,182,183]. Niclosamide exhibits poor solubility in aqueous and biorelevant media [184]. Reduction in particle size by supercritical crystallization methods in combination with cocrystallization could offer a method of nanoparticle production for improved solubility of Niclosamide. Niclosamide-urea cocrystals have been reported in literature prepared by screening methods such as co-evaporation, and a scalable spray drying method [147,184]. Preparation of the cocrystal by spray drying gave small, uniform particles, but the residual isopropanol (IPA) content was just at International Council for Harmonization (ICH) guidelines limit (~0.5%) [184]. Therefore, formation of the pure cocrystal in $scCO_2$ could be advantageous for removal of residual solvent.

The aim of this study was to investigate formation of an NCS-urea (UR) cocrystal in $scCO_2$, despite the very low solubility of both components. In addition, impact of cosolvent on cocrystal formation and its connection to ternary phase diagrams are discussed.

5.3 Materials and Methods

5.3.1 Materials

Niclosamide (>98% purity) was used as received without further purification from Millipore Sigma (Oakville, ON, Canada), Lot # 058M4059V (Section 3.1.2 and 3.1.4) and or Lot # 000122971 (section 3.1.3 and 3.1.5). Urea was sourced from Fisher Scientific (Toronto, ON, Canada). Liquid CO_2 (99.9% with eductor) was sourced from Praxair, Inc (Dartmouth, NS, Canada). Solvents isopropanol (IPA) and cyclohexane were sourced from Fisher Scientific (Toronto, ON, Canada) and VWR (Mississauga, ON, Canada), respectively.

5.3.2 CSS

Recrystallization experiments in $scCO_2$ were done with a modified SFT-110 equipment (Supercritical Fluid Technologies, Inc., Newark, DE, USA) which is shown in Figure 5.1. Mixtures of Niclosamide (150 mg) and urea (1 molar equivalent) were gently mixed using a vortex mixer (for approximately 30 s) and then wrapped in a Kimwipe or placed in an aluminum dish of 13 mm diameter for experiments employing cosolvent. The solid mixtures were placed in a 100 mL high-pressure vessel, in an extractor oven (±0.5 °C). The vessel was pressurized with

CO_2 using an SFT-10 pump at 24 mL/min (based on CO_2 at 9.3 MPa and 35 °C), and the vessel was sealed by closing the valves at the inlet and outlet. The vessel was held at the specified temperature (40 or 60 °C) and pressure (between 3.3 and 25.1 MPa) for between 6 and 48 h without additional shaking or mechanical agitation. Experiments at conditions below 7.3 MPa are referred to as 'subcritical' throughout this manuscript. In select experiments water, IPA, or cyclohexane was added as cosolvent. The cosolvent was added directly to the bottom of the vessel by micropipette prior to adding NCS and urea mixtures and pressurizing the vessel. The pressure in the vessel was measured at 5 min intervals using an in-line monitoring system, comprising a PX309-10KGI pressure transducer (Omega; St-Eustache, QC, Canada) and an OM-CP-Process101A current data logger (Omega). The transducer/logger system interfaces with OM-CP Data Logger Software version 4.2.21.1 via an OM-CO-IFC200 USB (Omega). After the hold period, the vessel was de-pressurized over approximately 15 min through a nozzle with 1580 μm inner diameter (ID). In all experiments, there was almost no solid (<< 10 mg) collected in the collection vials through a rapid expansion from supercritical solution (RESS) process. The Kimwipe containing residual solid mixture was carefully removed from the vessel. In all experiments, the mass of the packet was measured before and after the experiment, giving a mass difference of less than 10 mg. NCS Lot # 058M4059V was used for experiments in neat CO_2 with 24 h hold time and Lot # 000122971 was used for experiments employing cosolvent and varying hold time (6-48 h).

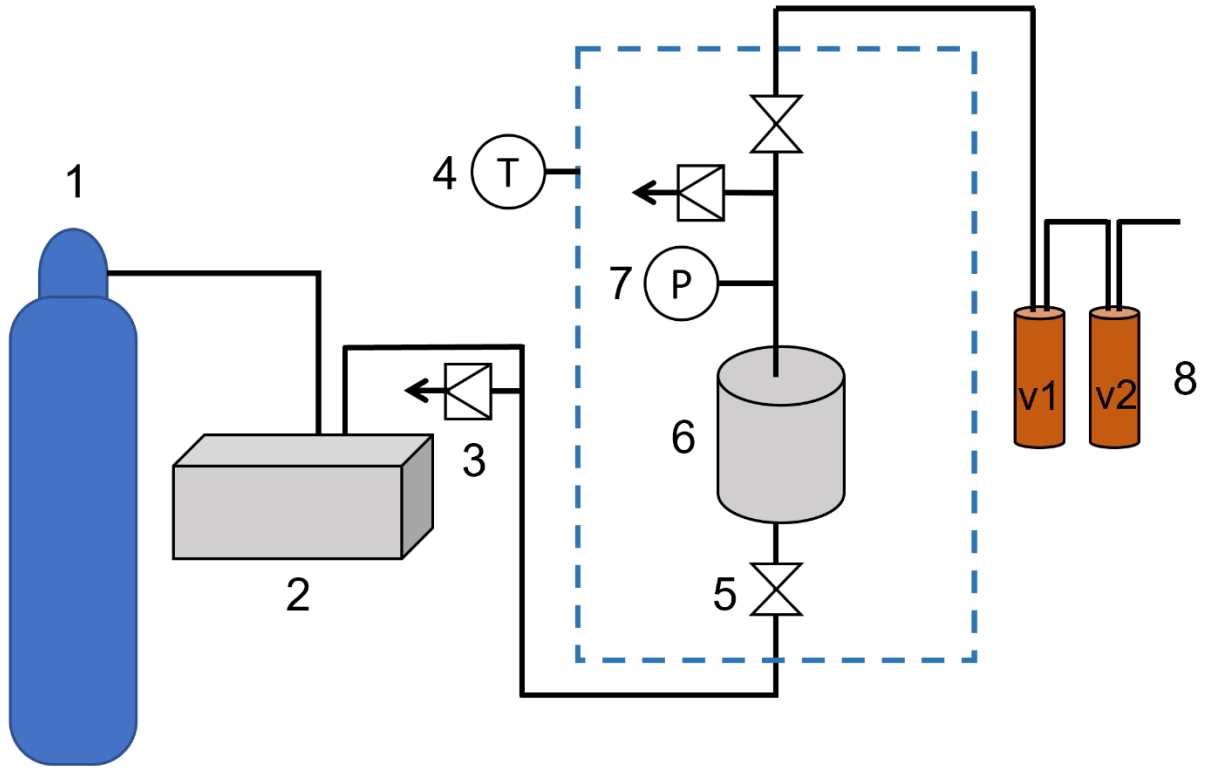

Figure 5.1- Schematic of the SFT-110 equipment. 1- CO2 source, 2- CO2 pump, 3- rupture disk, 4- thermocouple, 5- valve, 6- high-pressure vessel, 7- pressure transducer, 8- collection vials (v1 and v2). Dashed line indicates oven enclosure.

5.3.2.1 Solubility Assessment in CO2

Solubility of NCS was measured in $scCO_2$ using a simple gravimetric method at 40 °C and 20 MPa in the SFT-10 system described above. NCS was added to an Aluminum pan and weighed. The pan was covered with a Kimwipe and placed inside a 100 mL vessel. The vessel was pressurized, sealed, and held at the specified temperature and pressure for 24 h. After 24 h the vessel was purged with $scCO_2$ for 10 min and depressurized. The quantity of dissolved solids was calculated by mass difference of the pan before and after the measurement. The mass of CO_2 was calculated using the vessel volume (10.3 mL) and the CO_2 density as calculated by the Peng-Robinson equation of state. The experiments were done in duplicate.

5.3.2.2 Phase Monitoring in CO2

The phase change of urea, NCS, and NCS/urea physical mixture in $scCO_2$ was determined using a phase monitor (Supercritical Fluid Technologies (SFT) Inc., Newark, DE, USA) as described

by Bhomia et al[185]. Prior to the $scCO_2$ investigations, free-flowing NCS and urea particles were separately prepared by gentle grinding with a mortar and pestle to break any agglomerates. The NCS/urea mixture was formulated at a 1:1 molar ratio by mixing both components in a vortex mixer for 5 minutes. For the phase change studies, a glass capillary was filled with 3 to 5 mg of sample and placed in the sample holder, which was then tightly secured into the high-pressure vessel. The liquid CO_2 was then introduced into the vessel at 25 ± 2 °C and the pressure was allowed to equilibrate before any changes were made to the temperature and/or pressure. After equilibration, the temperature of the vessel was increased to 60 °C at a rate of 10 °C/min. The instrument was allowed to equilibrate for 15 minutes once the desired temperature was achieved in the vessel. The pressure was then adjusted to 20 MPa and kept constant during the experiment using a manually controlled syringe pump attached to the vessel. The possible phase change of the materials was monitored for up to 6 hours through a quartz window via a camera attached to the vessel.

5.3.3 Preparation of Anhydrous and Hydrate Forms of NCS

Niclosamide anhydrous (NCS-A) and hydrate (NCS-H) pure phases were prepared through slurry crystallization. Approximately 500 mg NCS was slurried in either 5 mL isopropyl alcohol (IPA) or 6 mL of a mixture of IPA:water (1:1 v:v) at room temperature (RT; 20-22 °C) for two days. After confirming conversion to the desired form by X-ray powder diffraction (XRPD) the solids were isolated by vacuum filtration and dried under vacuum.

5.3.4 Solubility in Organic Solvent

Solubility measurements were conducted using a gravimetric technique in IPA and cyclohexane. An excess of solid was suspended in 1 mL of solvent at room temperature to form a slurry. The slurries were stirred for a minimum of two days to equilibrate. Supernatant from the slurries was weighed (m_{sup}) in a tared vial of known mass (m_v) on a Mettler Toledo balance (± 0.0001 g) and then evaporated to dryness at 50 °C in atmosphere and then 50 °C under vacuum. The solid residue was weighed (m_{sol}), and the masses were used to calculate solubility. In the case where mass difference between m_{sol} and m_{sup} was less than 0.0001 g (not detected) the solubility was reported as << 1 mg/mL.

5.3.5 XRPD

X-ray powder diffraction (XRPD) was performed using a Bruker D8 Advance in reflection mode

with a Cu Kα source. The scan range was 4-30° 2θ with 0.03° 2θ step size. Samples (10 mg) were prepared on Si zero-return wafers.

5.3.6 Estimation of Cocrystal Conversion to NCS-UR Using XRPD

Anhydrous niclosamide (NCS-A) was prepared by slurry crystallization with 20 volumes of IPA at RT. The solid was filtered and dried under vacuum for use in calibration line development. NCS-UR was prepared by co-evaporation of a 1:1 mixture in EtOH at 50 °C. Mixtures of NCS-A and NCS-UR were prepared at 10 mg-scale and evaluated by XRPD using the method already specified. Mixtures of NCS-A and NCS-UR were prepared using 0, 20, 40, 50, 60, 80 and 100 wt.% NCS-A. The 50 wt.% point was prepared in duplicate. A selected range of the diffraction data between 9 and 15 °2θ was selected to use for quantification since characteristic peaks of both NCS-A and NCS-UR were observed in the range. A classical least squares method was used to develop a calibration matrix. Unknown samples were evaluated using the same XRPD method and the concentrations of NCS-A and NCS-UR were estimated using the diffraction data and generated calibration matrix.

In select number of cases, a mixture of the hydrate form of NCS (NCS-H) and NCS-UR were obtained. Since a mixture of these was not often observed in this work, an estimation of the cocrystal quantity was done. To estimate the cocrystal quantity in such mixtures the area of the highest intensity NCS-UR peak (10.4 °2θ) was compared to the area of the highest intensity NCS-H peak (11.6 °2θ).

5.4 Results

5.4.1 XRPD Analysis of NCS and Urea and Estimation of Cocrystal Quantity

To understand the impact of pressure, temperature, cosolvent additive, and time on cocrystal conversion rate, it was necessary to find a suitable analytical method to estimate the ratio of cocrystal in the isolated products. Although differential scanning calorimetry (DSC) can often be used to determine phase purity of a cocrystal, it was not feasible in this work due to the low melting point of urea. In general, use of DSC to quantify cocrystal phase purity is used when the cocrystal melting point is lower than those of both individual components [96,178]. However, urea's low melting point facilitated formation of NCS-UR *in-situ* by co-melting during the DSC

measurement, leading to significant overestimation of cocrystal content. Therefore, XRPD analysis was the preferred technique for estimation of the conversion in this study.

NCS (anhydrous and hydrate form), urea, and its cocrystal were analyzed by XRPD to obtain a baseline. The diffractograms of NCS-H, NCS-A, unprocessed NCS, urea, and NCS-UR are shown in Figure 5.2. NCS-H has characteristic peaks at 7.7, 9.5, 11.7, 12.8, and 16.9 °2θ. NCS-A has characteristic peaks at 6.6, 13.1, 13.8, 17.3, and 19.9 °2θ. Urea shows a prominent peak at 22.3 °2θ, while the NCS-UR cocrystal exhibits characteristic peaks at 7.9, 9.4, 10.3, 13.0, 15.8, and 17.4 °2θ. NCS provided by the supplier showed characteristic peaks of both NCS-A and NCS-H indicating that it was a mixture of anhydrous and hydrate forms. In a previous study, thermogravimetric analysis (TGA) suggested that the unprocessed NCS (lot 058M4059V) comprises approximately 22 wt.% of NCS-H [184].

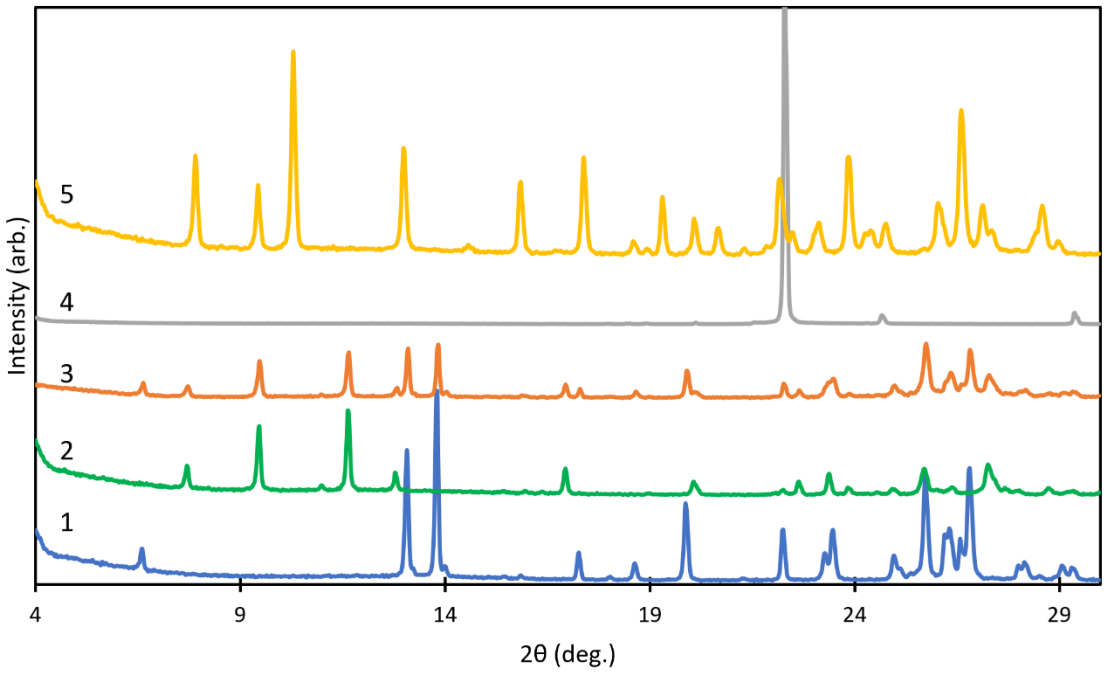

Figure 5.2- XRPD diffractograms of niclosamide, urea, and NCS-UR. 1- NCS-A; 2- NCS-H; 3- NCS unprocessed from supplier; 4- urea; 5- NCS-UR.

To better understand the impact of temperature, pressure, and cosolvent on conversion to the cocrystal, XRPD was used to build a multivariate calibration of NCS-A and NCS-UR. Multivariate analysis of XRPD data is a non-destructive tool for quantification of crystalline

multicomponent mixtures [186,187]. NCS-A was the selected form of NCS because it was frequently observed after exposure to $scCO_2$ (discussed in Section 3.3). First, an appropriate range for the multivariate analysis was determined. The range was selected to include characteristic peaks of both NCS-A and NCS-UR because those components were observed after exposure to $scCO_2$. The relative intensities of peaks for each phase should also be consistent to have a reliable calibration. NCS-UR prepared by two different methods (co-evaporation in EtOH, and exposure to 1 vol. IPA) showed varying relative peak intensities, indicative of preferred orientation effects in the samples. Notably, the relative peak intensity of the characteristic NCS-UR peaks at 7.9 and 15.8 °C varied significantly between the two samples as shown in Figure 5.3. Therefore, in a best attempt to avoid these two peaks skewing the conversion estimation result, a range of between 9 and 15 °2θ was selected. The range selected included four peaks related to NCS-UR (9.4, 10.3, 13.0, 14.6 °2θ) and three peaks related to NCS-A (13.1, 13.8, 14.0 °2θ).

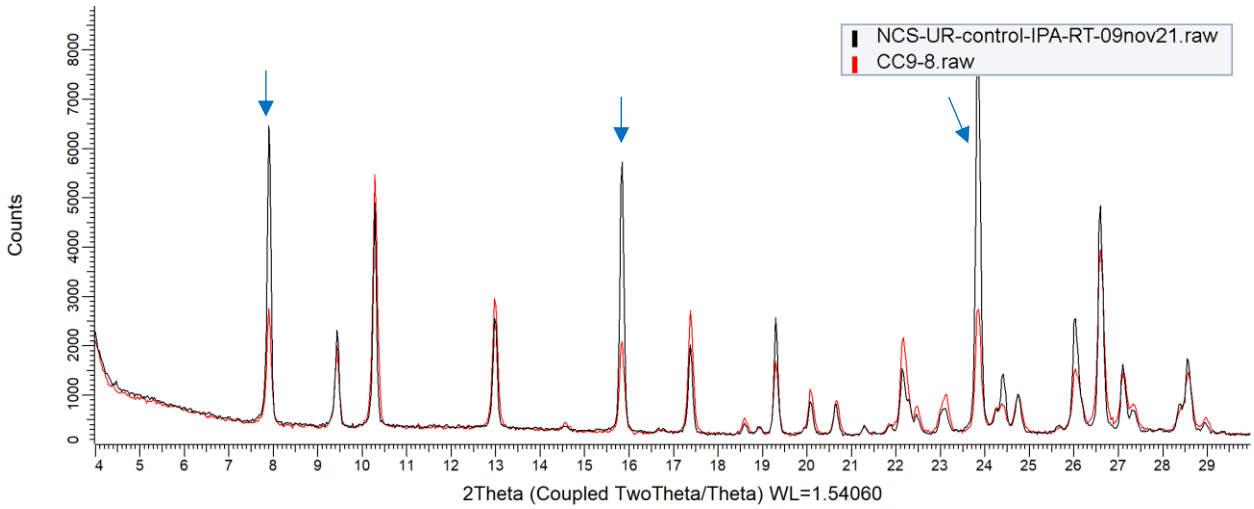

Figure 5.3- XRPD diffractograms of NCS-UR prepared by co-evaporation (red) and stagnant formation in IPA (black). Peaks showing the most significant variation in relative intensity are indicated with arrows.

The cocrystal conversion estimate was based on the Beer-Lambert law:

$$\boldsymbol{A = KC}$$

where $\boldsymbol{A}$ is the XRPD diffractogram, $\boldsymbol{K}$ is the matrix of calibration coefficients, and $\boldsymbol{C}$ is the matrix containing concentration data. The calibration was performed using the generated set of diffractograms with known concentrations of NCS-UR and NCS-A and the calibration coefficient matrix was calculated using:

$$\boldsymbol{K} = \boldsymbol{A}_{cal}\boldsymbol{C}_{\boldsymbol{cal}}^{\boldsymbol{T}}[\boldsymbol{C}_{\boldsymbol{cal}}\boldsymbol{C}_{\boldsymbol{cal}}^{\boldsymbol{T}}]^{-1}$$

where $\boldsymbol{A}_{cal}$ and $\boldsymbol{C}_{cal}$ are the matrices of calibration sample diffractograms and concentrations, respectively. The calibration was initially built using compositions of 0%, 20%, 50% (duplicate), 80%, and 100% NCS-UR. The calibration was validated using mixtures comprising 40% and 60% NCS-UR. The validation results showed that the calibration estimated the composition within ±7.5% NCS-UR which was acceptable for the qualitative nature of this work. The 40% and 60% points were then included in the calibration set used for estimating composition of unknown samples. The validation result (predicted values vs. expected values for NCS-UR %) for the complete calibration (including points with 40% and 60% NCS-UR) is shown in Figure 5.4.

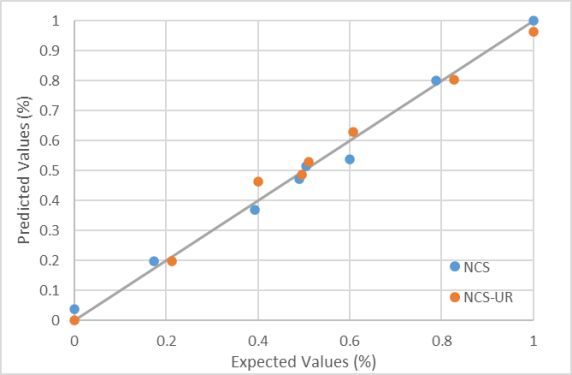

Figure 5.4- Validation result for calibration data set of NCS-A and NCS-UR.

The unknown concentration of NCS-UR and NCS-A in the isolated samples were then calculated by:

$$\boldsymbol{C}_{unk} = [\boldsymbol{K}^{T}\boldsymbol{K}]^{-1}\boldsymbol{A}_{unk}$$

where $\boldsymbol{A}_{unk}$ and $\boldsymbol{C}_{unk}$ are the matrices of unknown sample diffractograms and concentrations, respectively.

The wt.% of NCS-UR in the binary mixture (NCS and NCS-UR) was converted to wt.% NCS-UR in the ternary mixture (NCS, NCS-UR, urea) using the equation:

$$C^{t}_{NCS-UR} = {C^{b}_{NCS-UR}}\Big/{C^{b}_{NCS-UR} + \left(1 - C^{b}_{NCS-UR}\right) + \left(UR_{wt} - C^{b}_{NCS-UR} * UR_{wt}\right)}$$

where C^{t}_{NCS-UR} is wt.% NCS-UR in the ternary mixture, C^{b}_{NCS-UR} is wt.% NCS-UR in the binary mixture, and UR_{wt} is the wt.% urea in a 1:1 NCS-UR cocrystal.

5.4.2 Solubility of NCS, Urea, and NCS-UR

Solubility of the cocrystal components in CO_2 and cosolvents was measured. The solubility results of NCS, NCS-UR, and urea are summarized in Table 5.1. NCS and urea exhibit poor solubility in $scCO_2$ over the processing conditions used in this study, with solubility of less than 0.01 mg/g. The solubility of NCS (measured in this work) and urea on a molar basis was similar in $scCO_2$, both being on the order of 10^{-6} mole fraction [188]. NCS and NCS-UR also exhibited poor solubility in water, previously measured by MacEachern *et al.* [184]. NCS-UR was also observed to dissociate when slurried in water for 24 h in their study. However, urea is highly soluble in water with solubility greater than 1000 mg/g and is known to deliquesce at relative humidity (RH) above 74% [179]. In IPA, the solubility of NCS, urea, and the cocrystal are fairly similar on a mass basis, but urea is about 10 times more soluble than NCS and NCS-UR on a molar basis. The solubility of both NCS and urea was also very low in cyclohexane and the dissolved mass was below detection by the gravimetric method.

Table 5.1- Solubility of NCS, urea, and NCS-UR in various solvents.

Solvent	Solubility (mg/g)			
	$scCO_2$[a]	**Water**	**IPA**	**Cyclohexane**
NCS	0.01	~0.01[184]	14	<< 1
Urea	~0.005[188]	> 1000	32	<< 1
NCS-UR	-	~0.01[184]	20[184]	-

[a] Reported for 40 °C, 20 MPa for NCS and 40 °C, 15 MPa for urea

5.4.3 Cocrystal Formation at Atmospheric Conditions

Experiments were set up as a control to evaluate cocrystal formation of NCS-UR at ambient pressure. The control experiments comprised physical mixtures of NCS and urea at 1:1 molar ratio which were exposed to a specified condition for up to one week without mechanical

agitation, aside from the neat milling experiment. The control conditions included room temperature (RT) and 50 °C at ambient pressure (air), RT, 40 °C, and 50 °C at 75% RH, neat co-milling, and stagnant hold with 1 volume (1 mL/g) of IPA, water, and cyclohexane. All solids were analysed by XRPD after the specified hold time to check for characteristic cocrystal peaks.

After 24 h, the control experiments at ambient pressure with no mechanical agitation or solvent, did not show evidence of forming the cocrystal. The addition of moisture to the environment (RT and 75% RH) also did not promote cocrystal formation. Application of heat (50 °C) did not lead to cocrystal formation at ambient conditions within 24 h. The combination of humidity and heat (40 °C and 50 °C at 75% RH) did not show any cocrystal formation after 24 h or one week, but the unreacted NCS showed conversion to NCS-H.

The addition of solvent at ambient pressure without mechanical agitation was also explored with three different solvents. The addition of one volume of solvent (IPA) at 50 °C promoted cocrystal formation of the mixture after one day where about 100% conversion to the cocrystal was observed based on absence of NCS and urea characteristic peaks in the diffractograms. However, the addition of cyclohexane led to only partial cocrystal formation even after one week. In the case of cyclohexane addition, the extent of cocrystal conversion was not quantified because there was a mixture of NCS-H and NCS-A remaining, but the developed method was only suitable for mixtures with NCS-A. While adding water did not show any characteristic cocrystal peaks even after one week, all NCS converted to NCS-H within the first 24 h.

Neat grinding indicated partial formation of the cocrystal. The resulting solid after 48 sec of milling had lower crystallinity compared to other methods of generating the cocrystal. The extent of cocrystal conversion was not quantified but distinct cocrystal peaks were still observed.

After one week, the sample held at 50 °C also showed characteristic peaks of NCS-UR by XRPD. However, all other conditions aside from the afore-mentioned IPA, cyclohexane, and milling experiments, did not show any evidence of conversion to cocrystal even after one week in storage.

Table 5.2- Cocrystallization experiments at ambient pressure with NCS-UR.

Condition	XRPD Result	
	24 h	1 week
RT	NCS + urea	NCS + urea
RT, 75% RH	-	NCS + urea
40 °C, 75% RH	NCS + urea	NCS + urea[a]
50 °C	NCS + urea	NCS-UR (tr) + NCS + urea
50 °C, 75% RH	-	NCS + urea
50 °C, 1 vol. IPA	NCS-UR	-
50 °C, 1 vol. water	NCS + urea [a]	NCS + urea [a]
50 °C, 1 vol. cyclohexane	NCS-UR + NCS + urea	NCS-UR + NCS + urea
Neat grinding	NCS-UR (lc)+ NCS + urea[a]	-

Note. Hyphen (-) is not evaluated. 'lc' is low crystalline. 'tr' is trace.

[a] remaining NCS converted to NCS-H

5.4.4 Cocrystal Formation in Liquid and Supercritical CO_2

The formation of the NCS-UR cocrystal in the presence of subcritical or supercritical CO_2 without any mechanical agitation or shaking of the high-pressure vessel, was evaluated. For all experiments the mass of recovered material was compared to input material and showed less than a 10 mg (5 wt.%) difference before and after exposure to CO_2, confirming low solubility of the components. In addition, there were no solids collected in the collection vials during depressurization of the system.

A summary of the cocrystallization experiments in neat CO_2 is given in Table 5.3 and Figure 5.5. Exposure of the mixtures of subcritical CO_2 at 40 and 60 °C did not show cocrystal formation after a 24 h hold. XPRD analysis of the solids recovered showed physical mixtures of NCS and urea. Solid recovered from 40 °C (3.3 and 6.9 MPa) and 60 °C (5.8 MPa) showed mixtures of NCS-A, NCS-H, and urea while solid recovered from 60 °C (6.8 MPa) showed NCS-A and urea. Upon increasing the pressure to above critical in the system at 40 and 60 °C, partial conversion to the cocrystal was observed by XRPD in all experiments, evidenced by presence of characteristic NCS-UR peaks in the diffractograms. The XRPD diffractograms from the 40 °C series of experiments are given in Figure 5.6.

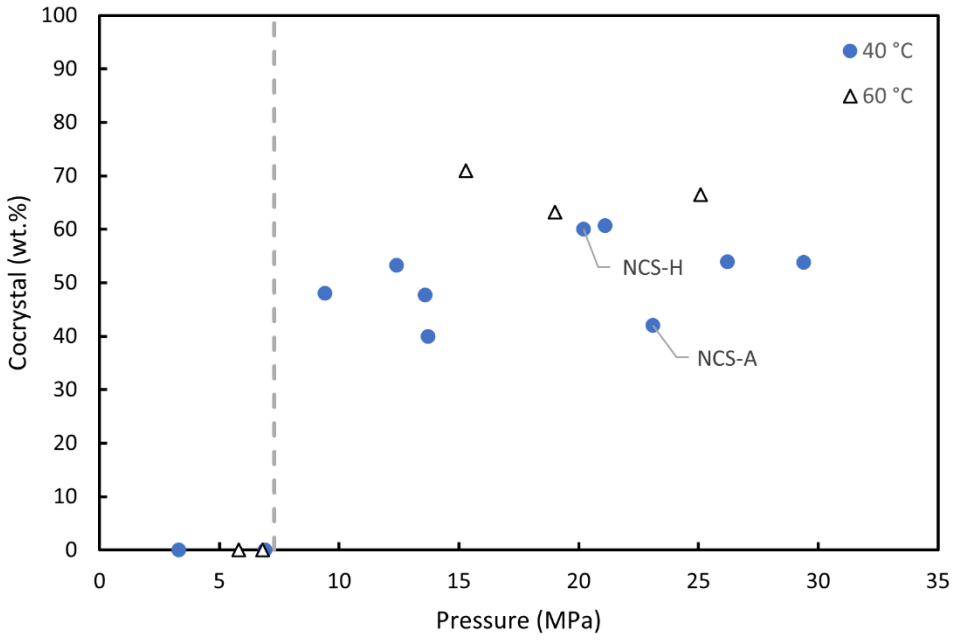

Figure 5.5- Conversion to NCS-UR cocrystal in CO2 at 40 and 60 °C at different pressures. Pc indicated with dashed line. All experiments used unprocessed NCS as input (mixture of NCS-A and NCS-H) unless otherwise specified.

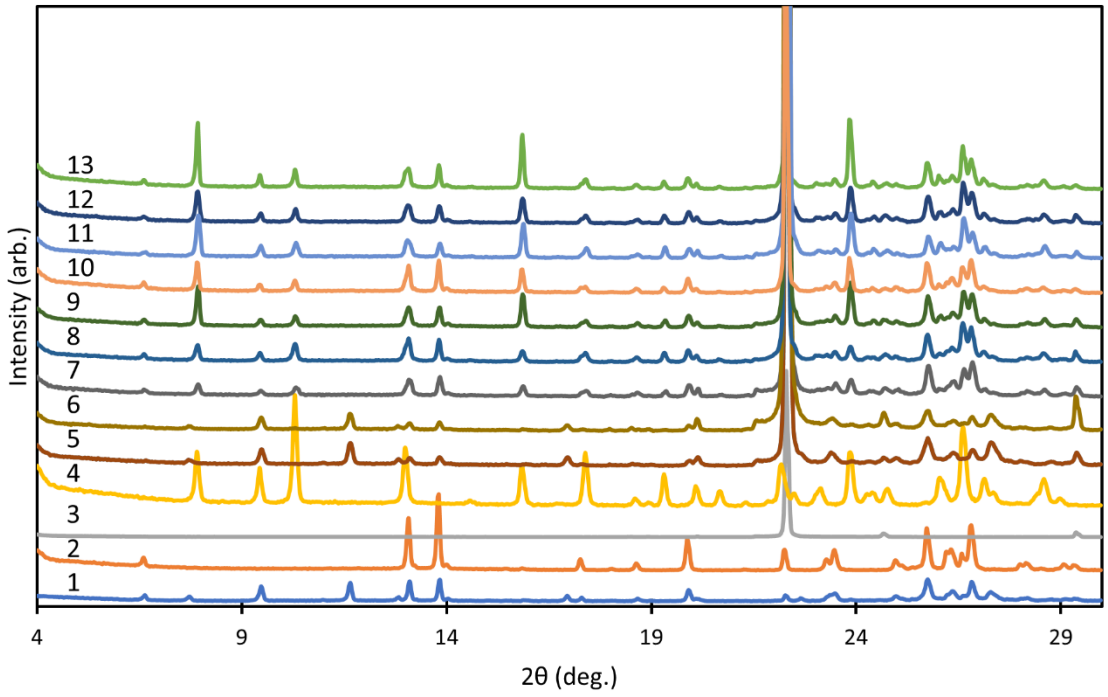

Figure 5.6- XRPD diffractograms from 40 °C experiments at different pressure with 24 h hold. 1-

NCS from Sigma; 2- NCS-A; 3- urea; 4- NCS-UR; 5- 3.3 MPa; 6- 6.9 MPa; 7- 9.4 MPa; 8- 12.4 MPa; 9- 13.6 MPa; 10- 13.7 MPa; 11- 21.1 MPa; 12- 26.2 MPa; 13- 29.4 MPa.

The conversion to cocrystal did not show a significant dependence on pressure above the critical pressure. An average 49% wt.% cocrystal was observed in supercritical conditions between 9.4 and 29.4 MPa at 40 °C. At 60 °C the cocrystal conversion was slightly higher with an average of 63% between 15.3 and 25.1 MPa. The XRPD quantification method used in this work is expected to estimate NCS-UR content with ±7.5%. The overall variability observed in the formation of NCS-UR at between 15 and 25 MPa at 60 °C was 8% which is near to the error of the quantification method. A duplicate point at 40 °C/13.6-13.7 MPa also illustrates this variability, giving between 37 and 44% cocrystal (a 7% difference, which agrees with the expected error in the method). As such, it is proposed that the pressure dependence of conversion to NCS-UR may be beyond the sensitivity of the quantification method. Nonetheless, the conversion is strongly dependent on the state of CO_2 (subcritical/liquid or supercritical).

In addition to cocrystal formation, unreacted NCS remaining after the experiments above the critical point consistently showed conversion from a mixture of NCS-H with NCS-A (input material) to only NCS-A. To test whether NCS-H converted to NCS-A or perhaps preferentially reacted to form the cocrystal, experiments were conducted using phase-pure NCS-A and NCS-H. Conversion to the cocrystal was observed when using either of the NCS polymorphs as input material, giving 39% wt.% cocrystal with NCS-A as input and 56% wt.% cocrystal when using NCS-H as input. However, when using NCS-H as input, the unreacted NCS-H after the experiment once again converted to NCS-A. Although the use of NCS-H showed greater conversion to the cocrystal compared to NCS-A (56% vs 39%), both results fell within ±10% of the average conversion (49%) at 40 °C. This difference may not be statistically significant. There was no evidence of polymorphic transformation of urea phase during all experiments.

Table 5.3- Summary of cocrystal formation experiments with NCS (lot 1) and urea in CO_2.

Temperature, °C	Pressure, MPa	Hold time, h	NCS-UR, wt.%
40	3.3	24	0 [a]
	6.9	24	0 [a]
	9.4	24	44
	12.4	23	49
	13.6	23	44
	13.7	23	37

Temperature, °C	Pressure, MPa	Hold time, h	NCS-UR, wt.%
	21.1	24	58
	26.2	24	50
	29.4	24	50
	20.2 (NCS-H)	24	56
	23.1 (NCS-A)	24	39
60	5.8	24	0 [a]
	6.8	25	0 [a]
	15.3	24	68
	19.0	18	60
	25.1	23	63

[a] No cocrystal observed in the XRPD, therefore CLS quantification not used.

5.4.5 Cocrystal Formation in $scCO_2$ with Cosolvent at Three Different Hold Times

In an attempt to improve the cocrystal formation in $scCO_2$, a small quantity of cosolvent was added. Three cosolvents were selected: water, IPA, and cyclohexane. Mixtures of NCS and urea were exposed to $scCO_2$ (or $scCO_2$ with cosolvent) for a specified time (6, 24, and 48 h) and the remaining solids in the vessel after the experiments were evaluated by XRPD. Cosolvents were selected to understand the impact on producing a congruent or incongruent system in relation to ternary phase diagrams. Water was selected as a solvent that would potentially give rise to an incongruent system because urea is highly soluble in water while NCS is not. IPA was selected because NCS and urea have similar solubilities in IPA and therefore it is suspected to form a congruent system. In addition, the control experiments in this work showed that NCS-UR formation can be facilitated by addition of just one volume of IPA to a physical mixture without mechanical agitation [184]. Cyclohexane was selected as a non-polar additive in attempt to solubilize the components slightly quicker compared to neat CO_2. The experiments with cosolvent were conducted at 40 °C and 20 MPa.

In neat $scCO_2$, NCS converted to NCS-A as expected at all hold times. Hold times of 24 and 48 h increased the cocrystal conversion by 41% and 50% compared to a 6 h hold, respectively. However, the cocrystal conversion only changed by 6% between 24 and 48 h.

When IPA was added as a cosolvent, some conversion to NCS-UR was observed in all experiments. Unreacted NCS converted to NCS-A when IPA was added as a cosolvent, similar

to the conversion observed in neat $scCO_2$ at similar conditions. However, although experiments in ambient pressure showed a complete conversion to the cocrystal in presence of one volume of IPA, complete conversion to the cocrystal was not observed within 48 h in supercritical conditions with the addition of 0.5 mL IPA. Conversion to cocrystal increased in the presence of IPA by between 50 to 60% compared with neat $scCO_2$ at all three hold times. Hold times of 24 and 48 h increased the cocrystal conversion by 47 and 46% compared to a 6 h hold, respectively. However, similarly to the experiments with neat $scCO_2$ the cocrystal conversion did not increase between 24 and 48 h.

Addition of a less polar solvent like cyclohexane had a slightly negative impact on cocrystal formation compared to IPA and neat $scCO_2$, reaching a maximum of 35% cocrystal conversion after 48 h. Conversion of NCS-H to NCS-A was also observed in experiments when cyclohexane was added. Compared to other cosolvent experiments, the time dependence between 6 and 48 h on the cocrystal formation was less pronounced with cyclohexane. The 6 and 24 h hold times did not show a significant change in cocrystal conversion, while 48 h showed an average 27% increase compared to 6 and 24 h. The cocrystal conversion in neat CO_2 and with the three cosolvent additives is shown in Figure 5.7 and Table 5.4.

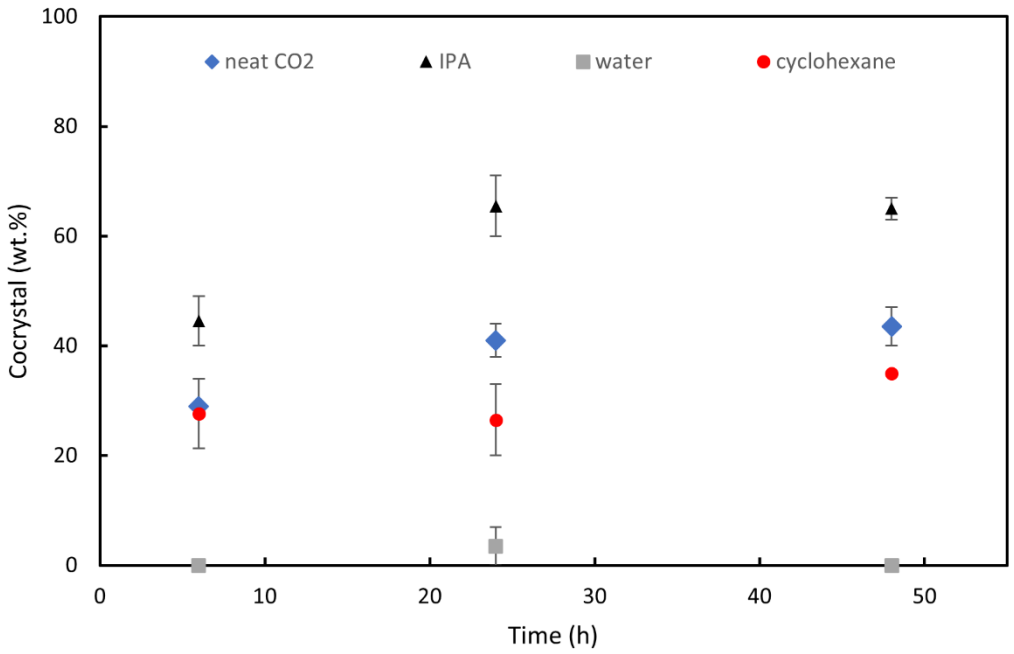

Figure 5.7- Estimated conversion to cocrystal vs time in neat CO2 and with three different cosolvents.

The use of water as cosolvent resulted in NCS converting to NCS-H. In addition, there was no evidence of cocrystal formation when water was added in most experiments, as indicated by the absence of characteristic peaks at 7.9, 9.4, 10.3, 13.0, 15.8, and 17.4 °2θ in the XRPD diffractograms as shown in Figure 5.8. Only two experiments showed a trace amount of cocrystal (estimated to be 2 wt.% and 7 wt.%), but overall experiments with water did not show any evidence of cocrystal formation. The hold time of 6, 24, or 48 h did not affect the result when water was added as cosolvent as all time points showed near zero conversion to the cocrystal.

Table 5.4- Summary of results from NCS-UR (with lot 2 of NCS) experiments in $scCO_2$ with 0.5 mL cosolvent at 40 °C and 20 MPa.

Cosolvent	Hold time, h	Result	Estimated cocrystal %[a]
none	6	NCS-UR + NCS-A + urea	29
		NCS-UR + NCS-A + urea	36
	24	NCS-UR + NCS-A + urea	38
		NCS-UR + NCS-A + urea	44
	48	NCS-UR + NCS-A + urea	40
		NCS-UR + NCS-A + urea	47
Water	6	NCS-H + urea	0
		NCS-H + urea + NCS-UR (trace)	2
	24	NCS-H + urea	0
		NCS-H + urea + NCS-UR (trace)	7
	48	NCS-H + urea	0
		NCS-H + urea	0
IPA	6	NCS-UR + NCS-A + urea	40
		NCS-UR + NCS-A + urea	49
	24	NCS-UR + NCS-A + urea	60
		NCS-UR + NCS-A + urea	71
	48	NCS-UR + NCS-A + urea	63
		NCS-UR + NCS-A + urea	67
cyclohexane	6	NCS-UR + NCS-A + urea	21
		NCS-UR + NCS-A + urea	34
	24	NCS-UR + NCS-A + urea	28
		NCS-UR + NCS-A + urea	20
	48	NCS-UR + NCS-A + urea	33
		NCS-UR + NCS-A + urea	35
		NCS-UR + NCS-A + urea	35

[a]Samples with no characteristic cocrystal peaks were not quantified using the CLS method.

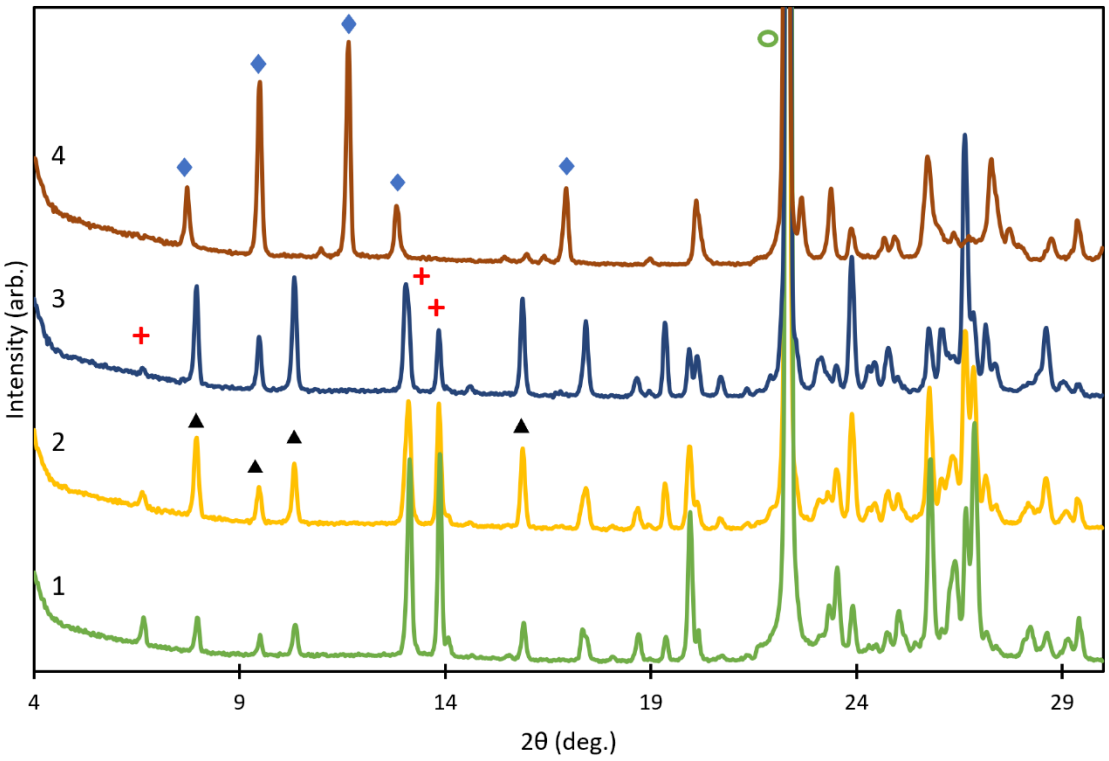

Figure 5.8- XRPD diffractograms of solids after 48 h hold-experiments using cosolvent 1- cyclohexane; 2- no cosolvent; 3- IPA; 4- water. Characteristic peaks indicated on figure for NCS-A (+), NCS-H (◊), NCS-UR (Δ), and urea (○).

5.4.6 Co-Melting Cocrystal Formation and Melting Point Depression

The effect of $scCO_2$ on the phase behavior of NCS and urea has not been previously studied. To eliminate the possibility of cocrystal formation by co-melting due to melting point depression in $scCO_2$, NCS and urea were held at process conditions with a viewing window to monitor for evidence of a phase change.

The behavior of NCS, urea, and an NCS/urea mixture was studied in $scCO_2$ at 60 °C and 20 MPa for 6 hours. These conditions were chosen to determine the phase change because they were near the upper limits of the pressure and temperature used for experiments in this study. There was no noticeable phase change (i.e., melting, complete solubilization, volume expansion, etc.) in the drug, urea, or drug-urea mixture at 60 °C and 20 MPa. The visual inspection of processed samples also indicated lack of melting as they remained free-flowing after the completion of the experiments.

5.5 Discussion

In this study, cocrystallization of NCS and urea in different conditions without mechanical agitation was compared under ambient conditions, with the addition of solvent or humid environment, and in $scCO_2$ with or without cosolvent.

Urea has been found to 'spontaneously' form cocrystals with caffeine and salicylic acid in other literature [179,180]. In one case particle-particle surface contact was proposed to influence cocrystal formation at low RH conditions [180]. In the case of higher humidity conditions, it has been shown that a thin urea saturated aqueous layer at the surface of urea particles gives rise to cocrystal formation [179]. But, in the case of NCS-UR neither the particle-particle contact nor the hygroscopicity of urea under atmospheric conditions was sufficient to give spontaneous cocrystal formation within 24 h; or in most cases, within one week at atmospheric pressure without mechanical agitation or addition of solvent. A low crystallinity NCS-UR was observed after the neat co-milling experiment, which may suggest that under this condition conversion of pure components to NCS-UR is facilitated by an amorphous intermediate phase, which has been proposed for numerous other cocrystals by researchers [189].

The impact of solvent choice on cocrystal formation in ambient, unmixed conditions was also observed during the initial experiments. In one case (IPA) complete conversion to cocrystal was observed, in another (cyclohexane) a mixture of all three components was observed, and in the third instance (water) no evidence of cocrystal formation was observed even after one week storage. The impact of solvent under these conditions may be related to the solubility of individual components and a theoretical TPD. As suggested by Chiarella et al. [87], if the relative solubility of both components in a given solvent is known then it is possible to estimate whether a system will have congruent or incongruent dissolution. With this in mind, the moderate and similar solubility of both components in IPA can allow for conversion to the cocrystal within a reasonably short time (> 24 h) and the mixture can fall within the cocrystal stability region as indicated by point (2) in Figure 5.9. In the cases of cyclohexane, the solubility of both components is similarly low, therefore a congruent system is expected and the conversion may trend towards point (2) in Figure 5.9. But the conversion rate in the presence of cyclohexane is hindered due to the low solubility and lower turnover to the cocrystal. While in IPA and cyclohexane the solubility of both cocrystal formers is similar, but the components have

dramatically different solubility in water. Therefore, following the estimation of congruency based on single component solubility it may follow that the TPD of NCS and urea in water is skewed heavily to an incongruent system. If this is the case, in the presence of water it is expected that a mixture will fall near a point such as point (4) in Figure 5.9, and cocrystal would not be observed which agrees with the observed results. However, it is also possible that NCS-UR simply is not favorable to form in aqueous systems due to the tendency to form its hydrated form, NCS-H, which is discussed in more detail below. Overall, it is hypothesized that in ambient conditions the NCS-UR cocrystal forms through an intermediate amorphous phase (in milling experiments) or by dissolution of its components followed by precipitation of the cocrystal in accordance with the theorized TPD (in the presence of solvents).

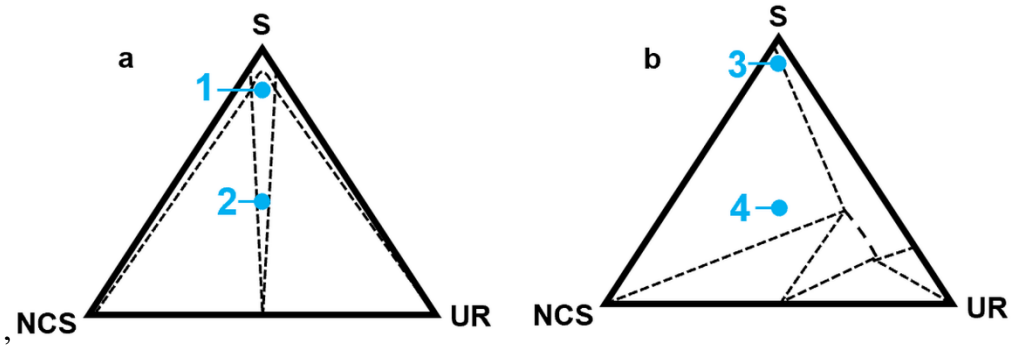

Figure 5.9- Theoretical TPD of NCS-UR in (a) congruent system and (b) incongruent system. 'S' indicates arbitrary solvent.

There is limited literature available on cocrystallization by CSS. Previous CSS cocrystallization studies have found that without mechanical agitation, phase-pure cocrystals are not typically isolated [34,94]. In general, either no cocrystal formation or a mixture of cocrystal and its components is observed. In one study cocrystallization of saccharin with six different coformers was evaluated and where partial cocrystal formation was observed without mixing, the conversion was improved with the addition of stirring [34,94]. However, in cocrystal pairs where no cocrystal formation was observed without mixing, the addition of stirring to the system did not offer an improvement. Therefore, there should be other reasons for lack of cocrystal formation aside from improving mass transfer via mechanical agitation.

Although improved mass transfer via mechanical agitation has been shown to promote cocrystal formation in unmixed conditions, our equipment was not suitable for studies with mechanical

agitation. Therefore, we attempt to provide an understanding of other parameters which influence cocrystal formation in unmixed conditions. In previous studies of CSS with cosolvent in mixed conditions, it has been consistently observed that addition of a small amount of cosolvent can improve cocrystal formation due to improved solubility of the components [34,97]. We have shown that NCS-UR has a tendency to cocrystallize in $scCO_2$ without mechanical agitation, despite low solubility of both components. In this work, although complete conversion to the cocrystal was not observed, it was found that the addition of cosolvent will impact the cocrystal formation in unmixed conditions. The impact may be positive or negative, sometimes completely hindering the formation of the cocrystal.

Despite the relatively low amount of cosolvent in the solvent mixture (0.5 mL), there was a notable impact on the extent of conversion to the cocrystal in the presence of different cosolvents. Since the CSS process is somewhat analogous to a conventional slurry crystallization experiment, ternary phase diagrams and equilibrium phase stability can be considered. Although a TPD has not been developed for the NCS-UR system at each condition used in this work, the aid of a theoretical TPD is considered to offer a reason for the observed phenomenon.

If we consider the formation of cocrystal in relation to a TPD of NCS, urea, and the $scCO_2$ solvent, we may get an idea of why formation is observed in neat CO_2. NCS, urea, and presumably the cocrystal all exhibit very poor solubility in $scCO_2$ and therefore the solubility line occurs at very small mole fraction of both compounds. The TPD will be similar to a congruently saturating system where an equimolar charge of both components allows for the system to fall near or within the cocrystal phase stability region at equilibrium (point (1) in Figure 5.9). Therefore, as the system is held at constant temperature and pressure, both materials are dissolving towards their equilibrium solubilities (with a near 1:1 ratio). Because the solubility of both components is very low the mixture trends into the cocrystal stability region on the TPD, but in an unmixed system it may not reach complete conversion due to lack of mass transfer or difference in dissolution kinetics as more reactants are consumed. NCS and urea in neat $scCO_2$ may behave as such a system.

When IPA is added to the system, the dissolution of components is anticipated to slightly improve leading to better conversion to the cocrystal and therefore higher percentage of cocrystal after a similar time compared to neat CO_2. The small quantity of IPA which improves dissolution

may allow for more cocrystal conversion and slightly facilitate mass transfer in the system, while still maintaining a nearly congruently saturating system (point (1) in Figure 5.9). In this work, addition of IPA increased conversion to cocrystal by between 50 and 60%. But when the mixture was exposed to one volume of IPA in ambient conditions, the components reacted to completely form the cocrystal within 24 h, at a composition similar to point (2) in Figure 5.9.

On the other hand, when cyclohexane is in the system as a nonpolar cosolvent, neither the solubility nor dissolution kinetics of components were improved. Solubility measurements of cocrystal components in cyclohexane also showed that it is a more considerable antisolvent, which may impede dissolution. Nonetheless, some cocrystal formation (up to 35%) was still observed because the system is expected to be congruently saturating (point (1) in Figure 5.9) and tend towards a 1:1 cocrystal because solubility of both components is similarly low. Unlike with IPA, the solubility of both components in cyclohexane was also poor in the neat solvent, therefore at ambient conditions in one volume of cyclohexane a mixture of cocrystal and its components was still observed.

Conversely in the case of added water, it may appear that the system tends towards an incongruently saturating system, where urea exhibits significantly higher solubility. Despite urea's tendency to easily cocrystallize in the presence of water at a particle's surface, water can impede the cocrystallization in a slurry-type system when a TPD is considered. When considering the extremely high solubility of urea in water, it could be that the addition of a small amount of water to $scCO_2$ would substantially improve the solubility of urea. Conversely, NCS has been shown to exhibit very poor solubility in both water and $scCO_2$ therefore the solubility in the mixture likely remains low. Under the assumption that differences in solubility of both components follows the suggested trend, an equimolar mixture of the API and coformer would be expected to fall into a region of the TPD where NCS is stable, but urea is dissolved (point (3) in Figure 5.9). The XRPD diffractograms of solids isolated from experiments with water show decreased urea peak intensity with longer hold time, supporting the preferential dissolution of urea and an incongruently saturating system. However, the possibility of a cocrystal simply not being thermodynamically favored in the aqueous systems must also be considered as a possibility.

In solvent systems where cocrystallization is favorable, TPDs can be used to identify regions of

cocrystal stability. However, in some solvents cocrystallization may not be favorable if the interaction between API and coformer is weaker than intramolecular interaction in the API or intermolecular interaction with API (or coformer) and solvent. As such it is important to consider that aspects aside from solubility of individual components contribute significantly to cocrystal formation. In the case of water as a solvent or cosolvent, it was observed throughout this work that NCS converted to NCS-H during experiments. In humid conditions, some tendency towards formation of NCS-H was also observed although it generally did not lead to complete conversion of NCS-A to NCS-H within the one-week time frame. In addition, all experiments with water or humid conditions did not show any evidence of cocrystal formation. The relative strength of hydrogen bonding (H-bonding) in the three crystalline forms is available from single crystal diffraction data and may be another indication why NCS-UR is not formed in aqueous systems.

In NCS-A, the molecules are intramolecularly bound by an O-H···O bond (d-a 1.92 Å) between the hydroxy group and amide oxygen as shown in Figure 5.10 (a) [147]. In NCS-H, each NCS molecule is H-bonded to water molecules in two locations, through an O-H···O bond (d-a 1.65 Å) between the NCS hydroxy group and water's oxygen and through an N-H···O bond (d-a 1.75 Å) between the NCS amide oxygen and water's hydrogen as shown in Figure 5.10 (b). NCS is H-bonded to urea at the same sites as NCS-H (hydroxy and amide oxygen) [148]. The NCS-UR H-bonding occurs through an O-H···O bond (d-a 1.80 Å) between the NCS hydroxy group and urea carbonyl and through an N-H···O bond (d-a 2.17 Å) between the NCS amide oxygen and the urea amine as shown in Figure 5.10 (c) [147]. Of the three crystalline forms, NCS-A has the longest bond lengths (weakest H-bond strength). In neat $scCO_2$ or $scCO_2$ with cyclohexane and IPA it was observed that NCS-A was the favored polymorph of NCS. In systems where NCS-A is the favored form, as the cocrystal components gradually dissolve the more strongly bound NCS-UR is crystallized. On the other hand, NCS-H has the shortest bond lengths (strongest H-bonds) of the three crystalline forms. In experiments with water, NCS-H remains the favored form and the anhydrous form converts to the hydrate. Despite the high solubility of urea in aqueous systems, formation of the cocrystal is not favorable due to the relative strength of he NCS-H crystal form in comparison.

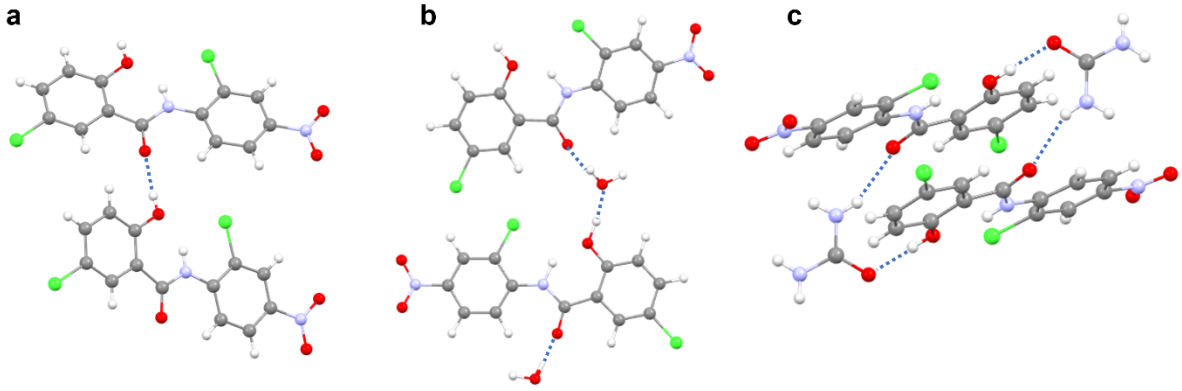

Figure 5.10- Hydrogen bonding in (a) NCS-A, (b) NCS-H, and (c) NCS-UR using single crystal diffraction data from Sanphui and Sovago [20,28].

The results in this work also indicate that a system without mechanical agitation and with or without cosolvent may trend towards equilibrium for between 6 and 24 h before a mass transfer limitation is reached. In the cases of neat CO_2 and IPA cosolvent conversion to cocrystal was roughly 50% greater at 24 h compared to 6 h, but no further improvement was observed with longer hold time. As has been previously suggested, it is possible that as the reactants in the system become more dilute mass transfer can be a limiting step. In addition, it has been previously shown that cocrystallization by CSS (with mechanical agitation) can follow a two-step process with a faster initial conversion followed by a slower rate second step [178]. Without mechanical agitation it could be that the second stage is further hindered due to lack of mixing or limited surface area of reactants to the extent that a full reaction is not achievable within a reasonable hold time (e.g. 48 h).

Interestingly, in neat $scCO_2$ cocrystal formation was improved at 60 °C compared to 40 °C over a similar range of pressures, despite a decrease in CO_2 density. The difference in cocrystal conversion at 40 °C and 60 °C was significant at $p < 0.05$ according to the null hypothesis. The observed behaviour may be related to the relatively high vapor pressure and solubility profile of urea. Catchpole *et al.* [188] found that the solubility of urea showed a stronger temperature dependence than pressure dependence. The crossover pressure is suspected to be in the range of 14-15 MPa based on Peng-Robinson equation of state, above which solubility of urea increased at higher temperatures [188]. However, only one solubility point below 15 MPa was used to model the data, therefore the crossover pressure has some uncertainty. A complete solubility

profile of NCS in CO_2 is not yet available. The temperature dependence observed for NCS-UR formation may be related to dependence of urea's solubility on temperature [188].

Finally, co-melting is a technique commonly employed in the screening of cocrystals whereby a mixture of API and coformer are heated to above the melting point of the lower melting component to facilitate formation of the cocrystal. In ambient conditions, the melt onset of urea and NCS was measured to be 134 °C and 230 °C, respectively. Although these temperatures are well above the operating temperatures in this work, the melting point depression in $scCO_2$ has been reported for a variety of materials such as pharmaceuticals, solid lipids, and polymers (depression in T_g) [190–192]. In this study, a simple phase monitoring experiment supports that melting of either component is not the reason for cocrystal formation in this system, therefore the solubility and dissolution of both components in the supercritical phase should be the main method of cocrystal formation of NCS-UR in this work.

5.6 Conclusions

Formation of an NCS-UR cocrystal was investigated without mechanical agitation under a wide range of conditions including atmospheric pressure with and without solvent, subcritical CO_2, $scCO_2$, and $scCO_2$ with cosolvent. In general, the cocrystal did not form in ambient conditions without mechanical agitation or addition of cosolvent. Also, cocrystal formation with urea was not facilitated by increased humidity in the case of NCS-UR.

Mixtures of NCS and urea were exposed to subcritical and supercritical CO_2 at pressures between 3 and 25 MPa without mixing. Samples at 40 °C and 60 °C that were held in liquid CO_2 did not show conversion to the cocrystal by XRPD analysis. However, when held at supercritical conditions for the same duration, partial conversion to cocrystal was observed in all cases. The conversion to cocrystal was somewhat higher at 60 °C compared to 40 °C, but did not show a strong dependence on pressure. The addition of 0.5 mL cosolvent (between 2.7 and 3.5 mole%) cosolvent to $scCO_2$ was found to have a substantial impact on conversion to the cocrystal. Addition of polar cosolvent (IPA) increased cocrystal conversion by between 50 and 60%. However, when cyclohexane was added conversion to cocrystal was lowered by between 5 and 35% compared to neat $scCO_2$ due to lower solubility of the individual components. In the presence of water, cocrystal formation was hindered completely likely due to the relatively higher strength of H-bonds in NCS-H compared to NCS-A and NCS-UR. The impact of

cosolvent on cocrystal formation is proposed to be dependent on the expected TPD, dissolution of cocrystal formers, and inter- and intra-molecular H-bonding of the relevant crystalline forms in comparison to the cocrystal. Since this was the first study of cocrystallization of NCS and urea in $scCO_2$, cocrystal formation due to a significant depression in melting point was ruled out by phase monitoring studies.

It is possible to form cocrystals under supercritical conditions without mixing even when solubility of the individual components is quite low, such as with NCS and urea. However, choice of cosolvent can significantly impact the results. The addition of cosolvent can improve or reduce cocrystal formation, and in some cases can hinder cocrystal formation completely. Therefore, it is recommended that solubility of individual components in neat organic cosolvent in ambient conditions is used to systematically select appropriate cosolvents for CSS cocrystal screening. Finally, without mechanical agitation, conversion to a cocrystal is slow and may be limited by mass transfer. Continued studies on determining impact of cosolvent choice in CSS cocrystallization with mixing may be suitable next steps in this research.

6 CHAPTER 6: DISCOVERY OF A NOVEL CRYSTALLINE FORM OF ANTHELMINTIC DRUG PRAZIQUANTEL USING HIGH-PRESSURE SUPERCRITICAL CARBON DIOXIDE

Reprinted with permission from L. MacEachern, A. Kermanshahi-pour, M. Mirmehrabi, Transformation under pressure: Discovery of a novel crystalline form of anthelmintic drug Praziquantel using high-pressure supercritical carbon dioxide, Int. J. Pharm. (2022).

6.1 Abstract

Supercritical carbon dioxide (CO_2) has been used as a processing technique to control polymorphism of pharmaceuticals. However, there are fewer reports of novel polymorphs being discovered by supercritical CO_2 processing. As supercritical crystallization methods gain attention for potential in pharmaceutical processing, they may become a critical screening tool for discovery of new polymorphs. In this work, a case study is presented for a novel crystalline form of the anthelmintic drug, Praziquantel, found through supercritical CO_2 processing. The novel form of Praziquantel was characterized by chromatography, nuclear magnetic resonance and infrared spectroscopy, X-ray powder diffraction, thermal analysis, and scanning electron microscopy. Furthermore, the novel form exhibited 13-20% improved solubility compared to commercial Form A between pH 1.6 and 7.5 and was physically stable under stressed conditions (40 °C and 75% relative humidity) for 7.5 weeks. Overall, this work showed that supercritical CO_2 processing is a valuable tool to screen for novel, and possibly viable polymorphs of pharmaceutical compounds with improved properties.

6.2 Introduction

The Food and Drug Administration (FDA) recommends that new drug applications investigate polymorphism of drug candidates. The FDA defines a polymorphic form as crystalline form with different arrangement of molecules in a crystal lattice, including solvates or hydrates [193]. Different polymorphs of an active pharmaceutical ingredient (API) can have different properties such as melting point and morphology, and also different bioavailability [50,156,193–195]. Conversion between polymorphs can occur during drug substance or drug product processing, for example during micronization, drying, grinding/milling, exposure to humidity, etc. [193,195,196]. An unexpected new polymorph can also have adverse impacts if discovered

during later phases of API development or manufacturing.

Many processing conditions can be simulated in a conventional polymorph screening using techniques such as slurries in different solvents, antisolvent crystallization, cooling crystallization, liquid assisted milling or grinding, evaporative crystallization and extended exposure to dry or humid conditions. However, as the pharmaceutical industry advances, so do drug substance manufacturing processes. Supercritical carbon dioxide ($scCO_2$) processing methods such as rapid expansion of supercritical solution (RESS) have gained attention for their potential to use in pharmaceutical processing [197–199]. One reason for the growing interest in supercritical crystallization is due to ability to produce sub-micron size particles, which could potentially be used in inhalers [99,200,201]. In addition, $scCO_2$ may offer environmental benefits in comparison with the conventional organic solvents if supercritical processed can be designed to give high yield with desirable throughput [140,177]. Therefore, it is important to begin incorporating supercritical processing conditions into polymorph screening studies.

There are several reports in literature about control of polymorphism of APIs using supercritical techniques for known polymorphs of pharmaceutical compounds [53,92,202–208]. For example, carbamazepine (CBZ) Form I and Form III have an enantiotropic relationship, where Form III is stable at ambient conditions and is the form used in the drug product [202]. Bettini *et al.* found that conversion to pure Form I could be facilitated by supercritical CO_2 using either static or dynamic methods at 55 °C above 30 MPa [202]. Kordikowski *et al.* observed a similar relationship for enantiotropically related polymorphs of sulfathiazole, whereby solution enhanced dispersion using supercritical fluids (SEDS) was used with methanol (MeOH) at 20 MPa up to 120 °C [203]. They found that the choice of temperature and CO_2 flow rate influenced which polymorph of sulfathiazole was isolated. In another paper, Rossmann *et al.* were able to control the polymorph of acetaminophen using supercritical antisolvent (SAS) with ethanol (EtOH) and acetone [207]. When using EtOH as solvent, Form I was always isolated, while acetone as solvent resulted in Form II. Control of polymorphism using supercritical processes is also reported for Salmeterol Xinafoate using SEDS, glycine and carbamazepine-saccharin cocrystal using SAS, tolbutamide, mefenamic acid, nabumetone and paracetamol using RESS [53,204,206,208,209].

However, there are fewer papers published whereby a novel crystalline form of a compound is

presented through supercritical fluid crystallization techniques. Tozuka *et al.* discovered a new crystalline form of deoxycholic acid (DCA), which can be used to form inclusion complexes with organic compounds, after exposing the material to supercritical CO_2 at 60 °C and 12 MPa [210]. After 1 h storage at the specified conditions, a new X-ray powder diffraction (XRPD) pattern was observed for the solid which was determined to be a new metastable form of DCA. While processing in nitrogen at the same conditions did not give the new form. Based on the differential scanning calorimetry (DSC) results, the new crystalline form was determined to be metastable. Bettini *et al.* found a new polymorph of Didanosine using a supercritical antisolvent (SAS) process with DMSO as solvent and CO_2 as antisolvent [211]. The new form, which was isolated between 10 and 20 MPa at 45 °C showed decreased particle size compared to commercial Didanosine with d_{90} 11.25 μm compared to 20.35 μm. The new form provided only slightly higher aqueous solubility at 26.9 mg/mL compared to 25.4 mg/mL. However, the new form showed conversion to amorphous during mechanical stress (milling) and extended stability study in stressed conditions is unknown.

Praziquantel is on the World Health Organization (WHO) list of essential medicines. It is an anthelmintic used to treat the parasitic worm disease, schistosomiasis [152]. Praziquantel is administered as a tablet of between 150 mg or 600 mg dosage [144]. Praziquantel has shown a minimum measured solubility of 0.4 mg/mL in water between pH 1.2 and 6.8 and is considered a BCS Class II drug [143]. Therefore some research efforts have focused on methods to improve the solubility of Praziquantel— for example, using milling for particle size reduction [154–156]. However, one study identified that milling and cryo-milling may be unsuitable for particle size reduction of Praziquantel due to significant loss of crystallinity and formation of impurities.[212] Therefore feasibility of alternative particle size reduction methods should be investigated.

Praziquantel can crystallize in different forms including (*RS*)-Praziquantel racemate (Form A), hemi-hydrates of both (*R*)- and (*S*)-enantiomers, and two lower-melting anhydrous forms (Form B and C), which were identified in 2018-2019 through solvent-free milling [156–158]. Form B melts 30 °C lower than Form A and has lower heat of fusion, indicating a metastable polymorph. Furthermore, the solubility of Form B in water was twice that of Form A and Form B was observed to be physically stable in ambient conditions for up to 12 months [156]. Form C was also a metastable, lower melting form which exhibited improved aqueous solubility compared to

Forms A and B. However, Form C showed limited physical stability and converted back to form A during storage [158].

There is not any existing literature for Praziquantel in the field of supercritical fluids. In this work, we present a case study of preparing a novel crystalline form of Praziquantel after supercritical CO_2 processing and discuss the benefits of utilizing supercritical CO_2 exposure or crystallization as a polymorph screening tool.

6.3 Materials and Methods

6.3.1 Materials

Praziquantel (>98% purity, Form A), was used as received without further purification from TCI America, Lot #: KM430-AB. Liquid CO_2 (99.9% with Eductor tube) was sourced from Praxair, Inc.

6.3.2 Preparing novel polymorph

Recrystallization experiments in $scCO_2$ were done with a modified SFT-110 equipment (Supercritical Fluid Technologies, Inc., Newark, DE) which is shown in Figure 6.1. Praziquantel (200 mg) was wrapped in a Kimwipe and was carefully placed in a 100 mL high-pressure vessel (Figure 6.1-6) in an extractor oven (±0.5 °C) (Figure 6.1-4). The vessel was pressurized with CO_2 using an SFT-10 pump at 24 mL/min (Figure 6.1-2) and the vessel was sealed by closing the valves at the inlet and outlet (Figure 6.1-5). The vessel was held at 40 °C/17.9 MPa for 22.5 h in the case of praziquantel. The pressure in the vessel was measured at 5 min increments using an in-line monitoring system (Figure 6.1-7) comprising a PX309-10KGI pressure transducer (Omega) and an OM-CP-Process101A current data logger (Omega). The transducer/logger system interfaces with OM-CP Data Logger Software version 4.2.21.1 via an OM-CO-IFC200 USB (Omega).

The vessel was held at the specified temperature and pressure for 22.5 h. After 22.5 h, the vessel was purged with CO_2 at the set pressure for 20 min at approximately 4-5 STD L/min. The pump was then stopped, and the vessel was de-pressurized. The solubilized solids were collected in the collection vials (Figure 6.1-8) through a rapid expansion from supercritical solution (RESS)

process through a nozzle with 1580 µm inner diameter (ID) and about 40 mm spray distance. The Kimwipe containing residual API (Praziquantel) was carefully removed from the vessel. The solid remaining in the Kimwipe after the experiment was simply exposed to high-pressure conditions for the duration of the experiment.

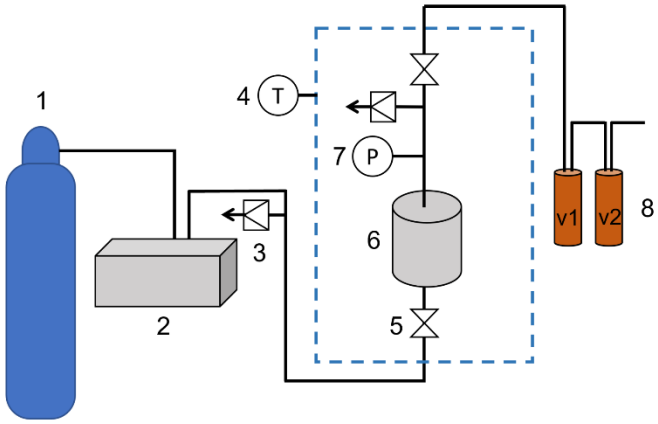

Figure 6.1- Schematic of the SFT-110 equipment. 1- CO_2 source, 2- CO_2 pump, 3- rupture disk, 4- thermocouple, 5- valve, 6- high-pressure vessel, 7- pressure transducer, 8- collection vials (v1 and v2).

6.3.3 XRPD and Indexing

X-ray powder diffraction (XRPD) was performed using a Bruker D8 Advance in reflection mode with a Cu Kα source. The scan range was 4-30° 2θ with 0.03° 2θ step size. Samples were prepared on Si zero-return wafers. Indexing of powder patterns was done using Rigaku PDXL2 software.

Variable-Temperature XRPD (VT-XRPD) analysis was performed using an Anton Paar CHC plus temperature- and humidity-controlled stage equipped with zero-background sample holder. Samples were heated at 10 °C/min under a stream of dry air.

6.3.4 Thermal Analysis

Differential scanning calorimetry (DSC) was performed using a TA Discovery DSC (TA Instruments). Samples (2-4 mg) were weighed directly into hermetic aluminum pans with pin-hole. All measurements were performed under nitrogen gas flow from 30-300 °C at a rate of 10.0 °C/min. In some instances, DSC was used for thermal treatment experiments to evaluate polymorph conversion after heating. For thermal treatment experiments, the solid was prepared

in the same fashion, but was heated to a specified temperature at a rate of 10.0 °C/min followed by cooling at 20 °C/min and then recovering the solid from the aluminum pan for XRPD analysis. The thermal treatment experiments were also conducted under nitrogen gas flow. Simultaneous thermogravimetric analysis and differential scanning calorimetry (TGA/DSC) was performed using a Mettler Toledo TGA/DSC^{3+}. Samples (5-10 mg) were weighed directly in hermetic aluminum pans with pin-hole and analyzed from 30-250 °C at a rate of 10.0 °C/min.

6.3.5 Water content by KF

KF titration for water determination was performed using a Mettler Toledo C20S Coulometric KF Titrator equipped with a current generator cell with a diaphragm, and a double-platinum-pin electrode. Aquastar™ CombiCoulomat fritless reagent was used in both the anode and cathode compartments. Samples were dissolved in the anode compartment and titrated until the solution potential dropped below 100 mV. Hydranal 1 wt. % water standard was used for validation prior to sample analysis.

6.3.6 Infrared Spectroscopy

IR spectroscopy was performed using a Thermo Scientific Nicolet iS10 FTIR Spectrometer with a helium-neon laser. The beam splitter was potassium bromide/germanium optimized for mid IR. The source type was Ever-Glo and tungsten/halogen. Samples were analyzed on the Smart iTX accessory with high-efficiency optic reflectors and diamond ATR crystal attenuator.

6.3.7 Liquid Nuclear Magnetic Resonance

^{1}H NMR was performed using a Bruker Avance 500 MHz spectrometer. Solids were dissolved in 0.75 mL deuterated DMSO. Solutions were transferred to NMR tube (Wilmad 5 mm thin wall 8″ 200 MHz, 506-PP-8). The measurement conditions were 16 scans with 1.0 s relaxation delay and 3.25 s acquisition time at 27 °C.

6.3.8 Scanning Electron Microscopy and Electron Dispersive Spectroscopy

SEM was performed using a TESCAN MIRA3-LMU FESEM with 5 kV beam, approximately 7 nm beam spot size, and 250-260 pA beam current. Samples were mounted on carbon tape and sputter coated with approximately 15 nm Au layer using a BIO-RAD PS3 sputter coater. EDS analysis was performed on the same samples. Unprocessed Praziquantel Form A was used as a

reference standard for C, N and O mass ratios. Between 6 and 12 unique points on each sample were analyzed using 5 kV beam and 40 s acquisition time.

6.3.9 Hot-Stage Microscopy

Hot-stage microscopy was performed Zeiss AxioScope A1 digital imaging microscope equipped with a Linkam hot stage with LTS420 Stage controller at 200X magnification using a 10 °C/min heating rate. Images were captured through a built-in Axiocam 105 digital camera and processed using ZEN 2 (blue edition) software provided by Zeiss.

6.3.10 Solubility in water and biorelevant media

Fasted state simulated gastric fluid (FaSSGF) was prepared using Biorelevant powder (Biorelevant.com) and FaSSGF concentrated buffer (Biorelevant.com). First, 3.678 g of FaSSGF concentrated buffer and 96.2 mL of distilled water were added to a beaker. FaSSGF powder, 6.0 mg, was then added and the mixture was stirred to dissolve before use.

Fasted state simulated intestinal fluid (FaSSIF) was prepared using Biorelevant powder (Biorelevant.com) and FaSSIF concentrated buffer (Biorelevant.com). First, 4.165 g of FaSSIF concentrated buffer and 96.1 mL of distilled water was added to a beaker. FaSSIF powder, 0.224 g, was then added and the mixture was stirred to dissolve before use.

Solubility in water and simulated fluids was measured at 37 °C in a stirred heating block (ThermoFisher). Solids (~5-6 mg) were weighed in 4 mL vials; and 3 mL of distilled water or simulated fluid was added. Unprocessed Praziquantel samples were prepared in triplicate and the new form in duplicate. The thin slurries were stirred until the sampling time. Approximately 1 mL of the slurry was drawn using a syringe and filtered through a 0.45 µm PTFE filter directly into a high performance liquid chromatograph (HPLC) vial for analysis. A calibration line was developed using unprocessed Praziquantel and the chemical purity HPLC method outlined below. Praziquantel was accurately weighed into volumetric flasks and diluted to volume with methanol:water (65:35 by volume). Calibration points were made at: 0.007, 0.010, 0.054, 0.098, and 0.342 mg/mL (0.342 mg/mL calibration point was injected in triplicate). Concentration of Praziquantel in the solutions was evaluated by comparing to the calibration line which is shown in Figure 6.2.

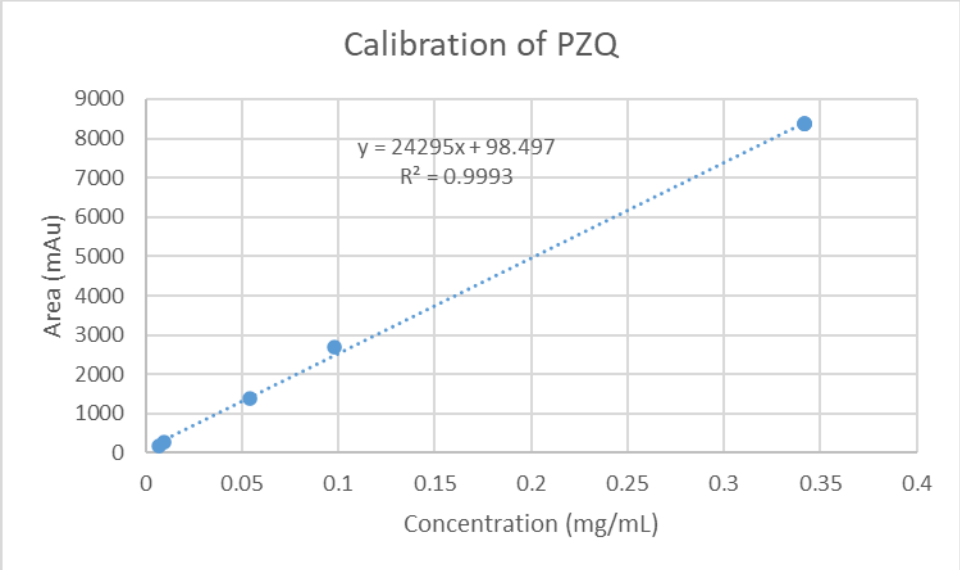

Figure 6.2- Calibration line for Praziquantel used for solubility measurement using HPLC.

6.3.11 High Performance Liquid Chromatograph (HPLC) analysis

HPLC analysis for chemical purity was done using an Agilent 1260 Infinity II HPLC equipped with a Waters XBridge C18 column (4.6 × 150 mm, 3.5 µm). The column temperature was uncontrolled. The mobile phase used was methanol:water (65:35 v/v) with a flow rate: 0.75 mL/min. Praziquantel was monitored at 220 nm and eluted at 6.1-6.2 min.

For chiral purity analysis an Agilent 1260 Infinity II HPLC equipped with a CHIRALPAK AD-H column (4.6 × 250 mm, 5 µm). The column temperature was 40 °C. The mobile phase used was heptane:isopropyl alcohol (82:18, v/v), at a flow rate of 1.25 mL/min. The column effluent was monitored at 220 nm. The measured retention times for R-Praziquantel and S-Praziquantel were 7.8 and 8.4 min, respectively.

6.3.12 Stability experiment

Physical form stability experiments were conducted by placing solids at 40 °C and 75% relative humidity (RH) in a Memmert HCP50 stability chamber. After storage, the solids were analyzed using XRPD.

6.4 Results and Discussion

In this work, a novel and stable form of Praziquantel was accidentally discovered through $scCO_2$ processing. The novel form was isolated after simply exposing Praziquantel to $scCO_2$ at 40 °C/17.9 MPa and also as a mixture of two crystalline forms through RESS. The novel solid form is presented here to serve as an example of the usefulness of $scCO_2$ as a tool in polymorph screening.

6.4.1 Characterization of Novel Form of Praziquantel

6.4.1.1 XRPD Analysis and Indexing

Solids collected from RESS and solids which remained in the Kimwipe after exposure to high pressure were analyzed by XRPD. Both solids exhibited an XRPD diffractogram different than unprocessed Praziquantel (Form A), as shown in Figure 6.3. Solids from RESS crystallization exhibited additional peaks in the XRPD diffractograms indicated with triangles in Figure 6.3, notably at 6.5 and 16.5 deg. 2θ, which are characteristic of Praziquantel hemihydrate (PZQ-HH) found by Zanolla *et al.* in 2020 [196]. This indicates that the solid remaining in the Kimwipe is likely a pure solid phase, while the solid from RESS is a mixture of two polymorphs.

The pure novel form, which remained in the Kimwipe, exhibits its highest intensity characteristic peaks at 7.3, 9.8, 13.1, 14.6, and 21.0 deg. 2θ. A comparison of the XRPD data of the solid in this work compared to predicted powder patterns of various anhydrous and hydrate forms obtained from the Cambridge Crystallographic Data Center (CCDC) is shown in Figure 6.4. The characteristic peaks of the novel form do not agree with previously reported data, illustrating that the solid isolated after exposure to high pressure is a novel form.

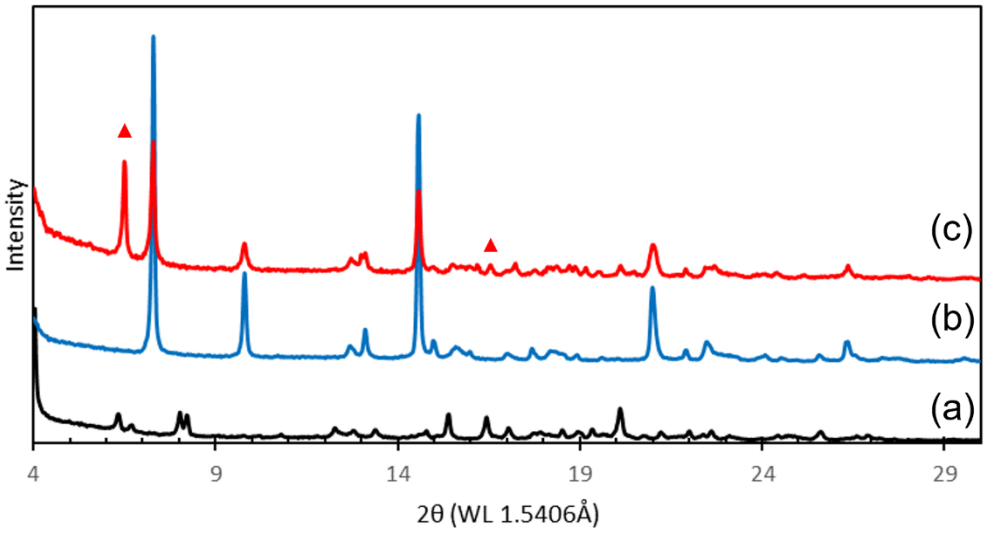

Figure 6.3- XRPD diffractograms of (a) Praziquantel Form A, (b) solid remaining in Kimwipe, and (c) solids isolated by RESS.

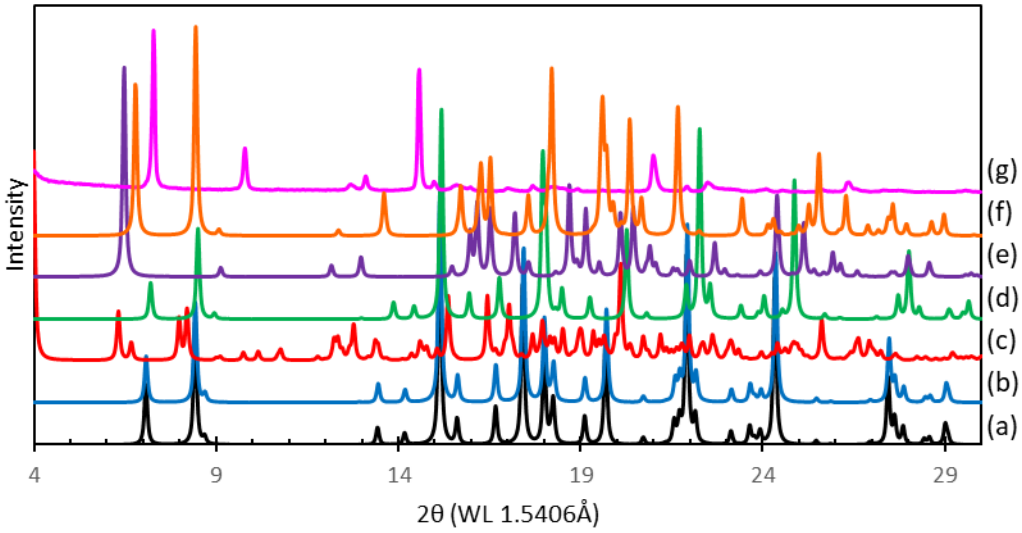

Figure 6.4- Comparison of XRPD powder pattern of new polymorph compared to predicted powder patterns from single crystal data available on the CCDC with associated Refcode. (a) SIGBUG (+)-Praziquantel hemihydrate [213]**; (b) SIGBUG01 (R)-(-)-Praziquantel hemihydrate** [214]**; (c) TELCEU (RS)-Praziquantel** [157]**; (d) LIVFED (R)-Praziquantel hydrate** [215]**; (e) WUHQAU Praziquantel hemihydrate** [196]**; (f) TELCEU01 Praziquantel Form B** [156]**; (g) Novel form from this work.**

Form A (unprocessed) Praziquantel crystallizes in the triclinic P-1 space group with four

molecules in the asymmetric unit and a unit cell volume of 3320 $Å^3$.[157] Racemic Praziquantel hemihydrate (PZQ-HH) also crystallizes in the P-1 space group with one molecule in the asymmetric unit and a unit cell volume of 860 $Å^3$.[196] However, a hemihydrate of the (*S*)-enantiomer was shown to crystallize in the monoclinic C2 space group with unit cell volume of 1708 $Å^3$.[157] The diffraction pattern of the novel form was indexed using PDXL2 software. Solutions were found using Ito13 and N-TREOR algorithms, with four of the five top solutions fitting a monoclinic space group and one solution fitting a triclinic space group which falls in line with space groups of previously reported Praziquantel forms. The solution with the best reliability (FOM value of 17.08) suggests that the novel form crystallizes in the monoclinic P2/m space group with unit cell volume of 2332.09 Å3 (a = 14.128 Å; b = 13.536 Å; c = 13.187 Å; $\alpha = \gamma = 90°$; $\beta = 112.368°$). A Z-value of 5 (rounded down from 5.2) can be calculated for the unit cell when using a predicted true density of 1.2 g/cm^3 calculated by the Immirzi and Perini method [216].

6.4.1.2 Confirmation of Chemical Structure

High-performance liquid chromatography (HPLC) analysis was done on the solids from high pressure experiments to ensure that the isolated solids were not degraded since this is the first report of Praziquantel exposed to $scCO_2$. Chemical and chiral purity were analyzed.

HPLC analysis of solids from high-pressure experiments do not show any signs of chemical degradation as shown in Figure 6.5 to Figure 6.7. Unprocessed Praziquantel eluted at 6.147 min and the solids after $scCO_2$ processing eluted at 6.129 min (residual solid) and 6.111 min (RESS). The chiral purity of the solid after exposure to high-pressure remained the same as input Praziquantel, showing a ratio of 49.8 to 50.2 (area) for the peaks at 7.75 min and 8.43 min and did not show conversion to either *(R)* or *(S)* enantiomer, as shown in Figure 6.8 and Figure 6.9. Therefore, it can be concluded that Praziquantel did not degrade or exhibit enantiomeric conversion during $scCO_2$ processing.

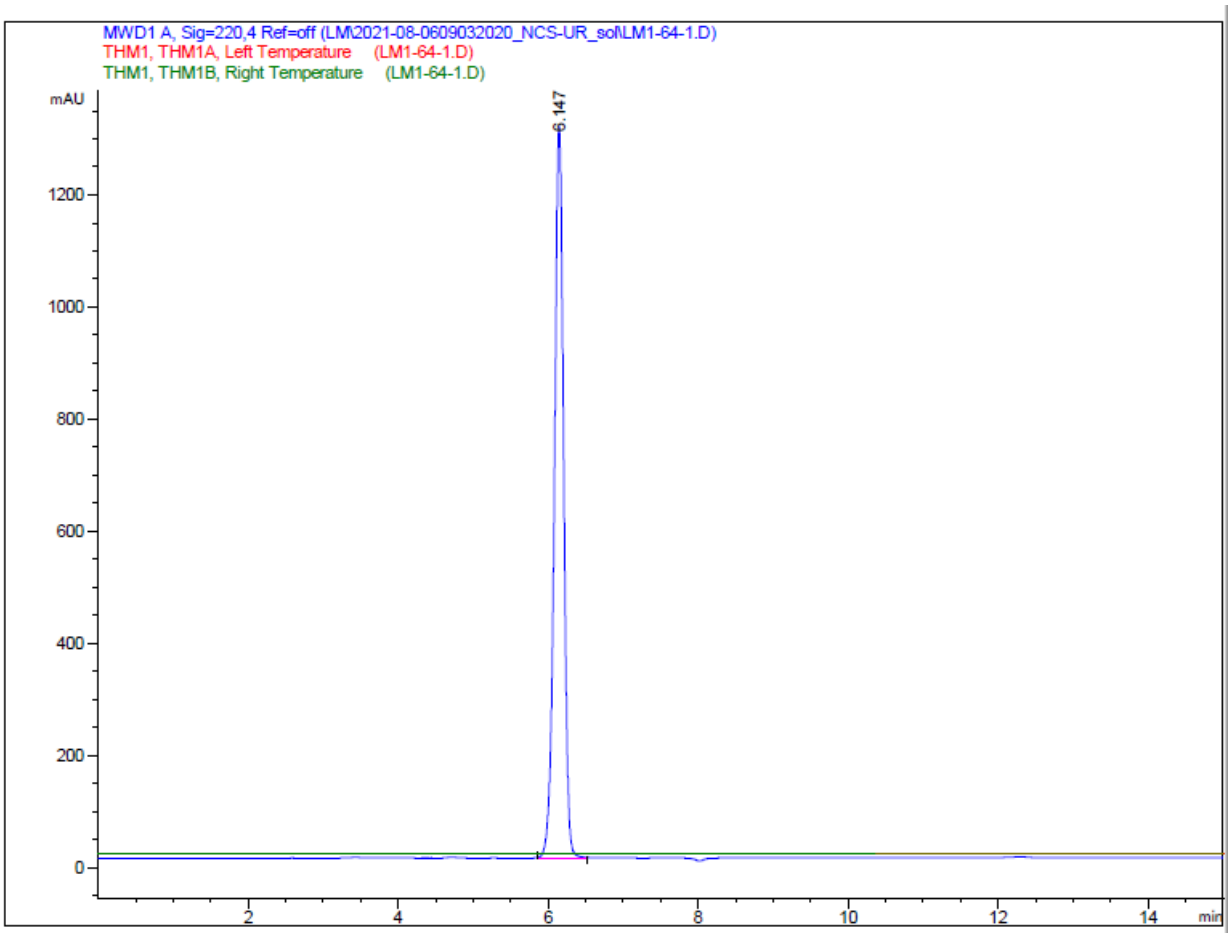

Figure 6.5- HPLC chromatogram of unprocessed Praziquantel.

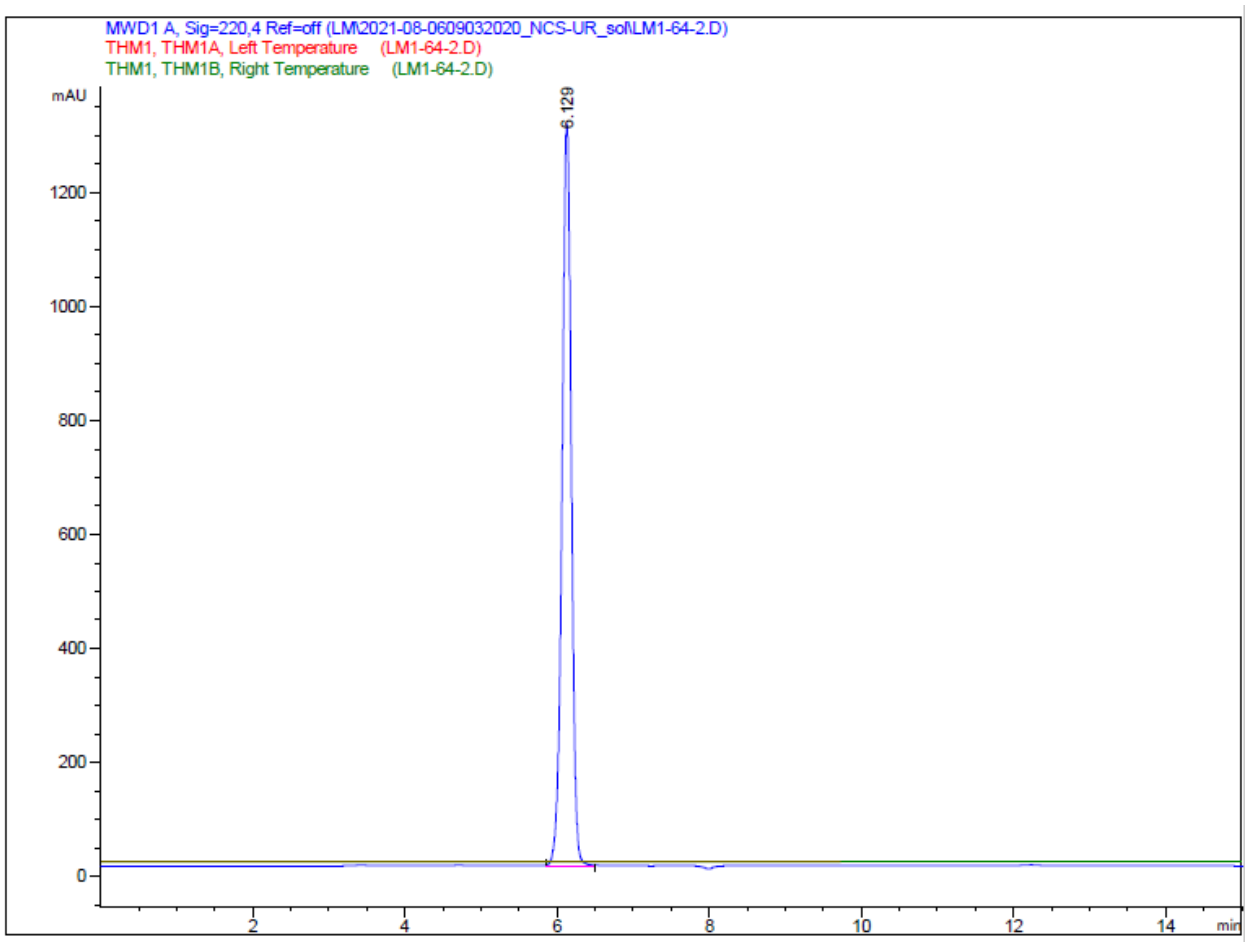

Figure 6.6- HPLC chromatogram of Praziquantel from vessel.

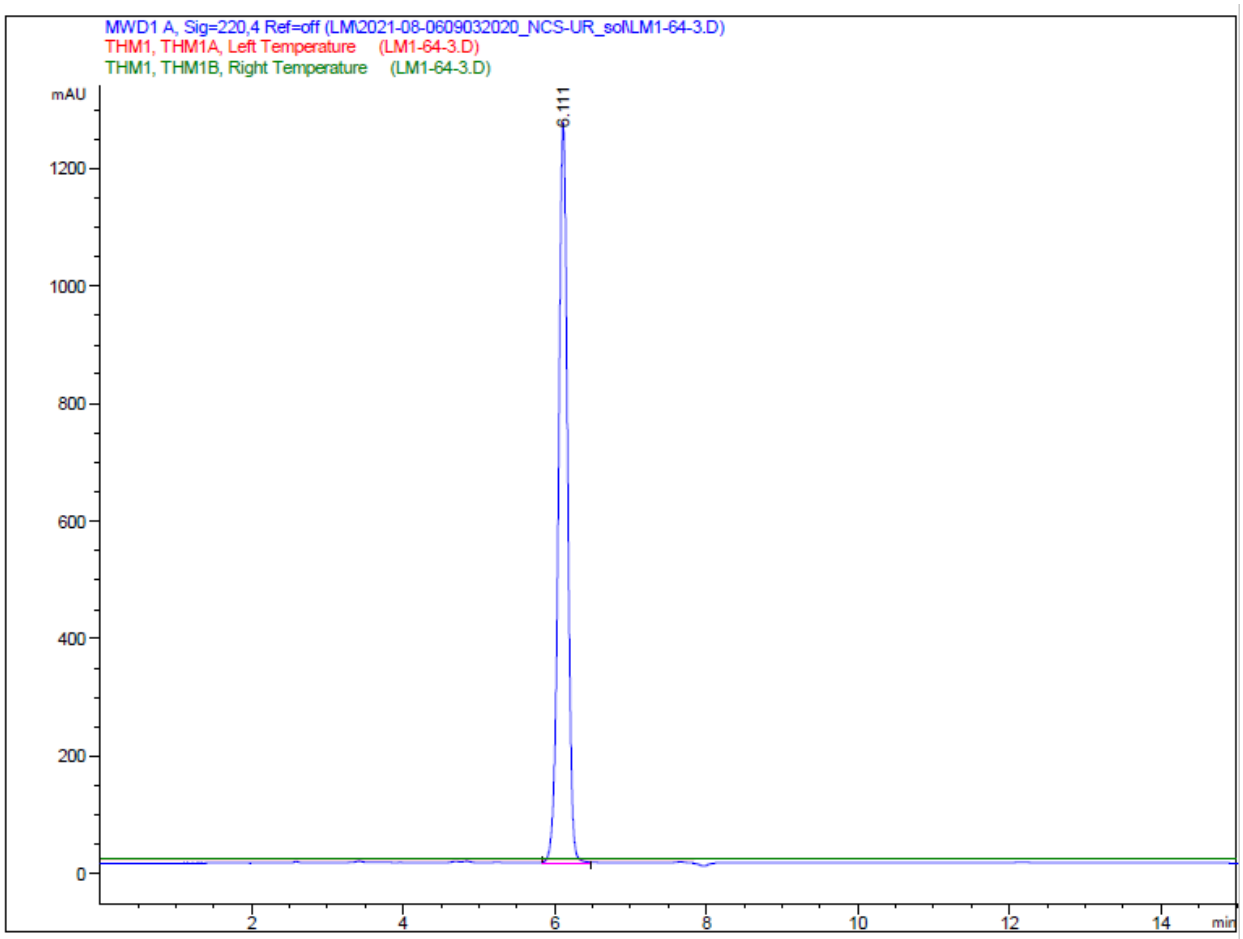

Figure 6.7- HPLC chromatogram of Praziquantel from RESS.

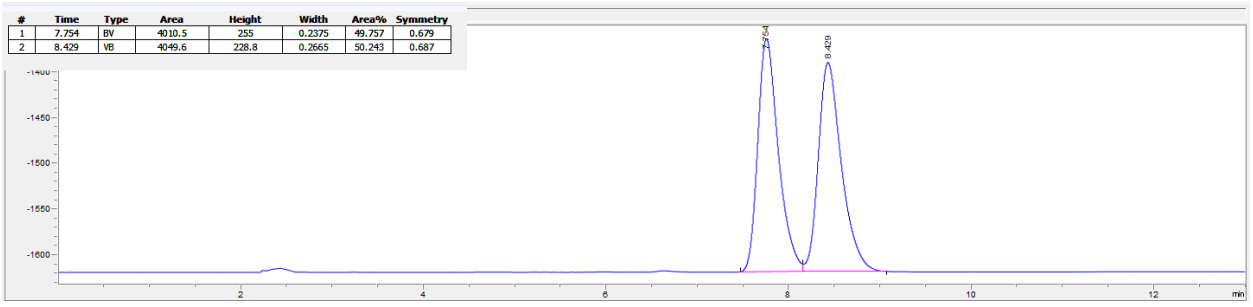

#	Time	Type	Area	Height	Width	Area%	Symmetry
1	7.754	BV	4010.5	255	0.2375	49.757	0.679
2	8.429	VB	4049.6	228.8	0.2665	50.243	0.687

Figure 6.8- Chiral HPLC chromatogram of unprocessed Praziquantel.

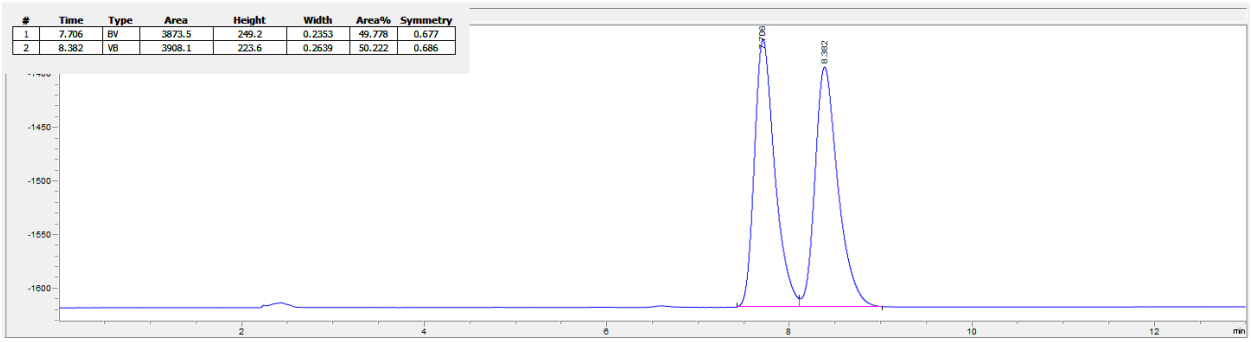

Figure 6.9- Chiral HPLC chromatogram of Praziquantel from vessel.

6.4.1.3 Spectroscopic Analysis

Solids isolated in high pressure experiments were analyzed by infrared (IR), liquid ^{1}H NMR spectroscopy, and EDS. Unprocessed Praziquantel (Form A) was also analyzed by three methods as a baseline.

The most notable differences in the IR spectrum of the solids, which were exposed to $scCO_2$ are the peak at 3586 cm^{-1} that is observed in the spectra of both solids, and the peak at 2321-2333 cm^{-1} that is observed only in the spectrum of the solid, which remained in the Kimwipe after the experiment. A stack of the IR spectra of three solids is shown in Figure 6.10. Changes in the fingerprint region of the $scCO_2$-processed solids compared to unprocessed Praziquantel were not substantial as shown in Figure 6.11 and Figure 6.12.

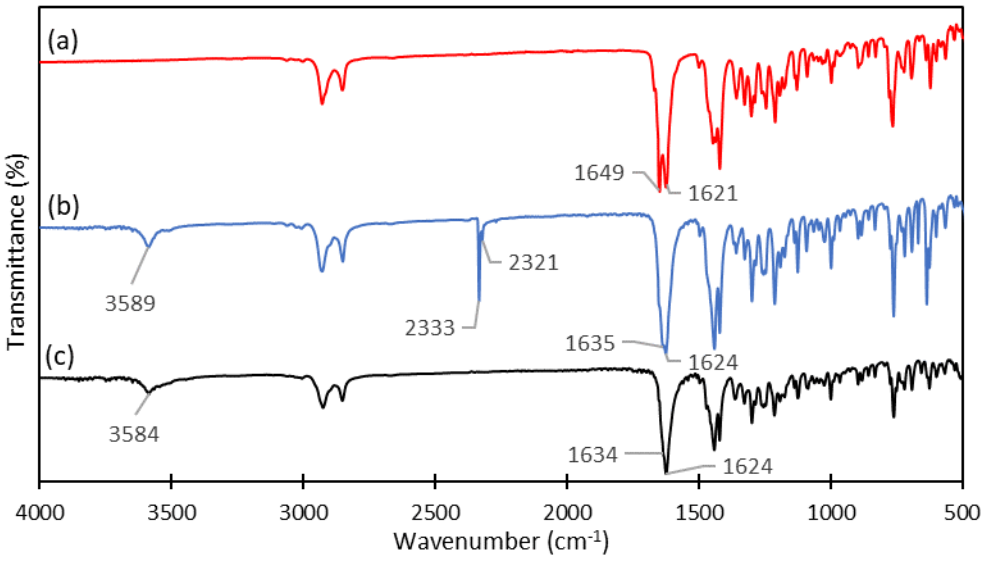

Figure 6.10- IR spectra of unprocessed Praziquantel and solids isolated after high-pressure CO_2 experiments. (a) Praziquantel Form A; (b) Praziquantel from Kimwipe; (c) Praziquantel from RESS.

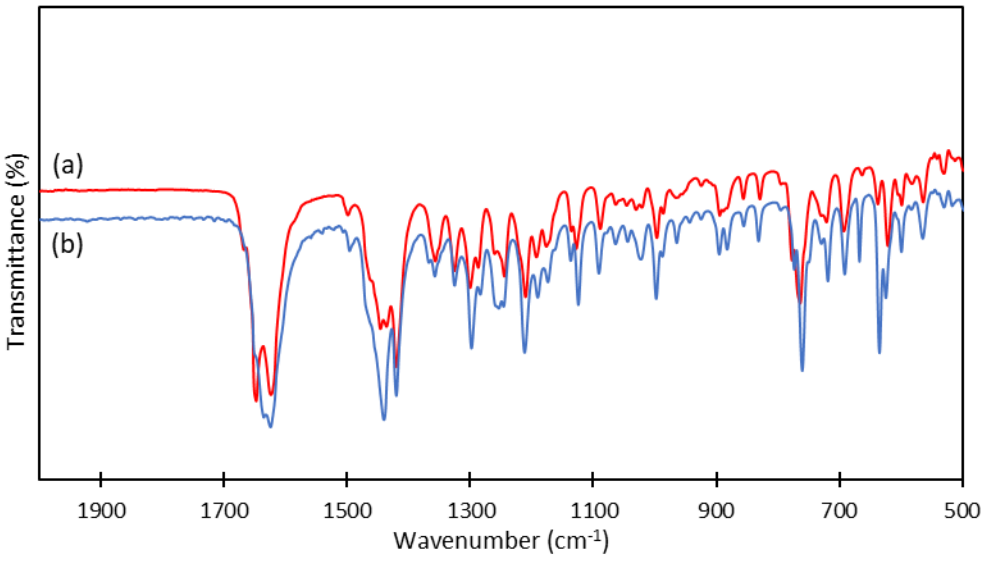

Figure 6.11- Comparison of fingerprint region of unprocessed Praziquantel (a) and solid remaining in Kimwipe after experiment (b).

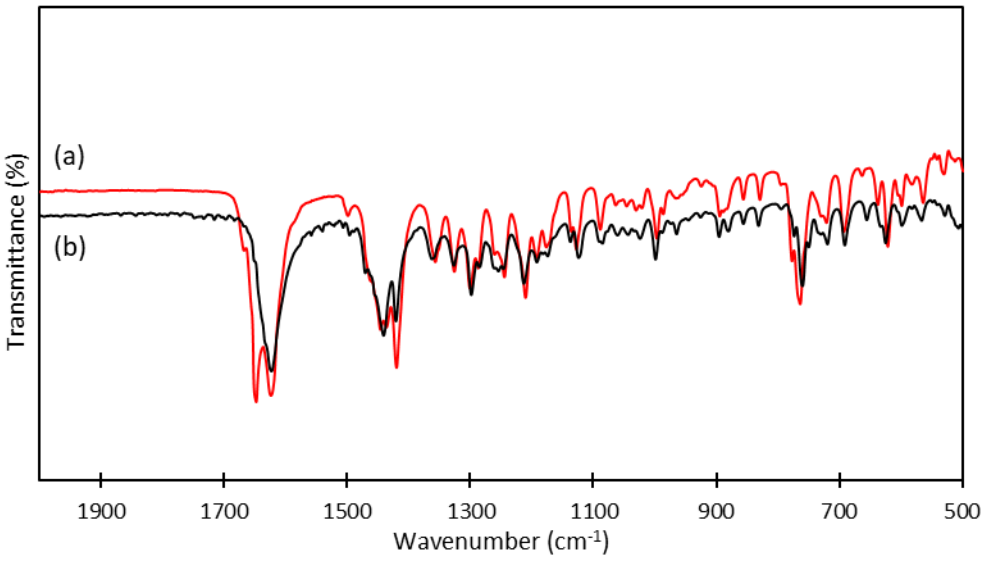

Figure 6.12- Comparison of fingerprint region of unprocessed Praziquantel (a) and solid from RESS (b).

Although the broad peak at 3584-3589 cm^{-1} is not observed in the spectrum for unprocessed Praziquantel, there are IR spectra of Praziquantel in literature which show peaks near that band. For example, Zanolla *et al.* report IR spectrum of three Praziquantel polymorphs, all with broad peaks near 3500 cm^{-1} [158,196]. In particular, the PZQ-HH form exhibited a more pronounced peak at 3543 cm^{-1} which was attributed to the OH typical of hydrates [196]. Some shifting of the C=O band at 1624-1649 cm^{-1} is also observed with the solids isolated from high-pressure compared to unprocessed Praziquantel, which has been reported for other polymorphs of Praziquantel which can be related to the conformation of the molecule [156,158,196]. Praziquantel has two main conformations which are related to the carbonyl moieties.[217] In the *syn* conformation, both carbonyl groups are on the same with respect to the piperazine ring while in the *anti* conformation the carbonyl groups are on opposite sides of the piperazine ring due to rotation of the C—N bond connecting to the cyclohexane-moiety. Density functional theory calculations by Borrego-Sánchez *et al*. have shown that the *syn* conformer— the conformer adopted by Form A— has greater frequency separation between the two C=O bands in a calculated IR spectrum compared to the *anti* conformer.[217] In addition, they calculated the dipole moment of both conformers, showing that the *syn* conformer was substantially more polar

than the *anti* conformer, thus the *anti* conformer may be more stable in nonpolar environments. Based on the circumstances under which the novel form was obtained (in non-polar scCO_2) and the smaller frequency difference in the C=O IR bands of the novel form compared to Form A (10-11 vs 28 cm^{-1}), it is possible that the form change induced by exposure to high pressure in a non-polar solvent is related to change in conformation of Praziquantel molecules from *syn* to *anti*. Change in conformation in supercritical conditions has also been observed for compounds such as Ibuprofen and Carbamazepine.[218,219] Further investigation of the system is needed to confirm the nature of this form change at a molecular level.

In addition, the peak at 2321-2333 cm^{-1} has not been observed in any reported IR spectra for known Praziquantel polymorphs and is not expected to be related to the structure of Praziquantel. Coincidentally, carbon dioxide IR spectrum shows the main characteristic peak in this range related to the asymmetric stretching mode. The peak related to the asymmetric stretch of CO_2 has also been shown to shift when dissolved in different environments, shifting from 2365 and 2333 cm^{-1} to 2343 cm^{-1} [220]. The inclusion of CO_2 in the crystals which remained in the vessel may be attributed to formation of persistent fluid bubble inclusions in the crystals which have been previously observed by Raman spectroscopy.[221] Bobo *et al.* found that under stagnant conditions in CO_2 the number of trapped fluid inclusions increased when pressure increased, which was also observed by increased intensity of the CO_2 bands in the associated Raman spectra. In this work, the solids which were isolated by RESS do not exhibit a CO_2 peak in the IR spectrum. If CO_2 is attributed to fluid inclusions in the crystals, the absence of such inclusions is possibly related to the rapid depressurization and small crystal size.

The liquid NMR spectra of the three solids are shown in Figure 6.13. The NMR spectra do not indicate any major degradation of the samples which were exposed to high-pressure. The spectra of the solids collected from RESS have an extra signal in the NMR around 0.8 ppm. However, the solids collected from the Kimwipe do not show any meaningful differences compared to unprocessed Praziquantel.

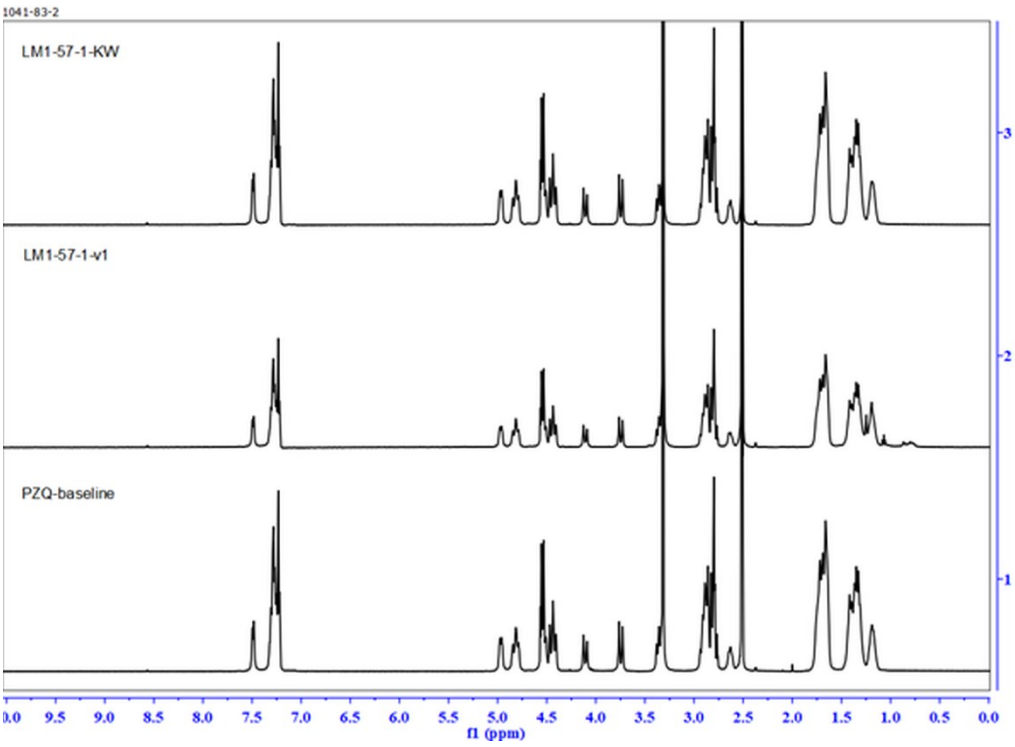

Figure 6.13- ^{1}H NMR spectra of Praziquantel samples.

The EDS results of solids obtained from supercritical experiments were within range of the expected composition for Praziquantel. EDS is a qualitative elemental analysis technique and is challenging for determining composition of light elements such as C, N, and O. However, the results from the samples are in fair agreement with the expected ratios (77 wt.% C, 9.5 wt.% N, 13.5 wt.% O for a hemi-hydrate) further corroborating other analyses that the isolated solids are the same chemical entity. The IR, NMR, and EDS analysis coupled with the HPLC data indicate that the chemical structure of Praziquantel remained in-tact after $scCO_2$ processing.

Table 6.1- EDS analysis results.

Sample	C (wt. %)	N (wt. %)	O (wt. %)
Unprocessed Praziquantel, Form A	78.0 ± 6.5	9.0 ± 2.3	12.9 ± 4.5
Sample from RESS	75.6 ± 3.2	10.8 ± 2.2	13.7 ± 3.0
Sample remaining in Kimwipe	74.9 ± 3.1	10.6 ± 1.0	14.5 ± 3.2

6.4.1.4 Thermal Analysis and Water Content

Both solids were analyzed by DSC to evaluate the melting point. The thermogram of unprocessed Praziquantel is shown in Figure 6.14 for comparison. The DSC of the solids isolated after $scCO_2$ processing showed multiple events in the DSC thermograms. The nature of the thermal events observed in the DSC thermograms was investigated though a combination of thermal treatment experiments in DSC, hot-stage microscopy, and VT-XRPD analysis.

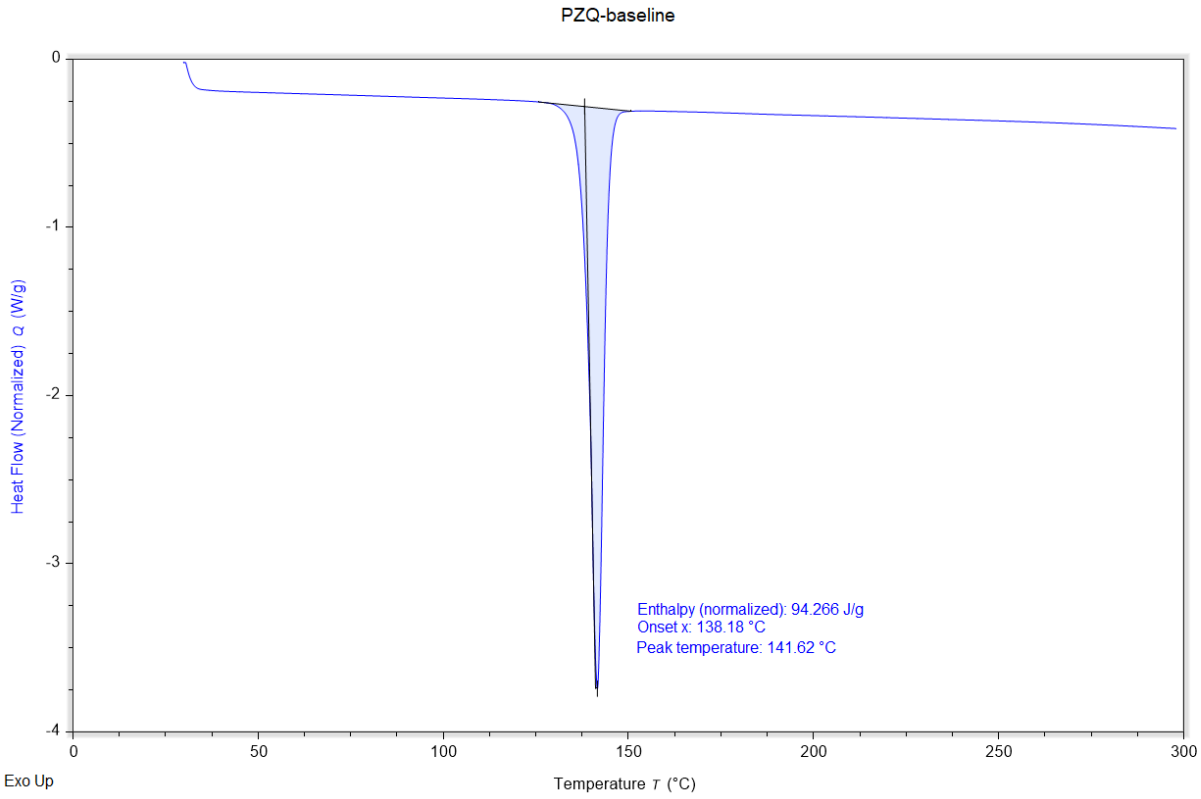

Figure 6.14- DSC thermogram for Praziquantel unprocessed.

The first endothermic peak in the thermogram of solids isolated from RESS (Figure 6.15) appears as two overlapping endotherms with onset of 66.2 °C (peak 83.6 °C). As aforementioned, the solids isolated from RESS are a mixture of the novel form presented in this paper and 'PZQ-HH' previously reported [196]. Hot-stage microscopy coupled with thermal treatment by DSC confirmed the first endotherm agrees with removal of water and subsequent melting of the previously reported 'PZQ-HH' form (appearing as a shoulder) followed by the

dehydration of the novel form to a new dehydrate form as illustrated in Figure S12-b,c [196]. The first exothermic event (onset 93.3 °C, peak 102.6 °C) corresponds to crystallization of the melt phase to previously reported Form B, with characteristic Form B peaks indicated with triangles in Figure 6.20 [156]. Subsequently, the new dehydrate form melts and crystallizes to yet another new form as indicated by the second endothermic and exothermic events with onsets at 110.42 °C (peak 113.2 °C) and 118.60 °C (peak 120.8 °C), respectively, as illustrated in Figure S12-e,f. Finally, the new higher temperature form melts with onset at 131.26 °C (peak 133.3 °C). The XRPD is in Figure 6.16 and thermal treatment and hot-stage microscopy results of the solids from RESS are shown in Figure 6.17.

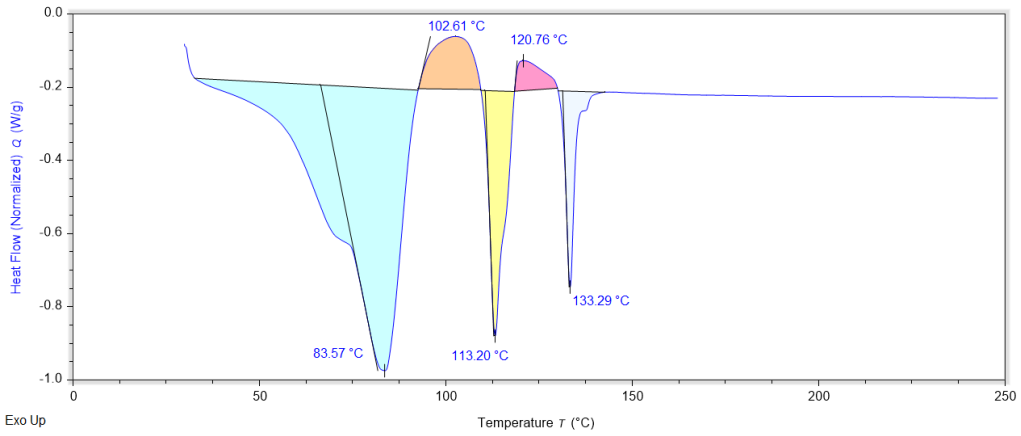

Figure 6.15- DSC thermogram of Praziquantel isolated from RESS.

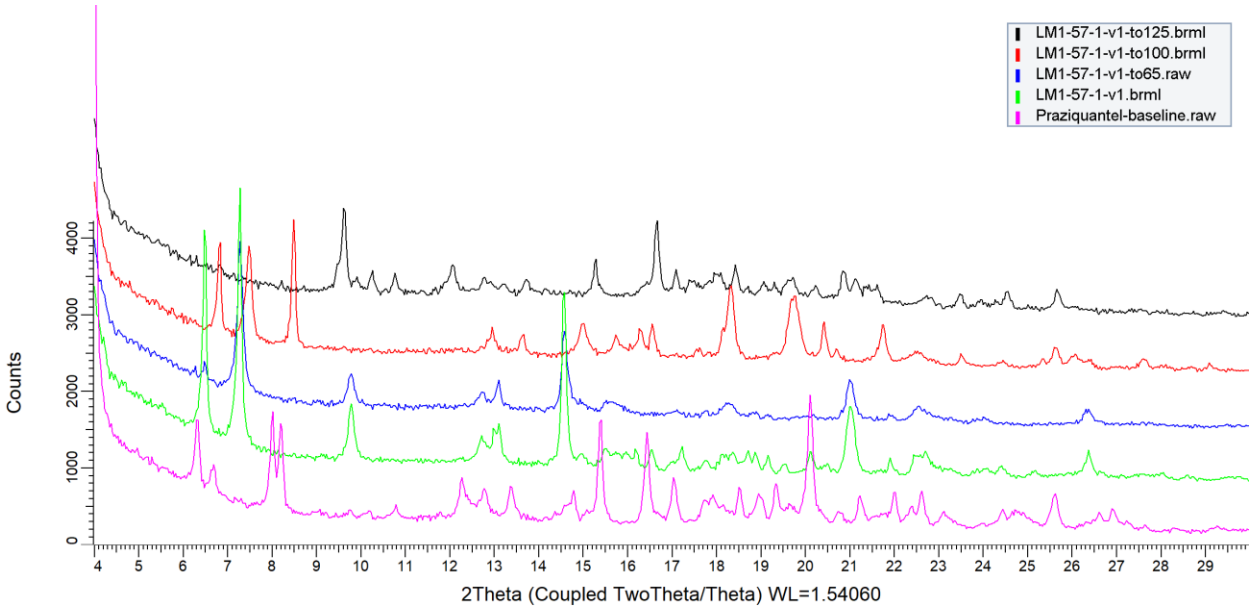

Figure 6.16- XRPD diffractograms from thermal treatment of PZQ from RESS. (pink) unprocessed; (green) PZQ from RESS; (blue) PZQ from RESS after thermal treatment to 65 °C; (red) PZQ from RESS after thermal treatment to 100 °C; (black) PZQ from RESS after thermal treatment to 125 °C.

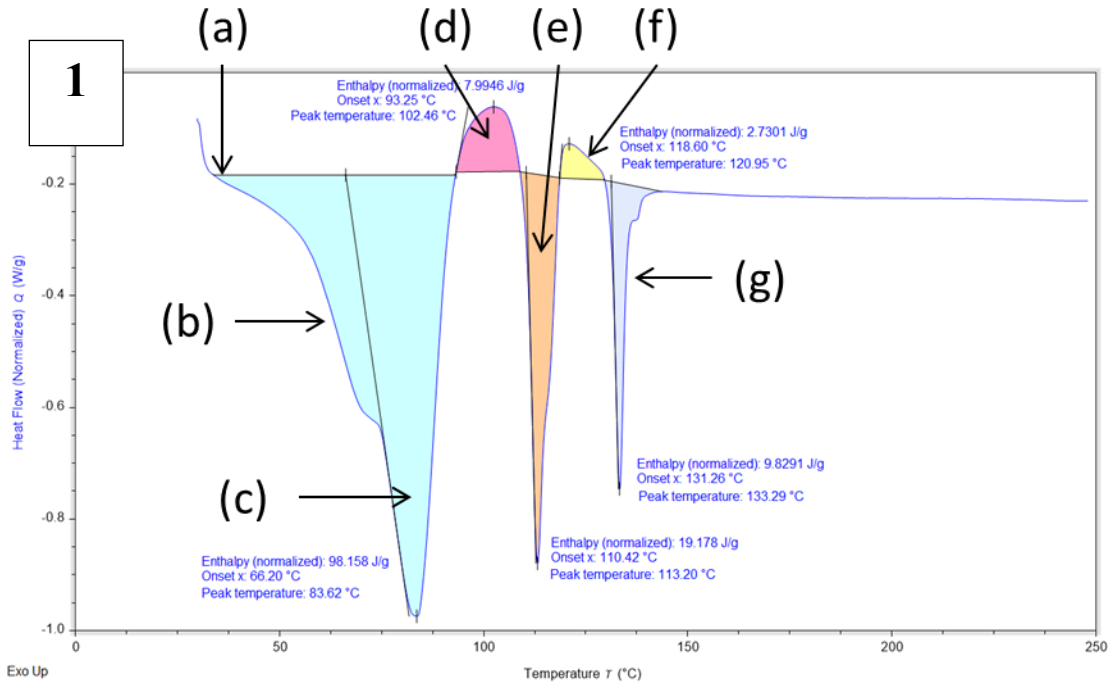

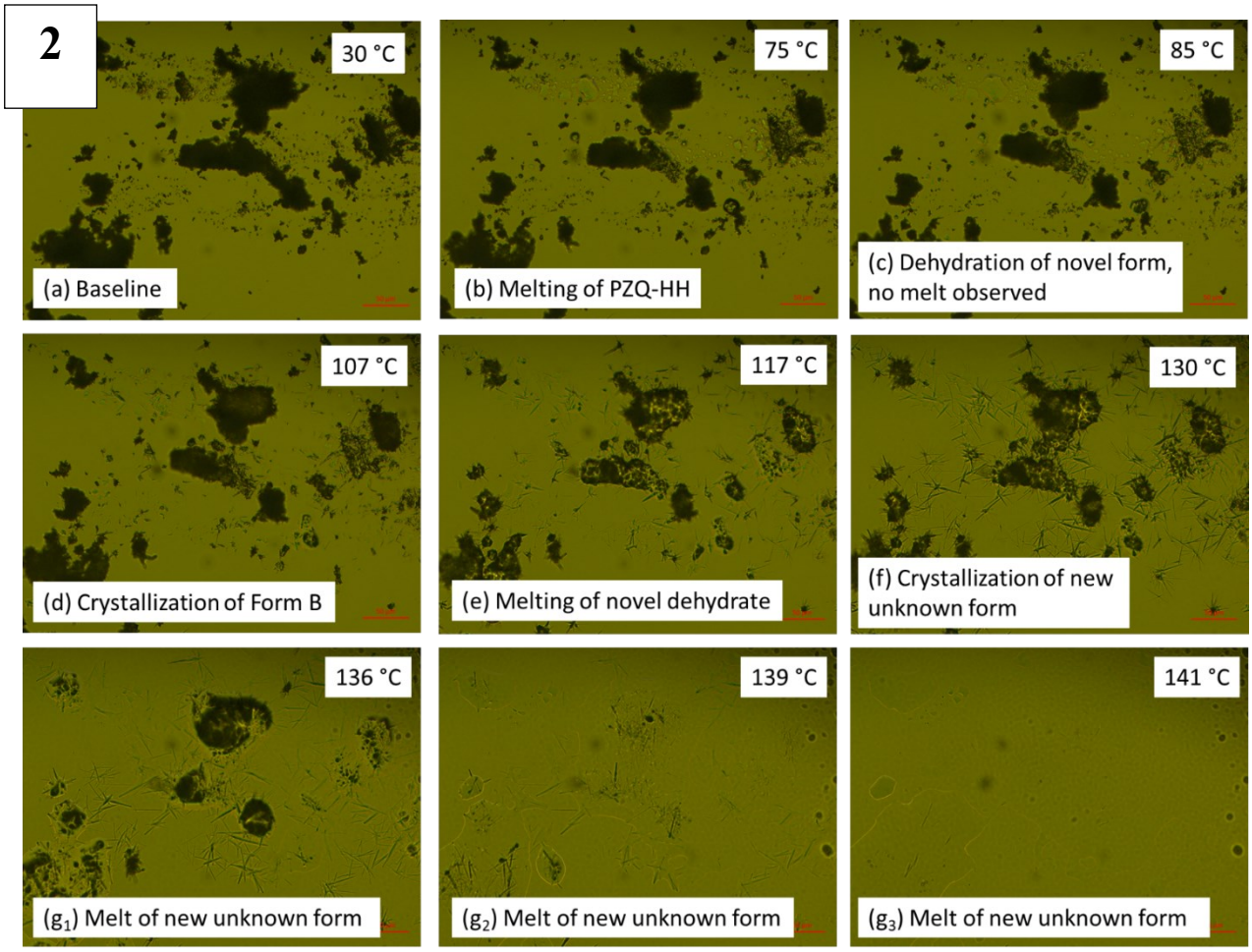

Figure 6.17- Hot-stage microscopy analysis of mixture of novel form and PZQ-HH. (1) DSC thermogram (2) microscope images.

The solid which remained in the Kimwipe also showed a complex DSC thermogram as shown in Figure 6.18. The first endotherm with onset at 83.11 °C (peak 92.5 °C) is related to dehydration of the novel form (to the same dehydrate observed after heating the solids from RESS). In this case, the dehydrate melted and then crystallized to Form A, as confirmed by VT-XRPD and thermal treatment by DSC. The final endotherm showed a melting event at 139.00 °C agreeing with the melt of Praziquantel Form A (141.6 °C), shown in Figure 6.14. The VT-XRPD results for the novel form are shown in Figure 6.19.

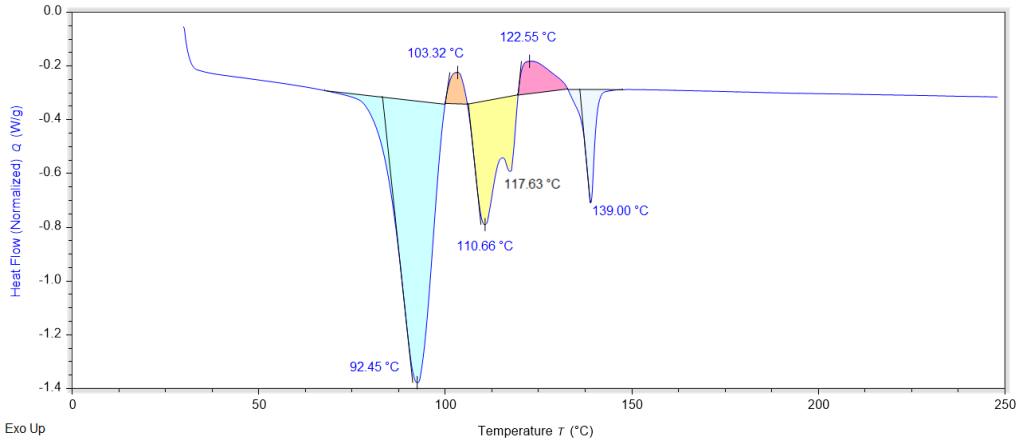

Figure 6.18- DSC thermogram of Praziquantel after exposure to high pressure.

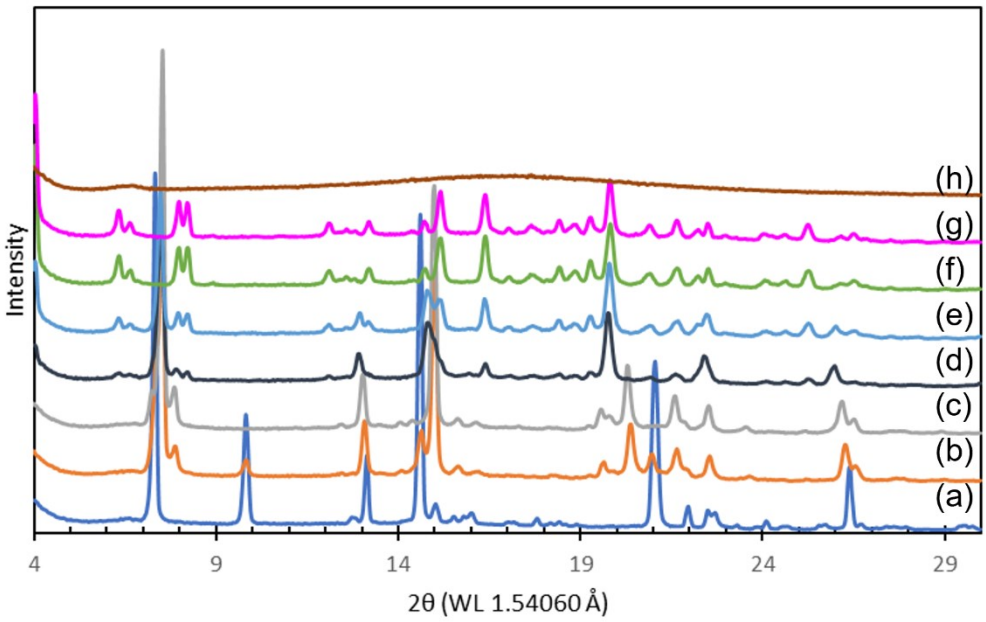

Figure 6.19- XRPD results from VT-XRPD experiment on sample remaining in Kimwipe. (a) 30 °C; (b) 70 °C; (c) 105 °C; (d) 115 °C; (e) 120 °C; (f) 130 °C; (g) 135 °C; (h) 140 °C.

Two new, unique diffraction patterns (compared to other papers and the CCDC database) were observed through thermal analysis. The two new forms are likely a new dehydrate and novel anhydrous form of Praziquantel, but neither were characterized beyond XRPD analysis in this

work. The diffractograms of the novel PZQ patterns obtained through thermal treatment experiments are shown in Figure 6.20-c (new dehydrate), Figure 6.20-d (new dehydrate as mixture with Form B), and Figure 6.20-e (new anhydrous form). The new dehydrate form has characteristic peaks at 7.5, 13.0, and 15.0 deg. 2θ, while the new anhydrous form has characteristic peaks at 9.6, 12.1, 15.3, and 16.7 deg. 2θ.

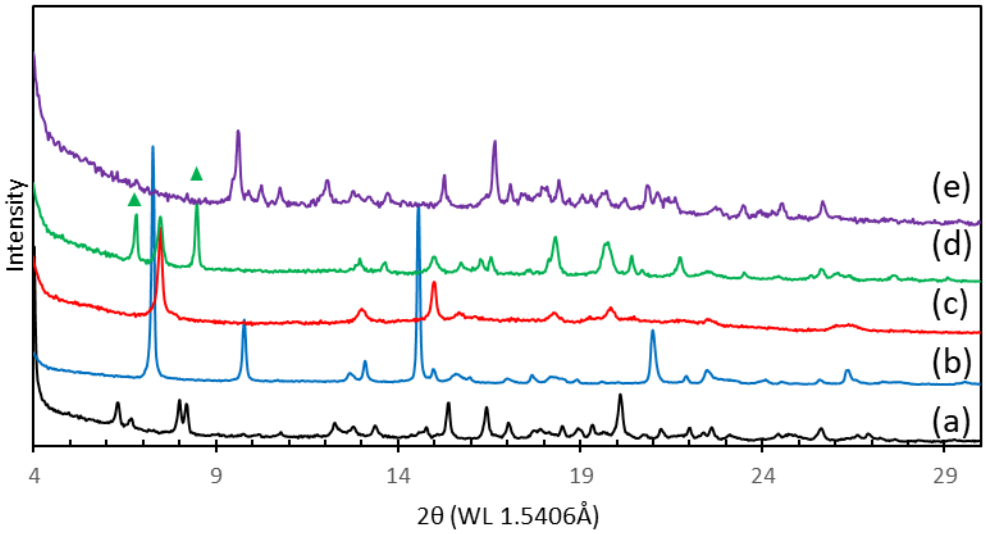

Figure 6.20- XRPD diffractograms of unique patterns obtained form thermal treatment experiments. (a) Praziquantel Form A; (b) Novel form (remaining in vessel after CO_2 exposure); (c) Novel form (remaining in vessel) after heating to 100 °C; (d) After heating mixture of novel form and PZQ-HH to 100 °C; (e) After heating mixture of novel form and PZQ-HH to 125 °C.

Thermogravimetric analysis was done on the solid remained in the Kimwipe after the experiment. A mass loss of 3.38 wt.% was observed, coinciding with the first endothermic event by DSC. The TGA thermogram is shown in Figure 6.21. KF titration for water content was done on the same sample. The water content for a 12.7 mg sample of the solid isolated from high-pressure vessel was 32397 ppm (3.24 wt.%), in close agreement with the mass loss observed by TGA (3.38 wt.%) indicating that the isolated solid is a hydrate with 0.6 eq. water. It is possibly a hemi-hydrate with a slight excess of surface water due to hygroscopicity. Other hemi-hydrates of PZQ are known [196]. It should be noted that a drying study was not completed to determine if there was surface or channel water. A single crystal analysis is recommended for further

evaluation.

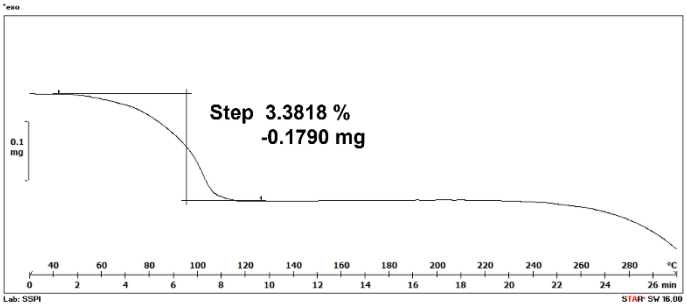

Figure 6.21- TGA thermogram of solid isolated from Kimwipe.

For generation of the new crystalline form, a 100 mL high pressure vessel was used for the conversion of 200 mg Praziquantel. The amount of water required for 0.6 molar equivalents of water with 200 mg Praziquantel is 6.7 mg. In 100 mL of CO_2 (with 10 ppm water) at the expected water content is 0.8 mg water which is not sufficient water to form the hydrate alone. Water content of the unprocessed material was 2.54 wt.%. In a coastal climate, such as in the lab where this work was conducted, relative humidity is often upwards of 60-70% relative humidity (RH). In addition, prior to pressurizing the vessel with CO_2, there was approximately 100 mL ambient air (60-70% RH) which was not purged from the system prior to pressurization. Therefore, the water incorporated into the novel hemi-hydrate should arise from combination of the water in the starting material and the humid air in the system which was not purged prior to processing.

6.4.1.5 Microscopic Analysis

Unprocessed Praziquantel, Praziquantel from RESS, and Praziquantel remaining in the vessel were analyzed by scanning electron microscopy (SEM), as shown in Figure 6.22. Both unprocessed Praziquantel and Praziquantel from RESS show agglomerates and fused particles comprising smaller individual crystals. Praziquantel recovered from the high-pressure vessel showed a distinct needle-like morphology with larger particle size compared to the unprocessed material. Praziquantel from the vessel were also at 500X is shown in Figure 6.23.

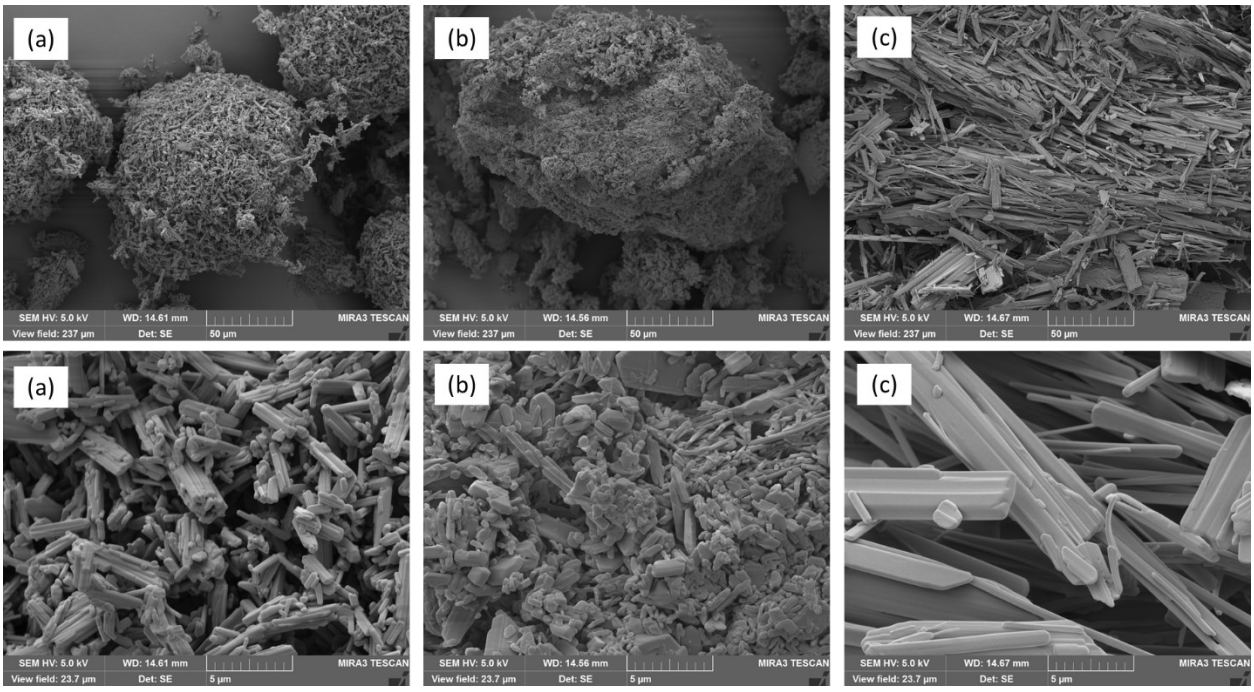

Figure 6.22- SEM images of (a) Praziquantel unprocessed; (b) Praziquantel from RESS; (c) Praziquantel from vessel.

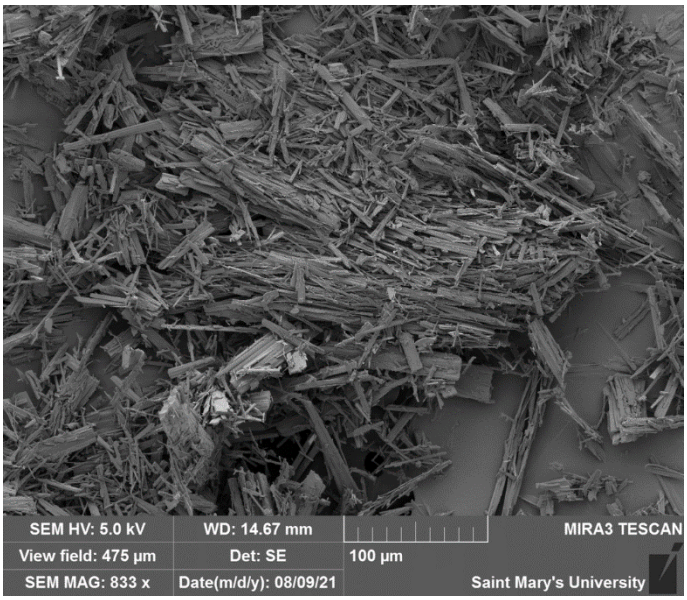

Figure 6.23- SEM (500X) of Praziquantel from vessel.

6.4.2 Physical Stability in Stressed Conditions

A sample of the solids remaining in the Kimwipe was stored at 40 °C/75% RH for 7.5 weeks to

assess its stability. After 11 days, 20 days, and 7.5 weeks at the stressed conditions, the samples were analyzed by XRPD showing the solids were physically stable and no changes in polymorph were observed, Figure 6.24.

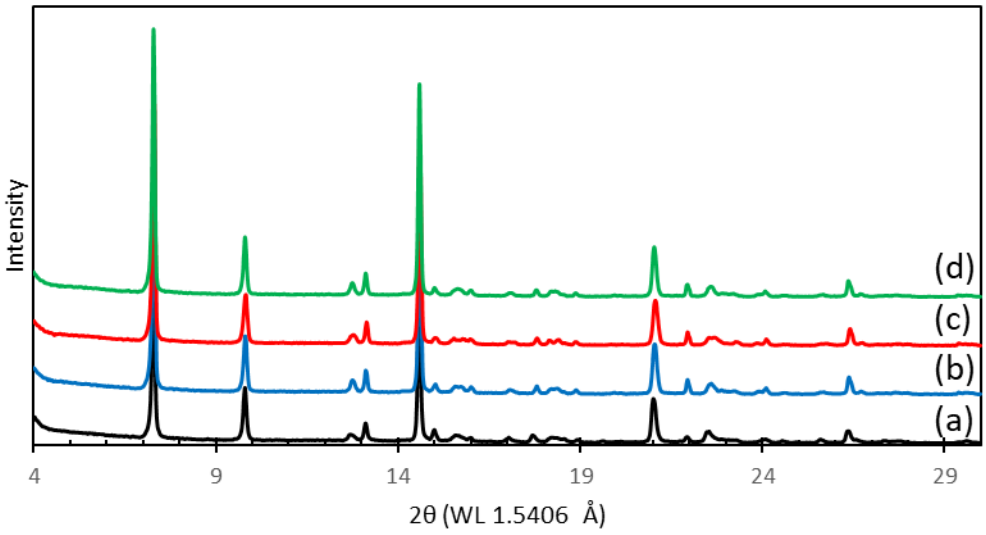

Figure 6.24- Solid form stability XRPD result after storage at 40 °C and 75% RH for 7.5 weeks. (a) solids from Kimwipe initial; (b) 11 days; (c) 20 days; (d) 7.5 weeks.

6.4.3 Solubility of Novel Form in Biorelevant Media

Solubility of unprocessed Praziquantel and the new polymorph (solids remaining in the vessel) was measured in water, FaSSGF (pH 1.6), and FaSSIF (pH 6.5) at 37 °C. The matrix of experiments is shown in Table 6.2. Any solid remaining in the vials after 24 h of stirring was analyzed by XRPD to assess if conversion to a different crystalline form occurred.

The solubility of Praziquantel Form A and the new polymorph did not show a strong dependence on pH and the solubility at pH 6.5 and 1.6 was similar. The solubility of the new polymorph was 1.2X greater than Praziquantel form A at the 30 min sampling point and 1.13X-1.18X greater at 24 h. The solids collected after 24 h showed that Praziquantel Form A was stable and did not change crystalline form as shown in Figure 6.25. In addition, the new hemihydrate did not show signs of conversion to a different hydrated of neat form after stirring in aqueous systems for 24 h, as shown in Figure 6.26.

Benet *et al.* presented a database with solubility of praziquantel reported at 0.4 mg/mL between pH 1 and 7.5 at 37 °C.[143] However, details on the polymorph which gave this solubility were not included. In a different work, Passerini *et al.* measured the solubility of praziquantel Form A in water at 25 °C as 0.304 ± 0.009 mg/mL.[222] Although the results in this work may not be compared directly to previous solubility reports for praziquantel since they are in different buffered media, they are similar in value. Differences between the solubility in this work compared to other data could possibly arise due to crystallinity/amorphous content, particle size, or the selected buffer media.

Table 6.2- Solubility of Praziquantel in water, FaSSIF, and FaSSGF.

Fluid	**Unprocessed Praziquantel (Form A)**		**New form**	
	30 min (mg/mL)	24 h (mg/mL)	30 min (mg/mL)	24 h (mg/mL)
Water	0.275 ± 0.003	0.291 ± 0.005 (pH 7.46 ± 0.11)	0.339 ± 0.001	0.333 ± 0.001 (pH 7.50 ± 0.01)
FaSSIF (pH 6.5)	0.281 ± 0.002	0.296 ± 0.001 (pH 6.46 ± 0.01)	0.338 ± 0.001	0.350 ± 0.001 (pH 6.46 ± 0.00)
FaSSGF (pH 1.6)	0.282 ± 0.003	0.303 ± 0.005 (pH 1.57 ± 0.02)	0.334 ± 0.004	0.343 ± 0.007 (pH 1.59 ± 0.01)

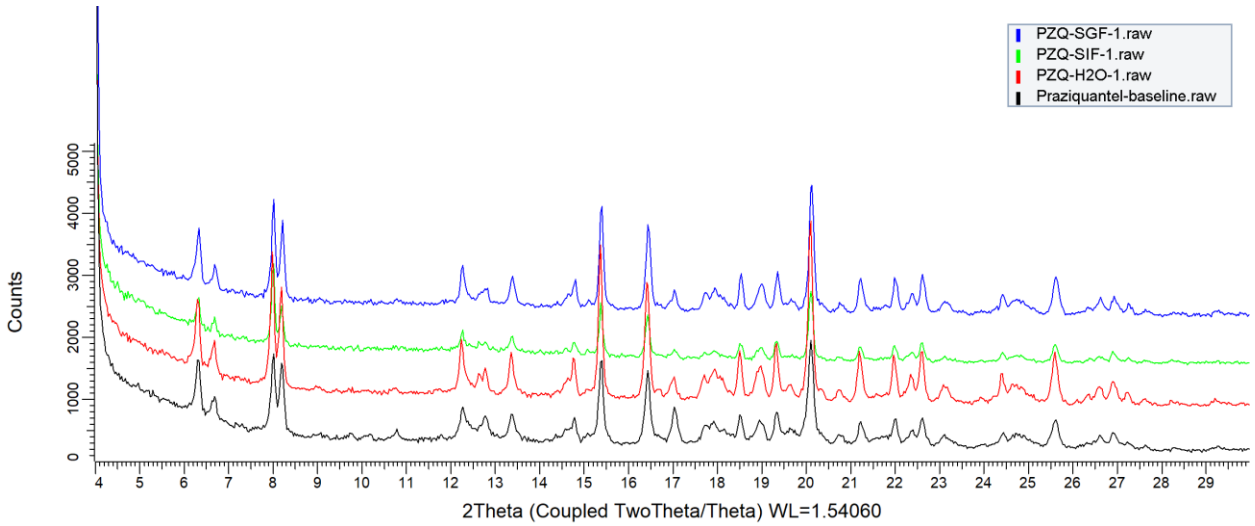

Figure 6.25- XRPD result for Praziquantel (unprocessed) after stirring in water, FaSSIF, and FaSSGF for 24 h.

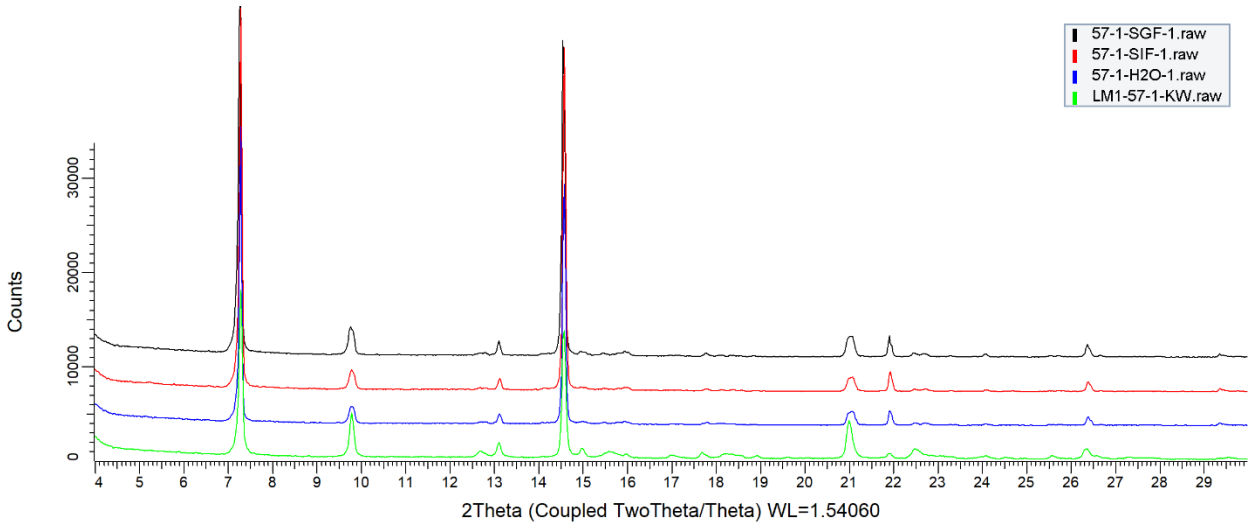

Figure 6.26- XRPD result for Praziquantel new form after stirring in water, FaSSIF, and FaSSGF for 24 h.

6.4.4 Review of Characterization of Novel Form

Although single crystal growth is the most conclusive method to confirm a new crystalline form of a compound, the XRPD, DSC, TGA, and microscopy results are indicative of a new crystalline form compared to other forms reported in literature. The combination of NMR, HPLC (both chemical and chiral), and IR analysis proves that the Praziquantel isolated after $scCO_2$ processing remained as the same chemical entity with high purity.

^1H NMR of the novel form shows the same spectrum as unprocessed Praziquantel, indicating the same chemical. The NMR data does not differentiate between enantiomers and would not indicate if a dimer or oligomer were formed. However, other analyses prove that the solid isolated remains the same, chemically. HPLC analysis shows that Praziquantel is chemically pure due to the compound eluting at the same retention time and there were no additional peaks in the chromatograms. Chiral HPLC analysis shows that the solid isolated after $scCO_2$ experiments remains racemic. This analysis is conclusive in showing that the enantiomeric composition did not change and the solid did not react to form a dimer or oligomer. IR analysis is consistent with the structure and did not indicate significant chemical change compared to unprocessed Praziquantel but shows that the solids which remained in the vessel after $scCO_2$ processing have trapped some residual CO_2. It should be noted that the CO_2 observed in the IR

spectrum does not indicate presence of stoichiometric amount of carbonic acid in the crystal structure. For example, VT-XRPD showed that upon heating, the novel form first dehydrates to a novel dehydrate form and then converts to Form A. If carbonic acid was present in a stoichiometric quantity, it would be expected to breakdown into CO_2 and water during the conversion to Form A, showing approximately 12 wt.% mass loss in TGA. There is no evidence of mass loss surrounding these transitions in the analysis presented. In addition, IR data suggests that the form change could be related to a change in the conformer of the molecule.

XRPD analysis shows unique peaks when compared to other Praziquantel solid forms in literature, which indicates a unique crystalline lattice. In addition, the solids collected by RESS is a mixture of the novel form and PZQ-HH; while the solid which remained in the vessel is a pure crystalline form [196]. Further investigation is needed to identify conditions which isolate a pure phase of the novel form through RESS crystallization. DSC shows a unique thermal profile compared to other polymorphs of Praziquantel. The unique endothermic events are indicative of a novel crystalline form. The first endotherm is due to loss of water (dehydration). The TGA result (3.38 wt.% mass loss which agrees with 0.61 eq. water) and KF result (3.24 wt.%, 0.58 molar eq. water) also indicate that the new solid form is a hydrate. It is possibly a hydrate with 3:5 stoichiometry (3 water to 5 Praziquantel molecules) or a hemihydrate with 0.1 eq. excess water due to hygroscopicity of the material. Different crystal forms of a compound also often demonstrate distinct morphology to one another. An evident morphology change was observed by microscopy and SEM for the solids remaining in the vessel compared to unprocessed Praziquantel, corroborating a form change after $scCO_2$ processing. Single crystal growth may not be feasible through supercritical crystallization. However, it can be used to produce seed which is useful for single crystal growth experiments.

6.5 Conclusion

In this work a novel form of Praziquantel was obtained by exposing to $scCO_2$ at 40 °C and 17.9 MPa. The novel form was isolated both as a pure form when collecting the solid residue remaining in the high-pressure vessel after the experiment, and as a mixture with a different, previously reported hemihydrate through RESS. The novel form in this work showed 0.6 eq. water and a unique thermal profile by DSC. HPLC, NMR, and IR analysis confirmed the

chemical structure and purity. The IR data suggests that the form change may be related to a change in conformer of Praziquantel. Attempts to further corroborate of the structure and conformer of the novel form through single crystal X-ray analysis are recommended. The novel form was stable under stressed conditions (40 °C and 75% RH) for at least 7.5 weeks. The novel form also exhibited improved solubility in biorelevant media and water, giving 13-20% higher solubility compared to unprocessed Form A of Praziquantel. Additional investigation is required to find conditions where the novel form can be isolated as a pure form with small particle size from RESS crystallization. Moreover, thermal treatment of the hydrated form isolated from high-pressure experiments also gave indication of other novel PZQ forms.

As interest in using $scCO_2$ processing for pharmaceuticals grows, it is important to include similar processing conditions during the polymorph screening process. Even if high-pressure processing may not be used for all APIs, novel and viable crystalline forms of organic compounds be discovered by simply exposing the solid to supercritical conditions [210]. Equipment designed to facilitate more routine screening will be advantageous. Therefore, we propose that investigating the polymorph of APIs after exposure to high-pressure conditions may be a valuable tool for screening the polymorphic landscape of new, innovative APIs. Case studies of different compounds are required to further support this recommendation.

7 CHAPTER 7: INFLUENCE OF SOLVENT SELECTION AND RESS PROCESSING CONDITIONS ON FORMATION OF A PRAZIQUANTEL-MALONIC ACID COCRYSTAL IN SUPERCRITICAL CO_2

7.1 ABSTRACT

Praziquantel (PZQ) is an anthelmintic drug with low aqueous solubility, therefore a combination of cocrystallization and particle size reduction is desirable to improve bioavailability. In this study, a PZQ-malonic acid cocrystal was micronized by rapid expansion of supercritical solution (RESS). Due to low solubility of both components in $scCO_2$, four cosolvents were screened as RESS modifiers. While addition of acetone or THF yielded mixtures of PZQ and its cocrystal, MeOH and EtOH were promising for producing pure cocrystal with yield as high as 52%. Impact of pressure (15-30 MPa), temperature (35-55 °C), and cosolvent loading (3-10 volumes) on product attributes such as phase-purity, yield, particle size, and residual solvent were investigated. Addition of a suitable cosolvent to RESS aided in dissolution of cocrystal formers in $scCO_2$ and facilitated crystallization of the cocrystal with modest yields (up to 68.5 wt.%), particle size as low as 600 nm, and acceptable residual solvent. These results show that for APIs with low solubility in $scCO_2$, cosolvent-modified RESS can be a suitable approach for simultaneous crystallization and micronization.

7.2 INTRODUCTION

Novel active pharmaceutical ingredients (APIs) often exhibit poor aqueous solubility and dissolution, and as such are considered to be Class 2 (low solubility, high permeability) according to the Biopharmaceutics Classification System (BCS).[143] APIs falling into BCS Class 2 should generally be modified in some aspect to improve such properties. For ionizable compounds, forming a salt often provides the desired outcome.[16] For non-ionizable compounds, salt formation is not possible and cocrystallization is an alternative approach.[3,4] In addition to altering the solid-form of an API, increasing surface area of particles through particle size reduction (micronization) can contribute to improved dissolution. A widespread industrial method for micronization of APIs is jet-milling, but jet-milling can introduce risks such as amorphous generation, yield loss due to solid sticking in the mill, change in polymorph or chemical degradation.[13,72]

Use of supercritical carbon dioxide ($scCO_2$) is an attractive alternative process for generation of small (sub-micron) particles and may also be combined with cocrystallization in a single step. However, many APIs and common coformers such as carboxylic acids, exhibit poor solubility in CO_2.[43,223–225] As a result, CO_2 is often used as an antisolvent for cocrystallization by supercritical antisolvent (SAS), gas antisolvent (GAS), and supercritical enhanced atomization (SEA) or atomization and antisolvent (AAS).[177] These methods require use of conventional organic solvent to dissolve the API and coformer. Methods such as rapid expansion from supercritical solution (RESS) and crystallization from supercritical solution (CSS) use $scCO_2$ as a solvent, requiring the API and coformer to dissolve in the supercritical phase. In the case of low solubility of APIs and coformers in $scCO_2$, the use of co-solvent (solubility modifier) is required to perform cocrystallization and micronization by RESS

To facilitate RESS crystallization of APIs with low solubility in $scCO_2$, researchers have introduced acetone, ethanol (EtOH), and methanol (MeOH) as cosolvents.[60,200,224] Acetone was used as cosolvent in a RESS process to crystallize griseofulvin, an antifungal which has poor solubility in $scCO_2$.[224] Addition of only 3 mol % acetone (CO_2 basis) improved the solubility of the drug in CO_2 by an order of magnitude and adding 2 mol % acetone (CO_2 basis) allowed the drug to be precipitated by RESS with a particle size as low as 0.84 μm. In another instance, EtOH (between 1 and 7 v/v % [CO_2 basis])was used to improve solubility of salicylic acid and taxol (paclitaxel) in $scCO_2$ in order to prepare the solids by RESS.[60] For both salicylic acid and taxol, changing the cosolvent loading gave rise to changes in particle size or morphology. To crystallize asthma drug, beclomethasone-17,21-dipropionate (BDP), by RESS, Charpentier *et al.* added 5 mol % MeOH (CO_2 basis) to dissolve the BDP in $scCO_2$, which was between approximately 2 and 45 volumes (mL/g; API basis) depending on the experiment.[200] The authors demonstrated the ability to crystallize BDP with sub-micron particle size by addition of MeOH when crystallization in neat $scCO_2$ would not have been feasible due to low solubility. Although cosolvent impact on particle attributes has been previously reported by various authors, the impact of cosolvent addition on process yields has not been discussed to the best of our knowledge. For example, Müllers *et al.* produced an ibuprofen (IBU)-nicotinamide cocrystal with yields up to 20 wt.%, but due to the relatively high solubility of IBU in $scCO_2$, cosolvent was not required.[226]

Praziquantel is a non-ionizable anthelmintic drug for treatment of schistosomiasis, a parasitic worm disease, first marketed by Bayer for human and veterinary use.[227] As such, it is on the World Health Organization's (WHO) list of essential medicines.[144] Praziquantel is considered a BCS Class 2 drug due to its low aqueous solubility.[143] Therefore, efforts have been made to improve solubility and dissolution through change of polymorph and cocrystallization. Solubility of Praziquantel in $scCO_2$ is relatively low [228].

Praziquantel has multiple known polymorphs including neat (anhydrous) forms, hydrates, and solvates, some of which have exhibited improved dissolution and solubility compared to commercial anhydrous Form A[156,196,228–231]. A lower melting, anhydrous Form B has about twice the solubility and intrinsic dissolution rate (IDR) compared to Form A.[156] A hemihydrate, PZQ-HH, also provided 43% improvement in aqueous solubility and twice the IDR compared to Form A.[196] Another potential hemihydrate isolated from $scCO_2$, PZQ-HH-B, provided 13-20% greater solubility in biorelevant media compared to Form A.[228] Finally, solvated forms of praziquantel with acetic acid, 2-pyrrolidone, and dimethylacetamide have been observed, but have less commercial relevance.[230,231] Cocrystals of Praziquantel have been identified with both aliphatic and aromatic carboxylic acids as well as phenolic compounds such as orcinol and hydroquinone.[153,155,157,232] Cocrystals of (RS)-Praziquantel with citric acid, DL-malic acid, salicylic acid, and L-tartaric acid prepared by liquid assisted grinding (LAG) exhibited between 1.5- and 2.1-fold improvement in solubility in simulated duodenal fluid at pH 4.5, while a cocrystal of (R)-praziquantel with L-malic acid crystallized from EtOAc acid showed a 12.5-fold improvement in intrinsic dissolution rate compared to Praziquantel Form A at pH 1.2.[155,232] Although many cocrystals have been identified, with some showing improved solubility in comparison to Praziquantel Form A, there is limited information available regarding their processability using scalable methods.

In this work, formation of a PZQ-malonic acid cocrystal by RESS is investigated, which may be a more scalable process compared to LAG and evaporative crystallization previously used to prepare the cocrystal.[157] Malonic acid is the second smallest dicarboxylic acid and is naturally occurring in some fruits and vegetables and forms a known 1:1 cocrystal with Praziquantel.[157] In this research, the aim was to meet two objectives using a single process: cocrystallization using a scalable method, and obtaining solid with desired small particle size. A scalable process

for crystallization a PZQ-L-malic acid cocrystal has been reported, but to our knowledge there is no literature on simultaneous cocrystallization and micronization of PZQ, specifically also utilizing $scCO_2$ technologies. This work presents one of the first systematic comparisons of different cosolvents used for one compound in RESS cocrystallization, with special attention to process yield which is often not reported for RESS. The impact of cosolvent type and quantity, and RESS processing conditions on attributes such as product yield, phase purity, and particle size of the PZQ-malonic acid cocrystal are investigated.

7.3 Materials and Methods

7.3.1 Materials

Praziquantel (>98% purity, Form A), was used as received without further purification from TCI America, lot ROPHF-NR. Malonic acid (Technipur®, for synthesis) was sourced from Sigma Aldrich, lot S7928987. Liquid CO_2 (99.9% with eductor) was sourced from Praxair, Inc. Solvents acetone and methanol (MeOH), were sourced from Fisher Chemical (ON, Canada). Ethanol (EtOH; anhydrous) was sourced from Commercial Alcohols (ON, Canada). Tetrahydrofuran (THF; containing 250 ppm butylated hydroxytoluene [BHT] as inhibitor) was sourced from Sigma Aldrich (ON, Canada).

7.3.2 RESS

Recrystallization experiments in $scCO_2$ were done using a custom HPR-Series High Pressure Chemical Reactor (Supercritical Fluid Technologies, Inc., Newark, DE, USA) which is shown in Figure 7.1. The system consists of pumps for CO_2 and cosolvent, reactor with overhead stirrer, and precipitation unit.

In each experiment, mixtures of Praziquantel (PZQ, 200-250 mg) and malonic acid (1 molar equivalent) were gently mixed using a vortex mixer (for approximately 30 s) and placed in a 50 mL high-pressure reactor vessel. The reactor was equilibrated to the crystallization temperature (35, 40, or 50 °C). The vessel was pressurized with CO_2 using an SFT-10 pump at 24 mL/min (based on CO_2 at 9.3 MPa and 35 ◦C). During the experiment the reactor contents were mixed (300 rpm) using a MagneDrive overhead stirrer equipped with a six-bladed, flat-blade turbine impeller. In some experiments, cosolvent (2-7 mol%, solute-free basis) was dosed into an overhead reactor port over 60 s using an LS-Class pump. The supercritical mixtures were kept at

the set temperature and pressure for 2 h with agitation to dissolve the cocrystal components. The pre-expansion line and back-pressure regulator valve were heated with heating tape to avoid clogging. After 2 h of mixing at the set temperature and pressure, supercritical solution was expanded through a nozzle into the collection chamber at atmospheric pressure which was vented to a fume hood. Two different capillary nozzle geometries were used during the course of this research. Experiments in neat $scCO_2$ and cosolvent screening experiments used a 14 cm long nozzle with 1580 µm inner diameter (ID), while experiments using MeOH cosolvent used a 5 cm long nozzle with 508 µm ID. All experiments had an average spraying distance of 45 mm into a 28 mm diameter collection vessel. The expansion process typically involved flushing at constant pressure for 20 min followed by gradual depressurization at the same rate. Approximate flow rates were monitored using either a MasterFlex digital flowmeter (neat CO_2 and cosolvent screening experiments) or Cole Parmer analog gas flowmeter (MeOH cosolvent experiments). In some cases, cosolvent was dosed during the flushing step at a rate of 0.13 mL/min for 20 min (10 volumes solvent with respect to the API and coformer mass) to improve recovery. The collection chamber temperature was typically kept at 60 °C unless otherwise noted. Product yield for RESS was calculated by weighing the collection chamber before and after the experiment and comparing it to input mass of reactants. In experiments where cosolvent was employed, the collection chamber was dried at 50 °C under vacuum for a minimum of 3 h before obtaining the final mass.

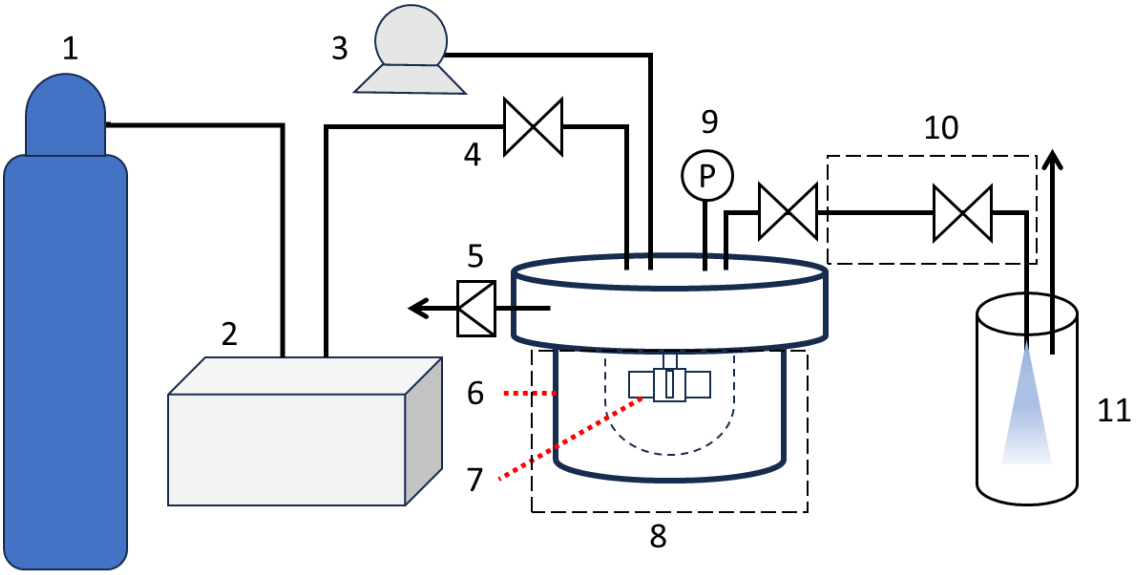

Figure 7.1- Equipment schematic for RESS. 1- CO_2 source; 2- CO_2 pump; 3- cosolvent pump; 4-

valve; 5- rupture disk; 6- reactor vessel; 7- impeller with overhead stirrer; 8- reactor heating jacket; 9- pressure gauge; 10- pre-expansion line heating tape; 11- heated collection chamber with vent.

7.3.3 Solubility in organic solvent and CO_2

Solubility measurements were conducted using a gravimetric technique in MeOH, EtOH, THF, and acetone. Excess solid was suspended in 1 mL of solvent at room temperature to form a slurry. The slurries were stirred for a minimum of two days to equilibrate. Supernatant from the slurries was weighed (m_{sup}) in a tared vial of known mass (m_v) on a Mettler Toledo balance (± 0.0001 g) and then evaporated to dryness at 50 °C in atmosphere and then 50 °C under vacuum. The solid residue was weighed (m_{sol}), and the masses were used to calculate solubility. In some cases solubility was approximated using a clear point method. A known mass of solid (30-40 mg) was added to a vial and solvent was added incrementally until a clear solution was observed. Solubility data obtained by the gravimetric technique are reported as the average of duplicate experiments.

Solubility was measured in $scCO_2$ using a simple gravimetric method at 40 °C and 18-20 MPa in the SFT-10 system using the method previously described by MacEachern *et al.*.[184]

7.3.4 Cocrystal screening methods

For co-evaporation experiments, approximately 40 mg PZQ and 1 molar equivalent malonic acid was added to a 4 mL vial followed by 2 mL of solvent (acetone, THF, MeOH, EtOH, or DCM:MeOH [1:1 v/v]). Solutions were evaporated to dryness with or without stirring at room temperature (RT). For solvent drop milling, approximately 40 mg PZQ and 1 molar equivalent malonic acid was added to a milling capsule followed by one volume (c.a. 40 µL) of solvent. Milling was conducted using a Patterson Dental Amalgamator mill for 2 × 16 s with a ¼" stainless steel ball as milling media. For low-energy mixing experiments, approximately 40 mg PZQ and 1 molar equivalent malonic acid was added to a vial followed by one volume (c.a. 40 µL) of solvent. The resulting pastes were stirred using a 10 mm stirbar at 250 rpm for 3 days.

For reactive crystallization, approximately 215 mg malonic acid (6.8 molar equivalents. with respect to 1 eq. PZQ) was dissolved in 0.6 mL acetone at RT with stirring. After dissolution, about 95 mg PZQ was added gradually as a solid. Solids were filtered, washed with 0.2 mL acetone, and dried at 50 °C under vacuum prior to analysis.

7.3.5 XPRD

X-ray powder diffraction (XRPD) was performed using a Bruker D8 Advance in reflection mode with a Cu Kα source. The scan range was 4–30° 2θ with 0.03° 2θ step size. Samples were prepared on Si zero-return wafers.

7.3.6 Thermal analysis

Differential scanning calorimetry (DSC) was performed using a TA Discovery DSC (TA Instruments). Samples (1-2 mg) were weighed directly into hermetic aluminum pans with pin-hole. All measurements were performed under nitrogen gas flow from 30 to 150-155 °C at a rate of 10.0 °C/min.

7.3.7 Scanning electron microscopy and particle size estimation

SEM was performed using a TESCAN MIRA3-LMU FESEM with 5 kV beam, approximately 7 nm beam spot size, and 250–260 pA beam current. Samples were mounted on carbon tape and sputter coated with approximately 15 nm Au layer using a BIO-RAD PS3 sputter coater. ImageJ software was used to estimate particle size distribution (PSD). Between 50 and 150 individual particles were measured for a given sample and used to calculate particle statistics and distributions.[172]

7.3.8 Gas chromatography

Gas Chromatography was performed using an Agilent 8890 equipped with a liquid autosampler and 7697A headspace sampler. An Agilent DB-624, 30 m x 0.32 mm, 1.8 µm column was used. Nitrogen was used as a carrier gas and the detector gases were helium (40 mL/min) and air (400 mL/min). Nitrogen was used as a make-up gas at 30 mL/min. The column temperature program was as follows: initial temperature 42 °C held for 4 min, ramp to 105 °C at 8 °C/min, then ramp to 240 °C at 30 °C/min followed by 1 min hold. The detector was maintained at 300 °C. The headspace oven, loop, and transfer line were maintained at 120 °C, 135 °C, and 145 °C, respectively and vial equilibration time was 10 min. Between 14 and 40 mg of sample was dissolved in 1 mL DMSO for analysis and compared to acetone and MeOH standards to determine residual solvent content.

7.4 Results

7.4.1 Baseline evaluation of PZQ and malonic acid

PZQ, malonic acid, and its cocrystal were analyzed by XRPD to obtain a baseline. The diffractograms of relevant polymorphs of PZQ, malonic acid, and PZQ-MLA are shown in Figure 7.2.[228] PZQ Form A was the commercially available form used in this work, and PZQ-HH-B diffraction data was obtained from MacEachern *et al.*.[228] Diffractograms for PZQ Form B, PZQ-HH, and PZQ-MLA cocrystal were obtained using single crystal data deposited in the Cambridge Structural Database.[156,157,196] PZQ Form A has characteristic peaks at 6.3, 8.0, 8.2, 15.4, and 20.1 °2θ. PZQ Form B has characteristic peaks at 6.8, 8.4, 13.6, 18.2, and 21.7 °2θ. PZQ-HH has characteristic peaks at 6.5, 17.2, 18.7, and 24.4 °2θ while PZQ-HH-B has characteristic peaks at 7.3, 9.8, 14.6, and 21.0 °2θ. Malonic acid has characteristic peaks at 17.7, and 23.7 °2θ. The PZQ-MLA cocrystal exhibits characteristic peaks at 6.7, 12.1, 15.9, 17.6, 19.4, and 23.4 °2θ.

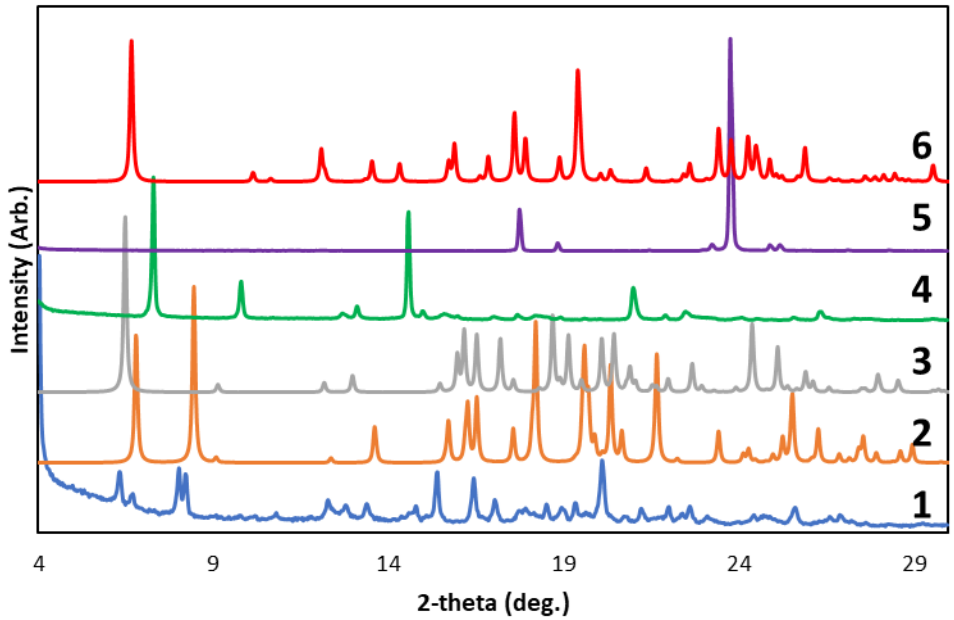

Figure 7.2- Comparison of XRPD powder patterns of select PZQ polymorphs, malonic acid, and PZQ-MLA cocrystal. 1- PZQ Form A sourced from TCI America; 2- PZQ Form B, TELCEU01[156]**; 3- PZQ-HH, WUHQAU; 4- PZQ-HH-B; 5- Malonic acid sourced from Sigma Aldrich; 6- PZQ-MLA cocrystal, TELDEV.**[156,157,196,228]

Solubility of the cocrystal components in a conventional organic solvent was measured at two

temperatures. PZQ Form A was used for solubility measurements. PZQ was determined to remain as Form A in all cases after collection from slurry in the respective solvents. The highest solubility of PZQ Form A was observed in THF (178 ± 3 mg/mL at RT; 290 ± 1 mg/mL at 40 °C) and MeOH (128 ± 2 mg/mL at RT; 313 ± 5 mg/mL at 40 °C), while slightly lower solubility was observed in acetone (73 ± 1 mg/mL at RT; 123±7 mg/mL at 40 °C) and EtOH (66 ± 1 mg/mL at RT; 137±1 mg/mL at 40 °C). The solubility of malonic acid was greater than PZQ in the four organic solvents tested, with malonic acid dissolving in 2 volumes (mL/g) of THF, EtOH, and MeOH and dissolving between 2-3 volumes of acetone at both temperatures. Conversely, the solubility of malonic acid in $scCO_2$ at 40 °C and 20 MPa was approximately 0.1 mg/g, while PZQ solubility at a similar condition (40 °C and 18 MPa) was significantly greater at 2.4 mg/g.

7.4.2 PZQ–MLA through conventional cocrystal screening methods

Formation of PZQ-MLA by LAG and evaporative crystallization has been previously reported.[157] In this work, cocrystal formation attempts were made in five solvents or solvent mixtures using three screening techniques. Solvents used for screening were selected based on solubility of cocrystal components and pharmaceutical acceptability. For instance, EtOH and acetone dissolved PZQ and malonic acid in less than 8 volumes of solvent at 40 °C and both solvents are Class 3 with low toxic potential.[63] Although THF and MeOH are Class 2 solvents with concentration limits of 720 and 3000 ppm, respectively, they are relatively low-boiling and therefore may be more easily removed from the drug substance. On the other hand, ACN and dioxane provided adequate solubility, but they are Class 2 solvents with lower concentration limits (410 and 380 ppm, respectively) and may be more challenging to remove by drying due to boiling point and vapor pressure.

Table 7.1 summarizes the results of the screening experiments in five solvent systems. Co-evaporation experiments without stirring resulted in formation of a glass or gel-like solid for all solvents tested. Glasses or gel-like materials were not further evaluated. When stirring was employed crystalline PZQ-MLA was successfully formed with systems containing alcohols, but a glass or gel-like solid was again obtained for acetone and THF. Solvent drop milling and low-energy mixing led to formation of crystalline PZQ-MLA in all solvents tested.

Table 7.1- Summary of conventional screening experiments with PZQ and malonic acid.

Screening Method	Co-evaporation (unstirred)	Co-evaporation (stirred)	Solvent drop milling	Low-energy mixing	Reactive Crystallization
Acetone	×	×	✓	✓	✓
EtOH	×	✓	✓	✓	-
MeOH	×	✓	✓	✓	-
THF	×	×	✓	✓	-

Formed cocrystal (✓); did not form cocrystal (×); not evaluated (-).

7.4.3 Crystallization in neat $scCO_2$

The feasibility of cocrystallization of PZQ-MLA by RESS in neat $scCO_2$ was evaluated. In this series of experiments, pure CO_2 without any added cosolvent was used. Approximately 270 mg total solid (API plus coformer) was used for each experiment, but product recovery in the RESS collection chamber was low (between 2.1 and 9.4 wt%) from all experiments. Experiments at each condition were done in duplicate. Yields for experiments at 15 MPa compared to 25 MPa were not statistically different at any given temperature using a student's t-test (α 0.05) and are represented in Figure 7.3. The bulk of solids remained in the 50 mL reactor vessel after the experiments. The results of the experiments are summarized in Table 7.2.

The solids isolated by RESS were characterized by XRPD to identify if cocrystal, PZQ, or coformer were collected. For all experiments (35-50 °C and 15-25 MPa) there was no evidence of PZQ-MLA cocrystal or malonic acid in the RESS product. Representative diffraction data for experiments conducted at 40 °C/15 MPa and 40 °C/25 MPa are given in Figure 7.4. Instead, the RESS product was predominantly a mixture of known forms of PZQ such as PZQ-HH, PZQ-HH-B, PZQ Form A, and PZQ Form B. PZQ-HH has previously been observed after RESS in $scCO_2$ (40 °C and 18 MPa). There was not a clear dependence of the form of PZQ in the RESS product on the experiment conditions in this work. The lack of cocrystal formation may be attributed to the poor solubility of malonic acid in $scCO_2$. Although the PZQ-MLA cocrystal was not observed in the RESS product, some cocrystal was observed in the solids remaining in the reactor after the experiment. Malonic acid was evident in the solids remaining in the reactor from all experiment conditions, as was PZQ-HH-B. PZQ Form A (matching the input form) was observed in the reactor vessel after experiments conducted at 15 MPa but was not observed after experiments conducted at 25 MPa. At 25 MPa PZQ-HH-B was the only crystalline form of PZQ observed remaining in the reactor after only 2 h of stirring in supercritical conditions.

Table 7.2- Yield and XRPD results of PZQ-malonic acid experiments in neat $scCO_2$.

Temperature (°C)	Pressure (MPa)	XRPD		RESS yield (%)
		Remained in reactor	RESS	
35	15	×✓	××	4.2 ± 1.4
	25	×✓	××	6.4 ± 3.1
40	15	×✓	××	5.3 ± 1.9
	25	×✓	××	5.5 ± 0.9
50	15	×✓	××	3.2 ± 1.1
	25	×✓	××	5.7 ± 1.4

Mixture of PZQ, MLA, and cocrystal (×✓); no cocrystal (××). Yield is reported as average of duplicate experiments.

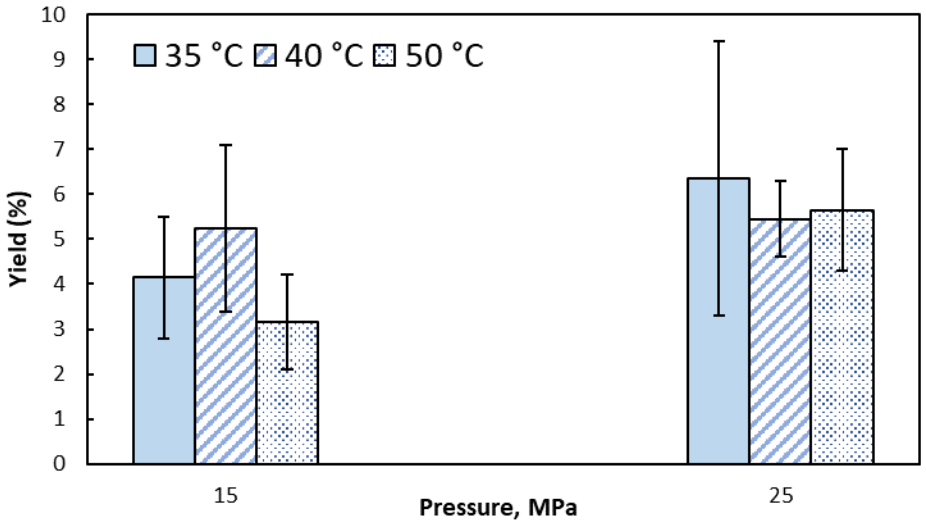

Figure 7.3- RESS yield for duplicate experiments with PZQ and malonic acid in neat $scCO_2$. Error bars indicate the range for each pair of experiments.

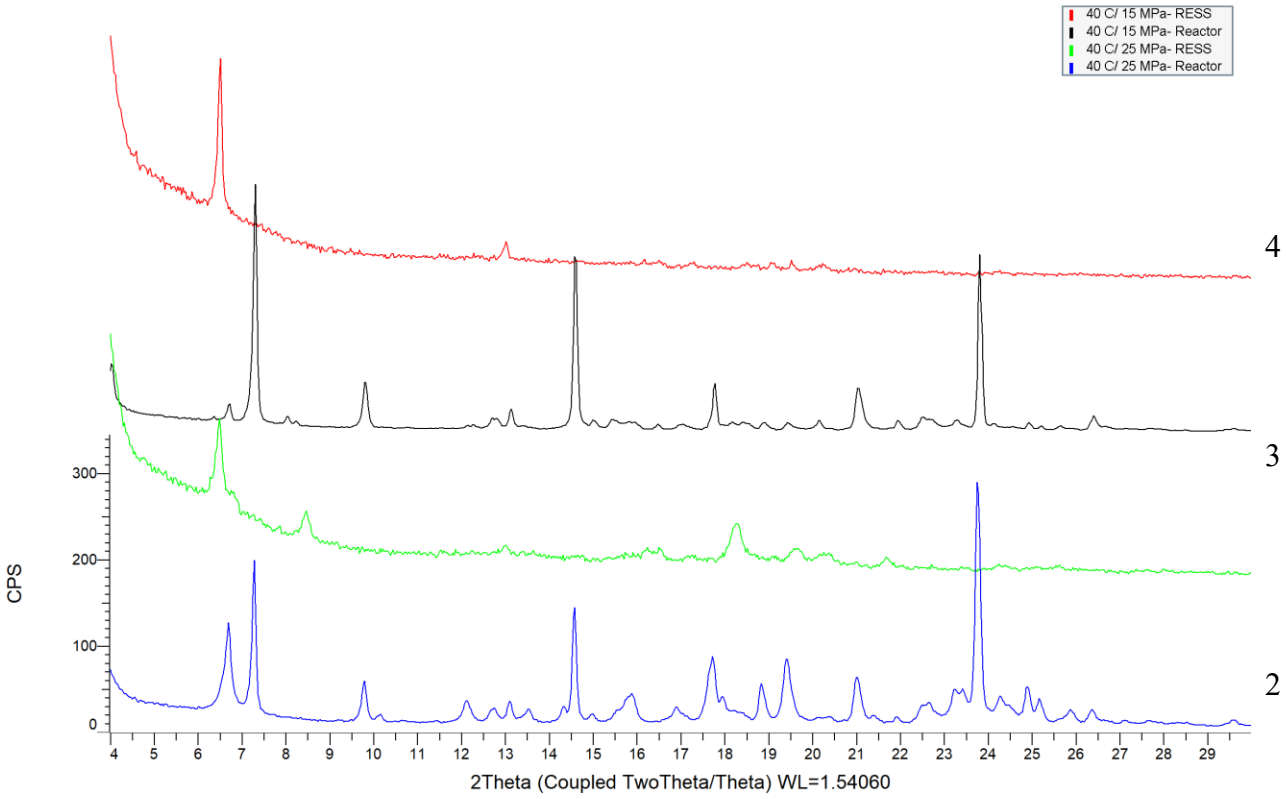

Figure 7.4- XRPD diffractograms from experiments in scCO2 without cosolvent. 1- 40 °C/25 MPa solids remaining in reactor; 2- 40 °C/25 MPa RESS solids; 3- 40 °C/15 MPa solids remaining in reactor; 4- 40 °C/15 MPa RESS solids.

7.4.4 Crystallization screening in $scCO_2$ with four cosolvents

In attempt to improve the yield from RESS and obtain the target cocrystal form, cosolvent (5 wt.% with respect to CO_2 mass) was added to the crystallization experiments. EtOH, acetone, MeOH, and THF were added as cosolvents prior to stirring for 2 h at 40 °C and 25 MPa. After stirring for 2 h at the specified conditions, a flushing rate of either < 0.3, 1-3.5, or 3.5-8.5 LPM was employed before depressurization. All experiments were done in duplicate and the flush time for all experiments was 40 min except for the low flush rate which was 90 min. Solid form, yield, and mass of solid remaining in the reactor was assessed for all experiments, while residual solids trapped in the pre-expansion line and nozzle were evaluated for one experiment with each solvent.

All experiments using EtOH and MeOH formed the cocrystal in the RESS product without evidence of crystalline PZQ or malonic acid by XRPD. When EtOH was used, cocrystal was

observed in the reactor after the experiment, while the quantity of solid remaining in the reactor after experiments with MeOH was too low to analyze. Experiments using acetone yielded a mixture of cocrystal and PZQ-A in the RESS product for one experiment, while another gave a mixture of PZQ Form A and Form B. Experiments using THF yielded a mixture of cocrystal and PZQ-A in the RESS product, but there was one unknown peak present in the diffraction data which may be due to a suspected dehydrated form. The solid which remained in the reactor after depressurization when using both acetone and THF were mixtures of cocrystal, PZQ, and coformer. XRPD results of RESS from the four cosolvents are presented in Figure 7.6. The differences in success of cocrystal formation in the presence of different solvents is suspected to be related to solubility of cocrystal components. Although solubility of malonic acid and PZQ in THF at ambient conditions was high, THF is less polar than the other cosolvents which may contribute to lower dissolution of solutes in the $scCO_2$ mixture. The solubility of malonic acid and PZQ in acetone was lower compared to the other solvents screened as well. Incomplete and possibly incongruent dissolution of components would lead to a molar excess of one component in the solution phase, in this case PZQ, resulting in an excess of PZQ mixed with the 1:1 cocrystal in the RESS precipitate. It follows that an excess of the coformer would then be observed in the remaining undissolved solid. It may be possible to design a process using acetone or THF as cosolvent and producing a phase-pure cocrystal by RESS. However, conditions should be selected where both cocrystal components are able to be solubilized at an equimolar ratio and therefore is expected to have lower throughput than the processes screened in this work which is a disadvantage.

Co-solvent was incorporated into neat CO_2 to improve yield and promote co-crystal formation. Potential recovery was measured by evaluating mass of solid collected by RESS, residue collected from the pre-expansion line and nozzle, and residue remaining in the reactor after the experiment. Preliminary experiments indicated potential for build-up of solids in the pre-expansion line which may lead to clogging. Therefore, after the experiments were complete the pre-expansion line and nozzle were washed with MeOH (10-15 mL), followed by evaporation to dryness to estimate the amount of solid trapped in the line. The material remaining in the reactor was also weighed and used as an indication of solubilized solids during the experiment. Although these three portions were not a complete mass balance for the experiments, they accounted for between 78 and 89% of the mass as represented in Figure 7.5.

Overall, THF and acetone gave similar outcomes in terms of phase purity and yield. THF and acetone provided similar RESS yield (8±2% and 12±3%, respectively). The mass of solid remaining in the reactor after using THF and acetone was also similar (45±2% and 42±7%). The amount of material collected from the line rinse was slightly higher for THF (35%) compared to acetone (25%), but duplicate data were not obtained for line rinse so the significance of the 10% difference is unknown. EtOH and MeOH both showed improvement over THF and acetone in terms of yield. The yield and solid mass remained in the reactor for experiments with EtOH were 9% and 30% when using a slow flushing rate, but improved to 20±2% and 16±1% when a faster flush rate was employed. About 42% of the mass was collected from the pre-expansion line indicating that yield could be increased if the flushing and depressurization method was improved. The experiments using MeOH with the 1-3.5 LPM flushing rate gave lower RESS yields compared to EtOH (13±5%), but the amount of solid remaining in the reactor after the experiment was low in comparison. In addition, it was found that the bulk of the solids (76%) were trapped in the pre-expansion line. Based on this result, an experiment using a faster flushing rate (3.5-8.5 LPM) was conducted in attempt to mitigate the potential clogging of the pre-expansion line. The results showed a significant improvement in yield up to 57±7% while also decreasing the mass of solid left in the pre-expansion line. The quantity of solid remaining in the reactor after both sets of experiments was similar. The mass of residue remaining in the reactor after each experiment may be considered as a qualitative comparison of solubility in the $scCO_2$/solvent mixtures. Addition of THF and acetone were not able to improve solubility to the same extent as MeOH and EtOH and therefore a larger amount of solid was undissolved. When comparing MeOH and EtOH, it would appear that the addition of more polar MeOH to the system provided a better improvement in solubility of the cocrystal compared to EtOH.

The results from the cosolvent screening suggested that both MeOH or EtOH provide an advantage over acetone and THF from a form purity and yield perspective. The combination of yield, reactor residue mass, and mass of solid collected from the line rinse support MeOH provides an advantage over EtOH for increasing product yield. Pharmaceutical acceptability of the cosolvent should also be considered when moving forward. Although MeOH is a Class 2 solvent with 3000 ppm ICH limit (compared to EtOH's 5000 ppm limit), the solvent limit is a significant deterrent. The selection of a Class 2 solvent in this instance may be justified by the significant improvement in yield.

Table 7.3- Summary of results from cocrystallization screening in $scCO_2$ with four cosolvents.

Solvent	Solvent loading (mL)	Flush rate (LPM, approx.)	XRPD		RESS yield (%)	Reactor residue (%)	Line rinse (%)
			Remained in reactor	RESS			
Acetone	2.80 mL	1-3.5	CC + MLA + PZQ[b]	PZQ/ PZQ-A + CC[c,d]	12 ± 3	42 ± 7	25
EtOH	2.90 mL	< 0.3[a]	CC	CC	9	30	-
		1-3.5	CC	CC	20 ± 2	16 ± 1	42
MeOH	2.78 mL	1-3.5	n/a	CC	13 ± 5	< 1	76
		3.5-8.5	n/a	CC	52 ± 7	< 1	31
THF	2.49 mL	1-3.5	CC + MLA + PZQ-HH-B[d]	CC + PZQ-A[d]	8 ± 2	45 ± 2	35

[a] Due to slower flushing rate, a 90 min flush time was used. All other experiments had 40 min flush time.
[b] Differences in PZQ polymorph were observed (1- PZQ-HH-B; 2- PZQ-HH-B + PZQ-HH-B suspected dehydrate).
[c] Differences in RESS solid were observed (1 & 2- peaks in agreement with mixture of PZQ-A + PZQ-B; 3- PZQ-A + CC)
[d] Single additional peak observed in XRPD (7.4-7.5 °2θ), unable to assign to a known solid form.

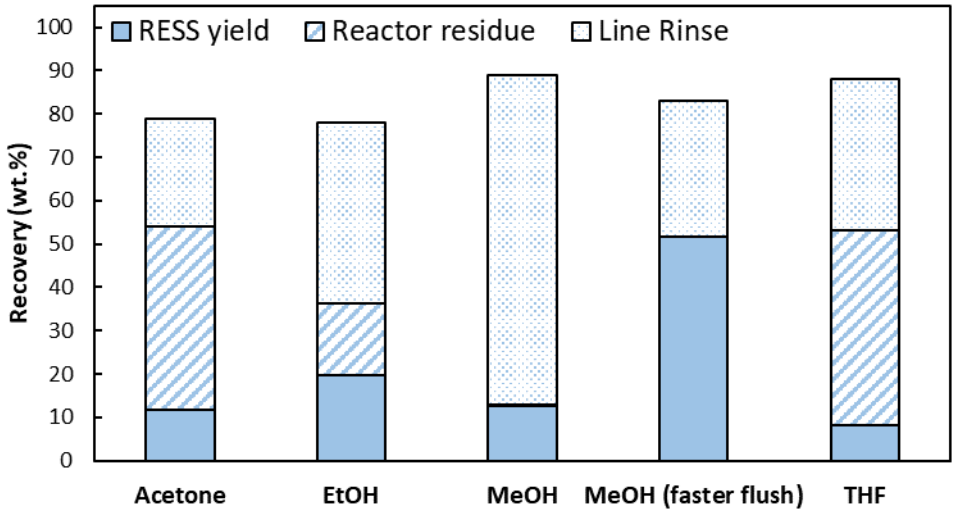

Figure 7.5- RESS yield, reactor residue, and line wash recovery from cosolvent screening at 40 °C and 25 MPa. Recovery for RESS yield and reactor residue are shown as the average of duplicate experiments while line rinse recovery is obtained from a single experiment.

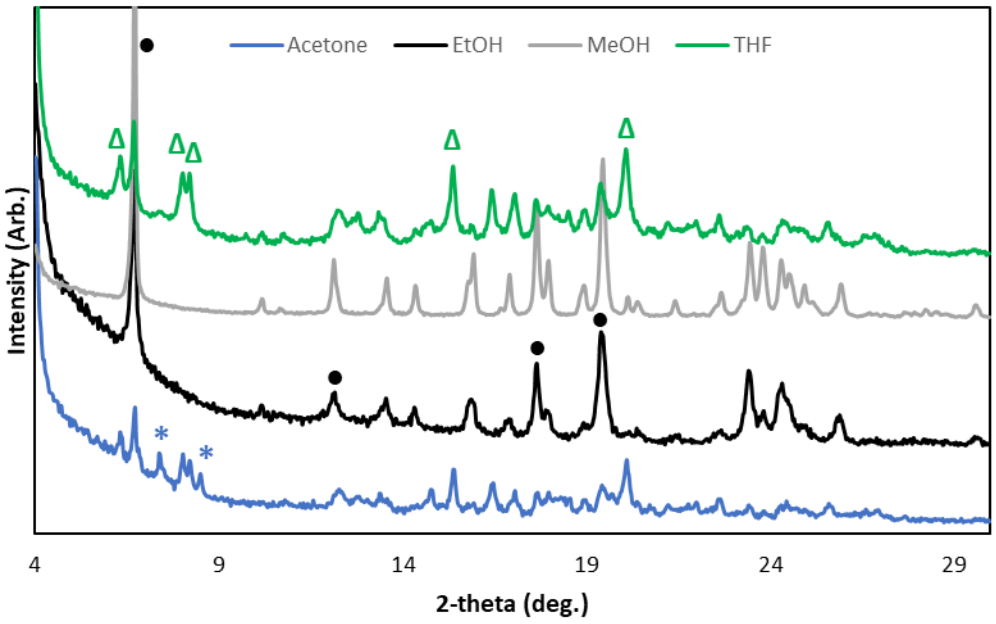

Figure 7.6- XRPD diffractograms of solids produced by RESS (40 °C and 25 MPa) with 10 volumes of various cosolvents. Open triangles (Δ) indicate characteristic PZQ Form A peaks; closed circles (●) indicate characteristic cocrystal peaks; asterisks (*) indicate peaks that may be characteristic of PZQ Form B or possible dehydrated form.[156,228]

7.4.5 Crystallization in $scCO_2$ using MeOH as cosolvent

The RESS process conditions used to investigate impact of process parameters when using MeOH as cosolvent are summarized in Table 7.4. Pre-expansion temperature and collection vessel were maintained at 60 °C for all experiments. Prior to depressurization, the system was flushed with $scCO_2$ at the experimental temperature and pressure conditions for 20 min at approximately 3 SLPM. To improve recovery and minimize clogging in the pre-expansion line and nozzle, MeOH was dosed at 0.13 mL/min during the flushing period, equivalent to 10 volumes of solvent. Reactive crystallization (ambient pressure) in acetone was chosen as a conventional process to compare to $scCO_2$ crystallization. Yield, solid form (XRPD), size and morphology of the precipitates (SEM), solvent content, and thermal properties were evaluated.

Table 7.4- Operating conditions and results for RESS experiments.

Operating condition			Form	Yield (%	Mean size	Solvent
P_r (MPa)	T_r (°C)	V_{sol} (vol.)	(0/1)[a]	w/w)	(µm)	content (wt.%)
15	35	10	1	39.8	1.15 ± 0.45	-

Operating condition			Form	Yield (%	Mean size	Solvent
P_r (MPa)	T_r (°C)	V_{sol} (vol.)	(0/1)[a]	w/w)	(µm)	content (wt.%)
15	35	3	0	18.5	-[b]	-
15	35	3	0	32.9	-[b]	-
15	55	10	1	47.8	1.90 ± 0.53	0.06 (MeOH)
15	55	3	1	35.5	1.50 ± 0.70	-
22.5	45	6.5	1	62.7	1.22 ± 0.51	0.08 (MeOH)
22.5	45	6.5	1	61.6	-	-
22.5	45	6.5	1	58.5	1.34 ± 0.55	-
30	35	10	1	59.4	0.94 ± 0.26	-
30	35	3	0	50.7	-[b]	-
30	35	3	0	40.7	-[b]	-
30	55	10	1	68.5	0.60 ± 0.27	0.05 (MeOH)
30	55	3	1	51.4	0.73 ± 0.28	-
-	22[c]	4.7[c]	1	63.0	9.41 ± 4.54	0.12 (acetone)

[a] 0 = mixtures, 1 = cocrystal.
[b] PSD not included due to product being mixture.
[c] Reactive crystallization performed in ambient condition at RT in 4.7 volumes acetone.

7.4.5.1 Solid Form

Solid form of RESS precipitates was evaluated by XRPD for all experiments. As shown in Figure 7.7, phase-pure cocrystal was observed for all experiments that were conducted at 45 and 55 °C using between 3 and 10 volumes MeOH and between pressures of 15 and 30 MPa. Phase-pure cocrystal was also obtained from reactive crystallization in acetone. Experiments conducted at 35 °C produced phase-pure cocrystal when 10 volumes of MeOH was used at both 15 and 30 MPa. However, when 3 volumes of MeOH was used, a mixture of cocrystal and PZQ was observed by XRPD in experiments at both 15 and 30 MPa. XRPD of solids from those experiments exhibited characteristic peaks of PZQ Form A in the diffractograms, notably peaks at 6.3, 8.0, and 8.2 °2θ can be observed. The experiments conducted at 35 °C using 3 volumes MeOH were duplicated at each pressure to verify the result, and in both cases PZQ Form A was observed by XRPD for the RESS precipitates. The solubility of malonic acid in neat $scCO_2$ was significantly lower than PZQ at similar conditions, therefore addition of 3 volumes MeOH at 35 °C between 15 and 35 MPa may not provide the solubility improvement required to dissolve malonic acid in the experiment. As a result, a sub-stoichiometric amount of malonic acid may be dissolved, giving rise to excess PZQ in the RESS precipitate. However, addition of cosolvent

improved the solid form purity compared to experiments without cosolvent where there was no evidence of cocrystal formation in RESS precipitates. Increasing cosolvent from 3 vol to 10 vol also provided an improvement in solid form purity for experiments at 35 °C.

Thermal properties of the cocrystals prepared by RESS were also compared to that of a reference cocrystal prepared by co-evporation and are shown in Figure 7.8. The reference cocrystal had a melting point of 145.8 °C and enthalpy of fusion (ΔH_f) of -107 J/g, which has not been previously reported. The cocrystals prepared by RESS melted 0.9— 2.1 °C lower than the reference, exhibiting single melting points between 143.7 and 144.9 °C. The thermogram of the solid from RESS at 55 °C/15 MPa/10 vol. exhibited a minor endothermic event prior to the melt (5 J/g, 116.4 °C) which could possibly correspond to trace amounts of a different polymorph (of PZQ, malonic acid, or its cocrystal) or eutectic, but a different crystalline phase was not detected by XRPD. All three RESS cocrystals had lower ΔH_f compared to the reference, indicating that the RESS products may be lower crystallinity compared to that of reactive crystallization although there was not a substantial difference in the XRPD results. The lowest ΔH_f (-69 J/g) was observed in the solid produced at 55 °C/15 MPa/10 vol. which also exhibited a small secondary thermal event which could also contribute to lower enthalpy due to phase impurities. However, solids from RESS at 45 °C/22.5 MPa/6.5 vol. and 55 °C/30 MPa/10 vol. had ΔH_f of -88 and -93 J/g, respectively, indicating a slight reduction in crystallinity compared to the reference.

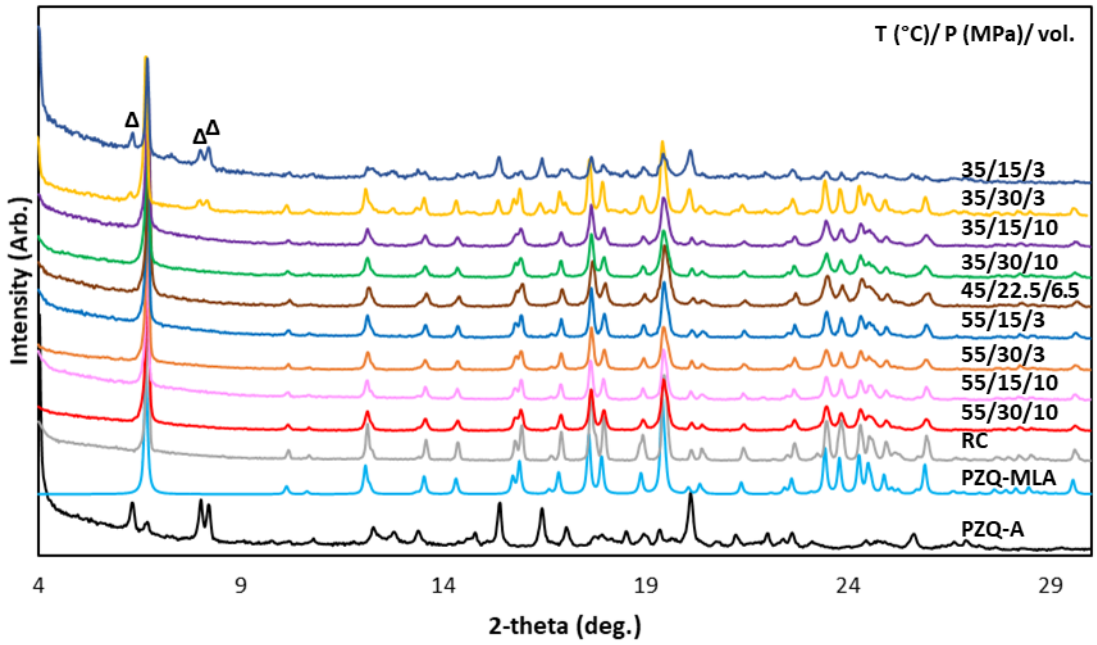

Figure 7.7- Diffractograms of precipitates from reactive crystallization (RC) and RESS compared to PZQ Form A (PZQ-A) and PZQ-malonic acid cocrystal (PZQ-MLA; TELDEV). Characteristic peaks of PZQ Form A indicated with open triangles (Δ).

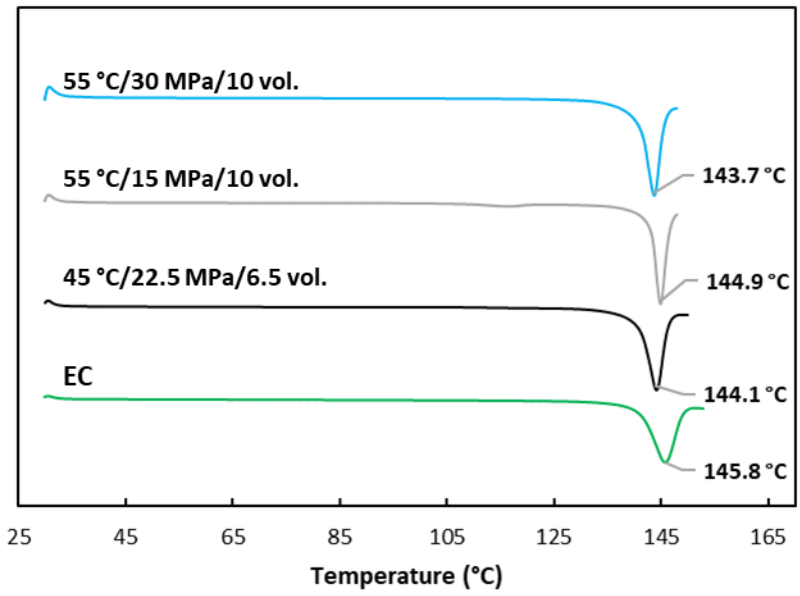

Figure 7.8-DSC thermograms of RESS products and reference cocrystal prepared by evaporative crystallization (EC).

7.4.5.2 Yield

The objective for using cosolvent in RESS crystallization is to improve the solubility of solutes, in turn improving the product yield. Without cosolvent, the yield from RESS processes using PZQ and malonic acid was less than 10 % (molar basis). When MeOH was employed as cosolvent (between 3 and 10 vol as cosolvent and 10 vol during flushing), the collected RESS product yields were between 18.5 and 68.5 % (molar basis). More specifically, experiments that resulted in phase-pure cocrystal (by XRPD analysis) gave yields above 35.5 %. In comparison, yield from reactive crystallization in acetone was 63 % (molar basis, PZQ as limiting reagent). Although consistent trends are observed for yield during this research and are suitable for process screening and understanding, it should be noted that the data can be considered for comparison only. Experiments that were conducted in duplicate or triplicate showed that the error in yield may be between 2 and 7 % yield (molar basis).

At each temperature and pressure tested, yield was between 12.3 and 17.1% higher when using 10 volumes versus 3 volumes solvent. For example, at 35 °C/ 30 MPa (ρ_{CO2} 0.952 g/cc) a 59.4 % yield was obtained using 10 volumes cosolvent compared to 45.7 % yield using 3 volumes cosolvent. Similarly, at 55 °C/ 30 MPa (ρ_{CO2} 0.852 g/cc) a 68.5 % yield was obtained using 10 volumes cosolvent compared to 51.4 % yield using 3 volumes cosolvent. The trend followed for the other pressure/temperature combinations- at 35 °C/ 15 MPa a 14.1 % increase was observed and at 55 °C/ 15 MPa a 12.3 % increase was observed when using 10 volumes versus 3 volumes of solvent. The trend in yield indicates that increasing MeOH content in the solvent mixture improves the solubility of the cocrystal components, allowing for better recovery. An increase in solubility with increasing cosolvent percentage in $scCO_2$ is commonly observed for polar organic compounds.[33,188,224,233,234]

Adding a MeOH dosing during the flush prior to depressurization significantly improved the loss of yield due to build-up in the pre-expansion line and nozzle compared to preliminary cosolvent screening experiments. During preliminary screening without cosolvent dosing during flushing the loss of product to the pre-expansion line and nozzle was between 25 and 76 wt.%, but addition of cosolvent during flushing reduced the product loss to an average of 5 wt.%.

Due to the relatively small scale of the experiments (c.a. 250 mg), loss of small quantities of solid during the process may have a substantial impact on the yield percentage. Loss of yield

arises due to solid build-up in the pre-expansion line and nozzle and also due to product escape through the venting system of the collection chamber. Further optimization of the pre-expansion line, nozzle, and collection chamber geometries may allow for continued improvement in yield. Nonetheless, yields obtained during the work indicate that use of a suitable cosolvent may provide RESS precipitate yields that can rival conventional crystallizations, such as reactive crystallization, for preparation of cocrystals. In this work conventional reactive crystallization was less solvent intensive compared to RESS with cosolvent. Reactive crystallization used about 6.3 volumes acetone, while RESS used between 13 and 20 volumes of MeOH (inclusive of wash and flush procedures).

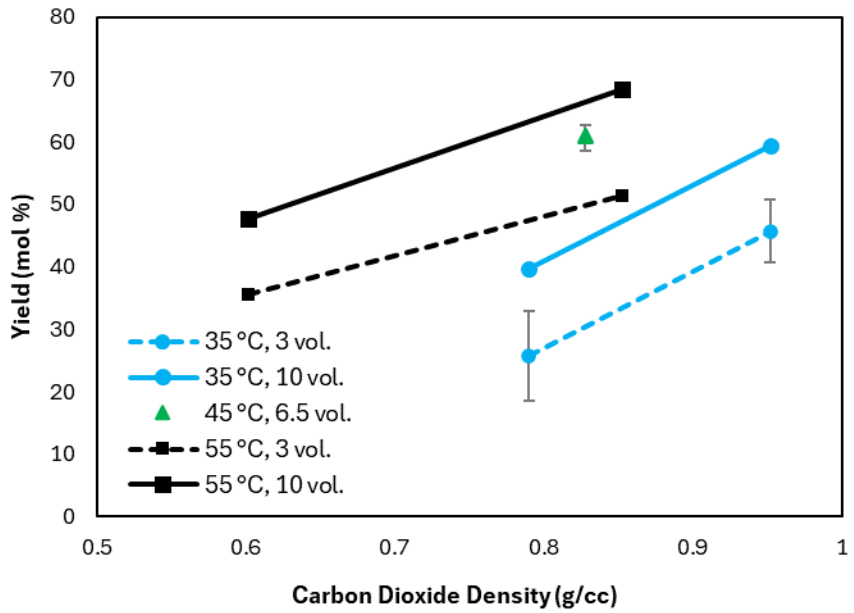

Figure 7.9- Yield of precipitates from RESS experiments with MeOH cosolvent. Density of CO_2 calculated on cosolvent/solute-free basis using PR-EOS.

7.4.5.3 Particle Size and Morphology

Size and morphology of RESS precipitates and the product from reactive crystallization were evaluated using a SEM and image analysis. Particles were generally three-dimensional with rhombus- or diamond-like morphology, consistent with a single crystal grown by Espinosa-Lara *et al.*[157] The morphology was well-defined with sharp particle edges for solids isolated from reactive crystallization and less defined for solids isolated from RESS. A comparison of the precipitate from reactive crystallization and RESS is shown in Figure 7.10. In both cases, the

PZQ-MLA cocrystal morphology differs from that of PZQ isolated from $scCO_2$, which has been shown to be characteristically needle-like.[228]

Particles obtained by reactive crystallization were larger, ranging from 2 to 22 μm, with a comparatively wide particle distribution. The average size of particles obtained by reactive crystallization was 9.41 ± 4.54 μm. Particles produced by RESS ranged from 0.2 to 4.5 μm and average particle size between 0.60 and 1.90 μm with overall narrower size distributions in comparison to reactive crystallization, depending on the processing conditions used. The larger particle size obtained by reactive crystallization is expected because conventional crystallization techniques are generally not expected to provide micron-size particles.[7] However, the wide distribution may be attributed to the relatively uncontrolled crystallization due to a high degree of supersaturation, rapid addition of cocrystal components together, and lack of seeding.

For solids isolated from RESS, particle size tended to increase as the reactor pressure decreased, with smaller particles obtained from experiments using 30 MPa operating conditions and larger particles from experiments using 15 MPa operating conditions. A clear temperature dependence was not observed within the data. The variation of particle size with cosolvent loading was also within the standard deviation of measurements for both 55 °C/30 MPa, and 55 °C/15 MPa. The smallest particles were obtained from experiments at 30 MPa and 55 °C, both of which yielded sub-micron particles on average. The experiments using 3 and 10 volumes cosolvent at those conditions gave particle size of 0.73 ± 0.28 μm and 0.60 ± 0.27 μm, respectively.

Perhaps the most notable trend within the data was the shape of the particle size distributions resulting from RESS. When experiments were conducted at 15 MPa the size distributions showed a distinct bi-modal or multi-modal shape and were wider than distributions from 22.5 and 30 MPa experiments. Solid from experiments at 22.5 and 30 MPa showed narrower, mono-modal distributions. In relation to Figure 7.9, the experiments that gave both pure cocrystal and monomodal distributions are the same conditions where higher solubility of the cocrystal components are anticipated. Therefore, it may follow that during flushing and depressurization, there is a higher degree of supersaturation which favors higher nucleation rates resulting in overall smaller more uniform particles.

Overall, it is not straightforward to identify a singular trend for impact of process parameters on particle size based on current literature, in particular for RESS processes employing cosolvent

for which literature is limited. Similar to the results presented in this work, Hu *et al.* found that higher extraction pressures (30 MPa) produced marginally smaller particles when compared to lower pressure (20 MPa) in their work with griseofulvin which is suspected to be related to a higher degree of supersaturation during depressurization.[224] Yildiz *et al.* also found that an increase in pressure gave marginally smaller particles.[60] However, Charpentier *et al.* found that a higher pressure generally resulted in larger particles and suggest that it may be related to aggregation, but as the authors noted, it is challenging to identify a universal trend when comparing available literature.[200] Hu *et al.* observed that increasing cosolvent (acetone) content from 0.5 to 2% led to smaller particles, but in this work particles obtained from different amount of solvent were within the standard deviation. Conversely, Yildiz *at al.* observed an increase in particle size when cosolvent (EtOH) was increased from 1 to 3 vol.% for salicylic acid particles produced by RESS and suggest it was related to increased coagulation among particles in the presence of cosolvent.[60]

However, perhaps it is the geometry of the crystallization system influencing the variability in literature, noting that the crystallization apparatus used for RESS with cosolvent have all been unique. In the above examples of RESS crystallization employing cosolvent, all three researchers found that the nozzle type and/or ID impact the particle size. In general, larger nozzle IDs yielded larger particles or wider particle size distribution to varying extent.[60,200,224] The collection vessel geometry (spray distance) was also found to impact particle size, but opposite trends were observed when comparing results of Hu *et al.* to Yildiz *et al.* In a broader literature review of cocrystallization in $scCO_2$, geometry of the experimental apparatus was also identified as having a significant impact on particle size.[177]

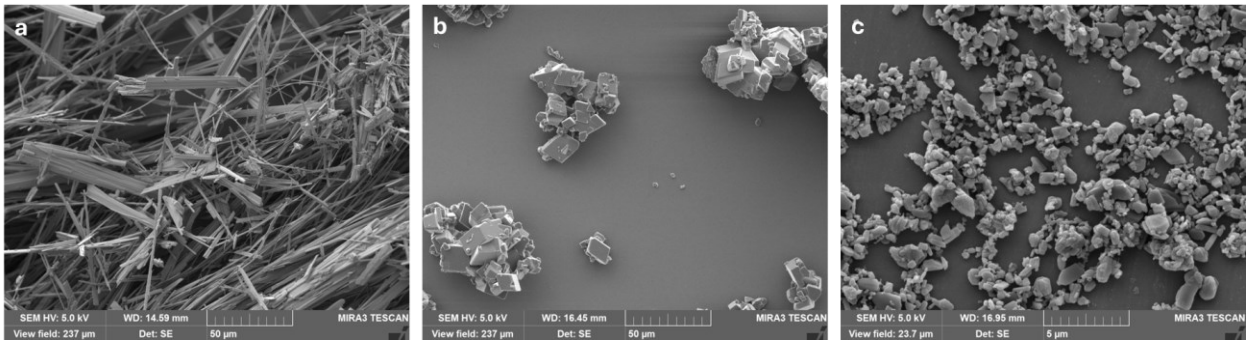

Figure 7.10- SEM images of PZQ-HH-B (a; 1000 X), precipitate from reactive crystallization (b; 1000 X) and RESS using 30 MPa, 55 °C and 10 vol cosolvent (c; 10,000X).

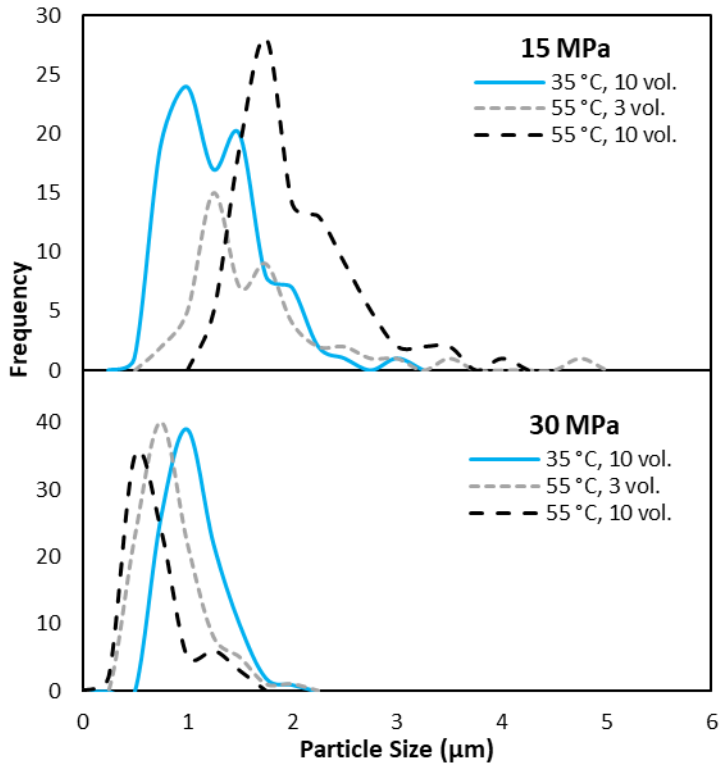

Figure 7.11- Particle size distribution evaluated at different RESS processing conditions.

7.4.5.4 Solvent Content

Residual solvent content of samples prepared by reactive crystallization and RESS were evaluated to determine if the isolated solids were within acceptable limits for acetone (ICH class 3) and MeOH (ICH class 2).[63] Solids from RESS with the largest and smallest particle size, along with an experiment at center-point conditions were evaluated. Solid with average particle size of 0.60 µm, 1.22 µm, and 1.90 µm had residual MeOH content of 0.05, 0.08, and 0.06 wt.%, respectively. The solvent content of three RESS-precipitated solids did not exhibit a clear trend with particle size and all fell well under the ICH limit for MeOH of 0.30 wt.%. The residual solvent content of solids prepared by reactive crystallization contained a slightly higher solvent content of 0.12 wt.% acetone, however the solvent content was still well within the 0.50 wt.% ICH limit of acetone. Despite the addition of up to 10 volumes of MeOH as cosolvent, RESS produced products with acceptable, low solvent content.

7.4.5.5 Comparison of RESS and reactive crystallization

A comparison of the process parameters and results from a conventional reactive crystallization in acetone to the best-performing RESS-cosolvent process is provided in Table 7.5. Reactive crystallization used a lower amount of organic solvent to provide similar process yield and did not require energy to heat or pressurize the system. However, an excess of coformer was required and the isolated product had significantly larger particle size compared to RESS. On the other hand, RESS-cosolvent crystallization required only a stoichiometric quantity of coformer and was able to produce sub-micron particles with similar yield to conventional crystallization. However, the RESS-cosolvent process used more solvent while also requiring energy to pressurize and heat the system. Both processes gave phase-pure cocrystal with acceptable residual solvent levels and similar yields. Overall, either process may be considered to have some advantage over the other, and determining the most suitable process will depend on the objective—whether it is potentially reducing energy usage and solvent consumption (RC may be favored) or producing sub-micron particles in a single step crystallization (RESS may be favored).

Table 7.5- Summary of process parameters and product attributes from RC and RESS-cosolvent processes.

Process type	Mol eq. malonic acid	Solvent quantity (mL/g)		$scCO_2$ quantity (g)	Pressure (MPa)	Temperature (°C)	Yield (mol.%)	Average particle size (µm)	Residual solvent content (wt.%)
		Main process	Wash/flush						
RC	6.8	4.7	1.6	-	-	20-22 °C	63.0	9.41 ± 4.54	0.12 (acetone)
RESS	1.0	10	10	~40	30	55 °C	68.5	0.60 ± 0.27	0.05 (MeOH)

7.5 Conclusion

Investigation of a PZQ-malonic acid cocrystal was carried out using conventional methods such as evaporation, grinding, and reactive crystallization. Due to low solubility of PZQ and malonic acid in $scCO_2$, cosolvents with different properties (acetone, EtOH, MeOH, THF) were screened to be used in a cosolvent-modified RESS process. During the cosolvent screening, it was found that the cosolvent type impacted both the solid-form precipitated by RESS and also the yield. In the case of acetone and THF, mixtures of PZQ and the PZQ-malonic acid cocrystal were collected by RESS with low yield and there was evidence that almost half of the input solid did not dissolve in the supercritical phase. Both EtOH and MeOH provided improved yields and between 0-16% of the solids did not dissolve in the supercritical phase, but MeOH showed the most promise in improving process yield.

The impact of process parameters such as pressure, temperature, and cosolvent loading on product attributes was investigated for RESS with MeOH as cosolvent. At 35 °C using 3 volumes of MeOH, the RESS product contained small amounts of PZQ Form A, while all experiments at 44-55 °C showed only cocrystal by XRPD. It is proposed that higher solubility and better dissolution of components is critical for promotion of cocrystal formation. Although XRPD did not show strong evidence of reduced crystallinity in the RESS products, DSC showed some evidence of lower crystallinity where a cocrystal prepared by reactive crystallization had ΔH_f of -107 J/g and the ΔH_f of RESS products were between -69 and -93 J/g. The highest process yields were obtained using 10 volumes of MeOH compared to 3 volumes, with the highest process yield of 68.5 wt.% from an experiment at 55 °C/30 MPa. Since the experiments were conducted at relatively small scale, small product losses may contribute significantly to the overall yield, however the yields obtained indicate that addition of a suitable cosolvent can rival a conventional crystallization, such as reactive crystallization. Particle sizes of the RESS-precipitated solids were evaluated using image analysis and it was determined that a higher pressure (30 MPa) generally led to generation of smaller particles. In the case of the PZQ-malonic acid cocrystal, an average size of 600 nm was obtained from an experiment conducted at 55 °C/30 MPa with 10 volumes of cosolvent. At lower pressures (15 MPa), the particle size distributions were typically multimodal, while the experiments at 22.5-30 MPa generated more

monodisperse particles. Finally, the solids collected by RESS had low residual solvent content, despite the use of MeOH as a cosolvent.

Literature available on RESS crystallization processes utilizing cosolvent are limited and in some cases the effect of process parameters on product attributes is contradictory. However, the geometry of the crystallization equipment, specifically the nozzle and collection chamber, may have a profound impact on crystallization by RESS. Overall, this research has shown that selection of a suitable cosolvent can allow for cocrystallization by RESS for compounds with low solubility in $scCO_2$. The choice of cosolvent and operating conditions can impact phase purity of the cocrystal, yield, and particle size.

8 CHAPTER 8: CONCLUSIONS AND FUTURE RESEARCH

In this work two anthelmintic drugs, PZQ and NCS, were selected to investigate simultaneous cocrystal formation and micronization processes. Instead of more conventional two-step process involving cocrystal formation and isolation followed by mechanical micronization, processes such as spray drying and RESS were explored due to their ability to produce micron or sub-micron cocrystal particles in a single process.

An NCS-urea cocrystal was attempted to be crystallized by two different methods known to produce small particle size— spray drying and RESS. Development of a TPD helped identify suitable conditions for spray drying and provided insight into advantages spray drying may have over conventional crystallization in the same solvent system, where an excess of coformer would be required to isolate a pure cocrystal. Spray drying was able to produce a pure cocrystal with average particle size as low as 2 μm by selecting an appropriate concentration and inlet temperature. Although spray drying was able to produce cocrystals with small particle size, it required use of high quantities of organic solvent (> 130 mL/g) and the residual solvent content in the product was relatively high (0.5 wt.%) when compared to ICH imposed limits for APIs. Therefore, scCO_2 was explored as a possible process solvent for preparing the cocrystal. Neat CO_2 and three different cosolvents (IPA, cyclohexane, and water) were tested, but the solubility of NCS and urea in the selected solvents were too low to prepare by RESS. Despite the low solubility, partial cocrystal formation was observed during the experiments with neat CO_2, and CO_2 mixtures with IPA and cyclohexane. This research investigated the impact of solvent choice and processing time on the extent of cocrystal conversion and related the findings to theorized TPDs and hydrogen bonding between the API, cosolvent, and coformer. Ultimately, the low solubility of NCS in scCO_2 was a limiting factor in this research and a second model compound, PZQ, was selected to facilitate investigation of RESS cocrystallization.

Prior to this research, scCO_2 as a process solvent for crystallization of PZQ had not been explored. As such, preliminary experiments with PZQ and scCO_2 were carried out to estimate solubility and evaluate for potential polymorphism. During this phase of the research a novel form of PZQ was identified. The novel form (since called PZQ-HH-B) was suspected to be a racemic hydrate, but with a possible change in conformer (from *syn*- to *anti*-) compared to the input material. PZQ-HH-B showed up to 20% improvement in solubility in biorelevant media

compared to commercial Form A and was stable for at least 7.5 weeks in humidity stressed conditions.

Following the investigation of PZQ in $scCO_2$, a PZQ-malonic acid cocrystal was selected to explore RESS as a crystallization method for simultaneous cocrystal formation and particle size reduction. Due to the relatively low solubility of PZQ and malonic acid in $scCO_2$, four different cosolvents (acetone, EtOH, MeOH, THF) were used to improve solubility. During screening with the four cosolvents, MeOH and EtOH were successfully able to produce a pure cocrystal by RESS while acetone and THF provided physical mixtures of cocrystal and PZQ. It was hypothesized that acetone and THF were not able to provide a sufficient solubility improvement to completely (and congruently) solubilize the material at the selected concentration and operating conditions. Eventually, MeOH was selected as the most promising cosolvent due to its suspected solubility improvement and volatility. The research explored the effect of pressure, temperature, and cosolvent loading on process yield and product attributes such as solid form, particle size, solvent content, and crystallinity. Cocrystal was able to be prepared with above 65 mol.% yield, average particle size of 600 nm, and residual solvent well below ICH limits for APIs (0.05 wt.% MeOH) by RESS with particular process conditions. Although RESS-cosolvent required more organic solvent (20 mL/g) compared to reactive crystallization (6.2 mL/g), both processes were less solvent-intensive than spray drying in this work. However, it should be noted that there was some evidence of loss of crystallinity in the RESS precipitate compared to cocrystal prepared by a more conventional reactive crystallization which could impact long-term stability.

Overall, this research showed that careful selection of process solvent(s) can allow simultaneous cocrystallization and generation of micron or sub-micron size particles, which may be advantageous over mechanical particle size reduction methods for APIs that are prone to chemical degradation or amorphization in such processes.

8.1 Recommendation for Future Research

In this work a niclosamide-urea did not provide a solubility advantage *in-vitro*, but it may provide an advantage *in-vivo*. Alternatively, different cocrystal forms of niclosamide may be more advantageous from a bioavailability perspective. Similarly, the novel crystalline form of praziquantel discovered in this research showed up to 20% improvement in solubility in biorelevant media, but the malonic acid cocrystal with small particle size was not yet evaluated.

The use of $scCO_2$ as a solvent is often limited by low solubility of APIs in neat CO_2. However, in this work it was demonstrated that crystallization in $scCO_2$ is a promising method to form cocrystals and produce sub-micron particles even for APIs with relatively low solubility by addition of a cosolvent. While there is a large body of research available for API crystallization by RESS, there is a small body of work exploring addition of a cosolvent to improve solubility to facilitate RESS crystallization, and even more limited research exploring the impact of using different cosolvents for crystallizing a given compound. Continued studies investigating systematic selection of cosolvent for use in $scCO_2$ processes should be done with a focus on pharmaceutically acceptable solvents for APIs. In the special case of cocrystallization, solubility measurement and/or modeling of both cocrystal components in mixtures of CO_2 with cosolvent can further aid in selection of suitable solvent systems that have a higher likelihood to produce phase-pure cocrystal in the RESS product. Expanding the body of work in this research area to develop a better understanding and identify trends for how cosolvent impacts particle attributes such as particle size, crystallinity, and residual solvent content will be beneficial. Based on the fact that sub-micron particles were produced in this work, there is promise to explore RESS for specialized applications that require nanoparticles such as APIs intended for pulmonary delivery. In literature there are sometimes conflicting trends observed, particularly when RESS-cosolvent processes are explored. Therefore, there is more work to be done to understand the parameters that influence particle size from similar processes. Furthermore, the impact of product attributes on bioavailability and long-term stability of the cocrystalline solids warrants exploration—in particular if a cocrystal is of high commercial or industrial interest.

In addition to systematic solvent selection, process optimization and scale-up potential should be considered with respect to throughput and yield. It is encouraged to evaluate and openly report process yields and mass balance for RESS crystallization which can help identify areas of

improvement, such as optimization of solids collection or equipment geometry. Future research can also investigate optimization of processes to reduce organic solvent intensity, improve throughput, while increasing product yields. For example, increasing pressure and temperature used to crystallize PZQ-malonic acid by RESS may decrease the organic solvent requirement to compete with reactive crystallization. Furthermore, optimization of equipment geometry and flush method could reduce the amount of organic solvent used during the flush steps. A broader exploration of processing conditions may also allow for use of solvents such as EtOH which is more pharmaceutically acceptable than MeOH. Improvement in throughput of RESS processes by changing operating conditions (pressure, temperature) and cosolvent (type and loading) may also make RESS more attractive for processing APIs.

BIBLIOGRAPHY

[1] Food and Drug Administration (FDA), M9 Biopharmaceutics Classification SystemBased Biowaivers: Guidance for Industry, (2021) 20. https://www.fda.gov/drugs/guidance-compliance-regulatory-information/guidances-drugs.

[2] T. Takagi, C. Ramachandran, M. Bermejo, S. Yamashita, L.X. Yu, G.L. Amidon, A provisional biopharmaceutical classification of the top 200 oral drug products in the United States, Great Britain, Spain, and Japan, Mol. Pharm. 3 (2006) 631–643. https://doi.org/10.1021/mp0600182.

[3] N. Blagden, M. de Matas, P.T. Gavan, P. York, Crystal engineering of active pharmaceutical ingredients to improve solubility and dissolution rates, Adv. Drug Deliv. Rev. 59 (2007) 617–630. https://doi.org/10.1016/j.addr.2007.05.011.

[4] N.J. Babu, A. Nangia, Solubility advantage of amorphous drugs and pharmaceutical cocrystals, Cryst. Growth Des. 11 (2011) 2662–2679. https://doi.org/10.1021/cg200492w.

[5] K.T. Savjani, A.K. Gajjar, J.K. Savjani, Drug Solubility: Importance and Enhancement Techniques, ISRN Pharm. 2012 (2012) 1–10. https://doi.org/10.5402/2012/195727.

[6] P. Khadka, J. Ro, H. Kim, I. Kim, J.T. Kim, H. Kim, J.M. Cho, G. Yun, J. Lee, Pharmaceutical particle technologies: An approach to improve drug solubility, dissolution and bioavailability, Asian J. Pharm. Sci. 9 (2014) 304–316. https://doi.org/10.1016/j.ajps.2014.05.005.

[7] H.H. Tung, Industrial perspectives of pharmaceutical crystallization, Org. Process Res. Dev. 17 (2013) 445–454. https://doi.org/10.1021/op3002323.

[8] G. Nykamp, U. Carstensen, B.W. Mu, Jet milling — a new technique for microparticle preparation, 242 (2002) 79–86.

[9] A. Ziaeea, A.B. Albadarina, L. Padrela, T. Femmer, E. O'Reilly, G. Walker, Spray drying of pharmaceuticals and biopharmaceuticals: Critical parameters and experimental process optimization approaches, Eur. J. Pharm. Sci. 127 (2019) 300–318.

[10] N.G. Sahoo, A. Abbas, Z. Judeh, C.M. Li, K.-H. Yuen, Solubility Enhancement of a Poorly Water-Soluble Anti-Malarial Drug: Experimental Design and Use of a Modified Multifluid Nozzle Pilot Spray Drier, J. Pharm. Sci. 98 (2009) 281–296. https://doi.org/10.1002/jps.

[11] J. Weng, S.N. Wong, X. Xu, B. Xuan, C. Wang, R. Chen, C.C. Sun, R. Lakerveld, P. Chi,

L. Kwok, S.F. Chow, Cocrystal Engineering of Itraconazole with Suberic Acid via Rotary Evaporation and Spray Drying, Cryst. Growth Des. 19 (2019) 2736–2745. https://doi.org/10.1021/acs.cgd.8b01873.

[12] L. Padrela, M.A. Rodrigues, A. Duarte, A.M.A. Dias, M.E.M. Braga, H.C. de Sousa, Supercritical carbon dioxide-based technologies for the production of drug nanoparticles/nanocrystals – A comprehensive review, Adv. Drug Deliv. Rev. 131 (2018) 22–78. https://doi.org/10.1016/j.addr.2018.07.010.

[13] S. Kitamura, A. Miyamae, S. Koda, Y. Morimoto, Effect of grinding on the solid-state stability of cefixime trihydrate, Int. J. Pharm. 56 (1989) 125–134.

[14] S. Kumar, D.J. Burgess, Wet milling induced physical and chemical instabilities of naproxen nano-crystalline suspensions, Int. J. Pharm. 466 (2014) 223–232. https://doi.org/10.1016/j.ijpharm.2014.03.021.

[15] K. Adrjanowicz, K. Kaminski, K. Grzybowska, L. Hawelek, M. Paluch, I. Gruszka, D. Zakowiecki, W. Sawicki, P. Lepek, W. Kamysz, L. Guzik, Effect of cryogrinding on chemical stability of the sparingly water-soluble drug furosemide, Pharm. Res. 28 (2011) 3220–3236. https://doi.org/10.1007/s11095-011-0496-4.

[16] A.T.M. Serajuddin, Salt formation to improve drug solubility, Adv. Drug Deliv. Rev. 59 (2007) 603–616.

[17] D.P. Elder, R. Holm, H. Lopez de Diego, Use of pharmaceutical salts and cocrystals to address the issue of poor solubility, Int. J. Pharm. 453 (2012) 88–100. https://doi.org/10.1016/j.ijpharm.2012.11.028.

[18] X. Lin, Y. Hu, L. Liu, L. Su, N. Li, J. Yu, B. Tang, Z. Yang, Physical Stability of Amorphous Solid Dispersions: a Physicochemical Perspective with Thermodynamic, Kinetic and Environmental Aspects, Pharm. Res. 35 (2018). https://doi.org/10.1007/s11095-018-2408-3.

[19] T. Peng, Y. She, C. Zhu, Y. Shi, Y. Huang, B. Niu, X. Bai, X. Pan, C. Wu, Influence of Polymers on the Physical and Chemical Stability of Spray-dried Amorphous Solid Dispersion: Dipyridamole Degradation Induced by Enteric Polymers, AAPS PharmSciTech. 19 (2018) 2620–2628. https://doi.org/10.1208/s12249-018-1082-4.

[20] X. Ma, R.O. Williams, Characterization of amorphous solid dispersions: An update, J. Drug Deliv. Sci. Technol. 50 (2019) 113–124. https://doi.org/10.1016/j.jddst.2019.01.017.

[21] US Food and Drug Administration, Regulatory Classification of Pharmaceutical Co-Crystals Guidance for Industry, 2018.

[22] C. Almansa, R. Mercè, N. Tesson, J. Farran, J. Tomàs, C.R. Plata-Salamán, Co-crystal of Tramadol Hydrochloride-Celecoxib (ctc): A Novel API-API Co-crystal for the Treatment of Pain, Cryst. Growth Des. 17 (2017) 1884–1892. https://doi.org/10.1021/acs.cgd.6b01848.

[23] A. Kumar, S. Kumar, A. Nanda, A review about regulatory status and recent patents of pharmaceutical co-crystals, Adv. Pharm. Bull. 8 (2018) 355–363. https://doi.org/10.15171/apb.2018.042.

[24] R. Kumar Bandaru, S.R. Rout, G. Kenguva, B. Gorain, N.A. Alhakamy, P. Kesharwani, R. Dandela, Recent Advances in Pharmaceutical Cocrystals: From Bench to Market, Front. Pharmacol. 12 (2021) 1–16. https://doi.org/10.3389/fphar.2021.780582.

[25] D. Douroumis, S.A. Ross, A. Nokhodchi, Advanced methodologies for cocrystal synthesis, Adv. Drug Deliv. Rev. 117 (2017) 178–195. https://doi.org/10.1016/j.addr.2017.07.008.

[26] M. Malamatari, S.A. Ross, D. Douroumis, S.P. Velaga, Experimental cocrystal screening and solution based scale-up cocrystallization methods, Adv. Drug Deliv. Rev. 117 (2017) 162–177. https://doi.org/10.1016/j.addr.2017.08.006.

[27] I. Pasquali, R. Bettini, F. Giordano, Supercritical fluid technologies: An innovative approach for manipulating the solid-state of pharmaceuticals, Adv. Drug Deliv. Rev. 60 (2008) 399–410. https://doi.org/10.1016/j.addr.2007.08.030.

[28] G.L. Perlovich, Thermodynamic characteristics of cocrystal formation and melting points for rational design of pharmaceutical two-component systems, CrystEngComm. 17 (2015) 7019–7028. https://doi.org/10.1039/C5CE00992H.

[29] F. Mao, Q. Kong, W. Ni, X. Xu, D. Ling, Z. Lu, J. Li, Melting Point Distribution Analysis of Globally Approved and Discontinued Drugs : A Research for Improving the Chance of Success of Drug Design and Discovery, 2 (2016) 357–368. https://doi.org/10.1002/open.201600015.

[30] C.A. Eckert, B.L. Knutson, P.G. Debenedetti, Supercritical fluids as solvents for chemical and materials processing, Nature. 383 (1996) 313–318.

[31] C.A. Ober, S.E. Montgomery, R.B. Gupta, Formation of itraconazole/L-malic acid

cocrystals by gas antisolvent cocrystallization, Powder Technol. 236 (2013) 122–131. https://doi.org/10.1016/j.powtec.2012.04.058.

[32] A.Z. Hezave, A. Mowla, F. Esmaeilzadeh, Cetirizine solubility in supercritical CO2 at different pressures and temperatures, J. Supercrit. Fluids. 58 (2011) 198–203. https://doi.org/10.1016/j.supflu.2011.05.017.

[33] R.G. Bitencourt, F.A. Cabral, A.J.A. Meirelles, Ferulic acid solubility in supercritical carbon dioxide, ethanol and water mixtures, J. Chem. Thermodyn. 103 (2016) 285–291. https://doi.org/10.1016/j.jct.2016.08.025.

[34] L. Padrela, M.A. Rodrigues, J. Tiago, S.P. Velaga, H.A. Matos, E.G. De Azevedo, Insight into the Mechanisms of Cocrystallization of Pharmaceuticals in Supercritical Solvents, Cryst. Growth Des. 15 (2015) 3175–3181. https://doi.org/10.1021/acs.cgd.5b00200.

[35] Q. Li, Z. Zhang, C. Zhong, Y. Liu, Q. Zhou, Solubility of solid solutes in supercritical carbon dioxide with and without cosolvents, 207 (2003) 183–192. https://doi.org/10.1016/S0378-3812(03)00022-0.

[36] X.Q. Bian, Q. Zhang, Z.M. Du, J. Chen, J.N. Jaubert, A five-parameter empirical model for correlating the solubility of solid compounds in supercritical carbon dioxide, Fluid Phase Equilib. 411 (2016) 74–80. https://doi.org/10.1016/j.fluid.2015.12.017.

[37] C. Si-Moussa, A. Belghait, L. Khaouane, S. Hanini, A. Halilali, Novel density-based model for the correlation of solid drugs solubility in supercritical carbon dioxide, Comptes Rendus Chim. 20 (2017) 559–572. https://doi.org/10.1016/j.crci.2016.09.009.

[38] C.Y. Huang, L.S. Lee, C.S. Su, Correlation of solid solubilities of pharmaceutical compounds in supercritical carbon dioxide with solution model approach, J. Taiwan Inst. Chem. Eng. 44 (2013) 349–358. https://doi.org/10.1016/j.jtice.2012.12.004.

[39] G. Sodeifian, S.A. Sajadian, F. Razmimanesh, N.S. Ardestani, A comprehensive comparison among four different approaches for predicting the solubility of pharmaceutical solid compounds in supercritical carbon dioxide, Korean J. Chem. Eng. 35 (2018) 2097–2116. https://doi.org/10.1007/s11814-018-0125-6.

[40] G. Sodeifian, N. Saadati Ardestani, S.A. Sajadian, H.S. Panah, Measurement, correlation and thermodynamic modeling of the solubility of Ketotifen fumarate (KTF) in supercritical carbon dioxide: Evaluation of PCP-SAFT equation of state, Fluid Phase Equilib. 458 (2018) 102–114. https://doi.org/10.1016/j.fluid.2017.11.016.

[41] J. Li, J. Jin, Z. Zhang, Y. Wang, Measurement and correlation of solubility of benzamide in supercritical carbon dioxide with and without cosolvent, Fluid Phase Equilib. 307 (2011) 11–15. https://doi.org/10.1016/j.fluid.2011.04.021.

[42] M. Hojjati, Y. Yamini, M. Khajeh, A. Vatanara, Solubility of some statin drugs in supercritical carbon dioxide and representing the solute solubility data with several density-based correlations, 41 (2007) 187–194. https://doi.org/10.1016/j.supflu.2006.10.006.

[43] L. Manna, M. Banchero, Solubility of Tolbutamide and Chlorpropamide in Supercritical Carbon Dioxide, J. Chem. Eng. Data. 63 (2018) 1745–1751. https://doi.org/10.1021/acs.jced.8b00050.

[44] A. Cháfer, T. Fornari, R.P. Stateva, A. Berna, Trans-cinnamic acid solubility enhancement in the presence of ethanol as a supercritical Co2 cosolvent, J. Chem. Eng. Data. 54 (2009) 2263–2268. https://doi.org/10.1021/je900154x.

[45] L.H. Wang, S.T. Lin, A predictive method for the solubility of drug in supercritical carbon dioxide, J. Supercrit. Fluids. 85 (2014) 81–88. https://doi.org/10.1016/j.supflu.2013.10.019.

[46] G. Sodeifian, S.A. Sajadian, F. Razmimanesh, Solubility of an antiarrhythmic drug (amiodarone hydrochloride) in supercritical carbon dioxide: Experimental and modeling, Fluid Phase Equilib. 450 (2017) 149–159. https://doi.org/10.1016/j.fluid.2017.07.015.

[47] R.G. Bitencourt, A.M. Palma, J.A.P. Coutinho, F.A. Cabral, A.J.A. Meirelles, Solubility of caffeic acid in CO2 + ethanol: Experimental and predicted data using Cubic Plus Association Equation of State, J. Supercrit. Fluids. 138 (2018) 238–246. https://doi.org/10.1016/j.supflu.2018.04.008.

[48] R.G. Bitencourt, A.M. Palma, J.A.P. Coutinho, F.A. Cabral, A.J.A. Meirelles, Prediction of solid solute solubility in supercritical CO 2 with cosolvents using the CPA EoS, Fluid Phase Equilib. 482 (2018) 1–10. https://doi.org/10.1016/j.fluid.2018.10.020.

[49] M. Mirmehrabi, S. Rohani, An approach to solvent screening for crystallization of polymorphic pharmaceutical and fine chemicals, J. Pharm. Sci. 94 (2005) 1560–1576. https://doi.org/10.1002/jps.20371.

[50] M. Mirmehrabi, S. Rohani, Polymorphic Behavior and Crystal Habit of an Anti-Viral/HIV Drug: Stavudine, Cryst. Growth Des. 6 (2006) 141–149.

https://doi.org/10.1021/cg050242g.

[51] Y. Li, Y. Yu, H. Wang, F. Zhao, Effect of process parameters on the recrystallization and size control of puerarin using the supercritical fluid antisolvent process, Asian J. Pharm. Sci. 11 (2016) 281–291. https://doi.org/10.1016/j.ajps.2015.12.001.

[52] E.L. Paul, V.A. Atiemo-Obeng, S.M. Kresta, Handbook of Industrial Mixing Science and Practice, John Wiley and Sons Inc., 2004.

[53] I.A. Cuadra, A. Cabañas, J.A.R. Cheda, C. Pando, Polymorphism in the co-crystallization of the anticonvulsant drug carbamazepine and saccharin using supercritical CO 2 as an anti-solvent, J. Supercrit. Fluids. 136 (2018) 60–69. https://doi.org/10.1016/j.supflu.2018.02.004.

[54] J. Mullin, Crystallization, Fourth, Butterworth-Heinemann, 2001.

[55] N. Rodríguez-Hornedo, D. Murphy, Significance of Controlling Crystallization Mechanisms and Kinetics in Pharmaceutical Systems, J. Pharm. Sci. 88 (1999) 651–660.

[56] W. Beckmann, Nucleation phenomena during the crystallisation and precipitation of Abecarnil, Cryst. Growth. 199 (1999) 1307–1314.

[57] A. Markande, A. Nezzal, J.J. Fitzpatrick, L. Aerts, Investigation of the Crystallization Kinetics of Dextrose Monohydrate Using In Situ Particle Size and Supersaturation Monitoring, Part. Sci. Technol. 27 (2009) 373–388. https://doi.org/10.1080/02726350902994050.

[58] D. Jafari, S.M. Nowee, S.H. Noie, A kinetic modeling of particle formation by gas antisolvent process: Precipitation of aspirin, J. Dispers. Sci. Technol. 38 (2017) 677–685. https://doi.org/10.1080/01932691.2016.1188709.

[59] A.Z. Hezave, S. Aftab, F. Esmaeilzadeh, Micronization of creatine monohydrate via Rapid Expansion of Supercritical Solution (RESS), J. Supercrit. Fluids. 55 (2010) 316–324. https://doi.org/10.1016/j.supflu.2010.05.009.

[60] N. Yildiz, Ş. Tuna, O. Döker, A. Çalimli, Micronization of salicylic acid and taxol (paclitaxel) by rapid expansion of supercritical fluids (RESS), J. Supercrit. Fluids. 41 (2007) 440–451. https://doi.org/10.1016/j.supflu.2006.12.012.

[61] A. Erriguible, C. Neurohr, A.L. Revelli, S. Laugier, G. Fevotte, P. Subra-Paternault, Cocrystallization induced by compressed CO2 as antisolvent: Simulation of a batch process for the estimation of nucleation and growth parameters, J. Supercrit. Fluids. 98

(2015) 194–203. https://doi.org/10.1016/j.supflu.2014.12.013.

[62] I. De Marco, E. Reverchon, Influence of pressure , temperature and concentration on the mechanisms of particle precipitation in supercritical antisolvent micronization, J. Supercrit. Fluids. 58 (2011) 295–302. https://doi.org/10.1016/j.supflu.2011.06.005.

[63] International Council for Harmonization, Technical Requirements for Pharmaceuticals for Human Use Guideline for Impurities: Residual Solvents, in: 2016.

[64] M. Türk, B. Helfgen, P. Hils, R. Lietzow, K. Schaber, Micronization of pharmaceutical substances by rapid expansion of supercritical solutions (RESS): Experiments and modeling, Part. Part. Syst. Charact. 19 (2002) 327–335. https://doi.org/10.1002/1521-4117(200211)19:5<327::AID-PPSC327>3.0.CO;2-V.

[65] H.P. Stahl, C.G. Wermuth, Handbook of Pharmaceutical Salts Properties, Selection, and Use, Verlag Helvetica Chimica Acta, WILEY-VCH, n.d.

[66] Substances Generally Recognized as Safe, in: 21 C.F.R. § 182, 2020.

[67] J. Lu, S. Rohani, Synthesis and Preliminary Characterization of Sulfamethazine-Theophylline Co-Crystal, Pharm. Technol. 99 (2010) 4042–4047. https://doi.org/10.1002/jps.

[68] M. Lindenberg, S. Kopp, J.B. Dressman, Classification of orally administered drugs on the World Health Organization Model list of Essential Medicines according to the biopharmaceutics classification system, Eur. J. Pharm. Biopharm. 58 (2004) 265–278. https://doi.org/10.1016/j.ejpb.2004.03.001.

[69] M.K. Stanton, A. Bak, Physicochemical Properties of Pharmaceutical Co-Crystals: A Case Study of Ten AMG 517 Co-Crystals, Cryst. Growth Des. 8 (2008) 3856–3862. https://doi.org/10.1021/cg800173d.

[70] I. Sathisaran, S.V. Dalvi, Engineering cocrystals of poorlywater-soluble drugs to enhance dissolution in aqueous medium, Pharmaceutics. 10 (2018). https://doi.org/10.3390/pharmaceutics10030108.

[71] R.S. Dhumal, S. V. Biradar, S. Yamamura, A.R. Paradkar, P. York, Preparation of amorphous cefuroxime axetil nanoparticles by sonoprecipitation for enhancement of bioavailability, Eur. J. Pharm. Biopharm. 70 (2008) 109–115. https://doi.org/10.1016/j.ejpb.2008.04.001.

[72] J.-O. Waltersson, P. Lundgren, The effect of mechanical comminution on drug stability,

Acta Pharm. Suec. 22 (1985) 291–300.

[73] N. Qiao, M. Li, W. Schlindwein, N. Malek, A. Davies, G. Trappitt, Pharmaceutical cocrystals: An overview, Int. J. Pharm. 419 (2011) 1–11. https://doi.org/10.1016/j.ijpharm.2011.07.037.

[74] G.R. Desirju, Supramolecular Synthons in Crystal Engineering- A New Organic Synthesis, Agnew. Chem. Int. (1995) 2311–2327. https://doi.org/10.1002/anie.199523111.

[75] C.B. Aakeröy, D.J. Salmon, Building co-crystals with molecular sense and supramolecular sensibility, CrystEngComm. 7 (2005) 439–448. https://doi.org/10.1039/b505883j.

[76] P. Vishweshwar, J. McMahon, J.A. Bis, M.J. Zaworotko, Pharmaceutical Co-Crystals, J. Pharm. Sci. 95 (2005) 499–516.

[77] C.B. Aakeröy, A.B. Grommet, J. Desper, Co-crystal screening of diclofenac, Pharmaceutics. 3 (2011) 601–614. https://doi.org/10.3390/pharmaceutics3030601.

[78] R. Chadha, A. Saini, P. Arora, S. Chanda, Dharamvirsinghjain, Cocrystals of efavirenz with selected conformers: Preparation and characterization, Int. J. Pharm. Pharm. Sci. 4 (2012) 244–250.

[79] P. Kavuru, D. Aboarayes, K.K. Arora, H.D. Clarke, A. Kennedy, L. Marshall, T.T. Ong, J. Perman, T. Pujari, Ł. Wojtas, M.J. Zaworotko, Hierarchy of supramolecular synthons: Persistent hydrogen bonds between carboxylates and weakly acidic hydroxyl moieties in cocrystals of zwitterions, Cryst. Growth Des. 10 (2010) 3568–3584. https://doi.org/10.1021/cg100484a.

[80] K. Fucke, S.A. Myz, T.P. Shakhtshneider, E. V. Boldyreva, U.J. Griesser, How good are the crystallisation methods for co-crystals? A comparative study of piroxicam, New J. Chem. 36 (2012) 1969–1977. https://doi.org/10.1039/c2nj40093f.

[81] M.A. Solomos, C. Mohammadi, J.H. Urbelis, E.S. Koch, R. Osborne, C.C. Usala, J.A. Swift, Predicting cocrystallization based on heterodimer energies: The case of N,N′-diphenylureas and triphenylphosphine oxide, Cryst. Growth Des. 15 (2015) 5068–5074. https://doi.org/10.1021/acs.cgd.5b01039.

[82] G. He, P.S. Chow, R.B.H. Tan, Predicting Multicomponent Crystal Formation: The Interplay Between Homomeric and Heteromeric Interactions, Cryst. Growth Des. 9 (2009) 4529–4532. https://doi.org/10.1021/cg900538g.

[83] M.A. Mohammad, A. Alhalaweh, S.P. Velaga, Hansen solubility parameter as a tool to

predict cocrystal formation, Int. J. Pharm. 407 (2011) 63–71. https://doi.org/10.1016/j.ijpharm.2011.01.030.

[84] H. Barua, A. Gunnam, B. Yadav, A. Nangia, N.R. Shastri, An: Ab initio molecular dynamics method for cocrystal prediction: Validation of the approach, CrystEngComm. 21 (2019) 7233–7248. https://doi.org/10.1039/c9ce01436e.

[85] T. Friscic, S.L. Childs, S.A.A. Rizvic, W. Jones, The role of solvent in mechanochemical and sonochemical cocrystal formation: a solubility-based approach for predicting cocrystallisation outcome, CrystEngComm. 11 (2009) 418–426. https://doi.org/10.1039/b810822f.

[86] D.J. Berry, J.W. Steed, Pharmaceutical cocrystals, salts and multicomponent systems; intermolecular interactions and property based design, Adv. Drug Deliv. Rev. 117 (2017) 3–24. https://doi.org/10.1016/j.addr.2017.03.003.

[87] R.A. Chiarella, R.J. Davey, M.L. Peterson, Making co-crystals - The utility of ternary phase diagrams, Cryst. Growth Des. 7 (2007) 1223–1226. https://doi.org/10.1021/cg070218y.

[88] T. Rager, R. Hilfiker, Stability domains of multi-component crystals in ternary phase diagrams, Zeitschrift Fur Phys. Chemie. 223 (2009) 793–813. https://doi.org/10.1524/zpch.2009.5454.

[89] F. Fischer, G. Scholz, S. Benemann, K. Rademann, F. Emmerling, Evaluation of the formation pathways of cocrystal polymorphs in liquid-assisted syntheses, CrystEngComm. 16 (2014) 8272–8278. https://doi.org/10.1039/c4ce00472h.

[90] S.J. Diez, M.D. Eddleston, M. Arhangelskis, M. Milbled, M.J. Müller, A.D. Bond, D.K. Bučar, W. Jones, Crystallization at Solvent Interfaces Enables Access to a Variety of Cocrystal Polymorphs and Hydrates, Cryst. Growth Des. 18 (2018) 3263–3268. https://doi.org/10.1021/acs.cgd.8b00114.

[91] M.A. Rodrigues, J.M. Tiago, A. Duarte, V. Geraldes, H.A. Matos, E. Gomes Azevedo, Polymorphism in Pharmaceutical Drugs by Supercritical CO 2 Processing: Clarifying the Role of the Antisolvent Effect and Atomization Enhancement, Cryst. Growth Des. 16 (2016) 6222–6229. https://doi.org/10.1021/acs.cgd.6b00697.

[92] K. Moribe, Y. Tozuka, K. Yamamoto, Supercritical carbon dioxide processing of active pharmaceutical ingredients for polymorphic control and for complex formation, Adv.

Drug Deliv. Rev. 60 (2008) 328–338. https://doi.org/10.1016/j.addr.2007.03.023.

[93] C. Pando, A. Cabañas, I.A. Cuadra, Preparation of pharmaceutical co-crystals through sustainable processes using supercritical carbon dioxide: A review, RSC Adv. 6 (2016) 71134–71150. https://doi.org/10.1039/c6ra10917a.

[94] L. Padrela, M.A. Rodrigues, S.P. Velaga, H.A. Matos, E.G. de Azevedo, Formation of indomethacin-saccharin cocrystals using supercritical fluid technology, Eur. J. Pharm. Sci. 38 (2009) 9–17. https://doi.org/10.1016/j.ejps.2009.05.010.

[95] M.M. Ribas, G.S.B. Sakata, A.E. Santos, C. Dal Magro, G.P.S. Aguiar, M. Lanza, J.V. Oliveira, Curcumin cocrystals using supercritical fluid technology, J. Supercrit. Fluids. 152 (2019) 1–7. https://doi.org/10.1016/j.supflu.2019.104564.

[96] M.M. Ribas, G.P.S. Aguiar, L.G. Muller, A.M. Siebel, M. Lanza, J.V. Oliveira, Curcumin-nicotinamide cocrystallization with supercritical solvent (CSS): Synthesis, characterization and in vivo antinociceptive and anti-inflammatory activities, Ind. Crops Prod. 139 (2019). https://doi.org/10.1016/j.indcrop.2019.111537.

[97] I.A. Cuadra, A. Cabañas, J.A.R. Cheda, M. Türk, C. Pando, Cocrystallization of the anticancer drug 5-fluorouracil and coformers urea, thiourea or pyrazinamide using supercritical CO2 as an antisolvent (SAS) and as a solvent (CSS), J. Supercrit. Fluids. 160 (2020). https://doi.org/10.1016/j.supflu.2020.104813.

[98] C.C. Tsai, H. mu Lin, M.J. Lee, Phase equilibrium and micronization for flufenamic acid with supercritical carbon dioxide, J. Taiwan Inst. Chem. Eng. 72 (2017) 19–28. https://doi.org/10.1016/j.jtice.2017.01.011.

[99] H. Rostamian, M.N. Lotfollahi, Production and characterization of ultrafine aspirin particles by rapid expansion of supercritical solution with solid co-solvent (RESS-SC): expansion parameters effects, Part. Sci. Technol. 0 (2019) 1–9. https://doi.org/10.1080/02726351.2019.1573865.

[100] M. Charoenchaitrakool, F. Dehghani, N.R. Foster, H.K. Chan, Micronization by rapid expansion of supercritical solutions to enhance the dissolution rates of poorly water-soluble pharmaceuticals, Ind. Eng. Chem. Res. 39 (2000) 4794–4802. https://doi.org/10.1021/ie000151a.

[101] A. Alhalaweh, S.P. Velaga, Formation of cocrystals from stoichiometric solutions of incongruently saturating systems by spray drying, Cryst. Growth Des. 10 (2010) 3302–

3305. https://doi.org/10.1021/cg100451q.

[102] M. Herrmann, U. Förter-Barth, H. Kröber, P.B. Kempa, M. Del Mar Juez-Lorenzo, S. Doyle, Co-Crystallization and characterization of pharmaceutical ingredients, Part. Part. Syst. Charact. 26 (2009) 151–156. https://doi.org/10.1002/ppsc.200800046.

[103] C. Vemavarapu, M.J. Mollan, T.E. Needham, Coprecipitation of pharmaceutical actives and their structurally related additives by the RESS process, Powder Technol. 189 (2009) 444–453. https://doi.org/10.1016/j.powtec.2008.07.005.

[104] K.C. Müllers, M. Paisana, M.A. Wahl, Simultaneous formation and micronization of pharmaceutical cocrystals by Rapid Expansion of Supercritical Solutions (RESS), Pharm. Res. 32 (2015) 702–713. https://doi.org/10.1007/s11095-014-1498-9.

[105] P. Kotnik, M. Škerget, Ž. Knez, Solubility of nicotinic acid and nicotinamide in carbon dioxide at T = (313.15 to 373.15) K and p = (5 to 30) MPa: Experimental data and correlation, J. Chem. Eng. Data. 56 (2011) 338–343. https://doi.org/10.1021/je100697a.

[106] C.A. Ober, R.B. Gupta, Formation of Itraconazole–Succinic Acid Cocrystals by Gas Antisolvent Cocrystallization, AAPS PharmSciTech. 13 (2012) 1396–1406.

[107] N. Wichianphong, M. Charoenchaitrakool, Statistical optimization for production of mefenamic acid–nicotinamide cocrystals using gas anti-solvent (GAS) process, J. Ind. Eng. Chem. 62 (2018) 375–382. https://doi.org/10.1016/j.jiec.2018.01.017.

[108] M. Neurohr, Clémence Marchivie, S. Lecomte, Y. Cartigny, N. Couvrat, M. Sanselme, P. Subra-Paternault, Naproxen−Nicotinamide Cocrystals- Racemic and Conglomerate Structures Generated by CO2 Antisolvent Crystallization, Cryst. Growth Des. 15 (2015) 4616–4626.

[109] C. Neurohr, A.L. Revelli, P. Billot, M. Marchivie, S. Lecomte, S. Laugier, S. Massip, P. Subra-Paternault, Naproxen-nicotinamide cocrystals produced by CO2 antisolvent, J. Supercrit. Fluids. 83 (2013) 78–85. https://doi.org/10.1016/j.supflu.2013.07.008.

[110] A. Shikhar, M.M. Bommana, S.S. Gupta, E. Squillante, Formulation development of Carbamazepine–Nicotinamide co-crystals complexed with γ-cyclodextrin using supercritical fluid process, J. Supercrit. Fluids. 55 (2011) 1070–1078.

[111] G. Kotbantao, M. Charoenchaitrakool, Processing of ketoconazole-4-aminobenzoic acid cocrystals using dense CO2 as an antisolvent, J. CO2 Util. 17 (2017) 213–219. https://doi.org/10.1016/j.jcou.2016.12.007.

[112] A.S. Pessoa, G.P.S. Aguiar, J. Vladimir Oliveira, A.J. Bortoluzzi, A. Paulino, M. Lanza, Precipitation of resveratrol-isoniazid and resveratrol-nicotinamide cocrystals by gas antisolvent, J. Supercrit. Fluids. 145 (2019) 93–102. https://doi.org/10.1016/j.supflu.2018.11.014.

[113] A. Erriguible, C. Neurohr, A.L. Revelli, S. Laugier, G. Fevotte, P. Subra-Paternault, Cocrystallization induced by compressed CO 2 as antisolvent: Simulation of a batch process for the estimation of nucleation and growth parameters, J. Supercrit. Fluids. 98 (2015) 194–203. https://doi.org/10.1016/j.supflu.2014.12.013.

[114] A.L. Revelli, S. Laugier, A. Erriguible, P. Subra-Paternault, High-pressure solubility of naproxen, nicotinamide and their mixture in acetone with supercritical CO2 as an anti-solvent, Fluid Phase Equilib. 373 (2014) 29–33. https://doi.org/10.1016/j.fluid.2014.03.029.

[115] C. Harscoat-Schiavo, C. Neurohr, S. Lecomte, M. Marchivie, P. Subra-Paternault, Influence of isomerism on recrystallization and cocrystallization induced by CO2 as an antisolvent, CrystEngComm. 17 (2015) 5410–5421. https://doi.org/10.1039/c5ce00753d.

[116] R. Imchalee, M. Charoenchaitrakool, Gas anti-solvent processing of a new sulfamethoxazole−l-malic acid cocrystal, J. Ind. Eng. Chem. 25 (2015) 12–15.

[117] N. Wichianphong, M. Charoenchaitrakool, Application of Box-Behnken design for processing of mefenamic acid-paracetamol cocrystals using gas anti-solvent (GAS) process, J. CO2 Util. 26 (2018) 212–220. https://doi.org/10.1016/j.jcou.2018.05.011.

[118] H.H. Chen, C.S. Su, J.J. Liu, M.T. Sheu, Solid-state property modification and dissolution rate enhancement of tolfenamic acid by supercritical antisolvent process, J. Supercrit. Fluids. 101 (2015) 17–23. https://doi.org/10.1016/j.supflu.2015.02.031.

[119] W.Y. Wu, C.S. Su, Modification of solid-state property of sulfasalazine by using the supercritical antisolvent process, J. Cryst. Growth. 460 (2017) 59–66. https://doi.org/10.1016/j.jcrysgro.2016.12.017.

[120] W.-Y. Wu, C.-S. Su, Recrystallization and Production of Spherical Submicron Particles of Sulfasalazine Using a Supercritical Antisolvent Process, Crystals. 8 (2018) 295. https://doi.org/10.3390/cryst8070295.

[121] H.H. Chen, C.S. Su, Recrystallizing Primidone through Supercritical Antisolvent Precipitation, Org. Process Res. Dev. 20 (2016) 878–887.

https://doi.org/10.1021/acs.oprd.5b00279.

[122] C. Neurohr, A. Erriguible, S. Laugier, P. Subra-Paternault, Challenge of the supercritical antisolvent technique SAS to prepare cocrystal-pure powders of naproxen-nicotinamide, Chem. Eng. J. 303 (2016) 238–251. https://doi.org/10.1016/j.cej.2016.05.129.

[123] C. Neurohr, A. Erriguible, S. Laugier, P. Subra-Paternault, Challenge of the supercritical antisolvent technique SAS to prepare cocrystal-pure powders of naproxen-nicotinamide, Chem. Eng. J. 303 (2016) 238–251. https://doi.org/10.1016/j.cej.2016.05.129.

[124] I.A. Cuadra, A. Cabañas, J.A.R. Cheda, F.J. Martínez-Casado, C. Pando, Pharmaceutical co-crystals of the anti-inflammatory drug diflunisal and nicotinamide obtained using supercritical CO2 as an antisolvent, J. CO2 Util. 13 (2016) 29–37. https://doi.org/10.1016/j.jcou.2015.11.006.

[125] S. Hiendrawan, B. Veriansyah, E. Widjojokusumo, S.N. Soewandhi, S. Wikarsa, R.R. Tjandrawinata, Simultaneous cocrystallization and micronization of paracetamol-dipicolinic acid cocrystal by supercritical antisolvent (SAS), Int. J. Pharm. Pharm. Sci. 8 (2016) 89–98.

[126] Z. Zhao, G. Liu, Q. Lin, Y. Jiang, Co-Crystal of Paracetamol and Trimethylglycine Prepared by a Supercritical CO2 Anti-Solvent Process.pdf, Chem. Eng. Technol. 41 (2018) 1122–1131.

[127] R.R. Tjandrawinata, S. Hiendrawan, B. Veriansyah, Processing paracetamol-5-nitroisophthalic acid cocrystal using supercritical CO2 as an anti-solvent, Int. J. Appl. Pharm. 11 (2019) 194–199. https://doi.org/10.22159/ijap.2019v11i5.34554.

[128] L. Padrela, M.A. Rodrigues, S.P. Velaga, A.C. Fernandes, H.A. Matos, E.G. de Azevedo, Screening for pharmaceutical cocrystals using the supercritical fluid enhanced atomization process, J. Supercrit. Fluids. 53 (2010) 156–164. https://doi.org/10.1016/j.supflu.2010.01.010.

[129] L. Padrela, M.A. Rodrigues, J. Tiago, S.P. Velaga, H.A. Matos, E.G. De Azevedo, Tuning physicochemical properties of theophylline by cocrystallization using the supercritical fluid enhanced atomization technique, J. Supercrit. Fluids. 86 (2014) 129–136. https://doi.org/10.1016/j.supflu.2013.12.011.

[130] J.M. Tiago, L. Padrela, M.A. Rodrigues, H.A. Matos, A.J. Almeida, E.G. De Azevedo, Single-step co-crystallization and lipid dispersion by supercritical enhanced atomization,

Cryst. Growth Des. 13 (2013) 4940–4947. https://doi.org/10.1021/cg401131x.

[131] L. Padrela, M.A. Rodrigues, J. Tiago, S.P. Velaga, H.A. Matos, E.G. De Azevedo, Tuning physicochemical properties of theophylline by cocrystallization using the supercritical fluid enhanced atomization technique, J. Supercrit. Fluids. 86 (2014) 129–136. https://doi.org/10.1016/j.supflu.2013.12.011.

[132] M. Türk, P. Hils, B. Helfgen, K. Schaber, H.J. Martin, M.A. Wahl, Micronization of pharmaceutical substances by the Rapid Expansion of Supercritical Solutions (RESS): A promising method to improve bioavailability of poorly soluble pharmaceutical agents, J. Supercrit. Fluids. 22 (2002) 75–84. https://doi.org/10.1016/S0896-8446(01)00109-7.

[133] D. Bolten, M. Türk, Micronisation of carbamazepine through rapid expansion of supercritical solution (RESS), J. Supercrit. Fluids. 66 (2012) 389–397. https://doi.org/10.1016/j.supflu.2012.04.010.

[134] A.Y. Sheikh, S.A. Rahim, R.B. Hammond, K.J. Roberts, Scalable solution cocrystallization: case of carbamazepine-nicotinamide I, CrystEngComm. 11 (2009) 501–509. https://doi.org/10.1039/b810822f.

[135] A.S. Pessoa, G.P.S. Aguiar, J. Vladimir Oliveira, A.J. Bortoluzzi, A. Paulino, M. Lanza, Precipitation of resveratrol-isoniazid and resveratrol-nicotinamide cocrystals by gas antisolvent, J. Supercrit. Fluids. 145 (2019) 93–102. https://doi.org/10.1016/j.supflu.2018.11.014.

[136] S.J. Nehm, B. Rodrı, Phase Solubility Diagrams of Cocrystals Are Explained by Solubility Product and Solution Complexation 2006, Growth (Lakeland). (2006).

[137] K. Ito, K. Sekiguchi, Studies on the Molecular Compounds of Organic Medicinals. II., Chem. Pharm. Bull. 14 (1966) 255–262. http://www.mendeley.com/research/geology-volcanic-history-eruptive-style-yakedake-volcano-group-central-japan/.

[138] J. Fages, H. Lochard, J.J. Letourneau, M. Sauceau, E. Rodier, Particle generation for pharmaceutical applications using supercritical fluid technology, Powder Technol. 141 (2004) 219–226. https://doi.org/10.1016/j.powtec.2004.02.007.

[139] Knez, E. Markočič, M. Leitgeb, M. Primožič, M. Knez Hrnčič, M. Škerget, Industrial applications of supercritical fluids: A review, Energy. 77 (2014) 235–243. https://doi.org/10.1016/j.energy.2014.07.044.

[140] F. Kurniawansyaha, R. Mammucaric, A. Tandyaa, N.R. Foster, Scale − Up and economic

evaluation of the atomized rapid injection solvent extraction process, J. Supercrit. Fluids. 127 (2017) 208–216. https://doi.org/https://doi.org/10.1016/j.supflu.2017.03.006.

[141] S.H. Dale, M.R.J. Elsegood, M. Hemmings, A.L. Wilkinson, The co-crystallisation of pyridine with benzenepolycarboxylic acids: The interplay of strong and weak hydrogen bonding motifs, CrystEngComm. 6 (2004) 207–214. https://doi.org/10.1039/b404563g.

[142] D.J. Good, N. Rodríguez-Hornedo, Cocrystal eutectic constants and prediction of solubility behavior, Cryst. Growth Des. 10 (2010) 1028–1032. https://doi.org/10.1021/cg901232h.

[143] L.Z. Benet, F. Broccatelli, T.I. Oprea, BDDCS applied to over 900 drugs, AAPS J. 13 (2011) 519–547. https://doi.org/10.1208/s12248-011-9290-9.

[144] WHO, World Health Organization Model List of Essential Medicines, 21st List, 2019, 2019.

[145] E.C. Van Tonder, T.S.P. Maleka, W. Liebenberg, M. Song, D.E. Wurster, M.M. De Villiers, Preparation and physicochemical properties of niclosamide anhydrate and two monohydrates, Int. J. Pharm. 269 (2004) 417–432. https://doi.org/10.1016/j.ijpharm.2003.09.035.

[146] M.R. Caira, E.C. Van Tonder, M.M. De Villiers, A.P. Lotter, Diverse Modes of Solvent Inclusion in Crystalline Pseudopolymorphs of the Anthelmintic Drug Niclosamide, J. Incl. Phenom. Mol. Recognit. Chem. 31 (1998) 1–16. https://doi.org/10.1023/A.

[147] P. Sanphui, S.S. Kumar, A. Nangia, Pharmaceutical cocrystals of niclosamide, Cryst. Growth Des. 12 (2012) 4588–4599. https://doi.org/10.1021/cg300784v.

[148] I. Sovago, A.D. Bond, Expanding the structural landscape of niclosamide: A high Z′ polymorph, two new solvates and monohydrate HA, Acta Crystallogr. Sect. C Struct. Chem. 71 (2015) 394–401. https://doi.org/10.1107/S2053229615005847.

[149] E.C. van Tonder, M.D. Mahlatji, S.F. Malan, W. Liebenberg, M.R. Caira, M. Song, M.M. de Villiers, Preparation and physicochemical characterization of 5 niclosamide solvates and 1 hemisolvate, AAPS PharmSciTech. 5 (2004) 1–10. https://doi.org/10.1208/pt050112.

[150] D. Luedeker, R. Gossmann, K. Langer, G. Brunklaus, Crystal Engineering of Pharmaceutical Co-crystals: “nMR Crystallography” of Niclosamide Co-crystals, Cryst. Growth Des. 16 (2016) 3087–3100. https://doi.org/10.1021/acs.cgd.5b01619.

[151] F. Grifasi, M.R. Chierotti, K. Gaglioti, R. Gobetto, L. Maini, D. Braga, E. Dichiarante, M. Curzi, Using salt cocrystals to improve the solubility of niclosamide, Cryst. Growth Des. 15 (2015) 1939–1948. https://doi.org/10.1021/acs.cgd.5b00106.

[152] A. Fenwick, L. Savioli, D. Engels, N.R. Bergquist, M.H. Todd, Drugs for the control of parasitic diseases: Current status and development in schistosomiasis, Trends Parasitol. 19 (2003) 509–515. https://doi.org/10.1016/j.pt.2003.09.005.

[153] J.-J. Devogelaer, M.D. Charpentier, A. Tijink, V. Dupray, G. Coquerel, K. Johnston, H. Meekes, P. Tinnemans, E. Vlieg, J.H. ter Horst, R. de Gelder, Cocrystals of Praziquantel: Discovery by Network-Based Link Prediction, Cryst. Growth Des. (2021). https://doi.org/10.1021/acs.cgd.1c00211.

[154] N. Castro, H. Jung, R. Medina, D. González-Esquivel, M. Lopez, J. Sotelo, Interaction between grapefruit juice and Praziquantel in humans, Antimicrob. Agents Chemother. 46 (2002) 1614–1616. https://doi.org/10.1128/AAC.46.5.1614.

[155] M. Cugovčan, J. Jablan, J. Lovrić, D. Cinčić, N. Galić, M. Jug, Biopharmaceutical characterization of praziquantel cocrystals and cyclodextrin complexes prepared by grinding, J. Pharm. Biomed. Anal. 137 (2017) 42–53. https://doi.org/10.1016/j.jpba.2017.01.025.

[156] D. Zanolla, B. Perissutti, N. Passerini, M.R. Chierotti, D. Hasa, D. Voinovich, L. Gigli, N. Demitri, S. Geremia, J. Keiser, P. Cerreia Vioglio, B. Albertini, A new soluble and bioactive polymorph of praziquantel, Eur. J. Pharm. Biopharm. 127 (2018) 19–28. https://doi.org/10.1016/j.ejpb.2018.01.018.

[157] J.C. Espinosa-Lara, D. Guzman-Villanueva, J.I. Arenas-García, D. Herrera-Ruiz, J. Rivera-Islas, P. Román-Bravo, H. Morales-Rojas, H. Höpfl, Cocrystals of active pharmaceutical ingredients - Praziquantel in combination with oxalic, malonic, succinic, maleic, fumaric, glutaric, adipic, and pimelic acids, Cryst. Growth Des. 13 (2013) 169–185. https://doi.org/10.1021/cg301314w.

[158] D. Zanolla, B. Perissutti, P.C. Vioglio, M.R. Chierotti, L. Gigli, N. Demitri, N. Passerini, B. Albertini, E. Franceschinis, J. Keiser, D. Voinovich, Exploring mechanochemical parameters using a DoE approach: Crystal structure solution from synchrotron XRPD and characterization of a new praziquantel polymorph, Eur. J. Pharm. Sci. 140 (2019) 105084. https://doi.org/10.1016/j.ejps.2019.105084.

[159] L.N. Andrade, D.M.L. Oliveira, M. V. Chaud, T.F.R. Alves, M. Nery, C.F. da Silva, J.K.C. Gonsalves, R.S. Nunes, C.B. Corrêa, R.G. Amaral, E. Sanchez-Lopez, E.B. Souto, P. Severino, Praziquantel-solid lipid nanoparticles produced by supercritical carbon dioxide extraction: Physicochemical characterization, release profile, and cytotoxicity, Molecules. 24 (2019). https://doi.org/10.3390/molecules24213881.

[160] C.P. Price, A.L. Grzesiak, M. Lang, A.J. Matzger, Polymorphism of Nabumetone, Cryst. Growth Des. 2 (2002) 501–503. https://doi.org/10.1021/cg0255568.

[161] C. Engineering, O.F. Nabumetone, B.Y. Cocrystallization, Crystal engineering of nabumetone by cocrystallization, J. Biomed. Pharm. Res. 3 (2014) 22–29.

[162] C.S. Su, Y.P. Chen, Measurement and correlation for the solid solubility of non-steroidal anti-inflammatory drugs (NSAIDs) in supercritical carbon dioxide, J. Supercrit. Fluids. 43 (2008) 438–446. https://doi.org/10.1016/j.supflu.2007.08.006.

[163] C.S. Su, M. Tang, Y.P. Chen, Micronization of nabumetone using the rapid expansion of supercritical solution (RESS) process, J. Supercrit. Fluids. 50 (2009) 69–76. https://doi.org/10.1016/j.supflu.2009.04.013.

[164] J. Holaň, F. Štěpánek, P. Billot, L. Ridvan, The construction, prediction and measurement of co-crystal ternary phase diagrams as a tool for solvent selection, Eur. J. Pharm. Sci. 63 (2014) 124–131. https://doi.org/10.1016/j.ejps.2014.06.017.

[165] P.J. N, A.P. D, Development of efavirenz cocrystals from stoichiometric solutions by spray drying technology, Mater. Today Proc. 3 (2016) 1742–1751. https://doi.org/10.1016/j.matpr.2016.04.069.

[166] J. Wouters, L. Quéré, Pharmaceutical Salts and Co-Crystals, Royal Society of Chemistry, 2012.

[167] S.P. Patil, S.R. Modi, A.K. Bansal, Generation of 1:1 Carbamazepine:Nicotinamide cocrystals by spray drying, Eur. J. Pharm. Sci. 62 (2014) 251–257. https://doi.org/10.1016/j.ejps.2014.06.001.

[168] A. Alhalaweh, W. Kaialy, G. Buckton, H. Gill, A. Nokhodchi, S.P. Velaga, Theophylline Cocrystals Prepared by Spray Drying: Physicochemical Properties and Aerosolization Performance, AAPS PharmSciTech. 14 (2013) 265–276. https://doi.org/10.1208/s12249-012-9883-3.

[169] L. Henriques, F. Almada, M.I. Amaro, V.P. De Sousa, L. Claudio, R. Pereira, G.S. De

Almeida, C.R. Rodrigues, A.M. Healy, L.M. Cabral, Development and Characterization of Dapsone Cocrystal Prepared by Scalable Production Methods, 19 (2018). https://doi.org/10.1208/s12249-018-1101-5.

[170] K. Cal, K. Sollohub, Spray Drying Technique. I: Hardware and Process Parameters, J. Pharm. Sci. 99 (2010) 575–586. https://doi.org/10.1002/jps.

[171] R. Vehring, Pharmaceutical particle engineering via spray drying, Pharm. Res. 25 (2008) 999–1022. https://doi.org/10.1007/s11095-007-9475-1.

[172] M.D. Abràmoff, P.J. Magalhães, S.J. Ram, Image processing with imageJ, Biophotonics Int. 11 (2004) 36–41. https://doi.org/10.1201/9781420005615.ax4.

[173] M.A. Reus, A.E.D.M. van der Heijden, J.H. ter Horst, Solubility Determination from Clear Points upon Solvent Addition, Org. Process Res. Dev. 19 (2015) 1004–1011.

[174] R.A. Halliwell, R.M. Bhardwaj, C.J. Brown, N.E.B. Briggs, J. Dunn, J. Robertson, A. Nordon, A.J. Florence, Spray Drying as a Reliable Route to Produce Metastable Carbamazepine Form IV, J. Pharm. Sci. 106 (2017) 1874–1880. https://doi.org/10.1016/j.xphs.2017.03.045.

[175] I. Gouaou, S. Shamaei, M.S. Koutchoukali, M. Bouhelassa, E. Tsotsas, A. Kharaghani, Impact of operating conditions on a single droplet and spray drying of hydroxypropylated pea starch: Process performance and final powder properties, Asia-Pacific J. Chem. Eng. (2018) 1–18. https://doi.org/10.1002/apj.2268.

[176] C. Cortés, A. Gil, Modeling the gas and particle flow inside cyclone separators, Prog. Energy Combust. Sci. 33 (2007) 409–452. https://doi.org/10.1016/j.pecs.2007.02.001.

[177] L. MacEachern, A. Kermanshahi-Pour, M. Mirmehrabi, Supercritical carbon dioxide for pharmaceutical co-crystal production, Cryst. Growth Des. 20 (2020) 6226–6244. https://doi.org/10.1021/acs.cgd.0c00571.

[178] L. Padrela, M.A. Rodrigues, J. Tiago, S.P. Velaga, H.A. Matos, E.G. De Azevedo, Insight into the Mechanisms of Cocrystallization of Pharmaceuticals in Supercritical Solvents, Cryst. Growth Des. 15 (2015) 3175–3181. https://doi.org/10.1021/acs.cgd.5b00200.

[179] M. Silva, K. Barcauskaite, D. Drapanauskaite, H. Tian, T. Bučko, J. Baltrusaitis, Relative Humidity Facilitated Urea Particle Reaction with Salicylic Acid: A Combined in Situ Spectroscopy and DFT Study, ACS Earth Sp. Chem. 4 (2020) 1018–1028. https://doi.org/10.1021/acsearthspacechem.0c00051.

[180] P. Macfhionnghaile, C.M. Crowley, P. McArdle, A. Erxleben, Spontaneous Solid-State Cocrystallization of Caffeine and Urea, Cryst. Growth Des. 20 (2020) 736–745. https://doi.org/10.1021/acs.cgd.9b01152.

[181] A. Jayasankar, D.J. Good, N. Rodríguez-Hornedo, Mechanisms by which moisture generates cocrystals, Mol. Pharm. 4 (2007) 360–372. https://doi.org/10.1021/mp0700099.

[182] E.C. van Tonder, M.D. Mahlatji, S.F. Malan, W. Liebenberg, M.R. Caira, M. Song, M.M. de Villiers, Preparation and physicochemical characterization of 5 niclosamide solvates and 1 hemisolvate, AAPS PharmSciTech. 5 (2004) 1–10. https://doi.org/10.1208/pt050112.

[183] R. V. Manek, W.M. Kolling, Influence of moisture on the crystal forms of niclosamide obtained from acetone and ethyl acetate, AAPS PharmSciTech. 5 (2004) 1–8. https://doi.org/10.1208/pt050114.

[184] L.A. MacEachern, R. Walwyn-Venugopal, A. Kermanshahi-pour, M. Mirmehrabi, Ternary Phase Diagram Development and Production of Niclosamide-Urea Co-Crystal by Spray Drying, J. Pharm. Sci. (2020) 1–11. https://doi.org/10.1016/j.xphs.2020.11.036.

[185] R. Bhomia, V. Trivedi, J.C. Mitchell, N.J. Coleman, M.J. Snowden, Effect of Pressure on the Melting Point of Pluronics in Pressurized Carbon Dioxide, Ind. Eng. Chem. Res. 53 (2014) 10820–10825. https://doi.org/10.1021/ie501344m.

[186] M.D. Moore, R.P. Cogdill, P.L.D. Wildfong, Evaluation of chemometric algorithms in quantitative X-ray powder diffraction (XRPD) of intact multi-component consolidated samples, J. Pharm. Biomed. Anal. 49 (2009) 619–626. https://doi.org/10.1016/j.jpba.2008.12.007.

[187] M. Suda, K. Takayama, M. Otsuka, An accurate quantitative analysis of polymorphic content by chemometric X-ray powder diffraction, Anal. Sci. 24 (2008) 451–457. https://doi.org/10.2116/analsci.24.451.

[188] O.J. Catchpole, S.J. Tallon, P.J. Dyer, J.S. Lan, B. Jensen, O.K. Rasmussen, J.B. Grey, Measurement and modelling of urea solubility in supercritical CO 2 and CO2 + ethanol mixtures, Fluid Phase Equilib. 237 (2005) 212–218. https://doi.org/10.1016/j.fluid.2005.09.004.

[189] T. Friščič, W. Jones, Recent advances in understanding the mechanism of cocrystal formation via grinding, Cryst. Growth Des. 9 (2009) 1621–1637.

https://doi.org/10.1021/cg800764n.

[190] Y.S. Youn, J.H. Oh, K.H. Ahn, M. Kim, J. Kim, Y.W. Lee, Dissolution rate improvement of valsartan by low temperature recrystallization in compressed CO2: Prevention of excessive agglomeration, J. Supercrit. Fluids. 59 (2011) 117–123. https://doi.org/10.1016/j.supflu.2011.07.008.

[191] O.N. Ciftci, F. Temelli, Melting point depression of solid lipids in pressurized carbon dioxide, J. Supercrit. Fluids. 92 (2014) 208–214. https://doi.org/10.1016/j.supflu.2014.05.009.

[192] E. Kiran, J.A. Sarver, J.C. Hassler, Solubility and diffusivity of CO2 and N2 in polymers and polymer swelling, glass transition, melting, and crystallization at high pressure: A critical review and perspectives on experimental methods, data, and modeling, J. Supercrit. Fluids. 185 (2022). https://doi.org/10.1016/j.supflu.2021.105378.

[193] USFDA, Guidance for Industry ANDAs: Pharmaceutical Solid Polymorphism, (2007).

[194] M. Mirmehrabi, S. Rohani, Measurement and Prediction of the Solubility of Stearic Acid Polymorphs by the UNIQUAC Equation, Can. J. Chem. Eng. 82 (2008) 335–342. https://doi.org/10.1002/cjce.5450820214.

[195] E.H. Lee, A practical guide to pharmaceutical polymorph screening & selection, Asian J. Pharm. Sci. 9 (2014) 163–175. https://doi.org/10.1016/j.ajps.2014.05.002.

[196] D. Zanolla, D. Hasa, M. Arhangelskis, G. Schneider-Rauber, M.R. Chierotti, J. Keiser, D. Voinovich, W. Jones, B. Perissutti, Mechanochemical formation of racemic praziquantel hemihydrate with improved biopharmaceutical properties, Pharmaceutics. 12 (2020) 1–22. https://doi.org/10.3390/pharmaceutics12030289.

[197] L. Padrela, M.A. Rodrigues, A. Duarte, A.M.A. Dias, M.E.M. Braga, H.C. de Sousa, Supercritical carbon dioxide-based technologies for the production of drug nanoparticles/nanocrystals – A comprehensive review, Adv. Drug Deliv. Rev. 131 (2018) 22–78. https://doi.org/10.1016/j.addr.2018.07.010.

[198] E. Badens, Y. Masmoudi, A. Mouahid, C. Crampon, Current situation and perspectives in drug formulation by using supercritical fluid technology, J. Supercrit. Fluids. 134 (2018) 274–283. https://doi.org/10.1016/j.supflu.2017.12.038.

[199] B. Long, K.M. Ryan, L. Padrela, From batch to continuous — New opportunities for supercritical CO2 technology in pharmaceutical manufacturing, Eur. J. Pharm. Sci. 137

(2019) 104971. https://doi.org/10.1016/j.ejps.2019.104971.

[200] P.A. Charpentier, M. Jia, R.A. Lucky, Study of the RESS process for producing beclomethasone-17,21-dipropionate particles suitable for pulmonary delivery, AAPS PharmSciTech. 9 (2008) 39–46. https://doi.org/10.1208/s12249-007-9004-x.

[201] M. Türk, Manufacture of submicron drug particles with enhanced dissolution behaviour by rapid expansion processes, J. Supercrit. Fluids. 47 (2009) 537–545. https://doi.org/10.1016/j.supflu.2008.09.008.

[202] R. Bettini, L. Bonassi, V. Castoro, A. Rossi, L. Zema, A. Gazzaniga, F. Giordano, Solubility and conversion of carbamazepine polymorphs in supercritical carbon dioxide, Eur. J. Pharm. Sci. 13 (2001) 281–286. https://doi.org/10.1016/S0928-0987(01)00115-4.

[203] A. Kordikowski, T. Shekunov, P. York, Polymorph control of sulfathiazole in supercritical CO2, Pharm. Res. 18 (2001) 682–688. https://doi.org/10.1023/A:1011045729706.

[204] H.H.Y. Tong, B.Y. Shekunov, P. York, A.H.L. Chow, Characterization of two polymorphs of salmeterol xinafoate crystallized from supercritical fluids, Pharm. Res. 18 (2001) 852–858. https://doi.org/10.1023/A:1011000915769.

[205] A. Bouchard, N. Jovanović, G.W. Hofland, D.J.A. Crommelin, W. Jiskoot, G.J. Witkamp, Ways of manipulating the polymorphism of glycine during supercritical fluid crystallisation, J. Supercrit. Fluids. 44 (2008) 422–432. https://doi.org/10.1016/j.supflu.2007.09.016.

[206] H. Shinozaki, T. Oguchi, S. Suzuki, K. Aoki, T. Sako, S. Morishita, Y. Tozuka, K. Moribe, K. Yamamoto, Micronization and polymorphic conversion of tolbutamide and barbital by rapid expansion of supercritical solutions, Drug Dev. Ind. Pharm. 32 (2006) 877–891. https://doi.org/10.1080/03639040500529994.

[207] M. Rossmann, A. Braeuer, A. Leipertz, E. Schluecker, Manipulating the size, the morphology and the polymorphism of acetaminophen using supercritical antisolvent (SAS) precipitation, J. Supercrit. Fluids. 82 (2013) 230–237. https://doi.org/10.1016/j.supflu.2013.07.015.

[208] M. Türk, D. Bolten, Polymorphic properties of micronized mefenamic acid, nabumetone, paracetamol and tolbutamide produced by rapid expansion of supercritical solutions (RESS), J. Supercrit. Fluids. 116 (2016) 239–250.

https://doi.org/10.1016/j.supflu.2016.06.001.

[209] A. Bouchard, N. Jovanović, G.W. Hofland, E. Mendes, D.J.A. Crommelin, W. Jiskoot, G.J. Witkamp, Selective production of polymorphs and pseudomorphs using supercritical fluid crystallization from aqueous solutions, Cryst. Growth Des. 7 (2007) 1432–1440. https://doi.org/10.1021/cg060834e.

[210] Y. Tozuka, D. Kawada, T. Oguchi, K. Yamamoto, Supercritical carbon dioxide treatment as a method for polymorph preparation of deoxycholic acid, Int. J. Pharm. 263 (2003) 45–50. https://doi.org/10.1016/S0378-5173(03)00344-2.

[211] R. Bettini, R. Menabeni, R. Tozzi, M.B. Pranzo, I. Pasquali, M.R. Chierotti, R. Gobetto, L. Pellegrino, Didanosine Polymorphism in a Supercritical Antisolvent Process, J. Pharm. Sci. 99 (2010) 1855–1870. https://doi.org/10.1002/jps.

[212] D. Zanolla, B. Perissutti, N. Passerini, S. Invernizzi, D. Voinovich, S. Bertoni, C. Melegari, G. Millotti, B. Albertini, Milling and comilling Praziquantel at cryogenic and room temperatures: Assessment of the process-induced effects on drug properties, J. Pharm. Biomed. Anal. 153 (2018) 82–89. https://doi.org/10.1016/j.jpba.2018.02.018.

[213] Y. Liu, X. Wang, J.-K. Wang, C.B. Ching, Investigation of the Phase Diagrams of Chiral Praziquantel, Chirality. 18 (2006) 259–264. https://doi.org/10.1002/chir.

[214] T. Meyer, H. Sekljic, H. Bothe, D. Schollmeyer, C. Miculka, Taste, A New Incentive to Switch to (R)-Praziquantel in Schistosomiasis Treatment, PLoS Negl Trop Dis. 3 (2009) e357.

[215] A. Cedillo-Cruz, M. Aguilar, M. Flores-Alamo, F. Palomares-Alonso, H. Jung-Cook, A straightforward and efficient synthesis of praziquantel enantiomers and their 4 ’-hydroxy derivatives, Tetrahedron Asymmetry. 25 (2014) 133–140. https://doi.org/10.1016/j.tetasy.2013.11.004.

[216] A. Immirzi, B. Perini, Prediction of density in organic crystals, Acta Crystallogr. Sect. A. 33 (1977) 216–218. https://doi.org/10.1107/S0567739477000448.

[217] A. Borrego-Sánchez, C. Viseras, C. Aguzzi, C.I. Sainz-Díaz, Molecular and crystal structure of praziquantel. Spectroscopic properties and crystal polymorphism, Eur. J. Pharm. Sci. 92 (2016) 266–275. https://doi.org/10.1016/j.ejps.2016.04.023.

[218] R.D. Oparin, D. V. Ivlev, A.M. Vorobei, A. Idrissi, M.G. Kiselev, Screening of conformational polymorphism of ibuprofen in supercritical CO2, J. Mol. Liq. 239 (2017)

49–60. https://doi.org/10.1016/j.molliq.2016.10.132.

[219] R.D. Oparin, M. V. Kurskaya, M.A. Krestyaninov, A. Idrissi, M.G. Kiselev, Correlation between the conformational crossover of carbamazepine and its polymorphic transition in supercritical CO2: On the way to polymorph control, Eur. J. Pharm. Sci. 146 (2020) 105273. https://doi.org/10.1016/j.ejps.2020.105273.

[220] T. Schädle, B. Pejcic, B. Mizaikoff, Monitoring dissolved carbon dioxide and methane in brine environments at high pressure using IR-ATR spectroscopy, Anal. Methods. 8 (2016) 756–762. https://doi.org/10.1039/c5ay02744f.

[221] E. Bobo, B. Lefez, M.C. Caumon, S. Petit, G. Coquerel, Evidence of two types of fluid inclusions in single crystals, CrystEngComm. 18 (2016) 5287–5295. https://doi.org/10.1039/c6ce00956e.

[222] N. Passerini, B. Albertini, B. Perissutti, L. Rodriguez, Evaluation of melt granulation and ultrasonic spray congealing as techniques to enhance the dissolution of praziquantel, Int. J. Pharm. 318 (2006) 92–102. https://doi.org/10.1016/j.ijpharm.2006.03.028.

[223] G.S. Gurdial, N.R. Foster, Solubility of o-Hydroxybenzoic Acid in Supercritical Carbon Dioxide, Ind. Eng. Chem. Res. 30 (1991) 575–580. https://doi.org/10.1021/ie00051a020.

[224] G. Hu, H. Chen, J. Cai, X. Deng, Micronization of Griseofulvin by RESS in supercritical CO2 with Cosolvent Acetone, Chinese J. Chem. Eng. 11 (2003) 403–407.

[225] L. MacEachern, A. Kermanshahi-pour, M. Mirmehrabi, L. Ajiboye, V. Trivedi, S. Rohani, Q. He, Cocrystal formation of niclosamide and urea in supercritical CO2 and impact of cosolvent, J. Supercrit. Fluids. 201 (2023). https://doi.org/10.1016/j.supflu.2023.106029.

[226] K.C. Müllers, M. Paisana, M.A. Wahl, Simultaneous formation and micronization of pharmaceutical cocrystals by Rapid Expansion of Supercritical Solutions (RESS), Pharm. Res. 32 (2015) 702–713. https://doi.org/10.1007/s11095-014-1498-9.

[227] D. Cioli, L. Pica-Mattoccia, Praziquantel, Parasitol. Res. 90 (2003) 3–9. https://doi.org/10.1007/s00436-002-0751-z.

[228] L. MacEachern, A. Kermanshahi-pour, M. Mirmehrabi, Transformation under pressure: Discovery of a novel crystalline form of anthelmintic drug Praziquantel using high-pressure supercritical carbon dioxide, Int. J. Pharm. 619 (2022) 121723. https://doi.org/10.1016/j.ijpharm.2022.121723.

[229] D. Salazar-Rojas, R.M. Maggio, T.S. Kaufman, Preparation and characterization of a new

solid form of praziquantel, an essential anthelmintic drug. Praziquantel racemic monohydrate, Eur. J. Pharm. Sci. 146 (2020) 105267. https://doi.org/10.1016/j.ejps.2020.105267.

[230] D. Zanolla, L. Gigli, D. Hasa, M.R. Chierotti, M. Arhangelskis, N. Demitri, W. Jones, D. Voinovich, B. Perissutti, Mechanochemical synthesis and physicochemical characterization of previously unreported praziquantel solvates with 2-pyrrolidone and acetic acid, Pharmaceutics. 13 (2021). https://doi.org/10.3390/pharmaceutics13101606.

[231] M.G.F. de Moraes, A.G. Barreto Jr., A.R. Secchi, M.B. de Souza Jr., P.L. da Cunha Lage, A.S. Myerson, Polymorphism of Praziquantel: Role of Cooling Crystallization in Access to Solid Forms and Discovery of New Polymorphs, Cryst. Growth Des. 23 (2023) 1247–1258.

[232] O. Sánchez-Guadarrama, F. Mendoza-Navarro, A. Cedillo-Cruz, H. Jung-Cook, J.I. Arenas-García, A. Delgado-Díaz, D. Herrera-Ruiz, H. Morales-Rojas, H. Höpfl, Chiral Resolution of RS-Praziquantel via Diastereomeric Co-Crystal Pair Formation with l -Malic Acid, Cryst. Growth Des. 16 (2016) 307–314. https://doi.org/10.1021/acs.cgd.5b01254.

[233] A. Tabernero, S.A.B. Vieira De Melo, R. Mammucari, E.M. Martín Del Valle, N.R. Foster, Modelling solubility of solid active principle ingredients in sc-CO2 with and without cosolvents: A comparative assessment of semiempirical models based on Chrastil's equation and its modifications, J. Supercrit. Fluids. 93 (2014) 91–102. https://doi.org/10.1016/j.supflu.2013.11.017.

[234] K.C. Pitchaiah, N. Lamba, N. Sivaraman, G. Madras, Solubility of trioctylmethylammonium chloride in supercritical carbon dioxide and the influence of co-solvents on the solubility behavior, J. Supercrit. Fluids. 138 (2018) 102–114. https://doi.org/10.1016/j.supflu.2018.04.002.

[235] D. Peng, D.B. Robinson, A New Two-Constant Equation of State, Ind. Eng. Chem. 15 (1976) 59–64. https://doi.org/10.1021/i160057a011.

[236] F. Trabelsi, K. Abaroudi, F. Recasens, Predicting the approximate solubilities of solids in dense carbon dioxide, J. Supercrit. Fluids. 14 (1999) 151–161. https://doi.org/10.1016/S0896-8446(98)00117-X.

[237] Z.Z. Cai, H.H. Liang, W.L. Chen, S.T. Lin, C.M. Hsieh, First-principles prediction of

solid solute solubility in supercritical carbon dioxide using PR+COSMOSAC EOS, Fluid Phase Equilib. 522 (2020). https://doi.org/10.1016/j.fluid.2020.112755.

[238] S. Gracin, T. Brinck, Å.C. Rasmuson, Prediction of solubility of solid organic compounds in solvents by UNIFAC, Ind. Eng. Chem. Res. 41 (2002) 5114–5124. https://doi.org/10.1021/ie011014w.

[239] N. De Zordi, I. Kikic, M. Moneghini, D. Solinas, Solubility of pharmaceutical compounds in supercritical carbon dioxide, J. Supercrit. Fluids. 66 (2012) 16–22. https://doi.org/10.1016/j.supflu.2011.09.018.

[240] Y. Zhao, W. Wang, W. Liu, J. Zhu, X. Pei, Density-based UNIFAC model for solubility prediction of solid solutes in supercritical fluids, Fluid Phase Equilib. 506 (2020). https://doi.org/10.1016/j.fluid.2019.112376.

[241] A. Baghban, J. Sasanipour, Z. Zhang, A new chemical structure-based model to estimate solid compound solubility in supercritical CO 2, J. CO2 Util. 26 (2018) 262–270. https://doi.org/10.1016/j.jcou.2018.05.009.

[242] A. Daryasafar, N. Daryasafar, M. Madani, M. Kalantari Meybodi, M. Joukar, Connectionist approaches for solubility prediction of n-alkanes in supercritical carbon dioxide, Neural Comput. Appl. 29 (2018) 295–305. https://doi.org/10.1007/s00521-016-2793-7.

[243] J. Yang, P.R. Griffiths, Prediction of the Solubility in Supercritical Fluids Based on Supercritical Fluid Chromatography Retention Times, Anal. Chem. 68 (1996) 2353–2360. https://doi.org/10.1021/ac960371r.

[244] M. Lashkarbolooki, B. Vaferi, M.R. Rahimpour, Comparison the capability of artificial neural network (ANN) and EOS for prediction of solid solubilities in supercritical carbon dioxide, Fluid Phase Equilib. 308 (2011) 35–43. https://doi.org/10.1016/j.fluid.2011.06.002.

[245] S. Guha, G. Madras, Modeling of ternary solubilities of organics in supercritical carbon dioxide, Fluid Phase Equilib. 187–188 (2001) 255–264. https://doi.org/10.1016/S0378-3812(01)00540-4.

[246] Y. Zhao, Y.H. Sun, Z.Y. Li, C. Xie, Y. Bao, Z.J. Chen, J.B. Gong, Q.X. Yin, W. Chen, C. Zhang, Solubility measurements and prediction of coenzyme Q10 solubility in different solvent systems, J. Solution Chem. 42 (2013) 764–771. https://doi.org/10.1007/s10953-

013-9998-5.

[247] R. Dohrn, J.M.S. Fonseca, S. Peper, Experimental methods for phase equilibria at high pressures, Annu. Rev. Chem. Biomol. Eng. 3 (2012) 343–367. https://doi.org/10.1146/annurev-chembioeng-062011-081008.

[248] G. Sherman, S. Shenoy, R.A. Weiss, C. Erkey, A static method coupled with gravimetric analysis for the determination of solubilities of solids in supercritical carbon dioxide, Ind. Eng. Chem. Res. 39 (2000) 846–848. https://doi.org/10.1021/ie9906924.

[249] M. Muntó, N. Ventosa, S. Sala, J. Veciana, Solubility behaviors of ibuprofen and naproxen drugs in liquid "CO2-organic solvent" mixtures, J. Supercrit. Fluids. 47 (2008) 147–153. https://doi.org/10.1016/j.supflu.2008.07.013.

[250] A. Galia, A. Argentino, O. Scialdone, G. Filardo, A new simple static method for the determination of solubilities of condensed compounds in supercritical fluids, J. Supercrit. Fluids. 24 (2001) 7–17. https://doi.org/10.1016/S0896-8446(02)00009-8.

[251] E. Reverchon, G. Donsi, D. Gorgoglione, Salicylic acid solubilization in supercritical CO2 and its micronization by RESS, J. Supercrit. Fluids. 6 (1993) 241–248. https://doi.org/10.1016/0896-8446(93)90034-U.

[252] A. Stassi, R. Bettini, A. Gazzaniga, F. Giordano, A. Schiraldi, Assessment of solubility of ketoprofen and vanillic acid in supercritical CO2 under dynamic conditions, J. Chem. Eng. Data. 45 (2000) 161–165. https://doi.org/10.1021/je990114u.

[253] M. McHugh, M.E. Paulaitls, Solid Solubilities Of Naphthalene And Biphenyl In Supercritical Carbon Dioxide, J. Chem. Eng. Data. 25 (1980) 326–329. https://doi.org/10.1021/je60087a018.

[254] S.. Chung, K.. Shing, Multiphase behavior of binary and ternary systems of heavy aromatic hydrocarbons with supercritical carbon dioxide, Fluid Phase Equilib. 81 (1992).

APPENDIX A: COPYRIGHT AGREEMENTS

Ternary Phase Diagram Development and Production of Niclosamide-Urea Co-Crystal by Spray Drying

Author:
Lauren A. MacEachern,Rishi Walwyn-Venugopal,Azadeh Kermanshahi-pour,Mahmoud Mirmehrabi

Publication: Journal of Pharmaceutical Sciences

Publisher: Elsevier

Date: May 2021

Cocrystal formation of niclosamide and urea in supercritical CO2 and impact of cosolvent

Author:
L. MacEachern,A. Kermanshahi-pour,Mahmoud Mirmehrabi,L. Ajiboye,V. Trivedi,S. Rohani,Q. He

Publication: The Journal of Supercritical Fluids

Publisher: Elsevier

Date: October 2023

Transformation under pressure: Discovery of a novel crystalline form of anthelmintic drug Praziquantel using high-pressure supercritical carbon dioxide

Author: Lauren MacEachern,Azadeh Kermanshahi-pour,Mahmoud Mirmehrabi

Publication: International Journal of Pharmaceutics

Publisher: Elsevier

Date: 10 May 2022

APPENDIX B: COCRYSTAL SCREENING DATA

NICLOSAMIDE

NCS co-crystals are reported in the literature with caffeine, urea, 4-aminobenzoic acid, nicotinamide, imidazole, and isonicotinamide.[147,150] In this study, a cocrystal was not observed with 4-aminobenzoic acid, instead a mixture of NCS and coformer was obtained with both solvents. The cocrystals obtained in this work with caffeine, urea, nicotinamide, imidazole and isonicotinamide were in agreement with powder patterns previously reported.[147,150] Nicotinic acid appeared to give a cocrystal as well, but there was not literature data available for confirmation.

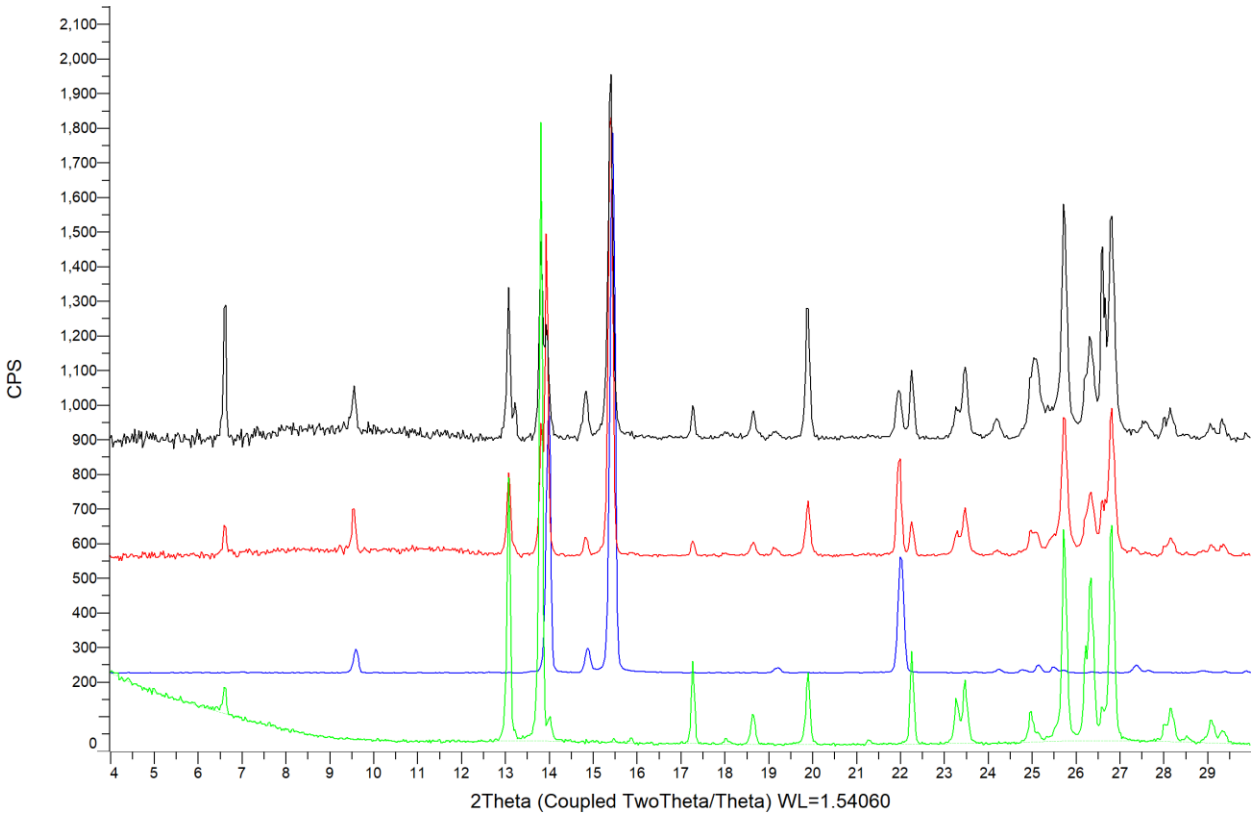

Figure A.1- XRPD result from NCS co-evaporation with 4-aminobenzoic acid in acetone (red) and EtOH (black).
NCS baseline and coformer shown in green and blue, respectively.

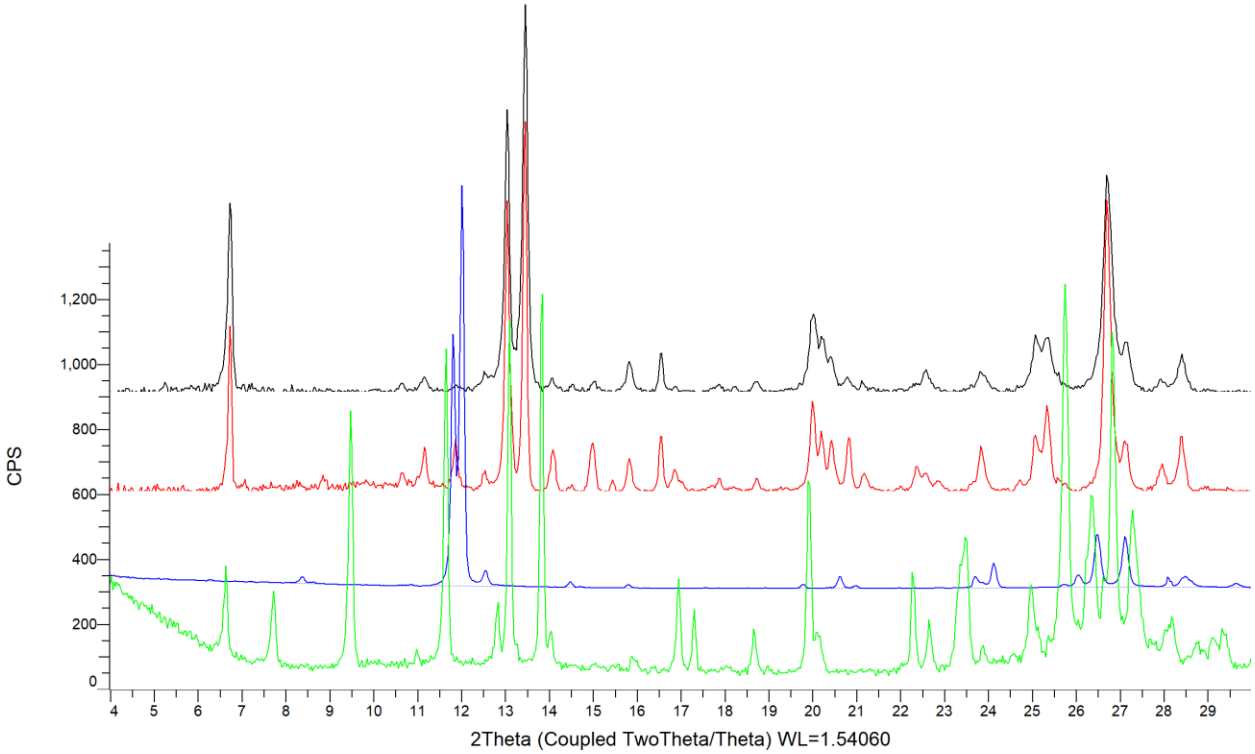

Figure A.2- XRPD result from NCS co-evaporation with caffeine in acetone (red) and EtOH (black).
NCS baseline and coformer shown in green and blue, respectively.

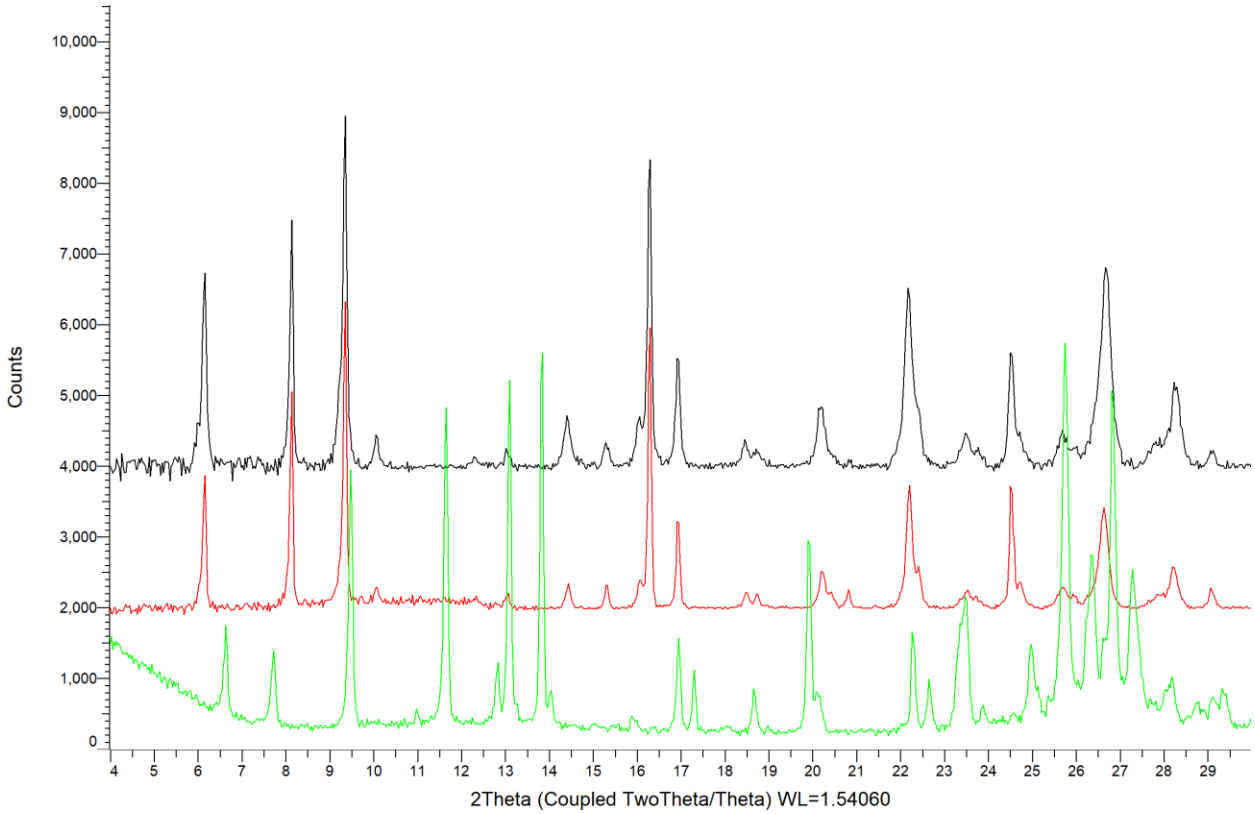

Figure A.3- XRPD result from NCS co-evaporation with imidazole in acetone (red) and EtOH (black).
NCS baseline shown in green.

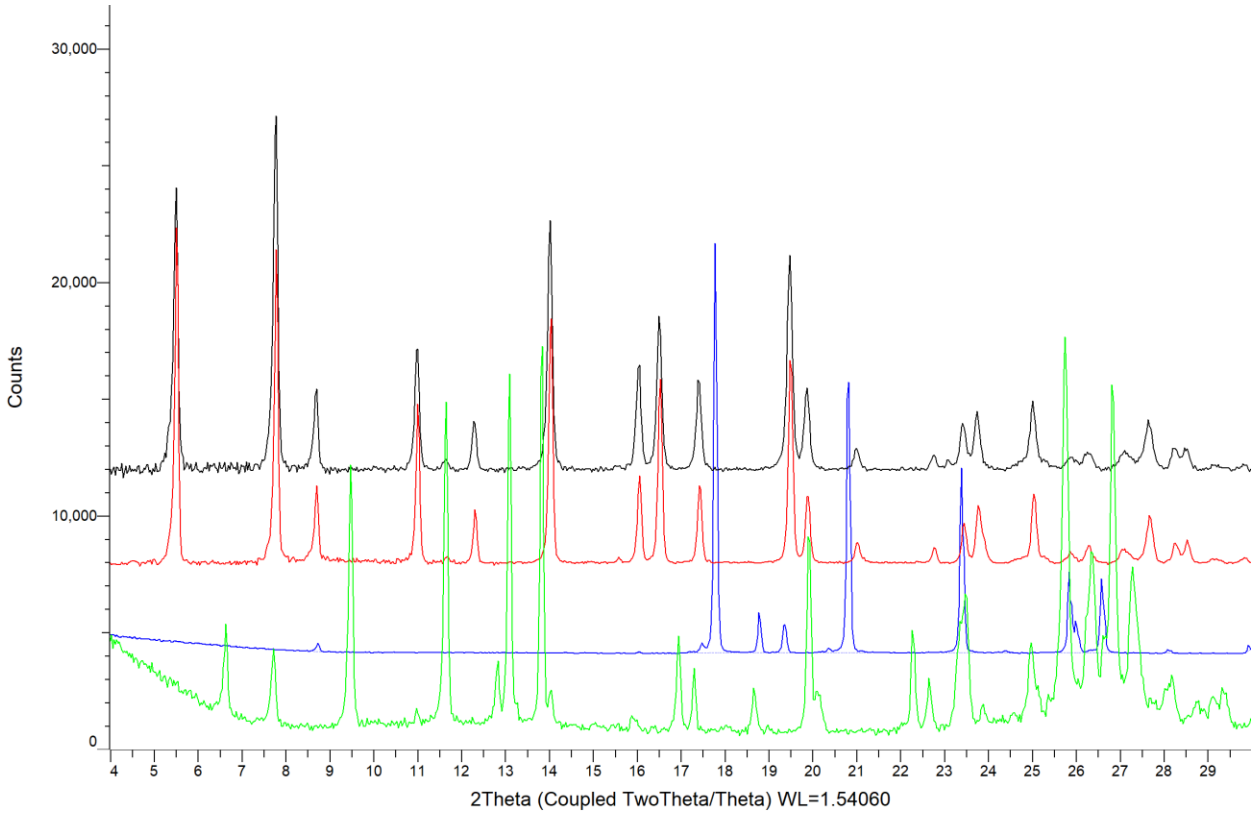

Figure A.4- XRPD result from NCS co-evaporation with isonicotinamide in acetone (red) and EtOH (black).
NCS baseline and coformer shown in green and blue, respectively.

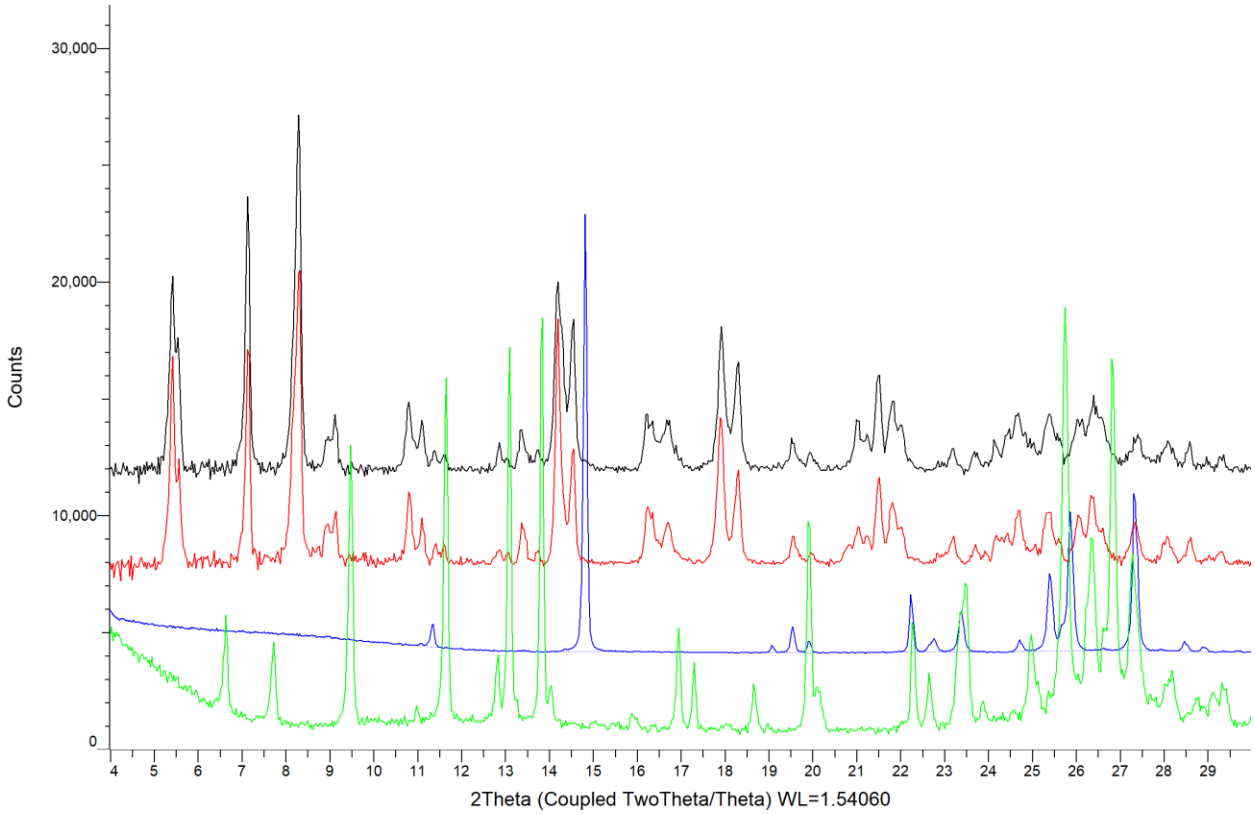

Figure A.5- XRPD result from NCS co-evaporation with nicotinamide in acetone (red) and EtOH (black).
NCS baseline and coformer shown in green and blue, respectively.

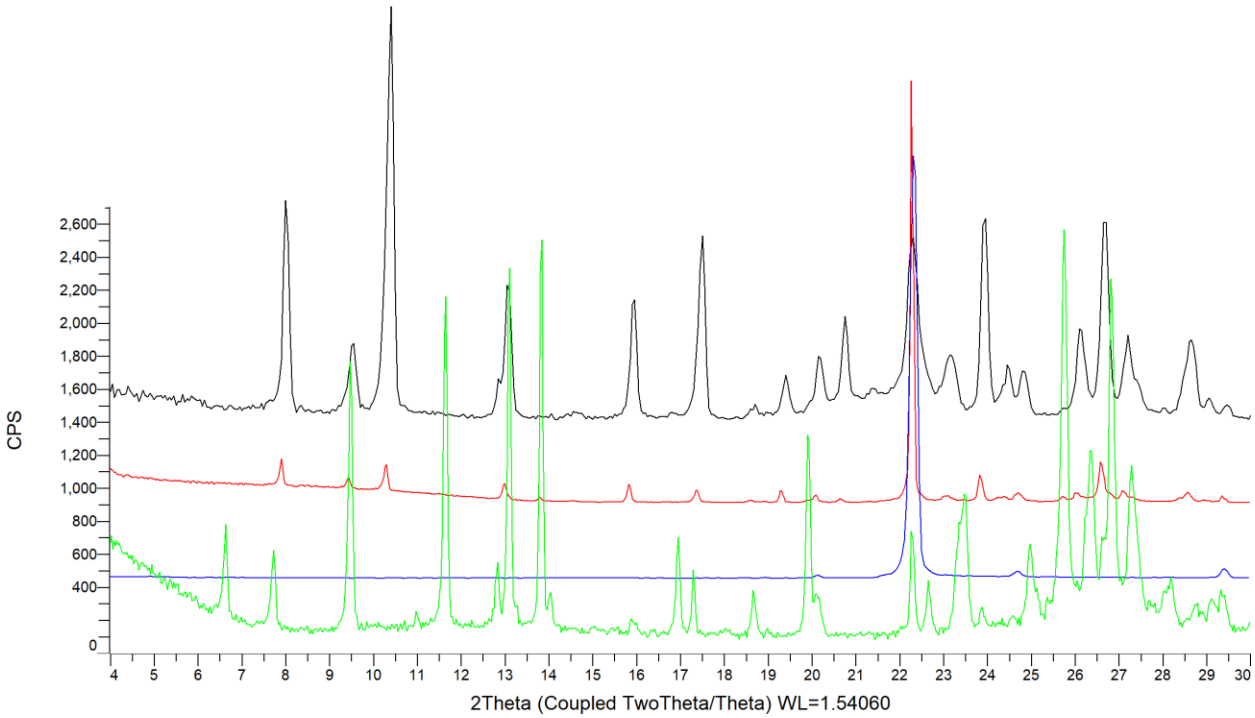

Figure A.6- XRPD result from NCS co-evaporation with urea in acetone (red) and EtOH (black). NCS baseline and coformer shown in green and blue, respectively.

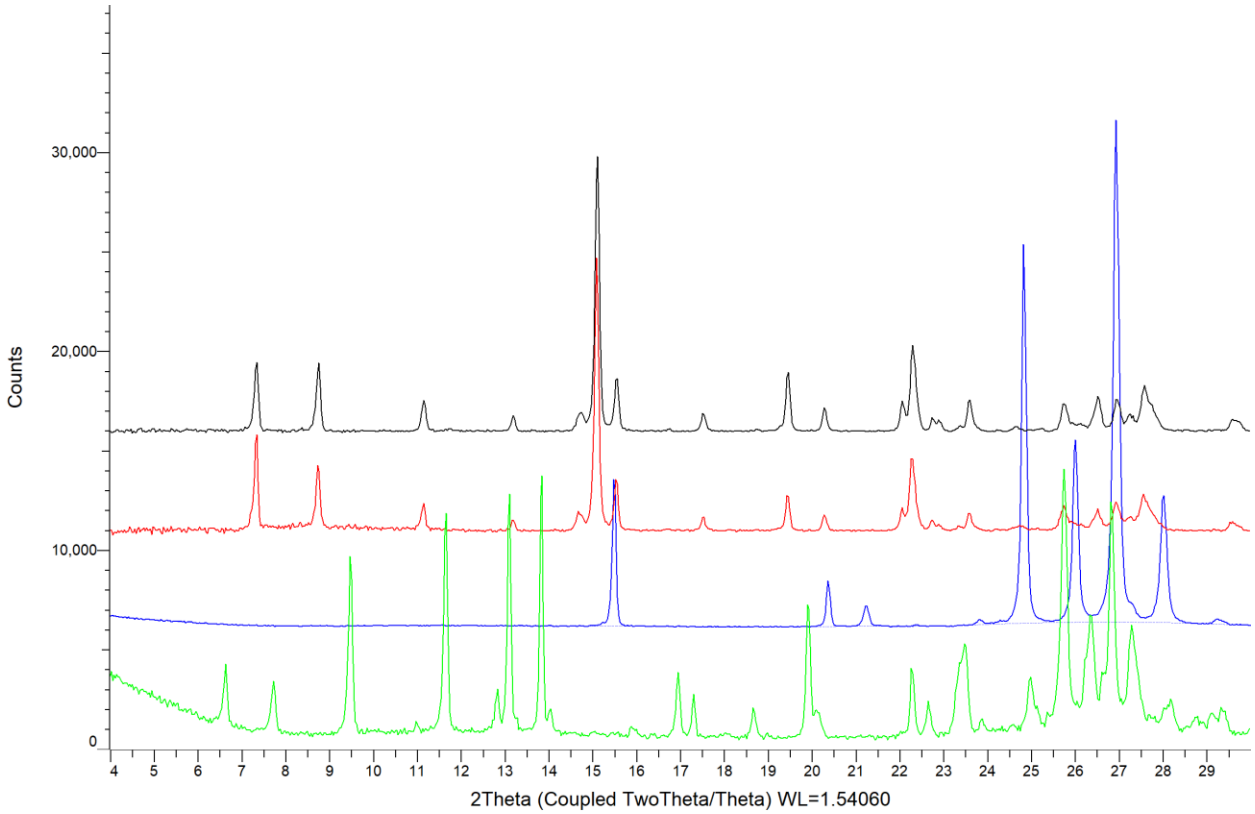

Figure A.7- XRPD result from NCS co-evaporation with nicotinic acid in acetone (red) and EtOH (black).
NCS baseline and coformer shown in green and blue, respectively.

Nabumetone

Co-crystals were not observed by XRPD from the co-evaporation experiments in acetone or EtOH using approximately 1.1 eq. of co-former. The XRPD results all show characteristic peaks only of NBM and co-former, indicating only physical mixtures were prepared. Therefore, no further characterization was carried out on the collected solids.

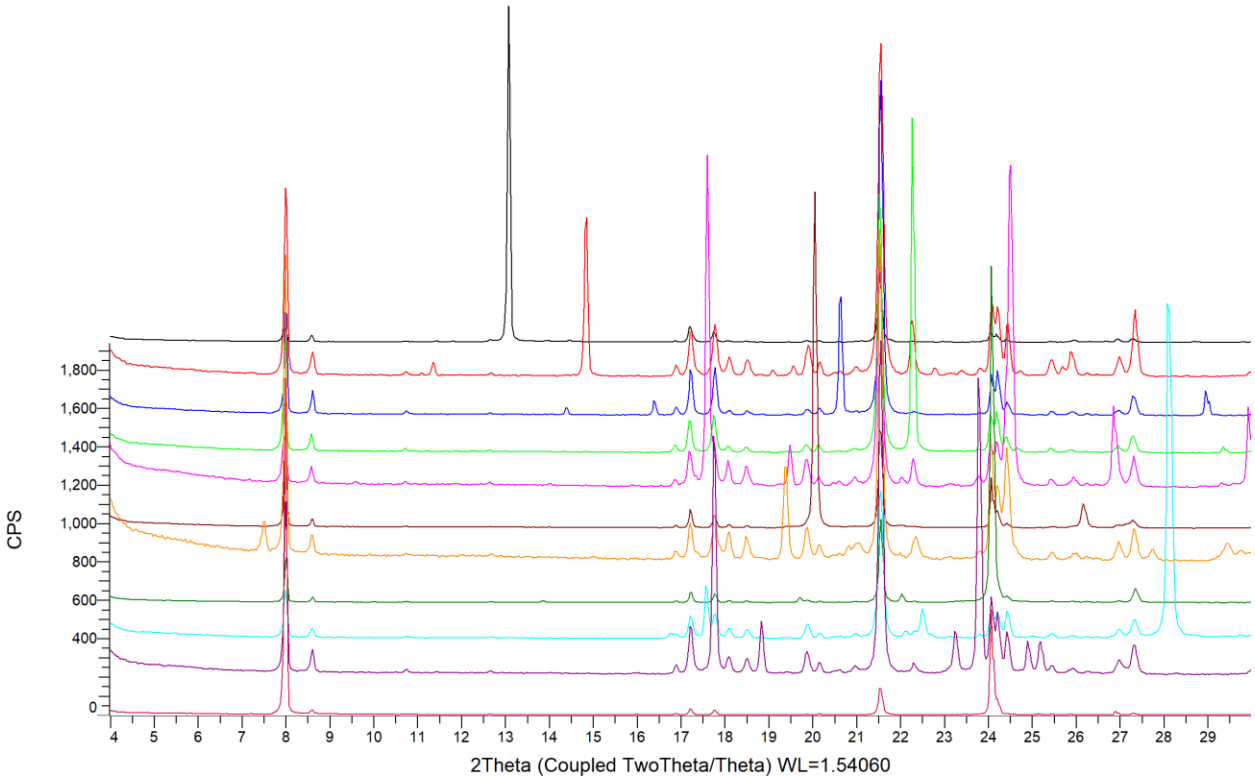

Figure A.8- XRPD result from NBM co-evaporation in acetone.
From bottom: NBM baseline, co-evaporation with: malonic acid, maleic acid, glutaric acid, malic acid, succinic acid, 4-hydrozybenzoic acid, urea, L-alanine, nicotinamide, vanillin.

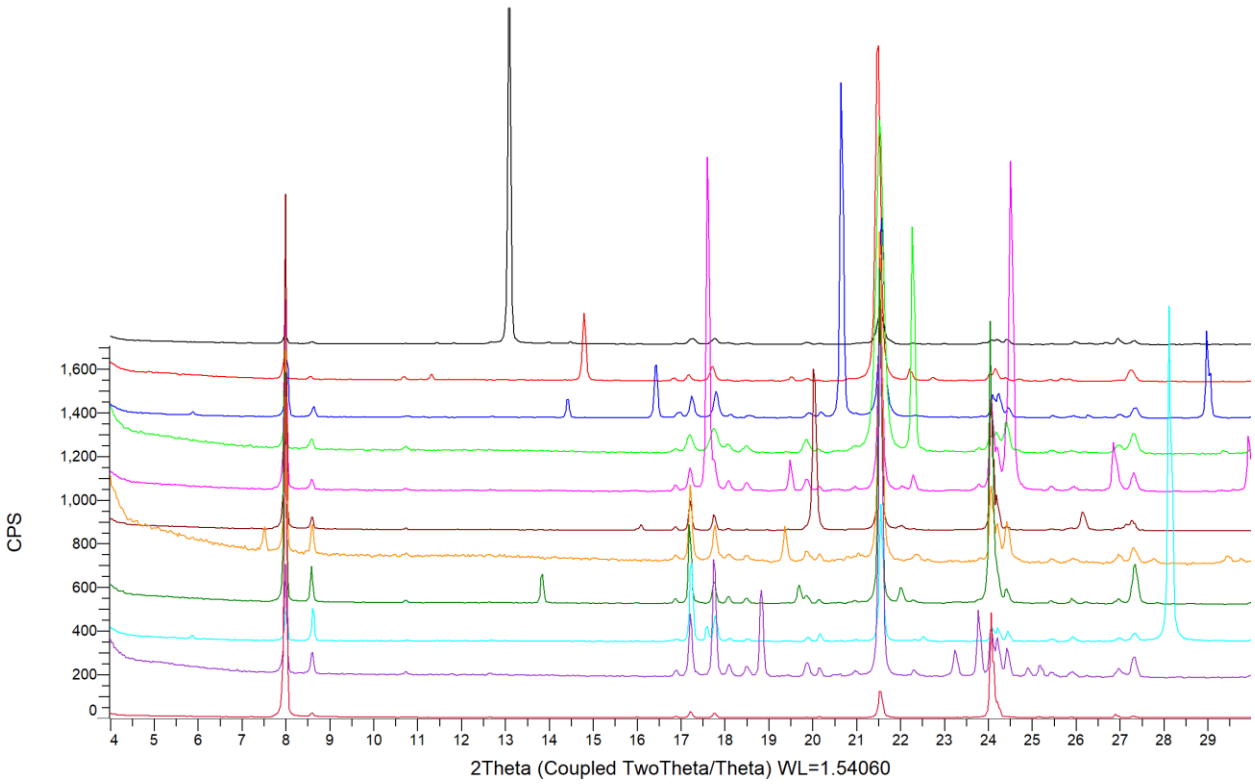

Figure A.9- XRPD result from NBM co-evaporation in EtOH.
From bottom: NBM baseline, NBM baseline, co-evaporation with: malonic acid, maleic acid, glutaric acid, malic acid, succinic acid, 4-hydrozybenzoic acid, urea, L-alanine, nicotinamide, vanillin.

PRAZIQUANTEL

The co-crystal recovered from co-evaporation with malonic acid (CC-MLA-1) showed the same crystalline pattern from both acetone and EtOH experiments (Figure A.10). A malonic acid co-crystal with 1:1 stoichiometry was prepared by Espinosa-Lara *et al.* through LAG and co-evaporation.[157] The co-crystal prepared by LAG and the simulated power pattern from single crystal (grown by co-evaporation) were the same, and agree with the XRPD of CC-MLA-1 in this study. DSC of CC-MLA-1 from EtOH showed a melting point of 145.79 °C (Figure A.11). DSC of CC-MLA-1 from acetone showed a similar melting point at 146.71 °C and a small endotherm at 116.97 °C with enthalpy of 4.5 J/g (Figure A.12). The origin of the second, smaller endotherm is unknown. However, based on XRPD the two co-crystals should be the same polymorph. DSC analysis was not part of the previous work, therefore there is not reference data for comparison.[157]

The co-crystal recovered from co-evaporation with glutaric acid (CC-GA-1) also showed the same crystalline pattern from both solvents. However, the solid isolated from co-evaporation in acetone exhibited lower crystallinity as indicated by the peak broadening in the diffractograms (Figure A.13). Espinosa-Lara *et al.* generated a 1:1 glutaric acid co-crystal through LAG and confirmed the stoichiometry through single crystal analysis.[157] CC-GA-1 in this study had the same XRPD pattern as the previously observed co-crystal. DSC of CC-GA-1 isolated from EtOH showed a small endotherm at 89.68 °C (1.5 J/g) and a melting endotherm at 124.95 °C (Figure A.14). The solid isolated from acetone showed similar DSC, but with slight depression of the melting point (121.98 °C, Figure A.15).

Only one co-crystal was observed from the co-evaporation experiment with L-malic acid in EtOH (CC-MA-1) as shown in Figure A.16, whereas the co-evaporation experiment in acetone yielded a peach-coloured gel. A DL-malic acid co-crystal was previously prepared by Cugovčan *et al.* using LAG and the powder pattern agreed with the solid isolated in this study.[155] It should be noted that the DSC of CC-MA-1 in this study differs from the co-crystal prepared by LAG in a previous paper.[155] The DSC of CC-MA-1 in this study shows two distinct endotherms with peaks at 117.16 °C and 232.24 °C (Figure A.17). The second endotherm is quite broad and could be related to decomposition of the solid or one of its components. The DSC from the previous paper does not show two separated thermal events, possibly due to

differences is sample preparation or crystallinity of the isolated co-crystal.

Co-evaporation with succinic acid gave two unique XRPD patterns. The solid isolated from acetone co-evaporation (CC-SA-1) was lower crystallinity compared to the solid isolated from EtOH (CC-SA-2) and the XRPD are shown in Figure A.18. Although CC-SA-1 and CC-SA-2 shared some common peaks in their diffraction patterns, there were notable differences including peaks at 8.8, 11.5, 13.09, 14.57 and numerous peaks above 20 deg. 2θ. In addition, DSC analysis of the two solids showed a difference in the melting points. CC-SA-1 had a melting peak at 138.79 °C and CC-SA-2 had a melting 142.16 °C as shown in Figure A.19 and Figure A.20. Two polymorphs of a succinic acid co-crystal have been reported in literature by Espinosa-Lara *et al.* and the XRPD patterns agree with the solid forms observed in this work.[157] The α form (CC-SA-2 in this work) was previously prepared using LAG in acetone and ACN. The β form (CC-SA-1 in this work) was previously prepared by evaporative crystallization and reactive crystallization in acetone.

Co-evaporation with 4-HBA also resulted in two solid forms. The solid isolated from co-evaporation in acetone (CC-HBA-1) appears to be a pure solid phase. A recent work by Devogelaer *et al.* was able to predict the formation of a PZQ co-crystal with 4-HBA using a network-based link prediction and they also prepared the 4-HBA co-crystal by LAG and co-evaporation.[153] The predicted co-crystal agrees with CC-HBA-1 in this work and a 1:1 stoichiometry was previously confirmed through single crystal analysis.[153] The solid from EtOH (CC-HBA-1+2) appears to be a mixture of CC-HBA-1 and a second solid phase, denoted as CC-HBA-2. The XRPD of both are shown in Figure A.21. The possible mixture of forms is corroborated by XRPD analysis because all peaks of CC-HBA-1 are present in the diffractogram of CC-HBA-1+2, but additional peaks are observed such as the peaks at 6.4, 8.7, 13.8, 15.8, 24.1 deg. 2θ. DSC analysis of the sample isolated from EtOH also shows evidence of a mixture by the presence of two endothermic peaks at 145.25 and 150.86 °C (Figure A.23). The DSC of CC-HBA-1 shows only a single melting endotherm with peak at 150.00 °C (Figure A.22). Therefore, it can be deduced that the melting point of CC-HBA-2 is 145.25 °C. The possible polymorph, CC-HBA-2, was not observed in the screening conducted by Devogelaer *et al.*[153]

A co-crystal was observed with vanillin from the co-evaporation experiment in EtOH (CC-VN-1), while the co-evaporation in acetone yielded a yellow gel. XRPD of the co-crystal is shown in

Figure A.24. DSC of CC-VN-1 showed that the vanillin co-crystal had a small endotherm at 71.54 °C (1.23 J/g) and a melt at 93.47 °C (Figure A.25). The melt of CC-VN-1 was the lowest melting point observed from the limited screening. There are no previous reports of a PZQ vanillin co-crystal to the best of our knowledge.

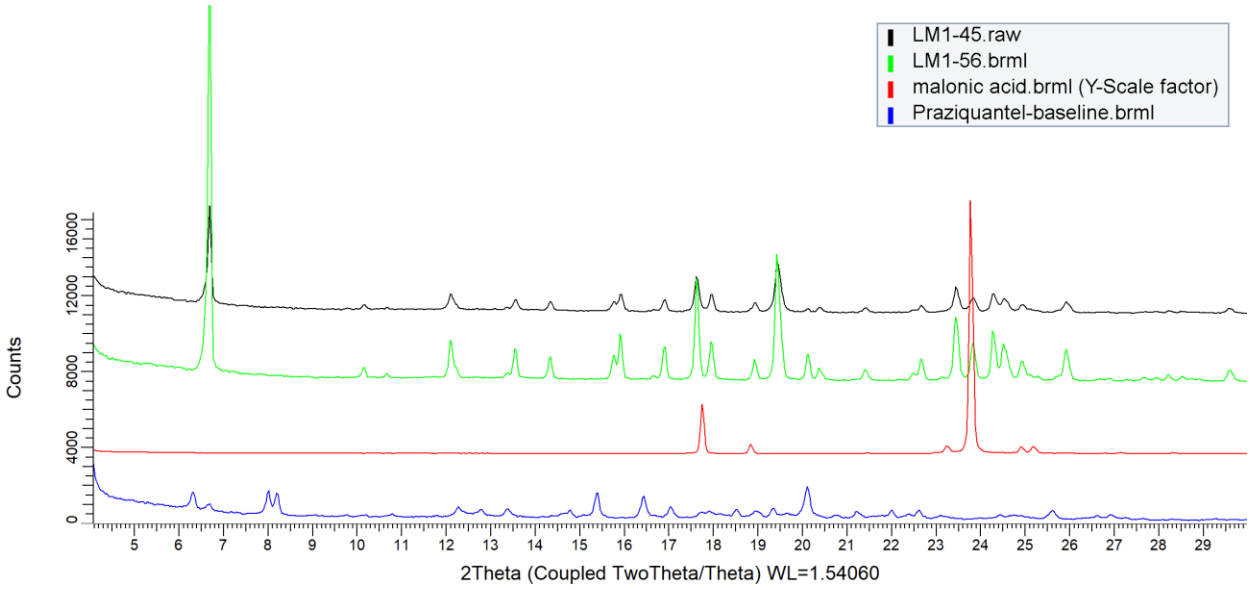

Figure A.10- XRPD result from PZQ co-evaporation with malonic acid in acetone (black) and EtOH (green).

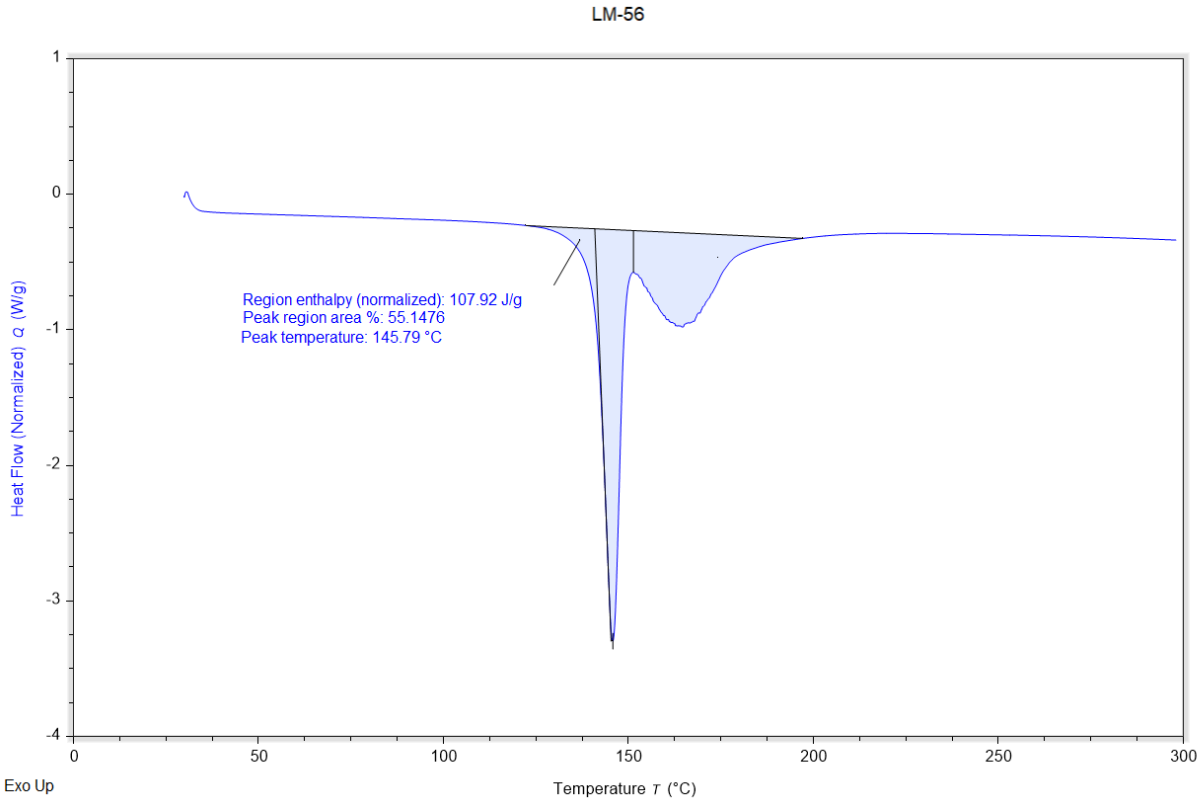

Figure A.11- DSC thermogram of solid from PZQ-malonic acid in EtOH.

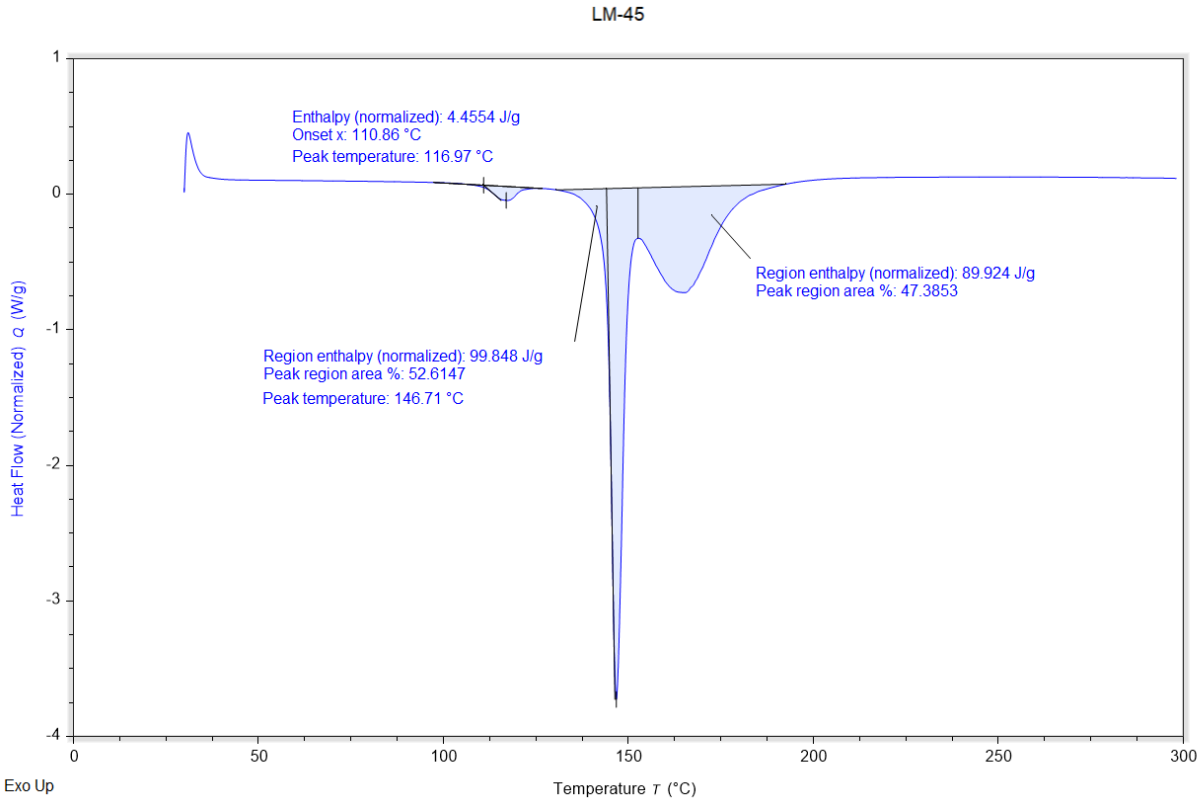

Figure A.12- DSC thermogram of solid from PZQ-malonic acid in acetone.

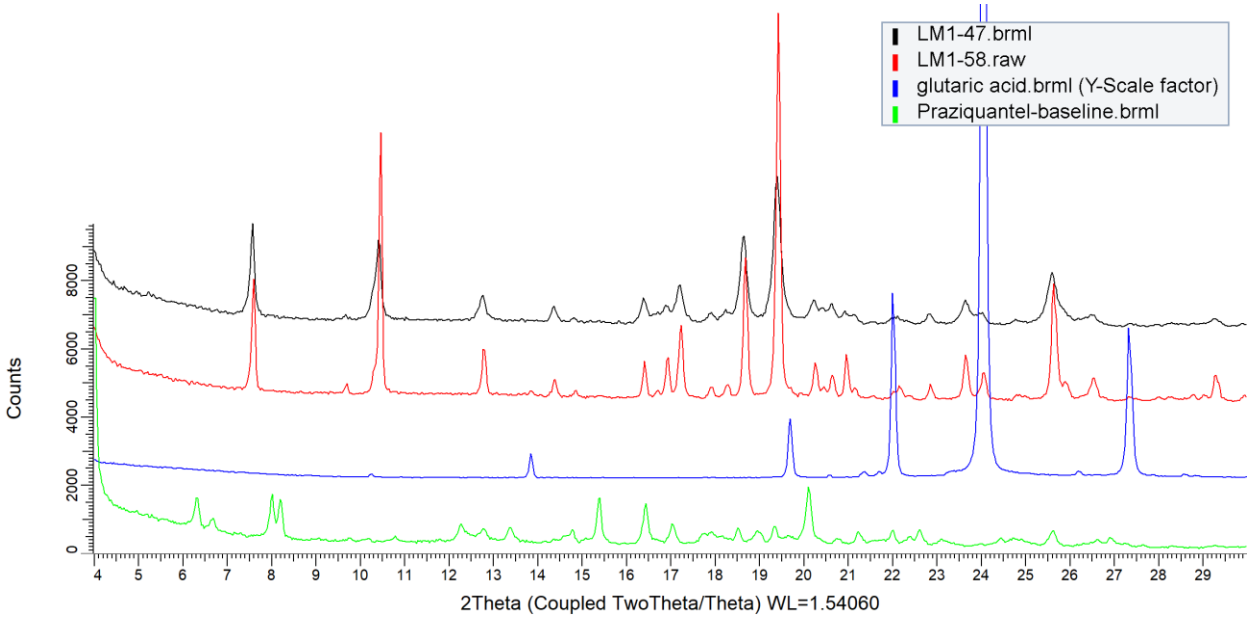

Figure A.13- XRPD result from PZQ co-evaporation with glutaric acid in acetone (black) and EtOH (red).

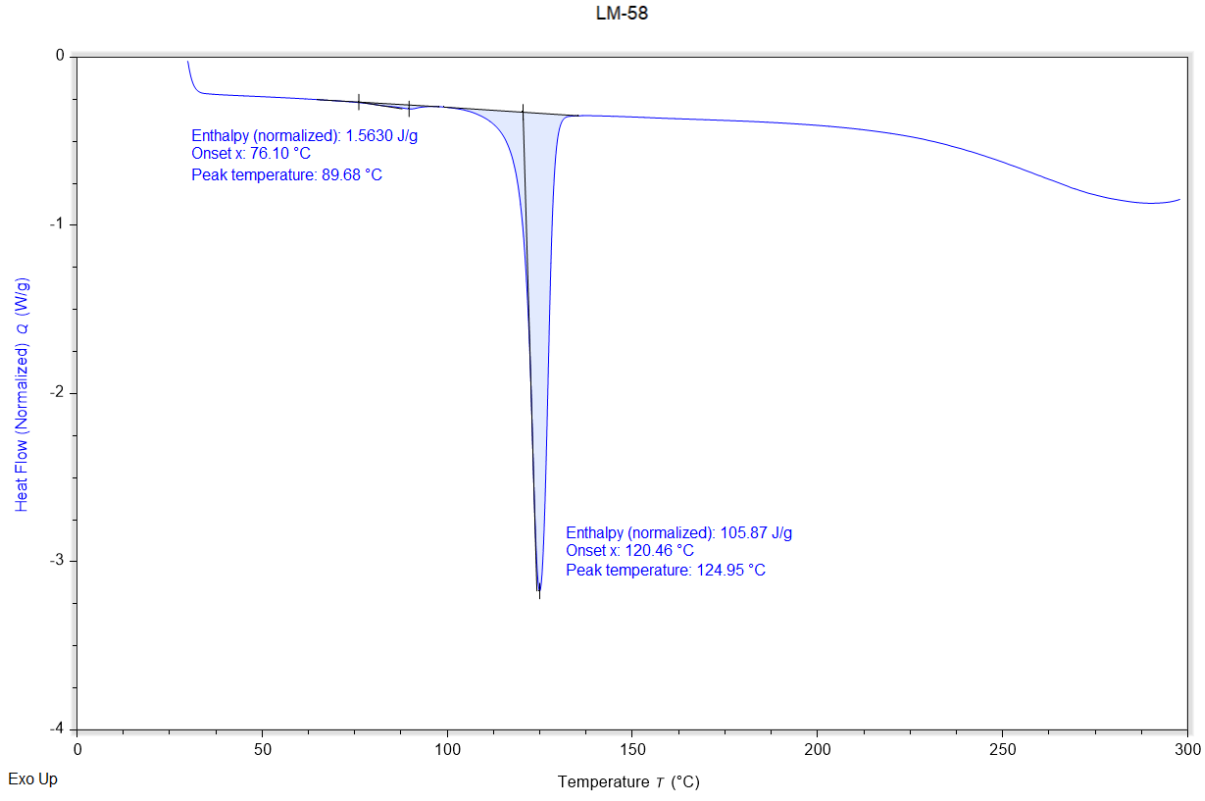

Figure A.14- DSC thermogram of solid from PZQ-glutaric acid in EtOH.

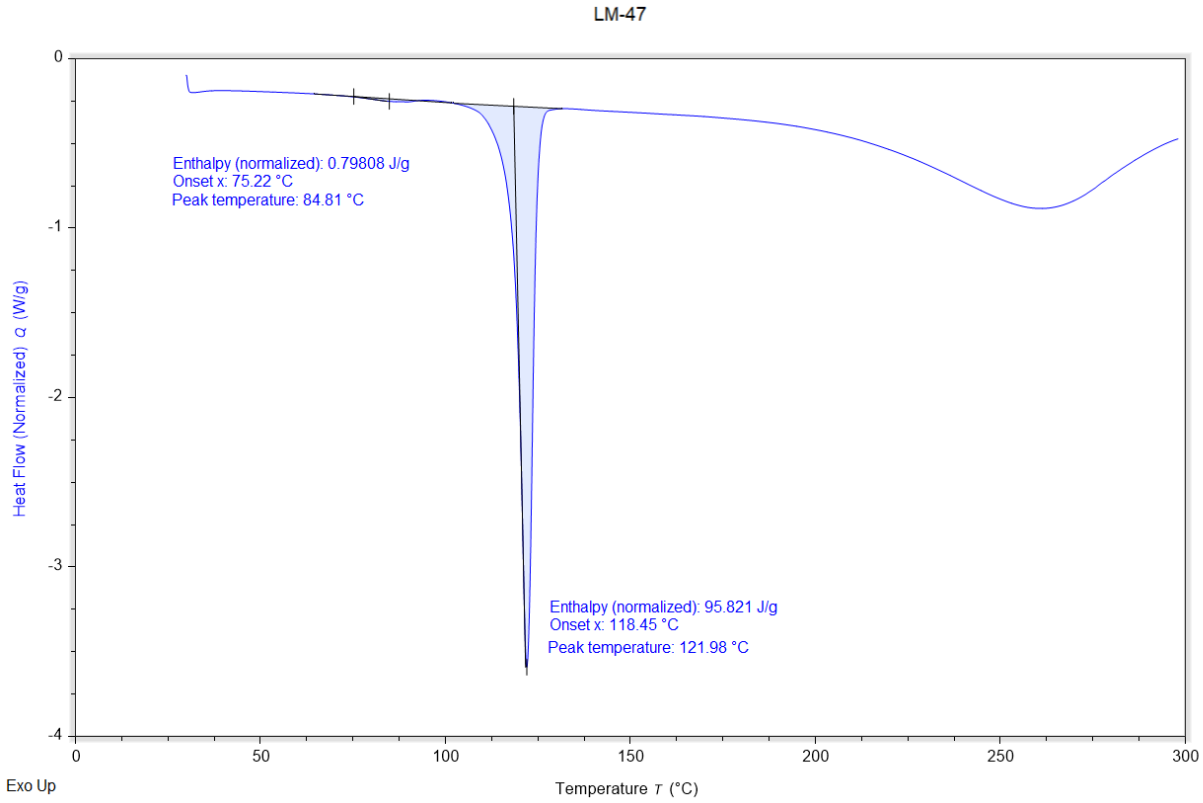

Figure A.15- DSC thermogram of solid from PZQ-glutaric acid in acetone.

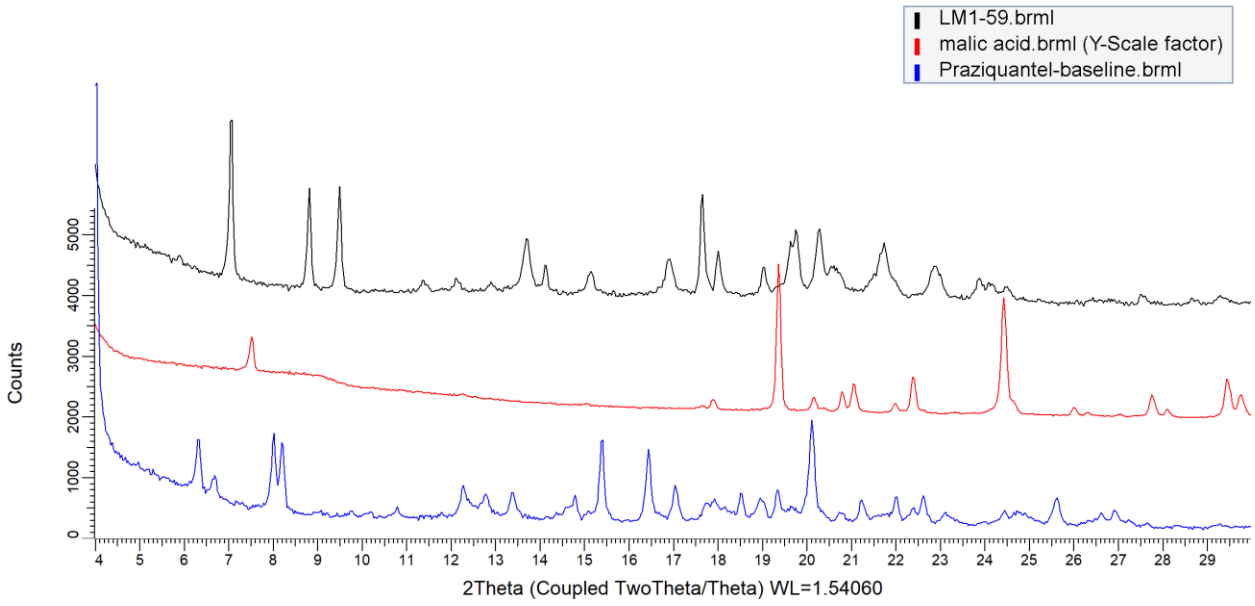

Figure A.16 - XRPD result from PZQ co-evaporation with malic acid in EtOH.

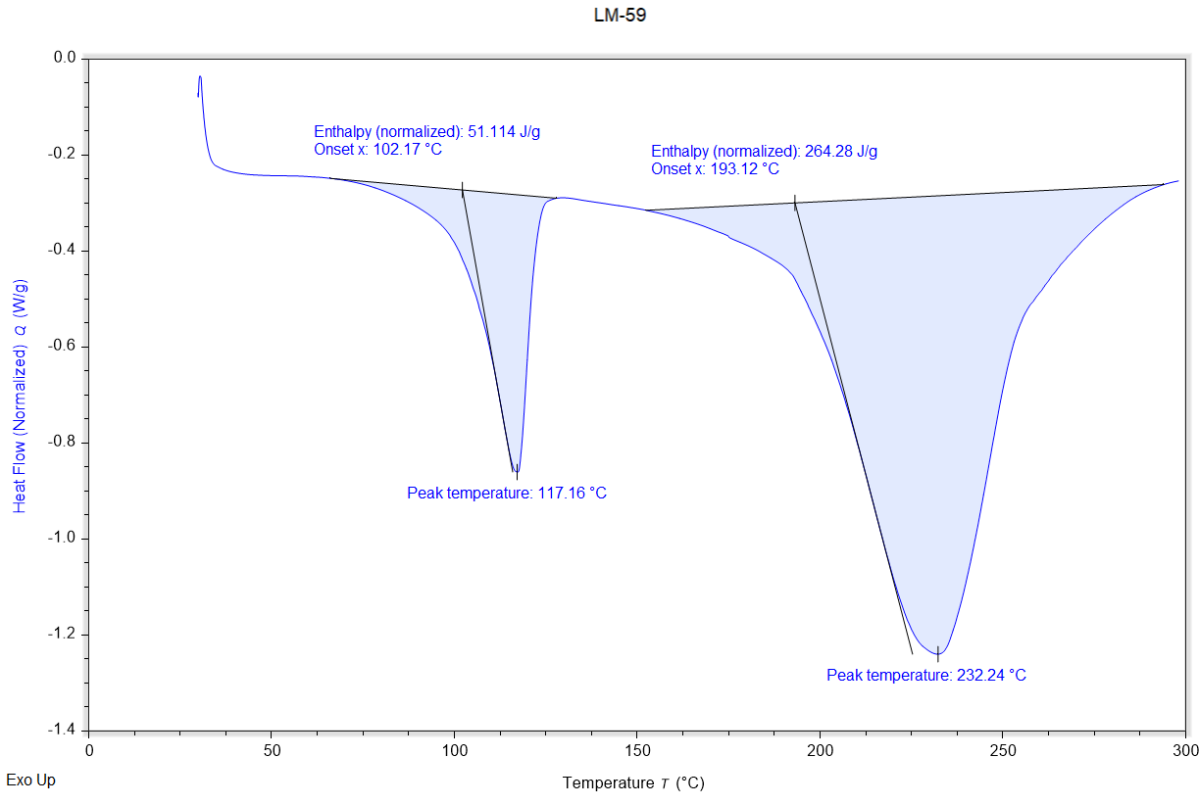

Figure A.17- DSC thermogram of solid from PZQ-malic acid in EtOH.

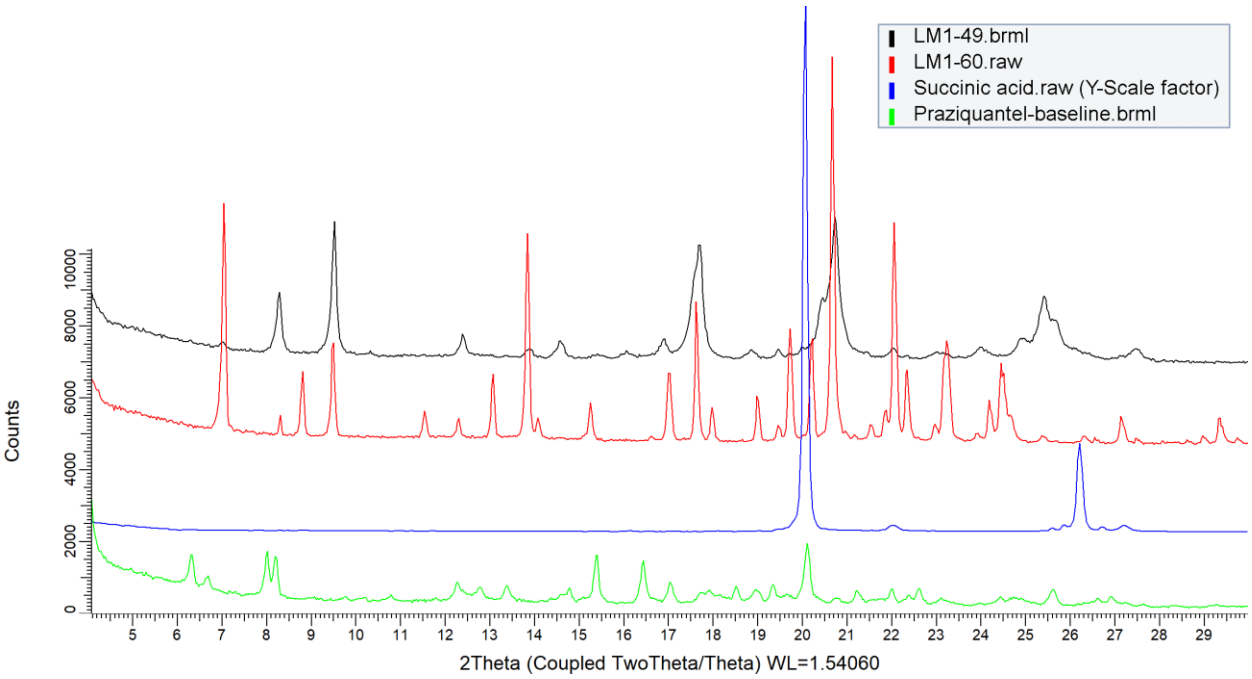

Figure A.18- XRPD result from PZQ co-evaporation with succinic acid in acetone (black) and EtOH (red).

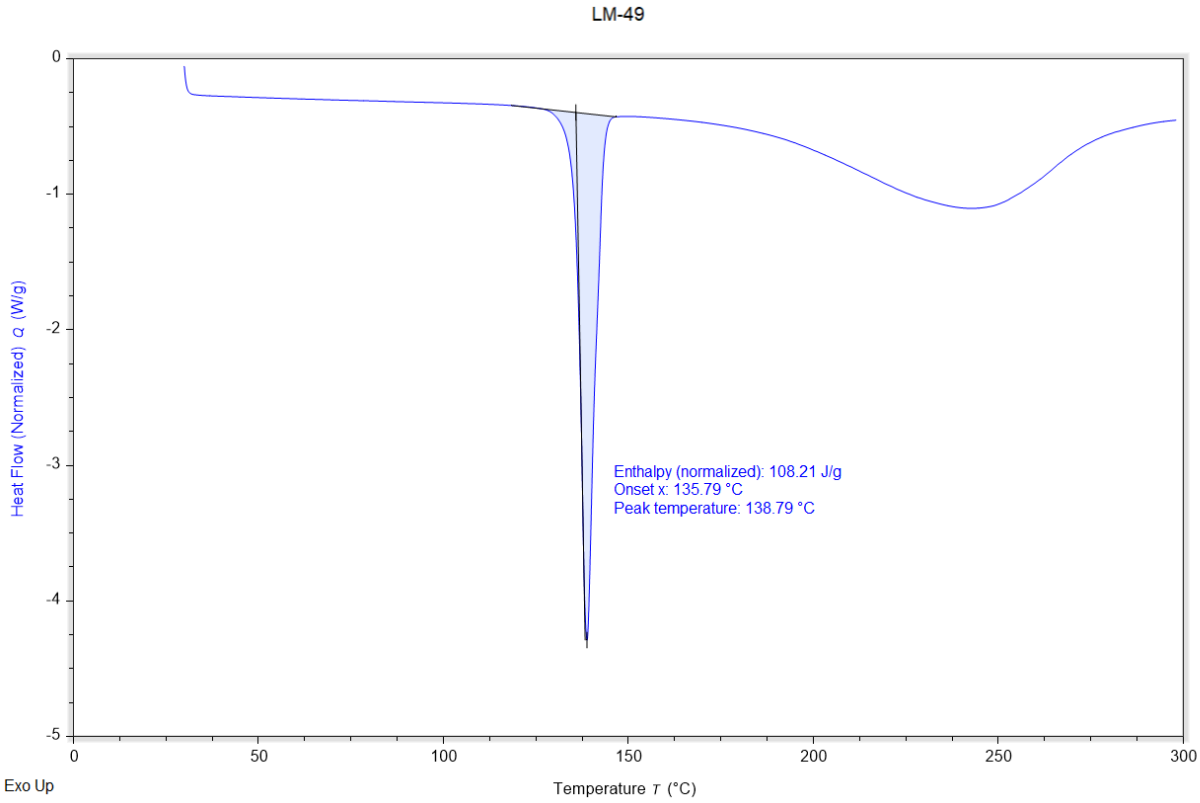

Figure A.19- DSC thermogram of solid from PZQ-succinic acid in acetone.

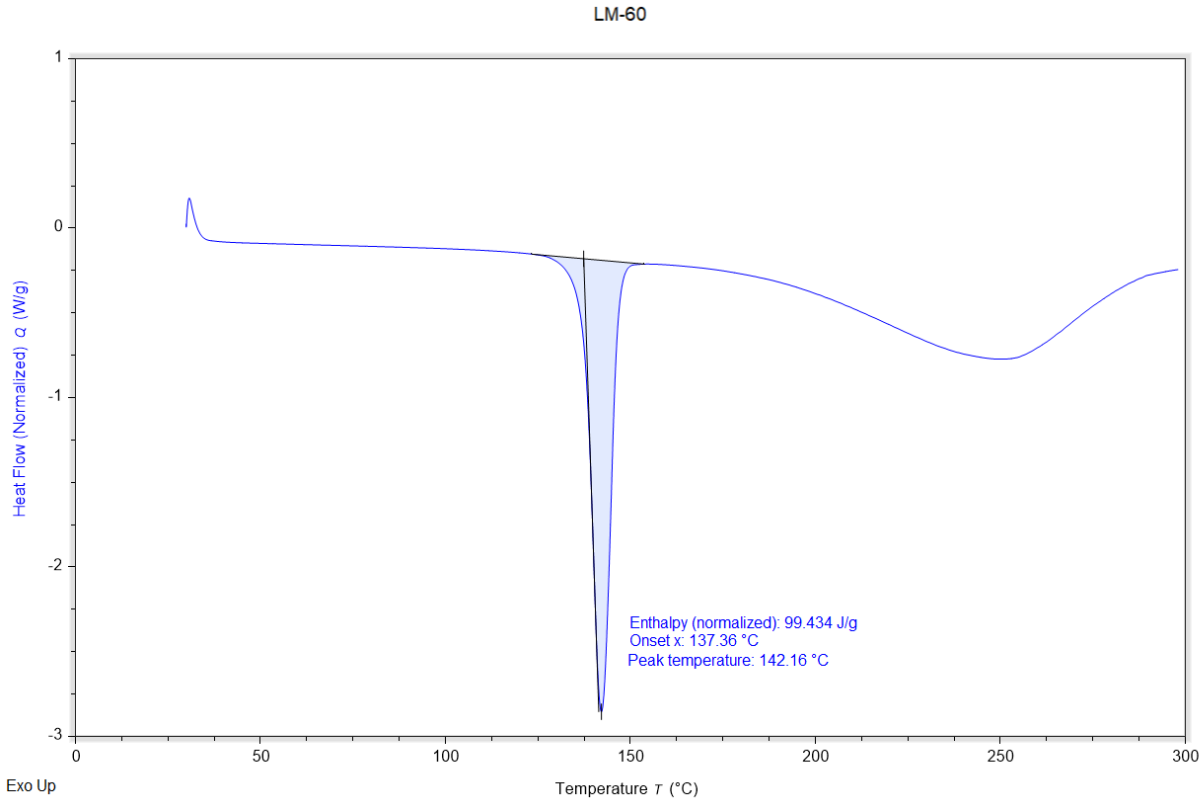

Figure A.20- DSC thermogram of solid from PZQ-succinic acid in EtOH.

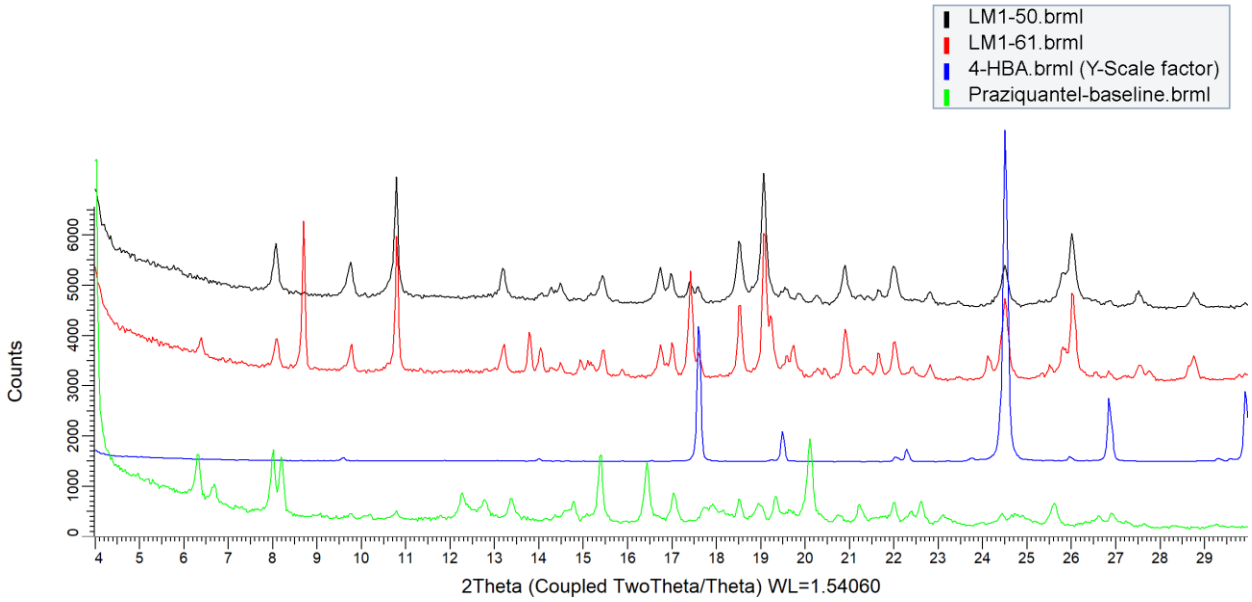

Figure A.21- XRPD result from PZQ co-evaporation with 4-HBA in acetone (black) and EtOH (red).

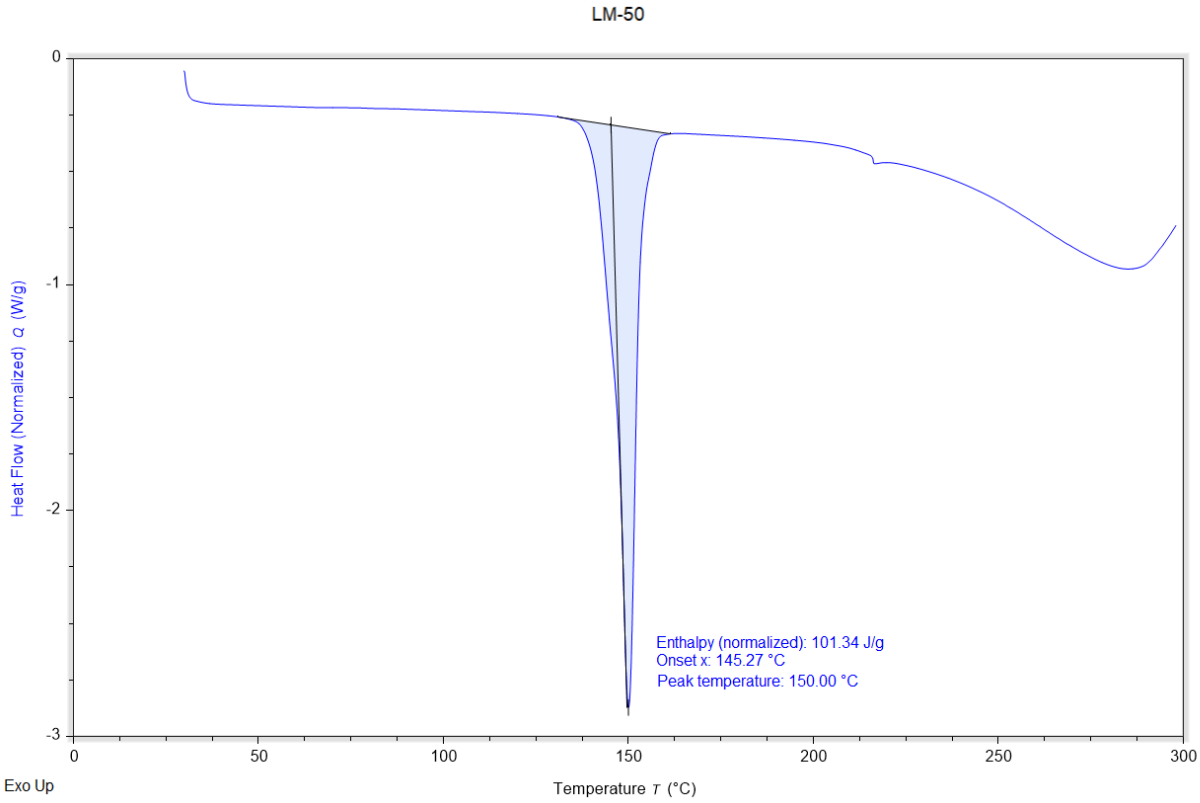

Figure A.22- DSC thermogram of solid from PZQ-4-HBA in acetone.

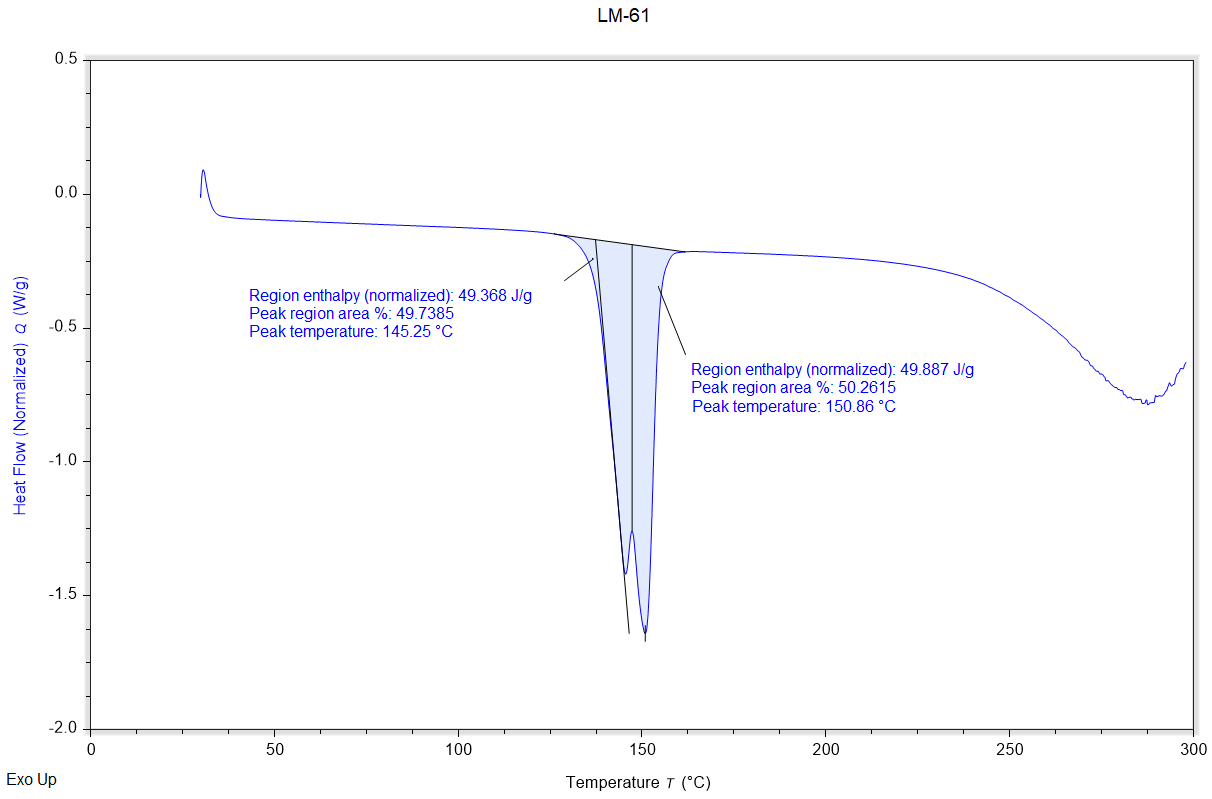

Figure A.23- DSC thermogram of solid from PZQ-4-HBA in EtOH.

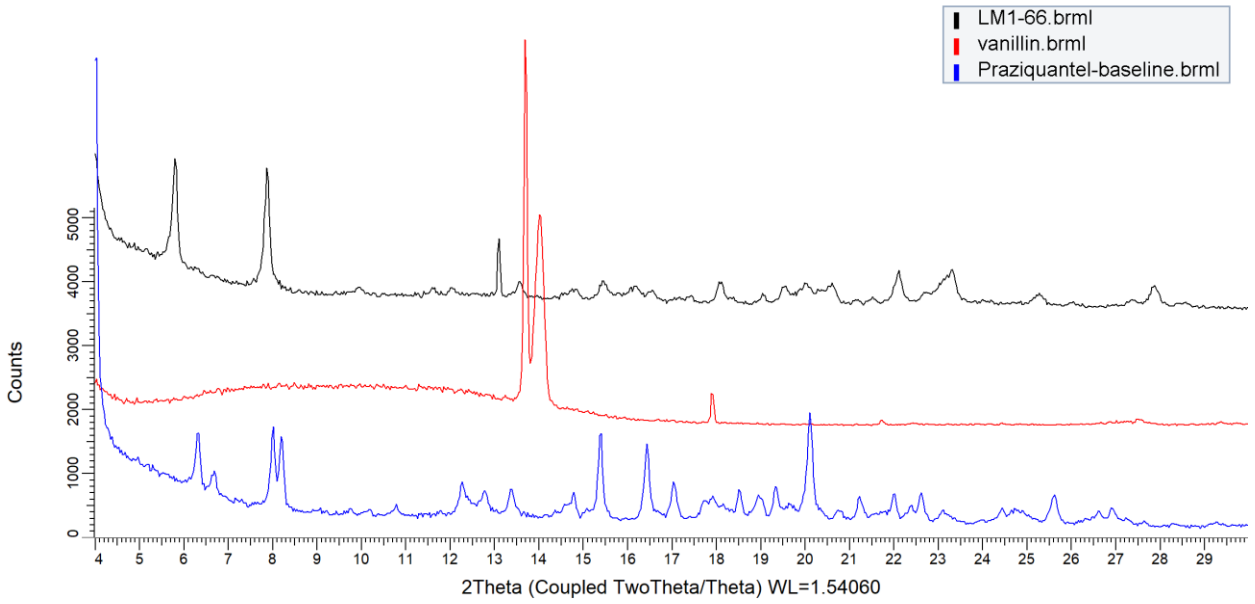

Figure A.24- XRPD result from PZQ co-evaporation with vanillin in EtOH (black).

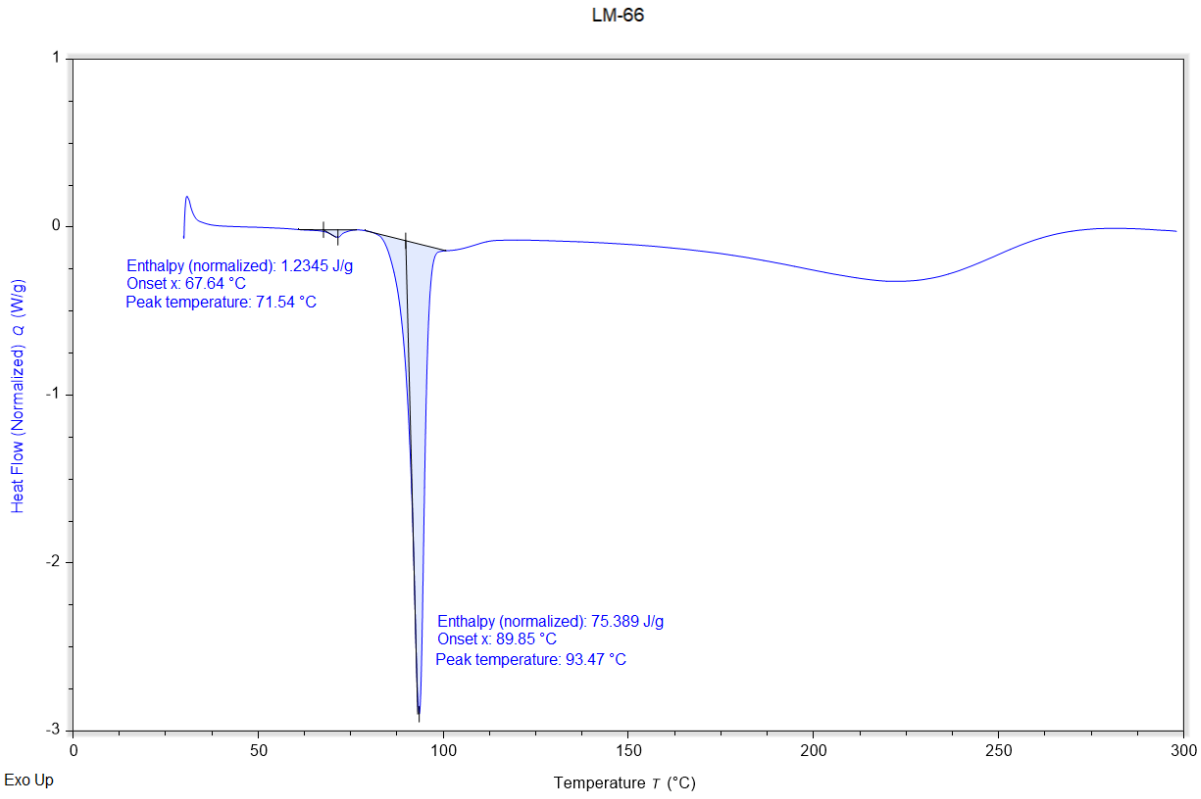

Figure A.25- DSC thermogram of solid from PZQ-vanillin in EtOH.

APPENDIX C: MATLAB SCRIPT FOR DESNITY CALCULATION OF CO_2 USING PENG-ROBINSON MODEL

The Peng-Robinson equation of state (PR-EOS) is a two-constant EOS which can be used to predict properties of single components systems, such as the density of CO_2.[235] The general PR-EOS equation is a modification of the van der Waals equation:

$$P = \frac{RT}{v-b} - \frac{a(T)}{v(v+b)+b(v-b)},$$

where parameters a and b follow the relationship

$$a = a_c \alpha$$

$$\alpha = \left[1 + \kappa\left(1 - \sqrt{T_r}\right)\right]^2$$

$$\kappa = 0.37464 + 1.54226\omega - 0.26992\omega^2$$

$$a_c = 0.45724 \frac{R^2 T_c^2}{P_c}$$

$$b = 0.07780 \frac{RT_c}{P_c}$$

in which T_c and P_c are critical temperature and pressure, respectively.

The equation above can be re-written as a function of three parameters A, B, C as:

$$Z^3 - (1-B)Z^2 + (A - 3B^2 - 2B)Z - (AB - B^2 - B^3) = 0,$$

where

$$A = \frac{aP}{R^2 T^2}$$

$$B = \frac{bP}{RT}$$

$$Z = \frac{Pv}{RT}.$$

In the above equations, R is the ideal gas constant, P is pressure, and T is temperature.

The script used for determination of supercritical CO_2 density with the Peng-Robinson model throughout this thesis is given below. The script was developed in Matlab R2020a.

```
function[rho, phi]=PREoS_CO2(T,P)
% PREoS for CO2 density at given T,P. Input is T (K) and P (MPa).
% Calculate the fugacity of PR-EoS 1 component. Output is density g/cc
and
% fugacity. CO2 props: MW 44.01, w 0.274, Tcrit 304.18, Pcrit 7.38 MPa

%DEFINE CONSTANTS OF THE PROBLEM
R =8.31433; %gas constant (J/molK)
P = P*1000000; %pressure, Pa
MW = 0.04401; %MW of compound, kg/mol
Tcrit = 304.18; %critical temp. of CO2, K
Pcrit = 7380000; %critical pres. of CO2, Pa
w = 0.274; %acentric factor of CO2, unitless
Tr =T/Tcrit; %relative temp, unitless

%DEFINE THE PR-EOS CONSTANTS, UNIVERSAL
a = 0.45724*R^2*Tcrit^2/Pcrit;
b = 0.07780*R*Tcrit/Pcrit ;
k = 0.37464+1.54226*w-0.26992*w^2; %kappa when w < 0.49
alpha = (1+k*(1-Tr^0.5))^2;

%REWRITE THE PR-EOS AS A FUNCTION OF Z
```

```
%PPR=(R*T/(V-b)-a*alpha/(V*(V+b)+b*(V-b)))

%FIND THE ROOTS OF Z. REAL ROOT USED FOR VOLUME at P,T

A = (a*alpha*P)/(R^2*T^2); %alpha used at conditions other than
critical

B = (b*P)/(R*T);

PRZ = [1 -(1-B) (A-3*B^2-2*B) -(A*B-B^2-B^3)];

PRZR = roots(PRZ); %PR Z roots of eqn

Z = PRZR(PRZR==real(PRZR)); %takes real root as Z

V = Z*R*T/P; %V from largest root only

rho = (MW/V)/1000; %density g/cc

%fugacity calculation for single component

phi = exp(Z-1-log(Z-B)-(A/(2*sqrt(2)*B)*...

    log((Z+(1+sqrt(2))*B)/(Z+(1-sqrt(2))*B))));

end
```

APPENDIX D: SOLUBILITY MEASUREMENT METHOD DEVELOPMENT AND COMPARISON TO LITERATURE

BACKGROUND

To aid in selection of a suitable compound for the work presented in this thesis, developing a method to estimate the solubility of various materials in $scCO_2$ was required. Firstly, a brief literature review of common solubility measurement techniques for SCF was done to identify a method that may be transferred to the available instrumentation (outlined in Chapter 5) followed by experiments to compare solubility of model compounds to literature values.

Solubility of a compound can be predicted when limited physicochemical and experimental data are available. However, there are few truly predictive models available for supercritical CO_2 ($scCO_2$) compared to the number of correlation models. In this regard, a truly predictive model is considered as a model to estimate solubility data using only molecular descriptors without the requirement of performing solubility measurements in the solvent of interest ($scCO_2$). Predictive models include UNIFAC, EOS coupled with COSMO- and DFT methods, and methods based on Abraham's euqations.[236–241] In addition there are many methods that are semi-predictive such as NRTL-SAC methods, variations of ANN, least square support vector machine approach (LSSVM), and even some methods using the retention time in supercritical fluid chromatography as indicators of solubility.[242–244]

However, solubility prediction in ternary (solid-CO_2-cosolvent) mixtures becomes more limited and often requires experimental data from the binary (solid-CO_2) system.[48,237,245] A disadvantage of predictive methods is that the predictions can vary depending on the method used for estimating the critical properties of the solute.[237] In addition, the ability to predict solubility of a compound may be limited by availability of essential model parameters or experimental binary data, which limits applicability to novel complex pharmaceuticals.[237] Therefore, to reliably determine solubility, experimental measurements must be conducted.

Solubility measurement in conventional and supercritical systems can be conducted using various techniques. For conventional solvents the methods include gravimetry, spectrophotometric methods, clear point through heating or solvent addition.[173,184,246] Similarly for supercritical fluids solubility measurement techniques include spectrophotometric,

gravimetric, and clear point methods.[114,223,247–249] A comparison of reported models identified that a gravimetric method was best suited to use with the available equipment.

Variations of static gravimetric methods for solubility measurement in CO_2 are reported in literature. In these measurements the vessel with solids is held at constant temperature and pressure for a given time without any flow of gas.[32] The high-pressure cell may be shaken. After the equilibration time (typical times reported are between 2.5 and 11 h) the vessel is depressurized and remaining undissolved solids are weighed.[32,248,250] Static methods tend to use mass of undissolved solid to calculate solubility, whereas the flow-through methods commonly measure the quantity of dissolved solids to calculate solubility.[223,251,252]

Static methods have been validated and reported for neat CO_2, but measurements using CO_2-cosolvent mixtures are not reported. Perhaps because the method of how the solid is added to the vessel (e.g. wrapped in a Kimwipe) is not conducive to addition of an organic co-solvent.[32] In this work we use a static gravimetric method to measure solubility in CO_2 and CO_2-cosolvent mixtures with between 5 and 15 mol.% co-solvent. Since the objective of the solubility measurements in $scCO_2$ presented in this thesis was for screening purposes rather than model development, obtaining values of the correct order of magnitude was most critical. To develop a pressure/temperature dependent solubility profile of a compound that is suitable for modeling, more extensive validation of the presented method is required.

EQUIPMENT MODIFICATION AND PRELIMINARY METHOD DEVELOPMENT

First the sample preparation method was assessed using the following conditions:

1. Solid wrapped in Kimwipe
2. Solid in an Al pan with Kimwipe secured with elastic band
3. Solid in an Al pan with Kimwipe secured with craft wire

The first method, while simple, lead to challenges in weighing and was somewhat messy. The second and third methods involved weighing the solid into an Al weigh dish and securing a Kimwipe to contain the solids allowing for a more reliable mass to be obtained after experiments and also offering flexibility for solubility measurement with cosolvent. The elastic band was found to swell during measurement and was not viable. Craft wire was found to remain secure throughout the experiment, therefore the third option was employed for all experiments described.

Upon initiating this work, the equipment was similar to what is described in Chapter 5, Figure 5.1, but the pressure transducer (Figure 5.1-7) and valve between the chamber and pump (Figure 5.1-5) were not standard from the manufacturer.

Without any modification to the equipment, although the vessel output is sealed the vessel remains open to the CO_2 pump. To maintain the pressure throughout an experiment, CO_2 is consistently being added to maintain the pressure over the measurement duration. This leads to concerns that the excess flow of fresh CO_2 would dissolve more of the solute leading to erroneous results. Therefore, a valve was added between the CO_2 pump and the vessel to close the connection between the pump and vessel. As a safety precaution, a rupture disk was also added between the vessel and the outlet valve in case of thermal runaway (Figure 5.1-3). Throughout the experiment the valve added between the vessel and collection vial remains closed. Addition of the second valve gave rise to another necessary equipment modification. Once the valves (Figure 5.1-5) are sealed, there was no pressure reading in the vessel. As such a PX309-10KGI pressure transducer (Omega) and an OM-CP-Process101A current data logger (Omega) were installed. The transducer/logger system interfaces with OM-CP Data Logger Software version 4.2.21.1 via an OM-CO-IFC200 USB (Omega). This allowed for the pressure inside the measurement vessel to be collected during a solubility experiment. Installation of the pressure transducer proved to be critical in obtaining reliable data to compare to literature, as some experiments illustrated that the pressure in the measurement vessel may be up to 500-900 psi above the set point on the pump or in some cases if there was a minor leak in the equipment it was identified prior to working up the solubility data. If there were not any leaks identified, the sealed vessel was able to maintain pressure for at least 48 h.

COMPARISON TO LITERATURE

Solubility of naphthalene, urea, and one of the APIs screened in Chapter 3, nabumetone, were evaluated using the static gravimetric method. A summary of the tests conducted on three compounds is given below and the suggested standard operating procedure (SOP) for solubility measurement is outlined in Appendix E.

Naphthalene was selected as a model compound because it exhibits relatively high solubility in $scCO_2$ and has been validated by multiple research groups.[252–254] The initial solubility measurements in this study using naphthalene were conducted prior to installation of the pressure

transducer. The values were all higher than the reported literature values, therefore it was suspected that the pressure in the cell during the experiments was above the set point. It should be noted that while the measured values in the first set of experiments were high, they were the same order of magnitude compared to literature and fell within between 16 and 35% of the literature value. After installation of the pressure transducer, one more experiment with naphthalene was performed to test this hypothesis. In that experiment, the pressure set point was 13.1 MPa, but the pressure measured in the vessel was 15 MPa. Taking into consideration the measured pressure, the solubility or naphthalene measured at 15 MPa and 35 °C fell nicely within the trend observed in literature. The data are shown in Figure A..

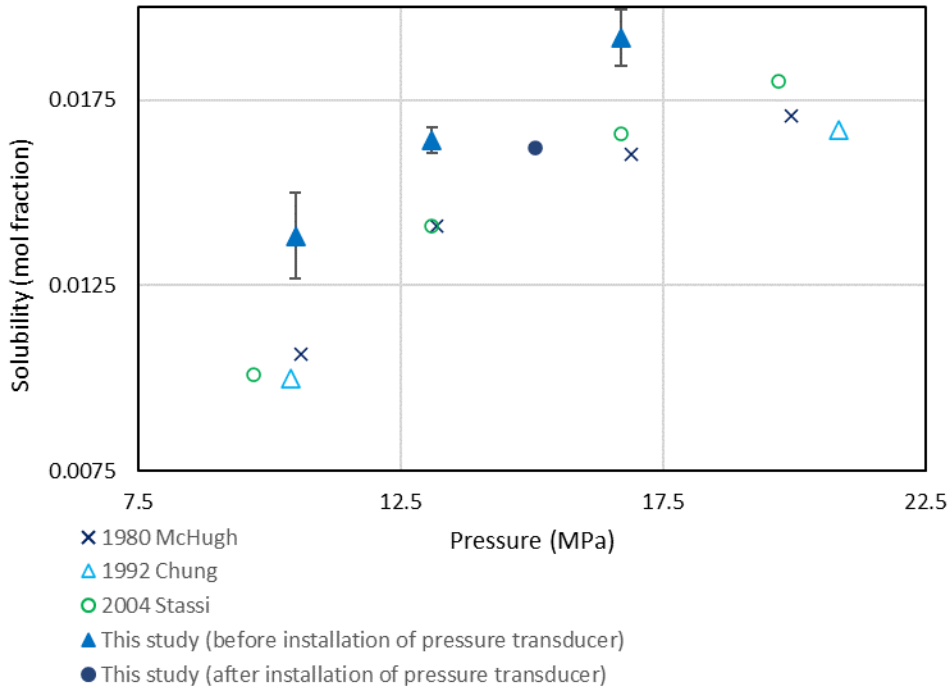

Figure A.26 - Solubility of naphthalene measured at 35 °C in this study compared to literature values.[252–254]

Solubility of nabumetone in $scCO_2$ has been measured and reported by Su *et al.*.[162] Although the solubility screening conditions in this study were slightly varied from the conditions used in literature, the results for NBM measured in this study were in fairly good agreement with the trend in previous data. The data are shown in Figure A..

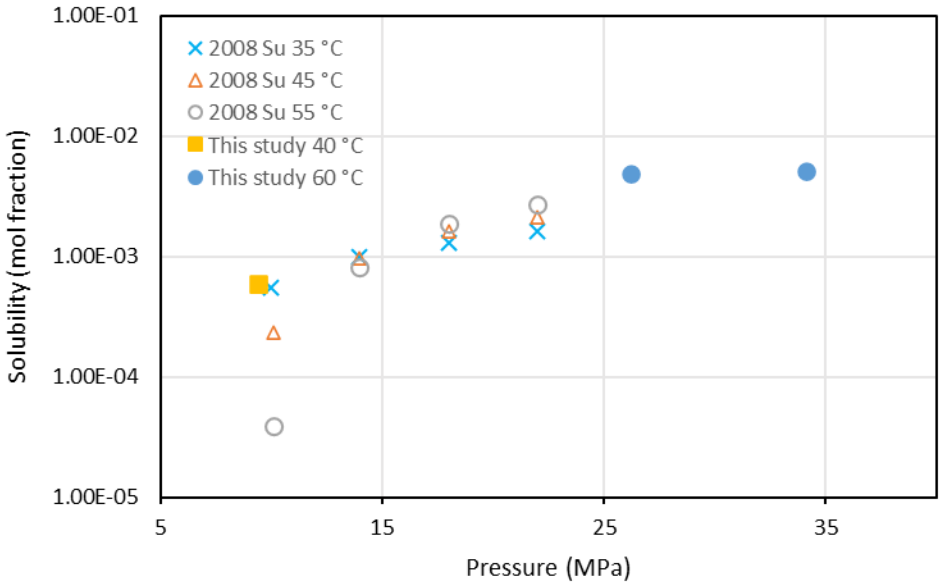

Figure A.27 - Solubility of nabumetone measured in this study compared to literature.[162]

Solubility measurement in the presence of cosolvent was tested using urea and EtOH cosolvent, comparing to Catchpole *et al.,* which was done using a flow-through method.[188] For these experiments, a specified amount of EtOH was added to the vessel prior to pressurization—0.5, 1.0, or 1.5 mL— which was approximately 5, 10, and 15 mol.% EtOH on a solute-free basis, respectively. An experiment without addition of solvent was also performed. Overall, the results were in good agreement with the literature with the exception of 5 mol% EtOH which was approximately 4-5 times higher than the literature value. The data are overlaid in Figure A.. Further validation of solubility measurement of solid in $scCO_2$ with cosolvent using this technique is warranted, but this preliminary work identified this method as a promising test for screening impact of cosolvent on solubility of a solid.

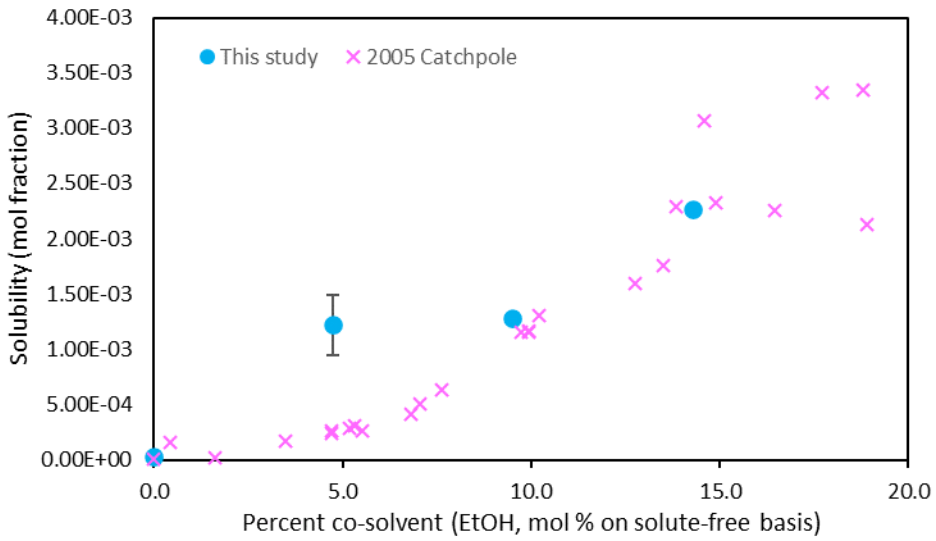

Figure A.28 - Solubility of urea in $scCO_2$ with varying EtOH content at 40 °C and 15 MPa compared to literature.[188]

For the purpose of the research presented in this thesis, the above summarized results were suitable for allowing solubility estimation of an unknown compound in $scCO_2$. Moving forward, if a more detailed solubility profile should be developed it is suggested to complete the validation using naphthalene with the modified equipment set-up to provide a larger body of data in order to estimate measurement error. In addition, continued investigation into solubility measurement in the presence of cosolvent (e.g. replicate measurements) would provide more confidence that the technique is suitable to measure previously unreported data. A complete validation of this solubility measurement method would provide a higher degree of confidence and allow for novel compounds to be measured and modeled in $scCO_2$ (with and without cosolvent) at publication quality.

APPENDIX E: STANDARD OPERATING PRODECURE FOR GRAVIMETRIC SOLUBILITY MEASUREMENT IN SUPERCRITICAL CO_2

1. Thoroughly clean high-pressure vessel (10 mL)
2. Set up SCF equipment according to SOP in closed mode
3. Set temperature and desired pressure according to SOP
4. Record mass of an empty aluminum weighing pan
    a. record mass m_{pan}
    b. add the solid to the pan and record the mass as m_1
        i. if particles/crystals are large then gently grinding in mortar and pestle is recommended before wrapping in KimWipe
    c. cover the pan using a KimWipe and craft wire (an elastic band will swell) and record the mass. This mass is not used in the calculation, but can serve as a second reference
5. Place solid (in pan) in the high-pressure vessel with the flat side of the pan facing down. The pan should not be put upside down, the outside of the vessel can be marked to indicate 'up' direction if needed.
6. Connect vessel to SCF equipment according to SOP.
    a. If cosolvent is used, the selected organic solvent can be added to the base of the sample vessel prior to sealing the vessel at the top. Care should be taken not to dispense solvent directly on the Al pan containing the solid.
7. Select 'run' to allow the vessel to reach the desired pressure (2-10 minutes) and then close the in-line valve to seal the vessel off from the pump.
8. Begin recording pressure using the in-line pressure transducer.
9. Record start time.
10. Let sit under selected conditions until equilibration (overnight—at least 12-15 h— is recommended).
    a. equilibration time may be compound dependent, preliminary tests of solubility vs time are recommended for new compounds.
    b. the insulating chamber must be closed during the temperature equilibration and measurement to avoid thermal runaway.

c. the equipment can be left unattended during equilibration. Rupture disks are installed in case of thermal runaway.

11. After holding for desired time purge the vessel for 10 min at the set pressure (isobaric) using CO_2
12. After purging, depressurize the vessel according to SOP.
13. Open the in-line valve and check that the display on the CO_2 pump reads 0 psi
14. Disconnect the high-pressure vessel and remove the solids in pan covered in Kimwipe for weighing
    a. open the vessel in a fume hood because small particles may be present
    b. be careful not to disturb the pan
    c. in cases where cosolvent is added, the Al pan with remaining sample should be dried under vacuum at 50 – 65 °C to remove residual solvent prior to weighing.
    d. record the total mass of pan/wire/solid after measurement
    e. carefully remove the Kimwipe and wire (without disturbing solids) and record the mass of the pan + solid, record mass as m_2
15. Clean the equipment and shut down according to SOP
16. The pan can be rinsed with a solvent such as MeOH and dried for re-use and the craft wire can be re-used.

Calculation and Example

1. Ensure consistent units used for all calculations below (e.g. mg or g)
2. Mass of solid dissolved
    a. $m_{diss} = m_1 - m_2$
3. Calculate volume of CO_2 (v_{CO2})
    a. assume KimWipe and craft wire volume is negligible
    b. calculate volume of the Al pan using the mass of the pan and Al density (v_{pan})
    c. use true density to calculate volume of solid added (mass of solid added is $m_1 - m_{KW}$)
        i. $v_{solid} = m_{solid}/\rho_{solid}$
    d. for 10 mL vessel: $v_{CO2} = 10.3\ mL - v_{pan} - v_{solid}$
4. Calculate mass of CO_2 at given pressure and temperature

a. use EoS to calculate density of CO_2 (ρ_{CO2}) at given temperature and pressure. Peng-Robinson EoS Matlab script
b. $m_{CO2} = v_{CO2} \times \rho_{CO2}$

5. Solubility (concentration of the dissolved component) is calculated using the following equation, assuming all masses are in g and mw_{sol} is the molar mass of the solute. The values of mol_{diss} and mol_{CO2} are moles of solute and CO_2 and are calculated using the molar mass of each.

$$C1\ \left(\frac{g}{g}\right) = {}^{m_{diss}}/_{m_{CO2}}$$

$$Y\ (\text{mole fraction}) = {}^{(mol_{diss})}\Big/_{(mol_{CO2}\ +\ mol_{diss})}$$

a. due to low solubility of solutes in SCF, mole fraction is often multiplied by 10,000 and reported as $Y \times 10^4$ in literature.

Symbol	Property/measurement	Calculation	Value	Unit
VV	vessel volume	-	10.33	mL
d_{Al}	Al density	-	2.7	g/mL
MW_{SA}	Salicylic acid molar mass	-	138.121	g/mol
d_{SA}	Salicylic acid density	-	1.44	g/mL
MW_{CO2}	CO_2 molar mass	-	44.01	g/mol
d_{CO2}	CO_2 density	-	1.00177	g/mL
m_{Al}	Al pan	-	0.20762	g
m_{PS}	Pan + solid	-	0.26239	g
m_{PSfin}	Final pan + solid	-	0.24955	g
m_{SAdiss}	Salicylic acid dissolved	m_{PSfin} - m_{PS}	0.01284	g
V_{SA}	Salicylic acid volume (total)	(m_{PS} - m_{Al})/ d_{SA}	0.03803	mL
mol_{SAdiss}	Salicylic acid dissolved	m_{SAdiss}/ MW_{SA}	9.2962E-05	mol
VV_{rem}	remaining chamber volume	VV - V_{SA} - m_{Al}/ d_{Al}	10.21728	mL
m_{CO2}	CO_2 mass in vessel	VV_{rem} * d_{CO2}	10.23537	g
mol_{CO2}	CO_2 mol in vessel	m_{CO2}/ MW_{CO2}	0.23257	mol
-	Salicylic acid solubility	mol_{SAdiss}/ (mol_{SAdiss} + mol_{CO2})	4.00E-04	mol fraction
		1000* m_{SAdiss}/ m_{CO2}	1.25	mg/gCO_2